

FEDERAL UNIVERSITY OF PERNAMBUCO
TECHNOLOGY AND GEOSCIENCES CENTRE
DEPARTMENT OF MECHANICAL ENGINEERING
POST-GRADUATE PROGRAMME IN MECHANICAL ENGINEERING

PAULA SUEMY ARRUDA MICHIMA

OPTIMIZATION OF PRISMATIC MOON POOL CONFIGURATION BY
OPERABILITY CRITERIA

RECIFE
2017

PAULA SUEMY ARRUDA MICHIMA

OPTIMIZATION OF PRISMATIC MOON POOL CONFIGURATION BY
OPERABILITY CRITERIA

Thesis submitted to the Post-Graduate
Programme in Mechanical Engineering of the
Federal University of Pernambuco in partial
fulfilment of the requirements for the degree of
Doctor of Science in Mechanical Engineering.

Concentration area: Energy.
Research field: Fluid dynamics.

Advisor: Prof. Dr. Ana Rosa Mendes Primo
Co-advisor: Dr. Hiroshi Kawabe

RECIFE
2017

Catálogo na fonte
Bibliotecária Margareth Malta, CRB-4 / 1198

M624o Michima, Paula Suemy Arruda.
Optimization of prismatic moon pool configuration by operability criteria /
Paula Suemy Arruda Michima. - 2017.
326 folhas, il., gráfs., tabs.

Orientadora: Profa. Dra. Ana Rosa Mendes Primo.

Coorientador: Prof. Dr. Hiroshi Kawabe.

Tese (Doutorado) – Universidade Federal de Pernambuco. CTG.

Programa de Pós-Graduação em Engenharia Mecânica, 2017.

Inclui Referências e Apêndices.

1. Engenharia Mecânica. 2. *Drill ship*. 3. Navio-sonda de perfuração.
4. *Moon pool*. 5. Otimização. 6. Operabilidade. 7. Algoritmo genético. I.
Primo, Ana Rosa Mendes. (Orientadora). II. Kawabe, Hiroshi.
(Coorientador). III. Título.

UFPE

621 CDD (22. ed.)

BCTG/2016-393

20 de outubro de 2017.

“OPTIMIZATION OF PRISMATIC MOON POOL CONFIGURATION BY
OPERABILITY CRITERIA”

PAULA SUEMY ARRUDA MICHIMA

ESTA TESE FOI JULGADA ADEQUADA PARA OBTENÇÃO DO TÍTULO DE
DOUTOR EM ENGENHARIA MECÂNICA

ÁREA DE CONCENTRAÇÃO: ENERGIA

APROVADA EM SUA FORMA FINAL PELO
PROGRAMA DE PÓS-GRADUAÇÃO EM ENGENHARIA
MECÂNICA/CTG/EEP/UFPE

Prof^a Dr^a ANA ROSA MENDES PRIMO
ORIENTADORA/PRESIDENTE

Prof. Dr. HIROSHI KAWABE
COORDENADOR

Prof. Dr. CEZAR HENRIQUE GONZALEZ
COORDENADOR DO PROGRAMA

BANCA EXAMINADORA:

Prof^a Dr^a ANA ROSA MENDES PRIMO (UFPE)

Prof. Dr. HIROSHI KAWABE (CLASSNK)

Prof. Dr. DARLAN KARLO ELISIÁRIO DE CARVALHO (UFPE)

Prof. Dr. JANARDAN SINGH ROHATGI (UFPE)

Prof. Dr. KAZUO NISHIMOTO (USP)

Prof. Dr. TSUGUKIYO HIRAYAMA (YOKOHAMA NATIONAL UNIVERSITY)

To my daughter Lara that teaches me, so deeply
and constantly, the patience and understanding.
To my son Dante who so naturally reveals to all,
at each moment, the vivid beauty of childhood.
To my beloved husband Marcelo.
To my eternal basis: mother Eliete (*in memo-
riam*), father Toshiyuki and my sister Lilian.

Acknowledgements

I believe in angels, even though they sometimes do not believe themselves.

When people say that being PhD candidate is a lifestyle, one doesn't trust until it has become truth. It was a big responsibility and heavy burden to impose such a long omission in the daily life of my dearest. Hence, first of all I deeply apologize and address my special thanks to my children Lara and Dante because I had to refuse to play together so many times during the past years, whilst always having your understanding. Also my sincere apologies and acknowledgement to my beloved husband Marcelo, my father Toshiyuki, my sister Lilian and my relatives. I also must apologize to my friends and Professors for keeping you all concerned about the timescales that took to conclude my thesis.

In parallel to each stage of my academic development I have experienced and learned a lot of concepts, techniques and about society, but in the past years I was caught off guard by the sincere and altruistic attitude from those who were beyond great Professors! For believing in looking into the eyes to teach, for taking students as individuals, for humbleness, dignity, hard working, faith, nobleness, for trusting my ability, for truly helping without charging, my most sincere thank you: Oscar Augusto and Moyses Szajnbock (*in memoriam*), Celio Taniguchi, Toshi-ichi Tachibana, Helio Morishita, Kazuo Nishimoto, Tsugukiyo Hirayama, Hiroshi Kawabe, Ana Rosa Primo. Although not my former professor, I include my chosen mother Ângela Buscema in this group. There is nothing else that I could say in return at the same level other than *I love you too*.

Thanks also to my colleagues, especially Professors Marco Petkovic, Marcos Pereira and Claudino Lira with whom I shared so many hours of planning, talking, being friends. Thanks to the Mechanical Engineering Department colleagues for trusting my potential, especially those from PPGEM, Professors Oscar de Araújo, Jorge Guerrero, Cezar Gonzalez, Darlan de Carvalho, for the many times I had you analyse my situation to help me with deadline, financial, administrative and psychological support. Many thanks to my student friends Tulio Cavalcante, Ícaro Fonseca, João Alves, Débora Mendonça and Danilo Bispo without whom I would not make it. It would also be too boring without you. Fillipe Silva, how precious your motivation was!

Thank you dears Hissae Fujiwara and Rita Tomina, you made the difference. Thanks to Lilian Yamamoto and Rogerio Takimoto for always being always there for me. Finally, thanks to everyone whom from the bottom of the heart supported me during this endeavour.

蔵焼けて 障るものなき 月見哉

水田 正秀

“Barn’s burnt down — Now I can see the moon”

Mizuta Masahide (1657–1723)

Abstract

A moon pool is an opening inside the hull of a floating system that allows access to the sea isolated from horizontal environmental forces. Despite those benefits, some disadvantages may occur when a resonant response to waves happens. Exaggerated oscillations might cause poor operation conditions or interruption of drilling procedures. The aim of this work is to, given a hull, find an optimal moon pool configuration that would result in the best stationary operation conditions for a typical sea state of the operation region. The proposal restricts it to be prismatic, free of appendages, recess, or any solution other than adequate contour shape. A drill ship is chosen as an example, but the method suits for floating systems in short and long term operation, granted that the response spectra can be calculated. Through an altered genetic algorithm applied to the set of parameters that define the shape and dimensions of the moon pool border, the optimum shape is searched based on hull and internal water response to wave excitation in various incidence angles and significant wave periods. A detailed development of the potential model used to describe the ship and free surface motions is presented, proposing a Rayleigh damping term and a boundary condition at the free surface inside the moon pool. The derivation of a set of formulae to transform into threshold significant wave height the acceptable limit values of each criterion: free surface height, ship motion, hull structure strength and positioning in azimuthal plane are also shown to determine a grade of fitness based on resultant operable conditions. Although there still are spaces for improvement of the resultant parameters' values due to computational limitations, transversal dimensions and border shape parameters have converged, and the small variation of longitudinal dimensions is limited by order of length and Length/Breadth ratio values range of the moon pool. It was found possible to define, from user input: hull geometry and limit values for operability, what is the optimum prismatic moon pool configuration, which can be very different from the standard rectangle. Further, once the results of optimization are obtained, still in design stage, it is possible to identify characteristics of the system (or ship) that would improve operability. The output of the optimization program provides a visualization file of the mesh of the hull with optimum moon pool, and a radar chart with the operable zone of a given sea state. The latter can be used for quick decision making upon interruption of procedures during operation. In terms of construction complexity the moon pool shape doesn't seem to present any limitations, since it is prismatic. A bow or stern shape is much more complex than the moon pool, and from mesh definition it is composed of only flat plates, demanding no extra work in plate conformation.

Keywords: Drill ship. Moon pool. Optimization. Operability. Genetic algorithm.

Resumo

Um moon pool é uma abertura no casco de um sistema flutuante que permite o acesso ao mar isolado das forças horizontais providas do ambiente. Apesar desse benefício, algumas desvantagens podem existir quando a resposta à excitação de ondas é ressonante. Oscilações exageradas podem provocar baixas condições de operação ou interrupção dos procedimentos de perfuração. O objetivo deste trabalho é, dado um casco, encontrar a configuração ótima do moon pool que resultará nas melhores condições de operação estacionária para um estado de mar típico da região de operação. A proposta restringe-o a ser prismático, livre de apêndices, recessos, ou qualquer outra solução que não seja o formato de sua borda. Um navio-sonda de perfuração (*drill ship*) foi escolhido como exemplo, mas o método se aplica a sistemas flutuantes em operação de curto e longo prazo, se os espectros de resposta puderem ser calculados. Utilizando um algoritmo genético alterado aplicado aos parâmetros que definem a forma e dimensões de seu contorno, a configuração ótima do moon pool é buscada para o casco, dada a resposta à excitação de ondas em vários ângulos de incidência e períodos significativos de onda. O modelo potencial usado para descrever os movimentos do navio e da superfície livre do moon pool é apresentada, com a proposta do termo de amortecimento de Rayleigh e a condição de contorno correspondente. A dedução das fórmulas para converter as informações de valores dos limites aceitáveis para cada critério (altura da superfície livre do moon pool, resposta do navio, resistência estrutural do casco e manutenção do posicionamento) é apresentada. As formulas definem a adequação do moon pool para as condições de operação resultantes. Embora haja pontos a serem melhorados nos valores dos parâmetros resultantes (devidos à limitação computacional), as dimensões transversais e parâmetros de forma convergiram, e a pequena variação nas dimensões longitudinais é limitada pela ordem de grandeza do comprimento e faixa de valores da razão de Comprimento/Boca do moon pool. Concluiu-se que é possível definir, a partir de dados de entrada do usuário: geometria do casco e valores limites para operabilidade, qual é a configuração ótima de moon pool prismático, que pode ser bastante diferente do retângulo convencional. Além disso, uma vez obtidos os resultados da otimização, ainda no estágio de projeto, é possível identificar características do sistema (ou navio) que podem melhorar a operabilidade se alterados de forma conveniente. Juntamente com os valores resultantes dos parâmetros de dimensões e forma, são fornecidos também a malha do casco com o moon pool ótimo integrado e um gráfico de radar com a zona operável em um dado estado de mar, que pode ser usado para tomadas rápidas de decisão sobre a interrupção das operações em curso. Em termos de complexidade construtiva, a forma do moon pool não parece apresentar limitações, por ser prismática. Formas como a da proa e da popa são muito mais complexas do que a do moon pool proposto que, pela própria definição da malha, é composto apenas de chapas planas, e não demandam trabalho de conformação.

Palavras-chave: *Drill ship*. Navio-sonda de perfuração. *Moon pool*. Otimização. Operabilidade. Algoritmo genético.

List of Illustrations

Figure 1 – Example of drill ship: Huisdrill 12000.	27
Figure 2 – Motion conditions of the internal water of a moon pool.	29
Figure 3 – Modes of water oscillation inside the moon pool	30
Figure 4 – Composed motion of the water inside a 2D moon pool	30
Figure 5 – Contribution of the vortex in the oscillatory motion and stagnation region of water at fore portion in a moon pool	31
Figure 6 – Oscillation modes and amplitude behaviours at ranges of reduced speeds, for different dimension ratios of rectangular moon pools.	32
Figure 7 – Numerically simulated moon pool water surface elevation at midpoint (encounter angle $\beta = 45^\circ$) in Series 60 hull	33
Figure 8 – Relation between the wave energy peak and the moon pool RAO peaks	34
Figure 9 – Elements of transfer function between incident wave and water column oscillation.	35
Figure 10 –Configurations studied with 2D numerical model by Day (1990)	37
Figure 11 –Different moon pool shapes.	39
Figure 12 –Simple U-tube	41
Figure 13 –Manometer	41
Figure 14 –Two tanks connected by a duct	42
Figure 15 –Vessel with moon pool, with no motion, in deep water	43
Figure 16 –Added draft obtained experimentally.	43
Figure 17 –Moon pool water surface elevation at mid	49
Figure 18 –Moon pool water surface relative elevation at surface mid. point ($\beta =$ 45°).	49
Figure 19 –Example of response spectrum in heave mode for different incidence angles.	50
Figure 20 –Threshold significant wave height \times significant wave period for each safety criterion.	51
Figure 21 –Effect of wave spectra on water surface elevation spectrum inside moon pool.	52
Figure 22 –Radar charts of threshold wave heights for specific significant periods	53
Figure 23 –Parameters of the moon pool contour.	55
Figure 24 –Generic flowchart of a genetic algorithm.	56
Figure 25 –Sketch of moon pool RAO.	57
Figure 26 –Flowcharts of the algorithms.	58
Figure 27 –Overall view of the composition of the Gamma algorithm.	58

Figure 28 –General file flowchart of the optimization tool interacting with the hydrodynamic calculation module.	59
Figure 29 –Detailed moon pool geometry flow diagram.	60
Figure 30 –Coordinate system.	62
Figure 31 –Ship as a transfer function between incident wave and response to its excitation.	71
Figure 32 –Short and long waves and coordinate system	77
Figure 33 –Incident angle β	85
Figure 34 –Degrees of freedom in ship motions.	86
Figure 35 –Drill ship RAO: surge motion.	89
Figure 36 –Drill ship RAO: sway motion.	90
Figure 37 –Drill ship RAO: heave motion.	91
Figure 38 –Drill ship RAO: roll motion.	92
Figure 39 –Drill ship RAO: pitch motion.	93
Figure 40 –Drill ship RAO: yaw motion.	94
Figure 41 –Drill ship RAO: vertical bending moment.	96
Figure 42 –Drill ship RAO: lateral drift.	97
Figure 43 –Drill ship RAO: MP water motion at mid.	98
Figure 44 –Overview of the strategy used for optimization	101
Figure 45 –Mesh of the hull without opening used as input in the present work .	102
Figure 46 –Border parameters of the moon pool, symmetric about the longitudinal centre line	103
Figure 47 –Illustration of size ratio dimensions	113
Figure 48 –Drill ship mesh with 1748 elements.	115
Figure 49 –Free surface mesh regions used for element generation order. . .	116
Figure 50 –Example of hull mesh in gmsh visualization	117
Figure 51 –Resonance peaks of the centre of the moon pool at different incidence angles	118
Figure 52 –Ship motion RAO for various values of Rayleigh damping coefficient	119
Figure 53 –Piston mode resonance peak amplitude for each Rayleigh damping coefficient	120
Figure 54 –Dimensions of the model, positions of the sensors and tank's depth.	122
Figure 55 –Mesh of the model used for validation.	123
Figure 56 –Responses inside and outside MP: comparison between literature and calculation.	124
Figure 57 –Comparison of the predicted response of the rectangular hull with moon pool	125

Figure 58	–Rectangular hull with moon pool used for empirical data acquisition	126
Figure 59	–Time history records of the exciting transient wave and the responses in each motion mode	128
Figure 60	–RAO in each motion mode: transient wave with incidence angle 90° : experimental and calculated	129
Figure 61	–Surge RAO at incidences 0° and 90° , comparison between calculations by WAMIT [®] and hydrodynamic module	130
Figure 62	–Sway RAO at incidences 0° and 90° , comparison between calculations by WAMIT [®] and hydrodynamic module	131
Figure 63	–Heave RAO at incidences 0° and 90° , comparison between calculations by WAMIT [®] and hydrodynamic module	132
Figure 64	–Roll RAO at incidences 0° and 90° , comparison between calculations by WAMIT [®] and hydrodynamic module	133
Figure 65	–Pitch RAO at incidences 0° and 90° , comparison between calculations by WAMIT [®] and hydrodynamic module	134
Figure 66	–Yaw RAO at incidences 0° and 90° , comparison between calculations by WAMIT [®] and hydrodynamic module	135
Figure 67	–Cylinder platform with a moon pool with a duct-type restriction on its bottom	136
Figure 68	–Mesh used for calculation in the hydrodynamic module.	137
Figure 69	–Comparison between numerical and experimental data obtained by Torres (2007) and the calculation by the hydrodynamic module	138
Figure 70	–Configuration of the floating ring used by Mavrakos (1988)	139
Figure 71	–Meshes of hull with free surface inside moon pool of the simulated floating rings	140
Figure 72	–Nondimensional added mass and damping coefficients in surge of the cylinder hull.	141
Figure 73	–Basic geometries assessed: rectangle, ellipsoid, octagon and rhombus	142
Figure 74	–Response charts of the moon pool internal water: rectangle moon pool	146
Figure 75	–Response charts of the heave motion: rectangle moon pool	147
Figure 76	–Response charts of the vertical bending moment: rectangle moon pool	148
Figure 77	–Response charts of the lateral drift motion: rectangle moon pool	149
Figure 78	–Response charts of the moon pool internal water: ellipse moon pool	150
Figure 79	–Response charts of the heave motion: ellipse moon pool	151
Figure 80	–Response charts of the vertical bending moment: ellipse moon pool	152
Figure 81	–Response charts of the lateral drift motion: ellipse moon pool	153
Figure 82	–Response charts of the moon pool internal water: rhombus moon pool	154
Figure 83	–Response charts of the heave motion: rhombus moon pool	155
Figure 84	–Response charts of the vertical bending moment: rhombus moon pool	156

Figure 85 –Response charts of the lateral drift motion: rhombus moon pool . . .	157
Figure 86 –Response charts of the moon pool internal water: octagon moon pool	158
Figure 87 –Response charts of the heave motion: octagon moon pool . . .	159
Figure 88 –Response charts of the vertical bending moment: octagon moon pool	160
Figure 89 –Response charts of the lateral drift motion: octagon moon pool . . .	161
Figure 90 –Operability charts of each sample for period $T_s = 10s$ in big axis range	168
Figure 91 –Operability charts of each sample for period $T_s = 4s$ in big axis range	169
Figure 92 –Operability charts of each sample for period $T_s = 10s$ in small axis range	170
Figure 93 –Operability charts of each sample for period $T_s = 10s$ in small axis range	171
Figure 94 –Results of the performance analysis of each geometry	172
Figure 95 –Common characteristic of the optimum solutions in moon pool water oscillation and ship motion criteria	181
Figure 96 –Common characteristic of the optimum solutions in drift criterion . . .	181
Figure 97 –Common characteristic of the optimum solutions in vertical bending moment criterion	182
Figure 98 –Radar charts of the resultant configurations of optimization by all criteria	185
Figure 99 –Wave harmonic nodes inside the hull	202
Figure 100 –Map of sea areas of the scope of global coverage	205
Figure 101 –Directional classes of joint probability distribution of wave heights and periods	206
Figure 102 –Joint probability distribution with threshold wave heights of the ship	207
Figure 103 –Moon pool elements with different size ratio dimensions	210
Figure 104 –Heave and drift charts at different moon pool element length ratios, both for $\beta = 90^\circ$	211
Figure 105 –Midship vertical bending moment and moon pool water surface ele- vation at mid with different moon pool element length ratios, both for $\beta = 0^\circ$	211
Figure 106 –Charts of drift force response value evolution with length ratio . . .	212
Figure 107 –Charts of heave motion response value evolution with length ratio . .	212
Figure 108 –Charts of moon pool water surface elevation at mid response value evolution with length ratio	212
Figure 109 –Charts of heave motion response value evolution with length ratio . .	213
Figure 110 –Length ratio of the elements in the MP	214
Figure 111 –Length ratio of the elements in the moon pool	214

List of Tables

Table 1 – Dimensions of drill ships	28
Table 2 – Dimensions of AHTS and CSV ships	29
Table 3 – Genetic algorithm characteristics table	46
Table 4 – Evolutionary strategy characteristics table	47
Table 5 – Units of the motion RAOs	85
Table 6 – General operability limiting criteria for ships	111
Table 7 – Length ratio of the element lengths: hull's to moon pool's	113
Table 8 – Variation of the results for each case taking as reference the case 5	114
Table 9 – Principal dimensions of the models used for comparison	120
Table 10 –Experiment parameters.	123
Table 11 –Dimensions of the model	127
Table 12 –Details of the tested models for validation	136
Table 13 –Collection of sets of parameters used in each sample of the basic geometries analysed	144
Table 14 –Threshold significant wave heights and differences between chosen L/B cases.	163
Table 15 –Incidence angles at which the impact is more significant	164
Table 16 –Comparison of highest L/B ratio in each incidence angle for moon pool internal water oscillation response.	165
Table 17 –Comparison of lowest L/B ratio in each incidence angle for moon pool internal water oscillation response and vertical bending moment at midship response.	165
Table 18 –Samples of the best L/B in each geometry with the same internal water plane area.	167
Table 19 –Values used as parameters for the evaluation criteria of operability	175
Table 20 –Three best configurations of optimization by moon pool water oscillation criterion only	177
Table 21 –Three best configurations of optimization by ship motion criterion only	178
Table 22 –Three best configurations of optimization by drift criterion only	179
Table 23 –Three best configurations of optimization by vertical bending moment amidship criterion only	180
Table 24 –Three best configurations of optimization by overflow + drift criteria only	183
Table 25 –Three best configurations of optimization by all criteria	184

List of abbreviations and acronyms

ABNT	Associação Brasileira de Normas Técnicas
AHTS	Anchor Handling Tug Supply Vessel
BEM	Boundary Element Method
CFD	Computational Fluid Dynamics
CLV	Cable Laying Vessel
CrOFW	Criterion: overflow of moon pool's internal water
CrSTR	Criterion: exceedance in stroke of the heave compensator equipment
CrVBM	Criterion: exceedance in vertical bending moment at midship section
CrDFT	Criterion: exceedance in drift power over DPS system limit
CSV	Construction Support Vessel
DNV	Det Norske Veritas
DPS	Dynamic Position System
DSV	Diving support vessel
FPSO	Floating Production, Storage and Offloading (system)
FVM	Finite Volume Method
HF	High Frequency
IACS	International Association of Classification Societies
IMR	Inspection, maintenance and repair
ISO	International Organization for Standardization
JONSWAP	Joint North Sea Wave Project
LF	Low Frequency
LWI	Light well intervention
MP	Moon pool

MPS	Moving Particle Semi-Implicit Method
OCLV	Offshore cable laying vessel
OCSV	Offshore Construction Support Vessel
PLSV	Pipe Laying Support Vessel
RAO	Response Amplitude Operator
SPH	Smoothed Particle Hydrodynamics Method
VOF	Volume Of Fluid
WF	Wave Frequency
1D	1-Dimension
2D	2-Dimensions
3D	3-Dimensions

List of symbols

β	Incidence Angle of the waves on the ship
ε	Rayleigh's Viscosity
π	Ratio of a circle perimeter to its diameter (approx. 3.1415)
Φ	Time-dependent velocity potential
ϕ	Time-independent velocity potential
φ	Time-independent velocity potential by unit motion
Φ_0	Velocity potential of incident wave
Φ_D	Velocity potential of diffracted wave
Φ_R	Velocity potential of radiated wave
Φ_S	Velocity potential of dynamic buoyancy restoration
ρ	Water specific weight in kg/m^3
ω	Angular frequency of the wave
ω_0	Natural frequency of the internal water of the moon pool
A	Added Mass
a	Wave amplitude
B	Breadth
B	Coefficient of wave radiation damping (in the equation of motion)
C	Restoration Coefficient
C_b	Block coefficient
d	Ship's draught
E	Wave Exciting Force
F	External force
F_D	Diffraction forces/moments

F_R	Radiation force
F_s	Static force
F_0	Froude-Krylov forces/moments
G	Green's Function
g	Gravity Acceleration
h	Oscillation Amplitude of the internal water of the moon pool
I_{xx}	Moment of Inertia of the ship along the longitudinal axis
I_{yy}	Moment of Inertia of the ship along the transversal axis
I_{zz}	Moment of Inertia of the ship along the vertical axis
L1	Longitudinal Fore-length
L2	Transversal Half-length
L3	Longitudinal Aft-length
M	Mass of the ship
m1	Transversal Coordinate of the fore corner polygon
m2	Longitudinal Coordinate of the fore corner polygon
m3	Longitudinal Coordinate of the aft corner polygon
m4	Transversal Coordinate of the aft corner polygon
nf	Number of vertices of the fore corner polygon
nt	Number of vertices of the aft corner polygon
n_x	Normal vector component in x direction
P_D	Power by drift force
S_a	Surrounding region at a finite distance far away the ship
S_h	Ship hull's surface
S_M	Moon pool wall surface
t	Time
X_j	Force or moment on the j -th movement mode of the ship

x	Longitudinal coordinate of the ship
x_Q	Limit value allowed for a criterion to be attended.
y	Transversal coordinate of the ship
z	Vertical coordinate of the ship

Summary

1	INTRODUCTION	21
1.1	MOTIVATION	22
1.2	OBJECTIVES	23
1.3	STRUCTURE OF THE THESIS	24
2	LITERATURE	26
2.1	DRILL SHIP CHARACTERIZATION	26
2.1.1	Water oscillation mechanism	28
2.2	LITERATURE SURVEY	34
2.2.1	Path 1: Resonant oscillation	35
2.2.2	Path 2: Evolutionary algorithm	45
2.3	DETAILED REVIEW	48
3	THEORETICAL FOUNDATION	60
3.1	SHIP RESPONSE IN WAVES	61
3.1.1	Coordinate system	62
3.1.2	General equation of motion	62
3.1.3	Linear theory model	64
3.1.4	Linear equation of motion	65
3.1.5	Ship response model	66
3.1.5.1	Frequency domain	67
3.1.5.2	Time domain	71
3.2	BOUNDARY VALUE PROBLEM WITHOUT MOON POOL	73
3.2.1	Wave drift force	76
3.2.2	Vertical bending momentum	81
3.3	BOUNDARY VALUE PROBLEM WITH MOON POOL	82
3.4	EFFECT OF MP ON MOTION RAO	84
4	METHODOLOGY	99
4.1	PERFORMANCE AND FITNESS GRADING	99
4.2	ASSESSMENT FORMULAE	103
4.2.1	Moon pool water oscillation	106
4.2.2	Ship motion	107
4.2.3	Station keeping problem	108
4.2.4	Structural problems	108
4.2.5	Workability	110

5	CALIBRATION	112
5.1	MESH CALIBRATION	112
5.2	RAYLEIGH COEFFICIENT CALIBRATION	116
6	VALIDATION	121
6.1	RECTANGULAR 2D MODEL	121
6.2	FPSO MODEL	126
6.3	SINGLE COLUMN	135
6.4	CYLINDRICAL MODEL	139
7	RESULTS AND DISCUSSION	142
7.1	CHARACTERISTICS INVESTIGATIONS	142
7.1.1	Aspect ratio variation	143
7.1.2	Shape variation	166
7.2	OPTIMIZATION	174
8	CONCLUSIONS	187
9	ONGOING AND FURTHER WORKS	190
10	CONTRIBUTIONS	192
	REFERENCES	193
	APPENDIX A MATRIX-SHAPED EQN. OF THE POTENTIAL	199
	APPENDIX B LONG TERM OPERABILITY DISCUSSION	204
	APPENDIX C MOON POOL MESH CALIBRATION DATA	209
	APPENDIX D INPUT FILES PICTURES	215
	APPENDIX E OUTPUT FILES DESCRIPTION	225
	APPENDIX F OUTPUT FILES PICTURES	248
	APPENDIX G CODE	273

1 Introduction

“The time to begin writing an article is when you have finished it to your satisfaction. By that time you begin to clearly and logically perceive what it is that you really want to say.”

— Mark Twain, *Notebook, 1902–1903*

A moon pool (MP) is a wall-sided flooded opening inside the hull of a ship through which procedures, equipment and operators access the ocean from the deck to the operation place (drills reach the sea floor, divers access the bottom part of the hull for fixing and inspections, ROV are launched, etc.). Using this passageway instead of the direct access to the ocean from one of the sides of the ship is justified by the isolation from horizontal environmental forces that it provides. Nonetheless, if the moon pool is located near or coincident with the centre of gravity of the vessel it will minimize the effects of the angular motions of the hull.

Although there are benefits of having MP to access the ocean, some problems might arise regarding the environmental actions on the hull, which could be worsened by the existence of such opening. The effects of those excitations, particularly when resulting in resonant wave response, lead to oscillations that, according to Day, Lee and Kuo (1989), can reach 3 to 4 times the exciting wave height. This behaviour can result in situations ranging from poor operation conditions to interruption of drilling procedures, or structural or mooring problems directly related to flooding of equipment handling areas – which are usually located above the moon pool – or indirectly cause excessive loads inside the opening.

The most critical factors are the vertical motions inside the moon pool, causing a potential large load on any object being launched through the water surface in the splash zone. Another aggravating environmental problem arises in risk of ice. With the associated cold climate, an ice element eventually entrapped in a MP, can be a demanding and time-consuming work to remove, as highlighted by Nesjø (2015).

As stated by Day (1990), the aggravation and its intensity are directly related to the shape, dimensions and location of the moon pool. Also, there is a criterion that should be considered in any engineering project, that is the long term downtime. In the MP case, this could happen due to a diversity of causes: inadequate structural design, build failure, accidental damages or excessive oscillation of the water column inside it, to which one can also refer as MP water or water plug.

In this sense, it is important to find an optimal combination of those characteristics that would result in the best operation conditions for a given wave spectrum that represents the sea state of the operation region. Besides the operation conditions

exclusively intrinsic to the vessel and its equipment, there is also the inoperability that results from the vibration effects on the crew, quantified in the ISO (1997) regulation, which accounts for comfort and workability.

A qualitative analysis of the safety of a drill ship based in a set of parameters, such as the Response Amplitude Operator (RAO) or response spectrum of the ship, hydrodynamic loads and internal characteristics. Dynamic Positioning System (DPS) amongst others can be a very useful tool.

If such analysis is summarized in a safety zone chart, this would be an operability chart, that might be useful not only for design details of the shape and dimensions of the MP, but also for usage during operation, as when in severe sea state. In critical situations, quick decision making becomes mandatory, and such tool would be helpful as an information source on which one can rely to decide about interruption of the procedure in course.

This research work presents the development of an optimization tool for shape, dimensions and location of prismatic moon pools centred around midship, given an input hull and chosen sea states. The search for the optimum solution focuses in operation condition (no advance speed), and is carried out through evolutionary strategy applied to a set of parameters that define the shape and dimensions of the MP in any section parallel to the waterline. The analysis can be done either in frequency or in time domain, and the resultant output is a visualization file for checking the mesh of the ship with the resultant moon pool coupled in the proposed hull, and a radar chart.

1.1 Motivation

Predicting the performance of a ship either in still water or rough sea is one of the main concerns of the naval architect. Combined to it, optimizing the shape of the hull from the hydrodynamic approach is a very important aspect since the early design stage.

As stated by the classification society Det Norske Veritas in DNV (2011)¹, marine operations consist of two phases: design and planning, and execution of the operations. The design and planning phase shall select seasons when the marine operations can be carried out and provide weather criteria for starting and interrupting the operations (the availability analysis). In this sense, it is important to conceive the ship design with the point of view of operability.

Due to its high complexity, it is still not usual to properly model the moon pool considering detailed phenomena originated in its internal water oscillation. One can,

¹ Former DNV, became DNV GL in 2013, after merging of Det Norske Veritas (Norway) and Germanischer Lloyd (Germany).

for example, refer to that practice recommended by that classification society, which describes a simplified wave condition of the water inside the MP internal water. Either for simplified or comprehensive analysis of moon pool-related operations, it assumes that the water plug inside it (internal water of the moon pool) is modelled as a fluid body moving only in vertical direction. Specially for simplified analysis, it also presumes that the moon pool dimensions are small compared to the breadth of the ship, what restrains the availability of the calculation method for moon pools with main dimensions at the same order as of the beam of the ship, for example.

In addition, still according to DNV (2011), the use of Computational Fluid Dynamics (CFD) may not be recommended for MP dynamics. Even though CFD can analyse the fluid dynamic interaction between the object inside² and the water plug inside the MP, it is difficult to couple with the dynamic characteristics of the ship in waves and the response of the installed system. In this case force predictions may hence be uncertain.

The resistance curve prediction in an early design phase, according to van't Veer and Tholen (2008), relies mostly on scaled model tests in combination with experiences based on previous designs. Unfortunately, an accurate estimate of the added resistance contribution from the moon pool remains difficult, whilst its magnitude can be significant. The variation in hull and moon pool designs is large and the available test data is often too limited for an accurate trend prediction.

Hence, it will be useful to have means to assess the performance of a MP in a more comprehensive and detailed manner, comprising flexible sizes and shapes, and allowing access to more precise information that can be reliable for decision making upon operation.

1.2 Objectives

General objectives

To develop tools for application in design stage, based on performance simulation and evaluation of operability of a drill ship operating in wave condition, without advance speed. This is intended to be carried out using system response calculation in time and frequency domain and an evolutionary algorithm for optimal solution searching. The solution should also be useful for ships as a chart of operation safe zones for a given sea state, and for quick decision making upon interruption of procedures during operation.

² Referred to as lifted object and lifting system in the original, but which can be understood as the drilling equipment for our case of a drill ship.

Specific objective

Hand over a tool to be used in design stage. The tool will have an operability evaluation approach to optimize the shape and dimensions of a prismatic moon pool for a fixed hull shape. It should be possible for the user to set the size restrictions, types of wave spectrum and analysis and sea states to be considered. In addition, an operability zone chart for those conditions should be provided.

The methodology through which the developments will lead to the achievement of the above described objectives is presented in the next section.

1.3 Structure of the thesis

This thesis is composed of this first chapter, introduction, in which were introduced the concept of moon pool, its utility, benefits and drawbacks, and problems due to its existence. It highlights also the importance of resonant responses to wave excitations and the idea to mitigate it in design stages, obtaining also a tool for quick decision making upon interruption during operation procedures. Inside the same section there are the motivation which explains the importance of having a detailed analysis of the moon pool and the objectives.

The following chapter contains information from the literature survey carried out in several approaches: the Drill ship characterization explains in more details particular aspects of such kind of ship and how the oscillation happens inside its moon pool. Two approaches of descriptions of previous researches by several authors are then presented: a literature survey with an overview of works about resonant oscillation and about evolutionary algorithm, and a detailed review of works that served as basis for the development of the present work.

Theoretical concepts needed to develop this research are presented in details inside the Theoretical Foundation chapter, describing the wave response of a ship in waves, and the mathematical model based on linear theory, with the boundary value problems for the conditions with and without moon pool, including calculation of vertical bending moment and wave drift force.

The subsequent chapter, of Methodology, contains the derivation of the assessment formulae of operability to each criterion, allowing performance and fitness grading for optimization. Some comments about the crew safety criterion (that is not implemented in this work) are also made in that section.

Parameters used in the calculation of response and the refinement of the mesh were adjusted before numerical simulation. The calibration is presented in the next chapter, prior to the validation chapter. Since it was not possible to run experiments for

the present research, the validation of the hydrodynamic response calculation model is presented using numerical and empirical results from other target publications.

In the chapter of Results and Discussions, results of investigations of trends in aspect ratio and shapes are presented, as well as the shape and dimensions of the optimal moon pool considering the proposed operability criteria. The Conclusions is then presented in a chapter followed by the list of ongoing and proposals of future works. The last chapter is presented to address the contribution of this work to scientific research community.

After a references list, appendices is also attached to enrich the descriptions of the material presented in this thesis.

2 Literature

This thesis presents the study of a way to mitigate the resonant motion of the water oscillation inside a moon pool by means of an evolutionary algorithm for optimizing its shape and dimensions. Hence, the literature survey has two paths: the first, about the resonant oscillation, and the second about the usage of evolutionary algorithms in naval architecture.

2.1 Drill ship characterization

The research and development in the offshore oil and gas industry have increased in order to attend the demand for energy sources. A good description of drill ships characterization is given by Vijith, Viswanathan and Panneerselvam (2014), as follows. In the early stages, the marine operations and researches were confined to shallow and intermediate water depths (less than 600m). At later stages, the oil and gas industries have developed new concepts applicable for deep water and ultra deep water. Structures of the offshore industry can be classified into three broad categories: fixed, compliant and floating structures, respectively for shallow, intermediate and deep waters. Examples of fixed structures are Jacket structures, Gravity structures etc., example of compliant structures are TLP, guyed towers, articulated towers, etc., while floating structures include TLPs, Spars, FPSOs, FDPSOs, Semi-submersibles, etc.

All marine operations in deep water fields are performed with highly specialized vessels with advanced equipment and features, and moon pools are one of the dominant features of certain vessels.

Among the offshore vessels, some classifications can also be done, as follows:

- IMR: Inspection, maintenance and repair
- DSV: Diving support vessel
- LWI: Light well intervention
- OCLV, CLV: Offshore cable laying vessel
- PLSV: Pipe laying support vessel
- OCSV, CSV: Offshore construction support vessel
- AHTS: Anchor handling tug supply vessel

The drill ship is a kind of CSV. More detailed descriptions of the drill ship and its particular characteristics are presented as follows.

There are two solutions for offshore drilling operations: the floating drilling platforms (drill rigs) and drill ships. Drill rigs are more stable for seakeeping, while the drill ships are more convenient for transit between two drilling positions. The choice of using one or the other is based on the depth of operation region and the distance between the locations where the drilling will take place. For locations that are close to each other, it may be more convenient to opt for drill rigs, while drill ships will perform better for drilling in sparse locations.

A drill ship is a vessel used for drilling of the seabed, usually for oil and gas exploration. It is equipped with a drill held on vertical position by a tower on the top of its deck. The drill reaches the seabed through an opening that usually is located at midship, and transversally centred. (See Figure 1).

Figure 1: Example of drill ship: Huisdrill 12000.



Source: www.huismanequipment.com (access in sep. 9th, 2016)

According to Day, Lee and Kuo (1989), the drilling equipment is located at midship for two reasons:

- Structurally, near the centre of the hull, the required forces to tension risers or other lines that connect the ship to the seabed can be better withstood
- In terms of seakeeping, the effects of angular motions of the ship – particularly roll and pitch – are minimized.

Depending on the application of the floating system, the dimensions of the moon pool will be smaller or larger to allow respectively access of people or equipment to the sea. Some examples of dimension order of the vessels and their corresponding moon pools are shown below in Tables 3 and 4. The first, extracted from van't Veer

Table 1: Dimensions of drill ships

Design	Year	Ship Dimensions		Moonpool dimensions	
GustoMSC designs:		LOA(m)	B (m)	L (m)	B (m)
Pelican Class	1972	147.70	27.00	7.20	8.20
Pride Africa / Angola	1999	204.52	29.87	12.01	10.00
GSF C.R.Luigs / J. Ryan	2000	231.34	35.97	12.80	12.80
Gusto WIV	2004	127.40	24.00	9.60	9.00
PRD12k - Oribis	2007	156.00	29.90	16.90	10.40
PRD12k - Bully	2007	166.50	32.00	19.60	12.60
Not designed by GustoMSC					
Deepwater Expedition	1989	171.00	28.40	8.53	8.00
Deepwater Frontier	1999	221.28	42.06	14.63	14.63
Deepwater Pathfinder	1999	221.28	42.06	25.60	12.40
Discovery Enterprise	1999	254.51	38.10	24.38	9.41
Deepwater Discovery	2000	227.38	42.06	18.37	12.47
Saipem 10000	2000	227.00	42.00	25.60	10.26
Belford Dolphin	2000	204.80	39.90	24.38	10.06
Chikyu	2005	210.00	38.00	22.00	12.00

Source: van't Veer and Tholen (2008)

and Tholen (2008) are of drill ships, and the latter, extracted from Nesjø (2015) are of Anchor Handling Tug Supply Vessels (AHTS) and Construction Supply Vessels (CSV).

2.1.1 Water oscillation mechanism inside a moon pool

Although the usage of moon pools bring advantages, the oscillation inside it should be understood to allow mitigation when it is a drawback or for maximizing the profits when it is advantageous. The excitation of the water column has basically two origins:

- Vertical acceleration due to the ship motion
- Pressure fluctuation at the bottom of the MP, due to encounter waves (when in forward speed), wave reflection and hydrodynamic reactions to the motions of the system. The oscillation of the water column itself also causes a hydrodynamic reaction to this motion.

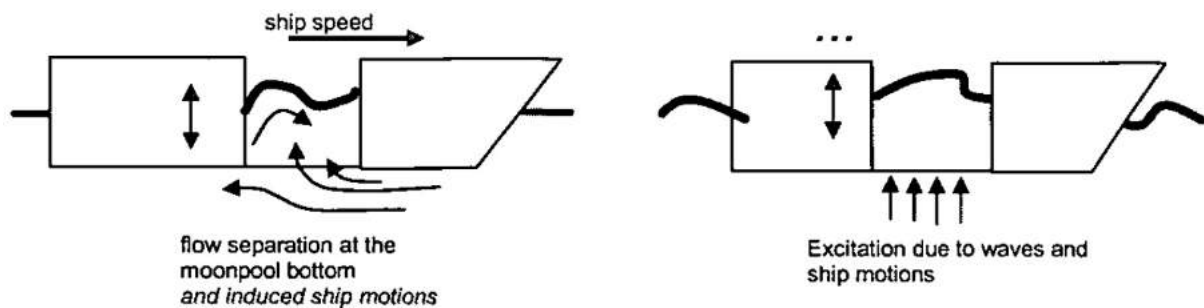
Usually, the study of such phenomenon is based on a ship with advance speed in calm waters, and ship without advance speed subjected to waves. There are also the combinations of both, as ship in seaway with waves and ship in operation with waves and current, but they are not so easily modelled. The first two basic conditions are the commonly studied ones, like in the illustration showed in Figure 2.

Table 2: Dimensions of AHTS and CSV ships

Vessel Data				Moonpool Geometry		
Vessel Name	LOA	B	D	L	B	S
-	m	m	m	m	m	m^2
Anchor Handling Tug Supply Vessels (AHTS)						
Skandi Vega	109.5	24.0	7.8	7.2	7.2	51.84
Construction Support Vessels						
Skandi Acergy	156.9	27.0	8.5	7.2	7.2	51.84
Skandi Aker	156.9	27.0	8.5	7.2	7.2	51.84
Skandi Artic	156.9	27.0	8.5	7.25	7.25	52.56
Skandi Constructor	120.2	25.0	8.0	8.0	8.0	64.00
Geosea	84.8	15.0	5.0	5.5	6.0	33.00
Geosund	98.5	18.8	5.9	7.1	6.0	42.60
Skandi Hercules	109.5	24.0	7.8	7.2	7.2	51.84
Skandi Neptune	104.2	24.0	6.3	7.2	7.2	51.84
Skandi Niteroi	142.2	27.0	8.5	7.2	7.2	51.84
Ocean Protector	105.9	21.0	6.6	7.2	7.2	51.84
Skandi Salvador	105.9	21.0	6.6	7.2	7.2	51.84
Skandi Seven	120.7	23.0	7.0	7.2	7.2	51.84
Skandi Skansen	107.2	24.0	7.8	7.2	7.2	51.84
Skandi Skolten	109.5	24.0	7.8	7.2	7.2	51.84
Skandi Vitoria	142.2	27.0	8.5	7.2	7.2	51.84
Newbuilding(CSV)						
EP9	139.9	28.0	8.5	7.2	7.2	51.84
EP10	139.9	28.0	8.5	7.2	7.2	51.84
NB800	160.9	32.0	9.25	9.4	7.2	67.68
NB823	146.0	30.0	8.5	9.1	7.2	65.52
NB824	146.0	30.0	8.5	9.1	7.2	65.52

Source: van't Veer and Tholen (2008)

Figure 2: Motion conditions of the internal water of a moon pool.



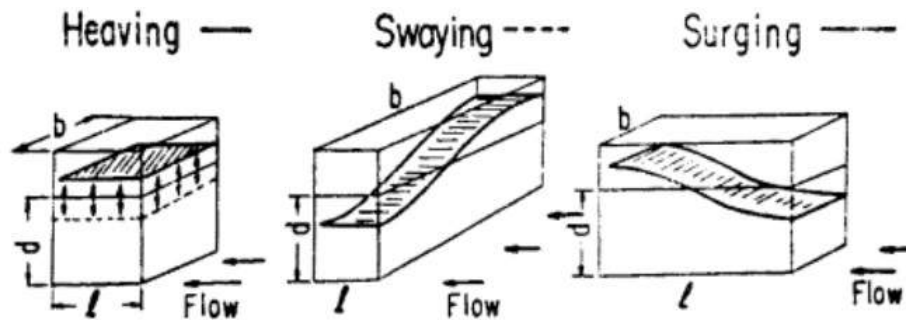
Source: Gaillardie and Cotteleer (2004)

contribution of the vortex in the oscillatory motion of the water free surface. Top view: stagnation region of water at fore portion in a moon pool

Fukuda (1977) described the oscillation mechanisms of the moon pool water

plug of a ship in transit: heaving, swaying and surging, respectively: vertical, transversal (parallel to the beacons) and longitudinal (parallel to the keel). Those motions also apply for the stationary condition (no forward speed, subjected to waves). The terms “piston” for the heave mode and “sloshing” for the other two modes are also used nowadays. The figure 3 illustrates those motions.

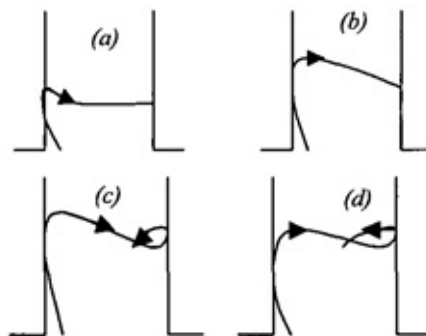
Figure 3: Modes of water oscillation inside the moon pool: heaving or piston for vertical, swaying or transversal sloshing for transversal and surging or sloshing for longitudinal mode.



Source: Fukuda (1977)

A composed motion (piston with sloshing modes together) in 2D is illustrated in the following Figure 4. Initially, the internal water level is low, when an elevation starts at back (a). This elevation is intensified together with the average waterline height (b), until the steepness becomes too high and the volume goes forward until it meets the opposite wall and reflects (c). The point where the forward and backward flows meet moves backwards to where the region that initially elevated now starts to get lower. At the same time, the water level starts lowering again, and the previously mentioned point vanishes when meeting the new generated wave, as in (a).

Figure 4: Composed motion of the water inside a 2D moon pool: simultaneous piston and sloshing. Vessel's speed to the right.

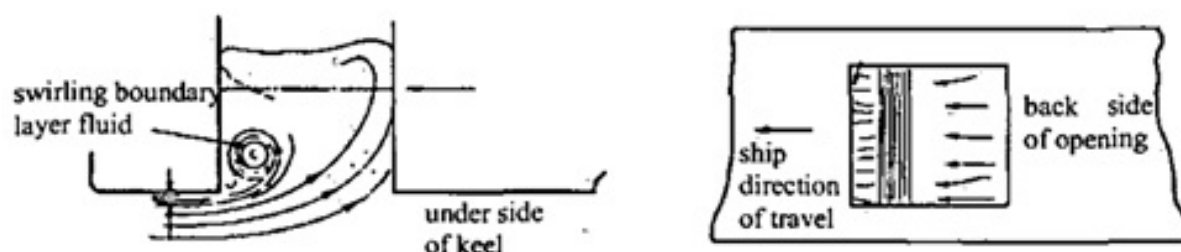


Source: Gaillardie and Cotteleer (2004)

The subsequent Figure 5 shows in a side view a transit situation, where the contribution of the vortex in that surface water motion is illustrated, and in the top view,

the stagnant water in the fore portion of the moon pool. In this case, the ship is assumed to have a forward speed from right to left.

Figure 5: Side view: contribution of the vortex in the oscillatory motion of the water free surface. Top view: stagnation region of water at fore portion in a moon pool.



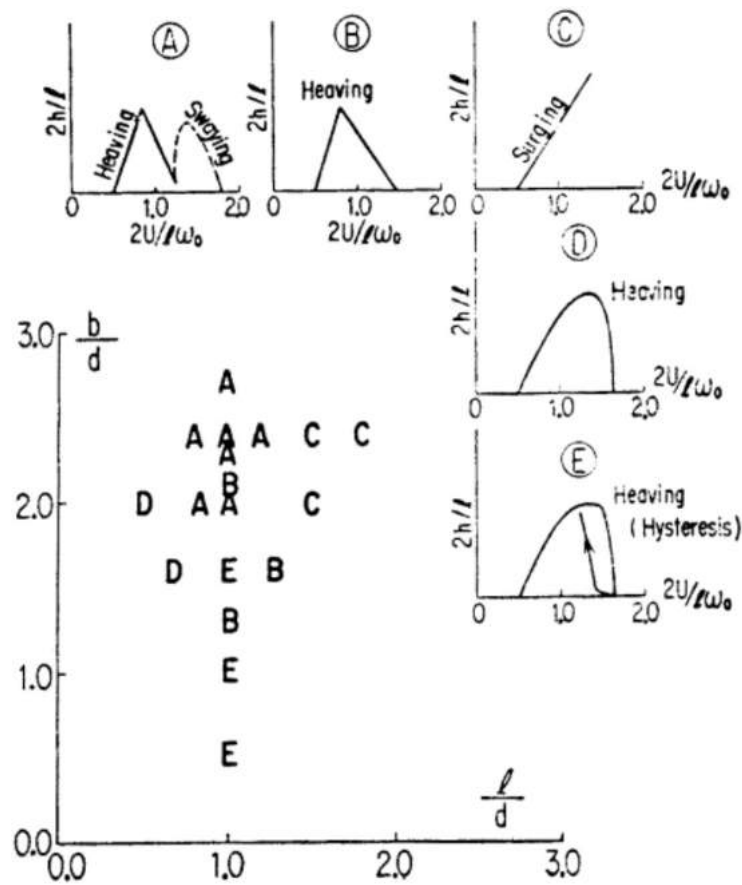
Source: English (1976)

A very simple way to understand how these two modes are dependent on the geometry of the moon pool in the ship with advance speed can be found when checking the illustration published by Fukuda (1977). The Figure 6 presents on the bottom of the left hand side the kinds of behaviour, from *A* to *E* speed functions, that can be observed according to each geometrical configuration, ranging the parameters l/d and b/d respectively, for length to draft ratio and breadth to draft ratio. In the behaviour diagrams surrounding it on the top and right side, h represents the oscillation amplitude, so that the vertical axis represents the proportion of oscillation height to draft of the MP. In a common square shaped moon pool with $b/d < 1$, for example, the expected oscillation behaviour would be like the described in *E*. Longer moon pools have dominant sloshing.

Aalbers (1984) explains also that, excitations in frequencies with modulus equivalent to half the natural frequency are also possible due to non-linearities. Sometimes, this leads to apparently resonant behaviours in frequencies different from the sea wave. In this way, for example, if a ship is cruising in waves, the encounter frequency can be increased until the natural frequency of the MP is reached, resulting in resonant excitation. On the other hand, the interaction between the ship motion in transit and the MP can suppress the excitation by the wave pressure. Then, the observed relative motion generally does not reach exceptionally high amplitudes. The figure 7 illustrates a typical curve with two peaks of amplitude response in oscillation of the free surface inside the MP.

According to van't Veer and Tholen (2008), recent measurements show that both types of oscillation can increase ship resistance to the same magnitude. The sloshing mode dominates in longer moon pools, while piston mode oscillations are dominant in shorter moon pools, what agrees with the statement by Fukuda (1977). With increasing

Figure 6: Oscillation modes and amplitude behaviours at ranges of reduced speeds, for different dimension ratios of rectangular moon pools.



Source: Fukuda (1977)

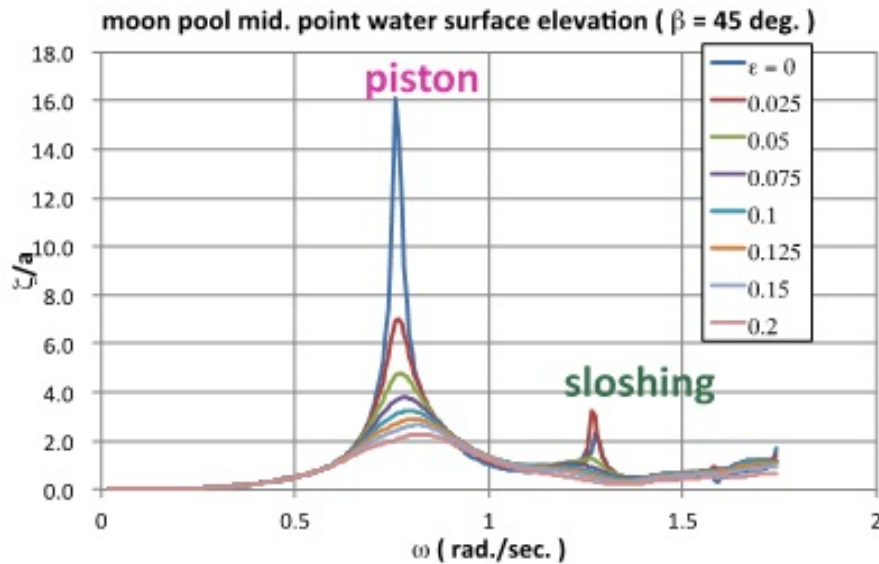
MP length over width, the sloshing oscillations were found to dominate above the piston mode, despite the fact that the piston mode always has a lower natural frequency.

A ship reacts to different regular frequencies with different amplifications or reductions of the excitation amplitudes. The collection of the reaction modulus to an unit excitation amplitude is called Response Amplitude Operator (RAO), which can be calculated in the frequency domain. More details and examples can be found in the section 6, of the validation results.

The characteristic curve of RAO presents the two resonance peaks, one for piston and other for sloshing. Usually the curve lowers to zero at high frequencies and approaches to a fixed non-zero value at low frequencies.

In the words of DNV (2011), a floating, moored structure may respond to wind, waves and current with motions on three different time scales, — high frequency (HF) motions — wave frequency (WF) motions — low frequency (LF) motions. The largest wave loads on offshore structures take place at the same frequencies as the waves, causing wave frequency (WF) motions of the structure. To avoid large resonant effects,

Figure 7: Numerically simulated moon pool water surface elevation at midpoint (encounter angle $\beta = 45^\circ$) in Series 60 hull. The graph presents several curves, simulating different damping coefficients. Neglecting the overdamped examples, most of them present two peaks of amplitude: lower frequencies are usually for piston mode and higher frequencies, sloshing.



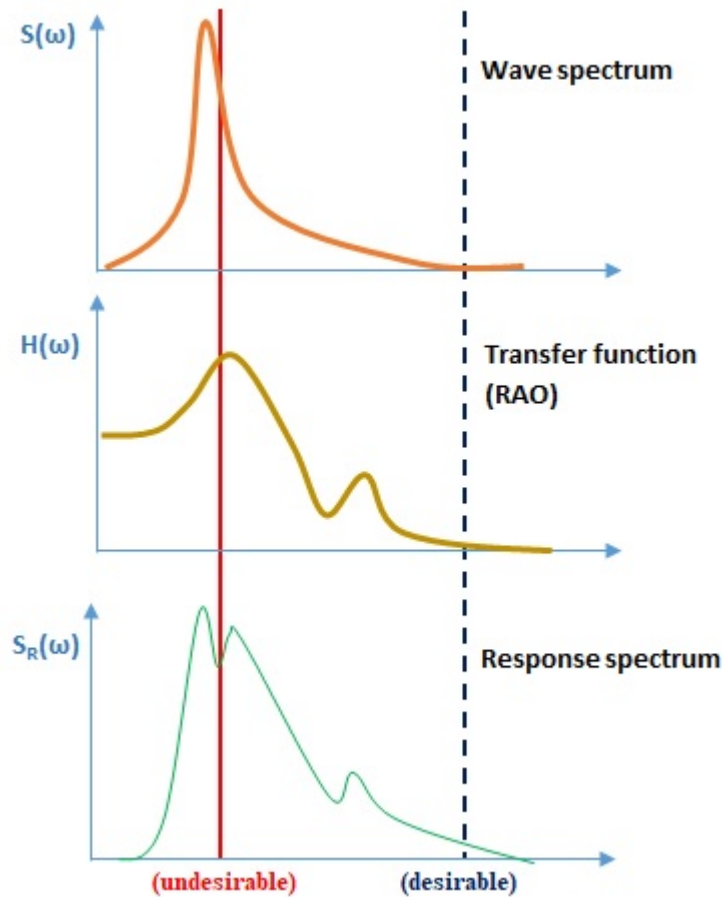
Source: adapted from Michima and Kawabe (2014b)

offshore structures and their mooring systems are often designed in such a way that the resonant frequencies are shifted well outside the wave frequency range. Figure 8 illustrates this relation between the wave energy peak and the moon pool RAO peaks.

It is important to highlight that the transfer function between the incident wave and the moon pool free surface oscillation cannot be decoupled from response of the external hull to wave. Despite formerly (until around the year of 2000, as already presented in section 2.2 (of the literature survey) it was assumed that there was no mutual influence between the hull and the water oscillation inside the MP. Nowadays it is known that there is this mutuality. This is illustrated in the scheme of the elements of transfer function between incident wave and water column oscillation of Figure 9.

According to Day (1990), there are basically two strategies that can be adopted by the designer to approach the problem of avoiding matching peaks. Either the moon pool can be modified to reduce the magnitude of the response peak, or shift the frequency peak to a frequency range far from the dominant wave energy of the operation area. In terms of analogy of a mechanic oscillator, the first approach requires an increase of the damping of the system, while the second requires the mass changes. In practice, the increase of damping will imply in decrease of the peak frequency and the mass change will also influence in damping, but the distinction between them regarding the above cited strategies does exist. For the piston mode, empirical tests presented by Nesjø

Figure 8: Relation between the wave energy peak and the moon pool RAO peaks. According to DNV (2011), offshore structures and their mooring systems are often designed in such a way that the resonant frequencies are shifted well outside the wave frequency range.



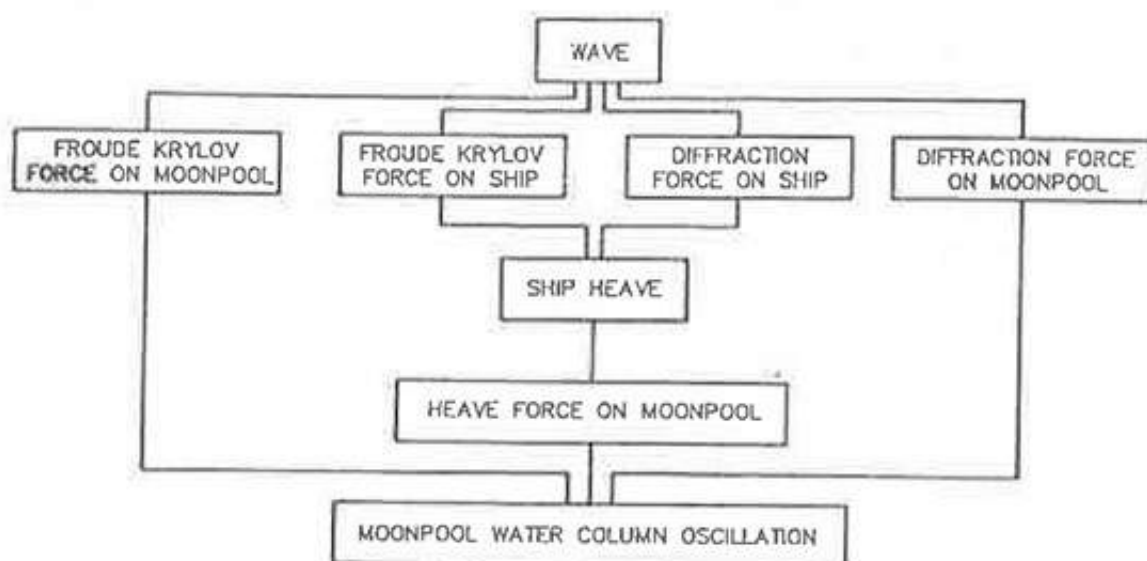
Source: Author

(2015) show that the natural periods increase as the draft becomes larger, as would be expected due to the increase of mass if we analyse from the viewpoint of a rigid mechanic oscillator.

2.2 Literature survey

This thesis presents the study of a way to mitigate the resonant motion of the water oscillation inside a moon pool by using means of an evolutionary algorithm for optimization of its shape and dimension. Thus, the literature survey was carried out in two paths: the first, about the resonant oscillation mitigation, and the second about the usage of evolutionary algorithms in naval architecture. The following contents will then start with the first path, that is the most important subject of this study, and then present some literature survey related to the second path.

Figure 9: Elements of transfer function between incident wave and water column oscillation.



Source: Day, Lee and Kuo (1989)

2.2.1 Path 1: Resonant oscillation

Investigations of the motions of the water inside the moon pool, here also referred to as water plug, and a possible connection between those oscillations and the resistance of the hull, were published by English (1976). In his work, towing tests of a model of unknown size with a square moon pool were done to observe the water motions in forward speed and find out how to reduce them by changing its geometry.

The mechanisms of oscillation of the water plug, were described by Fukuda (1977), where the names Heaving, Swaying and Surging, respectively, vertical, transversal and longitudinal motions are used as first description of the flow. The 2D composed motion was described. More details are presented in the section 2.1.1, of the internal water oscillation mechanism. Nowadays, the motion modes are also called “piston” for the vertical oscillation, and “sloshing” for the transversal and longitudinal motions.

Bales (1987) highlighted that knowledge of the prevailing wave environment is important, not only based on the wave height information, but on wave length and wave directions as well. Besides establishing practical applications that count on directional wave spectra, she identified some sensitivity of ship hull shapes to the wave spectrum, showing the importance of those parameters.

Some models of the water motion inside the MP were also proposed. Aalbers (1984) compares that motion to a mass-spring system, in which dynamic amplifications occur at a given frequency. The so-called natural frequency depends on the draft of the

hull – or better, of the water column height – and generally it is located above the sea waves frequency range. The variations of the water level, when measured in comparison to the ship, are called “relative motion of the water in the moon pool”.

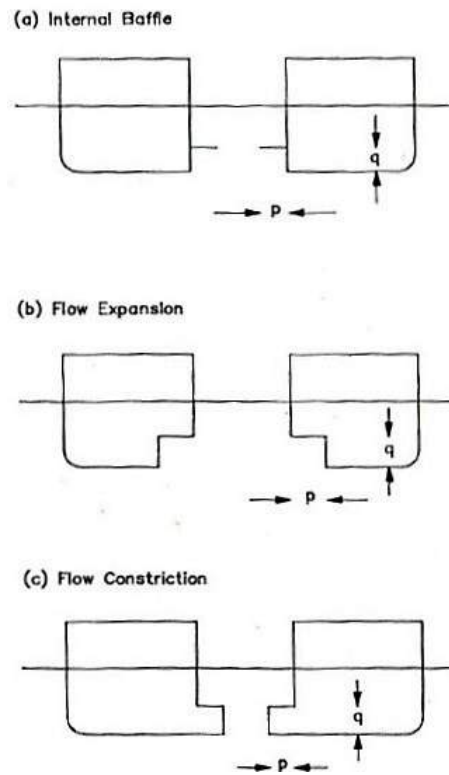
A method for assessing the performance of a MP with an operability approach was proposed by Day, Lee and Kuo (1989). In that work, the authors propose techniques to predict the water column oscillation and the forces on a unit in the moon pool for a given sea state. The experimental validation was done with all modes of motion restricted. In their words, “the methods proposed are only intended to allow individual designs to be studied and are not sufficient to allow the optimization of moon pool design. In order for this process to be carried out, a method of assessment of the performance of moonpools is required and some fundamental knowledge about the way in which different moonpool geometries affect the moonpool performance.” It indicates therefore the need for a more precise analysis of the MP performance for optimization, related to the geometry variation.

In the work that gives continuity to the mentioned above, Day (1990) indicates some geometries that can be used for improving the performance of a moon pool. A description of the ideal way how the prediction of performance should be carried out is detailed in the section 4.2, about the drill ship operability assess formulae. The variation of the water behaviour inside MP related to geometry changes in 2D was considered in 3 cases: a restriction added to the section parallel to the waterline, widening the section at the bottom of the opening, and narrowing the section at the bottom of the opening. The configurations are shown in figure 10.

In the 2D simulation with ideal flow, there are shifts of the range of wavenumber where the oscillation amplitude peaks happen. Those shifts caused by geometry changes are, in general, very small compared to the results of the original geometry when the moon pool is prismatic, with no recess. There is more influence in shift when widening and narrowing the bottom section. The author explains that the experimental trends indicate that for the 3D case with real fluid, those shifts would be much bigger. The simplistic justification is that the damping effect is the reduction both in magnitude and in frequency of the peak. Thus, the shifts in the wavenumber ranges in those peaks would be bigger than the values obtained in 2D for the MP with narrowed bottom section, and smaller than the values obtained in 2D for the one with wider bottom section. This leads to the conclusion that it is possible to change the position of the natural frequency of oscillation for higher or lower values by varying the shape of the MP.

That research development was done based on some assumptions about the procedures, such as minimizing transition effects between sea states, treating them as stationary processes, and assuming that the evaluation should be done by only observing effects involving the inoperability of the MP isolated. In this simplification, the

Figure 10: Configurations studied with 2D numerical model by Day (1990). In a) there is a slim restriction (internal baffle), b) an expansion of the bottom (flow expansion), and c) narrowing of the bottom (flow constriction).



Source: Day (1990)

author states that, given a sea state, there are no profits obtained by improving the moon pool's performance if the hull is already inoperable for other reasons not related to it. In addition, in preliminary design stages, the necessary information to calculate will not be available and the designer has no alternative than neglect the effect of hull performance and simply consider the downtime due to moon pool.

In other later work, however, it is noticed that the decoupling of responses of hull and MP can lead to presumption of non-existence of situations where the inoperability of the hull is reversed by the moon pool's influence with the oscillation of the water plug in opposite phase to the motion of the hull, as in the case of the cylindrical platform studied by Malta et al. (2006) and Torres (2007). In the latter work, a piston mode oscillation with the mass-spring-damper model was proposed, as a way to consolidate the usage of moon pools as motion reducing device for cylindrical platforms. After comparison between numerical and physical tests, it was concluded that the coupled motion of the platform and water plug will be reduced if the natural frequency of the plug (as if the hull was fixed) is smaller or equal to that of the platform (as if there was no moon pool).

The same conclusion that there is such mutual influence was presented by Vijith, Viswanathan and Panneerselvam (2014). In that work, two different configurations

(circular and rectangular shape) of the MP were selected to study their effects on the motions of a barge. The oscillation of water plug and its effects were also investigated, and the numerical results showed also that the sloshing mode was found to be dominant in the rectangular moon pool.

Gaillarde and Cotteleer (2004) say that there are two main ways to reduce the water oscillation inside a moon pool: reducing the excitation or reducing the motion with damping devices. For the first option, to reduce the importance of the excitations, some alternatives are presented, related to the ship with advance speed. As a second option to damp the already existent motions, besides devices that can be installed in the MP, draft variation is also proposed as a solution. The idea of this last proposal is that natural frequency of the water plug depends on its total mass, which in turn depends on the draft. When the ship is in operation, the excitation frequency depends on the wave frequency, thus for different wave frequencies, there are also different appropriate drafts to adopt.

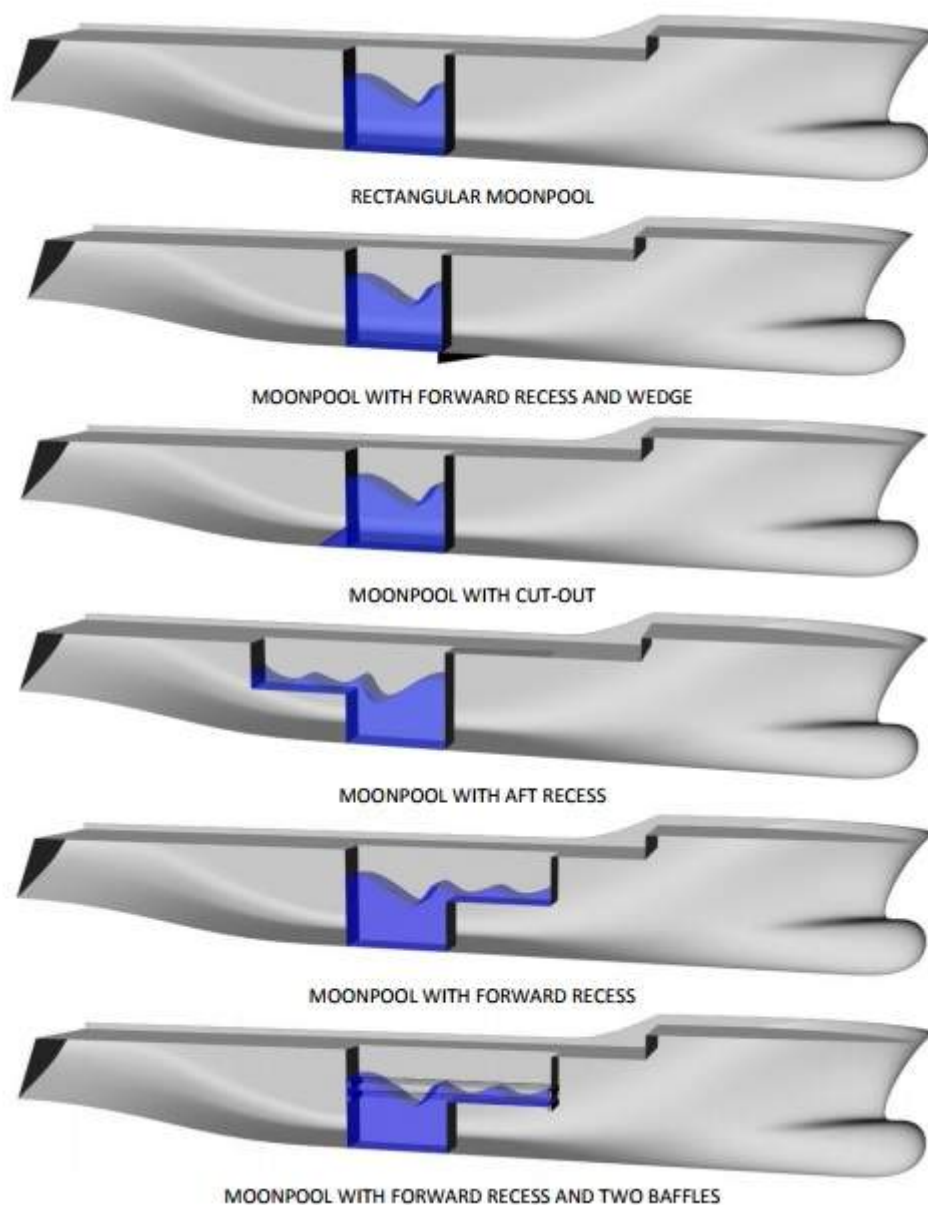
The authors also show some experimentally validated solutions for reducing the water plug oscillations caused by advance speed. Until then, the presented solutions were holistic and validated only experimentally. A numerical method is proposed to solve the transit problem in still water and stationary with waves, using the Volume Of Fluid (VOF) method, initially developed for the study of sloshing of liquid fuel in satellites. The VOF models suitability for solving MP problems was confirmed by numerical and experimental evaluation by Maisondieu et al. (2004).

Different strategies to model the water flow have been tried, besides the VOF approach. Somehow similar in terms of discretizing the space and deciding whether each unit is full or empty or water is the Smoothed Particle Hydrodynamics Method (SPH) by Gingold and Monaghan (1977), which considers the water as being a number of particles that interact as solids with walls and among themselves. In that method, pressures are statistically estimated by a kernel function, defined as a summation of the contributions of pressure of each neighbour particle. An adaptation made in the kernel function, that pre-calculates the pressure value for later correction inside a time step loop was made in the development of the Moving Particle Semi-Implicit Method (MPS), by Koshizuka and Oka (1996) and tested in (MICHIMA; KAWABE, 2014a). More recent studies have been merging potential theory with other methods that account for viscous effects, such as empirical results (MALTA et al., 2006) or the Finite Volume Method (FVM), also used in several CFD programs, as used by, for example, Fredriksen, Kristiansen and Faltinsen (2014).

Another investigation of the flow behaviour inside moon pools was carried out by Törnblom and Hammargren (2012), using an open source CFD program, called OpenFOAM. A 2D case was validated with empirical tests in small scale. In that work,

a general presentation of MP shapes and patented devices for free surface motion damping was carried out. The work addressed the case of transit in still water, testing different MP configurations (see figure 11). In general, the focus is towards to transit situations and most proposed solutions tend to restrict the bottom opening in order to reduce the resistance of the ship.

Figure 11: Different moon pool shapes.



Source: Törnblom and Hammargren (2012)

Although the case in discussion in this thesis accounts for the drill ship in operation, it is important to learn about how the phenomenon has been mitigated in transit, since it is not possible to decouple the solutions for transit from the ones for operation in the same ship. The restrictions in bottom section proposed in the above-

mentioned article are not interesting for drill ships from the operation point of view. Considering that it has as most important activity the operation without advance speed and subjected to waves, the present work prioritizes the operation ensuring, leaving the transit situation to a second plan.

Since the problems caused by the existence of a MP happen when resonance occurs, an important study is to find out the exciting frequencies at which it appears. About the investigation of the natural frequencies of oscillation, formulations have been developed and revisited by several authors, for both sloshing and piston modes of oscillation. For sloshing, Molin (2000) and Molin (2001) have proposed for a rectangular moon pool:

$$\omega_{n0} \simeq \sqrt{g \frac{n\pi}{l} \frac{1 + J_{n0} \tanh\left(\frac{n\pi}{l}d\right)}{J_{n0} + \tanh\left(\frac{n\pi}{l}d\right)}} \quad (2.1)$$

which had a more updated version proposed by Faltinsen and Timokha (2009):

$$\omega_n = \sqrt{g \frac{n\pi}{l} \tanh\left(\frac{n\pi}{l}d\right)} \quad (2.2)$$

where n is the mode of oscillation, g is the gravity acceleration, l and d are respectively the length and draft of the moon pool. In equation 2.2, $J_{n0} < 1$, is the integral over the length and beam dimensions of the moon pool. A comprehensive overview of most developments of sloshing natural frequencies for different configurations of confinements is presented in Faltinsen and Timokha (2012).

The piston mode was also modelled with several approaches. The main idea is that the water column oscillates in contact with the fluid at the bottom of the moon pool, so an added mass should be accounted. Usually, this added mass is taken as an additional draft of the MP, and this is the point where each author makes a different model proposal. An interesting observation about the structure of the natural frequency formula can be found.

Tajima (1972) shows in his book some examples of oscillation starting from a simple U-tube (see figure 12) of which the natural frequency is

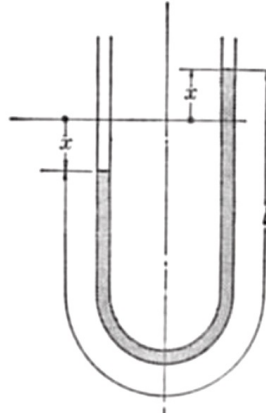
$$\omega_n = \sqrt{\frac{2g}{l}} \quad (2.3)$$

That has the following structure:

$$\text{frequency}^2 = \frac{\text{gravity}}{(L/2)} \quad (2.4)$$

where $L/2$ is the length of the tube filled with fluid, which ends up being:

Figure 12: Simple U-tube



Source: Tajima (1972)

$$k * \text{draft} + j * \text{breadth}$$

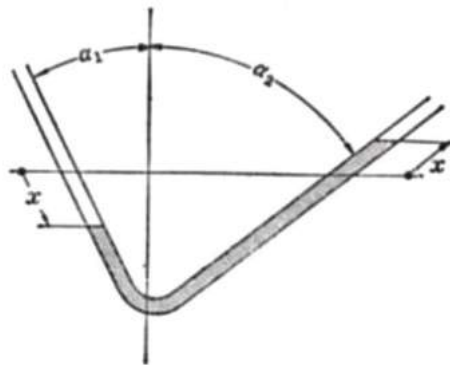
Here, k and j are constants and breadth is the distance between the ends of the tube. Thus it becomes

$$\text{frequency}^2 = \frac{\text{gravity}}{(k * \text{draft} + j * \text{breadth})} \quad (2.5)$$

Increasing the complexity of the examples, a derivation of the natural frequency of a manometer (figure 13) is obtained

$$\omega_n = \sqrt{\frac{g(\cos \alpha_1 + \cos \alpha_2)}{l}} \quad (2.6)$$

Figure 13: Manometer



Source: Tajima (1972)

which, similarly, has the following structure:

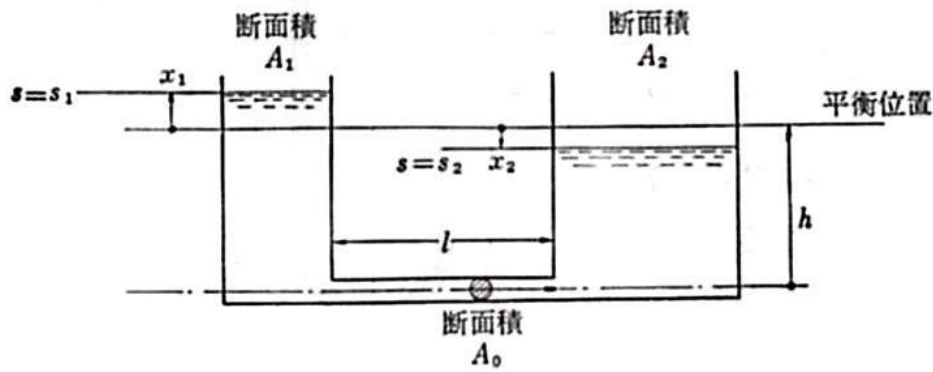
$$\text{frequency}^2 = \frac{\text{gravity}}{[L/(\cos \alpha_1 + \cos \alpha_2)]}$$

Once again, the shape is still the same, so it can be observed that the above equation has the same structure as equation 2.5.

Extending to an example that evolves towards to more expansion of dimension sizes, an example is presented of two tanks with different section areas, A_1 and A_2 connected by a duct of section area A_0 and a length L defining a breadth of the connected system (figure 14), to which the linearised natural frequency yields

$$\omega_n = \sqrt{\frac{(1 + (\frac{A_1}{A_2})g}{(1 + \frac{A_1}{A_2})h + \frac{A_1}{A_2}l}} \quad (2.7)$$

Figure 14: Two tanks connected by a duct



Source: Tajima (1972)

and this equation, if dividing all terms by $(1 + A_1/A_2)$, will again assume the same structure as in 2.5. If in the previous equation 2.7, $A_0 = A_1 = A_2$, the expression becomes exactly the first example of U-tube 2.4.

The author extrapolates that, if the area of one of the tanks, conveniently choosing A_2 , is very large (tends to infinity), the expression simplifies to

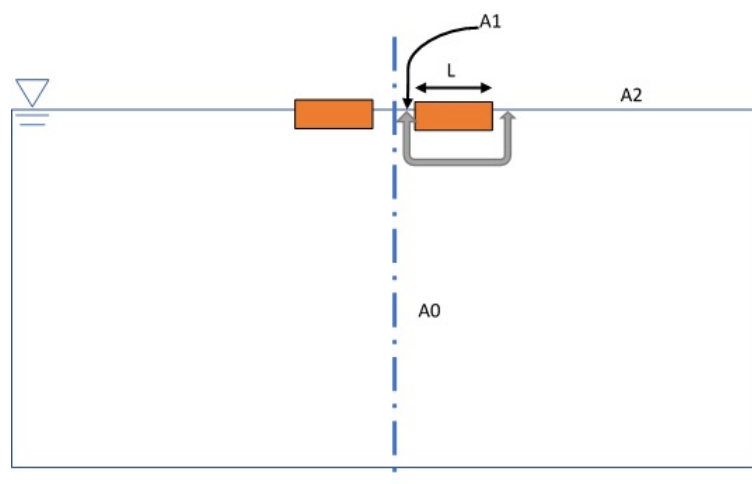
$$\omega_n = \sqrt{\frac{g}{h + \frac{A_1}{A_2}l}} \quad (2.8)$$

If in equation 2.8 the areas A_0 and A_1 are kept the same order, and tend to infinity, the natural frequency will become

$$\text{frequency}^2 = \text{gravity}/[\text{draft} + L]$$

and will represent the natural frequency in 2D of a moon pool of a vessel with no motion in deep water (figure 15).

Figure 15: Vessel with moon pool, with no motion, in deep water



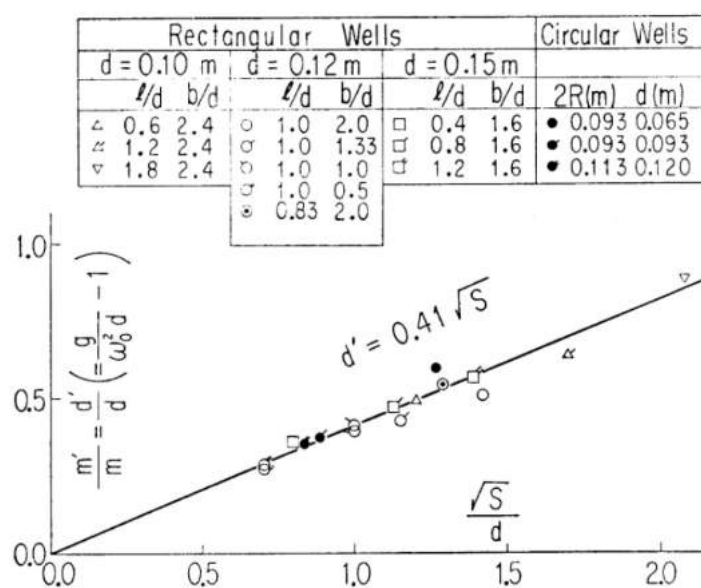
Source: Author

Such equation agrees with the model proposed by Fukuda (1977), who had published the following equation of natural frequency including the three dimensional effects of the moon pool

$$\omega_0 = \sqrt{\frac{g}{h + k\sqrt{A}}} \quad (2.9)$$

where A is the cross sectional area of the moon pool, h is the draft and $k = 0.41$, obtained empirically as shown in figure 16.

Figure 16: Added draft obtained experimentally.



Source: Fukuda (1977)

Once again, the same structure from 2.5 is kept even in 3D model, and is still used in some recent works, always validated, like in Vijith, Viswanathan and Panneerselvam (2014).

The above extrapolation from equation 2.8 is rather simplified, from a restricted depth situation to an infinite depth model.

Molin (1999) develops a procedure for the simplified 2D flow neglecting the far-field, in which a velocity potential composed of sources and sinks distribution. The obtained formula is

$$\omega_0 = \sqrt{\frac{g}{h} \frac{1}{1 + \frac{b}{\pi h} \left(\frac{3}{2} + \ln \frac{B}{2b} \right)}} \quad (2.10)$$

where g is the gravity acceleration, h is the average draft of the MP, b is its length, and B is the ship's length.

If L is very small, the right-hand side of the equation approaches the value 1, neglecting the added mass, and assumes the same shape as a pendulum solution, as shown in Faltinsen (1993), given by

$$\omega_0 = \sqrt{\frac{g}{h}} \quad (2.11)$$

The recommendations from DNV (2011) provide a flexible expression that includes the possibility for a cofferdam with an expansion of the cross-sectional area

$$\omega_0 = \sqrt{\frac{g}{\int_{-d}^0 \frac{S(0)}{S(z)} dz + \frac{S(0)}{S(-d)} k \sqrt{S(-d)}}} \quad (2.12)$$

Where S is the sectional area, d is the draft and $0.45 \leq k \leq 0.47$ for rectangular moon pools with aspect ratio between 0.4 and 1.0. If the moon pool is circular, the recommended parameter value is $k = 0.48$. As can be seen, there were several authors who proposed different models or parameter values for calculating the natural frequency, among which some were highlighted above. Currently the more updated one is the last presented, by DNV (2011).

It is known, however, that the linear theory over-predicts the fluid response in these types of systems due to lack of damping, since the only dissipation of energy happens through radiated waves, what was already explained earlier by Aalbers (1984) and reported also in Faltinsen, Rognebakke and Timokha (2007). The former explained that linear damping is dominant in small relative amplitudes, while the quadratic damping is dominant at high relative amplitudes. In those cases, the potential damping has a magnitude that is too small in comparison to friction and viscous pressure. Nonetheless,

the friction damping dissipates energy inside the boundary layer, but its magnitude in turn would be negligible in comparison to the vortex shedding damping.

The corner joint between the bottom of the hull and the moon pool is usually sharp and the in- and out- oscillating flow generates turbulence that results in a quadratic damping. Knott and Flower (1980) showed that for vessels with forward speed, the existence or not of vortices would depend on how rounded those joints are. They proposed thus to increase the vortex generation by varying the shape (position and sharpness) of that angle, or adding appendages for this purpose.

Kristiansen and Faltinsen (2008) have made an investigation about the influence of the viscous effects, that may act as a damping and non-linear effects associated with the free surface conditions. The authors explain that they may cause transfer of energy between the different modes. In the cases studied, they found that the effect on the piston mode associated with the non-linear free surface conditions are of minor importance, and also the effect of the in- and out-flow of the boundary layer is negligible to all practical purposes, whereas the flow separation explains the major part of the discrepancy between the measured response and that estimated by linear theory. The same was observed by Heo et al. (2014), with a comparison of numerical simulations of flow around a 2D rectangular body with a moon pool. The simulations were done with potential boundary element method solver (BEM) and finite volume method (FVM) based on Navier-Stokes equation. The vortex shedding was found to account for the most of the damping, and showed a better agreement of the viscous flow compared to the potential flow simulation.

Recently, not only for mitigation purposes is the moon pool resonance phenomenon being researched, but also amplification for energy generation, either by using the water pressure fluctuation or the air above the free surface inside the MP, enclosed in a chamber, as can be seen in Bull (2015).

2.2.2 Path 2: Evolutionary algorithm

The optimization of hull shapes has been tested by several researchers, with different techniques. They vary in number of objective functions (one, two or three), programming types (linear or non-linear) and algorithms.

Among others, the evolutionary algorithms and neural networks offer effective methods to conduct the optimization and data analysis. The evolutionary algorithm techniques are generic population-based and use mechanisms inspired by biological evolution, such as reproduction, mutation, recombination, and selection. Some sets of solutions to the optimization problem are taken as individuals of a population to be tested and classified according to a fitness function, which indicates how good or how

fit each solution is. The individuals with best performance are then selected to perform a breeding and other procedures that will create the next generation of that population according to the technique in usage. According to Eiben, Smith et al. (2003), the popular evolutionary algorithm variants are:

- Genetic algorithm;
- Evolution strategy;
- Evolutionary programming;
- Genetic programming;
- Learning classifier system;
- Differential evolution;
- Particle Swarm Optimization;
- Estimation of Distribution Algorithms.

Of those, the most used ones for changing the hull geometry are the genetic algorithm and evolutionary strategies.

The authors say that the genetic algorithm is the most widely known type, conceived by John Henry Holland as a means of studying adaptive behaviour, and together with Kenneth A. De Jong's thesis defined what has come to be the classical genetic algorithm and largely been considered as function optimization method. It is summarized in Table 3.

Table 3: Genetic algorithm characteristics table

Representation	Bit-Strings
Recombination	1-Point crossover
Mutation	Bit flip
Parent Selection	Fitness proportional - implemented by Roulette Wheel
Survival Selection	Generational

Source: Eiben, Smith et al. (2003)

Genetic algorithms traditionally have fixed workflow: given a population of π individuals, parent selection fills an intermediary population of π , allowing duplicates. Then the intermediary population is shuffled to create random pairs and crossover is applied to each consecutive pair with probability p_c and the children replace the parents immediately. The new intermediary population undergoes mutation individual by individual, where each of the l bits in an individual is modified by mutation with independent probability p_m . The resulting intermediary population forms the next generation replacing the previous one entirely. Note that in this new generation there might be pieces, perhaps complete individuals, from the previous one that survived crossover

Table 4: Evolutionary strategy characteristics table

Representation	Real-valued vectors
Recombination	Discrete or intermediary
Mutation	Gaussian perturbation
Parent Selection	Uniform random
Survival Selection	Deterministic elitist replacement by (μ, λ) or $(\mu + \lambda)$
Speciality	Self-adaptation of mutation step sizes

Source: Eiben, Smith et al. (2003)

and mutation without being modified, but the likelihood of this is rather low (depending on the parameters π, p_c, p_m).

In the early years of the field there was significant attention paid to trying to establish suitable values for GA parameters such as the population size, crossover and mutation probabilities. Recently the problem of how to choose a suitable fixed mutation rate has largely been solved by adopting the idea of self-adaptation, where the rates are encoded as extra genes in an individual's representation and allowed to evolve.

Evolution strategies were invented in the early 1960s by Ingo Rechenberg and Schwefel, and in the earliest proposal, there were simple two-membered algorithms denoted (1+1) (pronounce: one plus one) evolution strategies, working in a vector space. In the 1970s the concept of multi-membered evolution strategies was introduced, with the naming convention based on π individuals in the population and λ offspring generated in one cycle. The resulting $(\mu + \lambda)$ and (μ, λ) strategy gave rise to the possibility of more sophisticated forms of step-size control, and led to the development of a very useful feature in evolutionary computing: self-adaptation of strategy parameters. In general, self-adaptivity means that some parameters of the algorithm are varied during a run in a specific manner: the parameters are included in the chromosomes and coevolve with the solutions. A summary is shown in the Table 4.

A clear and detailed explanation about optimization problems and algorithms is presented by Bagheri and Ghassemi (2014), from where some of the following information was extracted. Day and Doctors (2001) studied the hull geometry optimization using genetic algorithm to minimize the resistance.

Among other researchers, Bales (1980) used optimization techniques for the performance in different speeds with head waves of a destroyer. Kükner and Sariöz (1995) optimized the seakeeping behaviour of a fast ship by generating different hull geometries, each one with different shape parameters from the original. Özüm, Şener and Yilmaz (2011) studied the characteristics of seakeeping of fast ships, varying systematically the main dimensions and hull shape parameters.

In most cases, the optimization procedures assume that the optimal hull is

obtained when the motions in vertical plane and the absolute vertical acceleration in regular head waves in pitch and heave are minimized. The same can be observed in the case of the drill hull. Due to its long length, the pitch motion has a strong influence on the vertical motion at the bow and a change in vertical motion far from the centre of gravity has a big impact, for example, in slamming of the bow or crew workability.

2.3 Detailed review

Some parts of the developed concepts have already been published in advance in bachelor thesis developed in collaboration to this research. the main concepts are revisited here and further details can be found in the originals, referenced along the text.

A study for a single example of hull with moon pool was presented in Michima and Kawabe (2014b) assessing operability parameters evaluated using threshold significant wave heights that would determine the limit at which the operability of the ship would not be assured any further. The hull was a Series 60 with a rectangular prismatic moon pool.

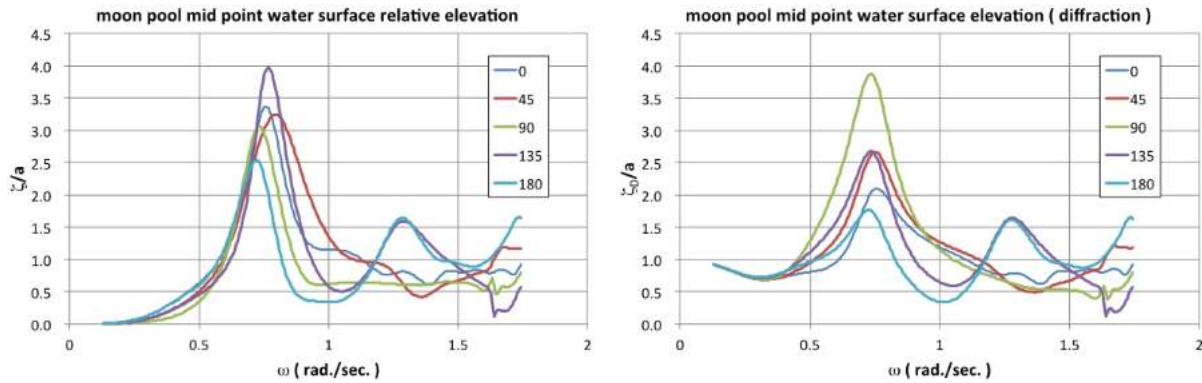
A comparison between the RAOs of the free water surface elevation in the centre of the moon pool for the total velocity potential and diffraction velocity potential showed that the dominant component is the diffraction ($\phi_0 + \phi_7$), especially at an incident wave of large frequency (sloshing mode). At piston mode resonance (around $\omega = 0.76$ rad/s), the highest peak in the chart obtained with total velocity potential happens mainly because the MP water surface elevation is combined with the radiation velocity potential, which means that the ship's vertical motion amplifies the elevation (see figure 17). This fact shows an agreement with the integration illustrated in figure 9 of section 2.1.1 of the water oscillation mechanism.

Also, another evident contribution of the vertical motion of the hull mainly on piston mode is the comparison of calculated responses for different damping coefficient values, shown in figure 18.

At the piston mode circular frequency, the response amplitudes increase fast for small decreasing of damping coefficient values, while comparatively the effects on sloshing are negligible. This behaviour becomes more evident at no damping situation, showing that the radiation contribution that is affected by the damping, and which is originated on the vertical oscillation, is concentrated at the piston mode response of the hull.

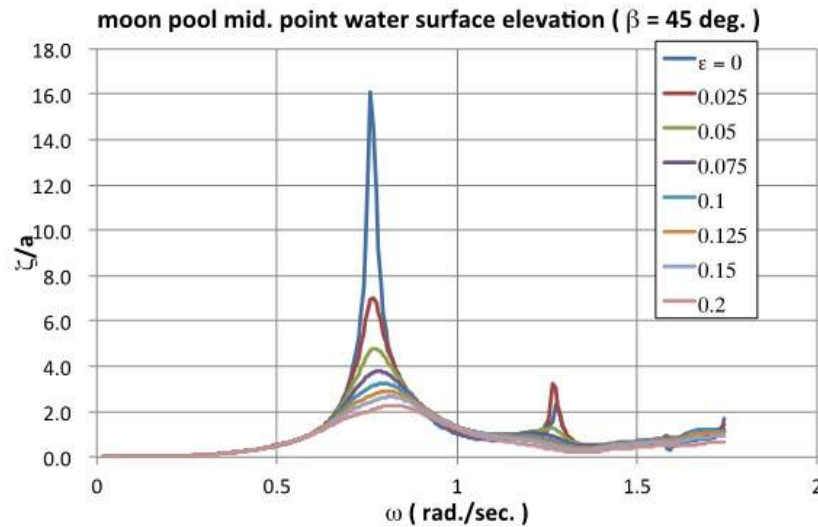
Irregular waves used in a numerical simulation of the ship response are closer representations of the specified real sea condition than the regular ones. An irregular wave is represented by a height or energy spectrum determined by the amount of

Figure 17: Moon pool water surface elevation at mid. The left figure shows the non-dimensional amplitude obtained with the total velocity potential, and the right figure shows the non-dimensional amplitude due to the diffraction potential only. From comparison, it is noticeable that there is a dominance of the diffraction potential, especially in sloshing mode (higher frequency peak). The piston mode (lower frequency peak) resonance is increased by radiation due to vertical motion of the ship.



Source: Michima and Kawabe (2014b)

Figure 18: Moon pool water surface relative elevation at surface mid. point ($\beta = 45^\circ$).



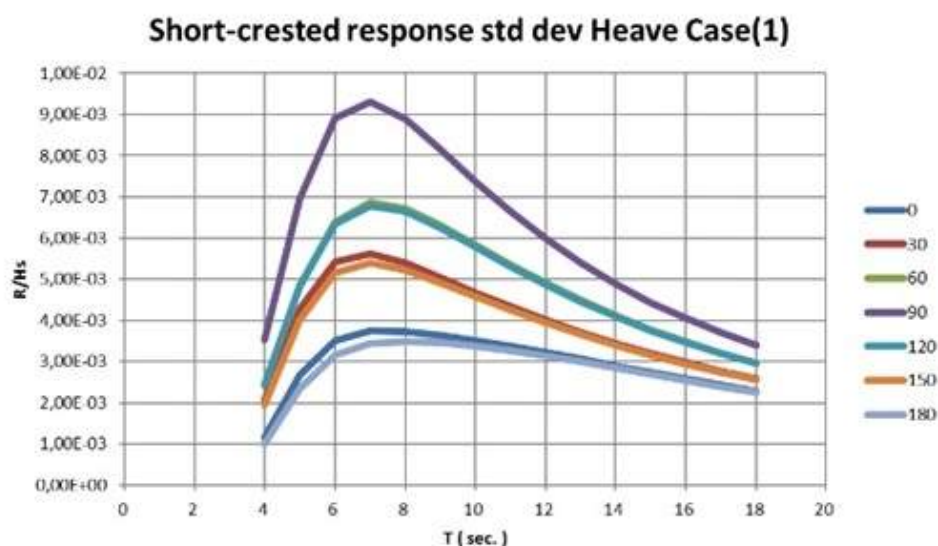
Source: Michima and Kawabe (2014b)

energy contained in a component of a specific regular period, and its characterizing parameters are the significant wave height, significant wave period and some variables that shape how spread or concentrated the energy distribution is around a range of main periods.

A response chart analogous to the RAO, called Response Spectrum, is obtained exclusively in time domain, from the standard deviation of the response of the ship to the irregular wave with each significant period and unit significant wave height. Based on those information, one can evaluate for each significant wave height what is the

maximum value that an incident irregular wave will result in ship motion at each degree of freedom. An example of those charts is presented in the figure 19.

Figure 19: Example of response spectrum in heave mode for different incidence angles.



Source: Author.

Since this development is done in the linear theory, the response to any significant wave height different from unit is obtained by simply multiplying the response by the modulus of that height. This response is the one to be used to find the limit wave height that matches with each criterion in each motion mode, as follows.

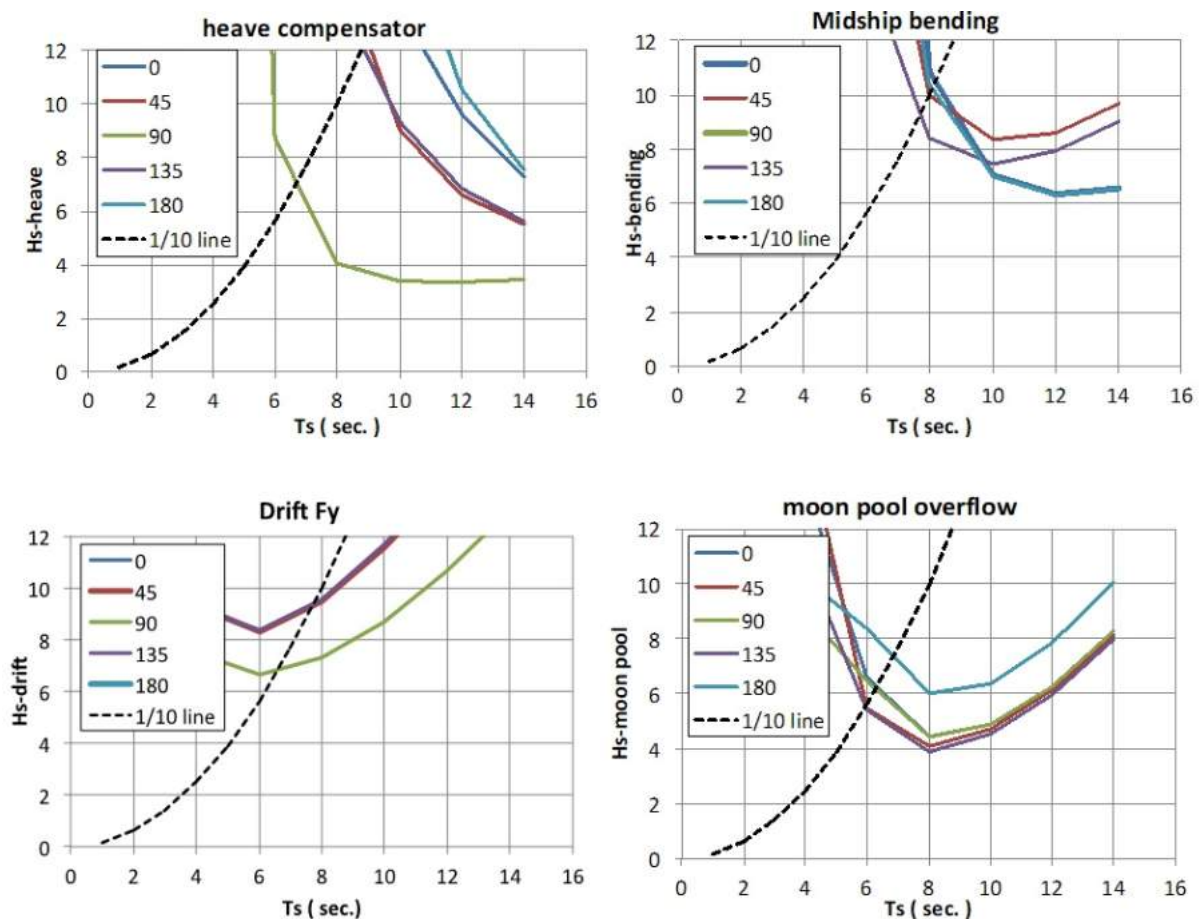
Given a sea state characterized by the parameters that define the wave spectrum, the response to a significant wave height with an incidence angle β is obtained from the respective mode chart, as in the example previously described. From this response, a decision can be made based on the specific criterion for each motion whether that significant height exceeds the allowed limit or not.

There will be the significant wave height that is the critical value above which the criterion is no more attended, that is the so-called threshold significant wave height. It indicates, thus, the limit of operability of the system for the given situation. The example shown in the figure 20 illustrates the TWH for each criterion in each incidence angle for a Series 60 hull adapted with a rectangular moon pool under JONSWAP wave spectrum condition. The criteria are the ones listed in the subsection 4.2 about the assessment formulae, except for the crew comfort. A short description of those criteria is:

- moon pool overflow, accounting to the relative motion between the water column and the moon pool, exceeding the free board for a number of times in a definite interval, according to specific recommendations (CrOFW);

- exceedance in heave amplitude, accounting to the heave motion of the hull, that cannot be compensated by the limited stroke of the heave compensator of the drill(CrSTR);
- occurrence of critical wave induced vertical bending moment at midship for a number of times in a definite interval, according to specific recommendations (CrVBM), and
- exceedance in drift power, regarding to what the DPS (dynamic positioning system) can compensate (CrDFT).

Figure 20: Threshold significant wave height \times significant wave period for each safety criterion. Northwest: heave, northeast: vertical bending moment at midship, southwest: average drift power and southeast: moon pool overflow. Black dashed lines indicate the breaking wave limit.

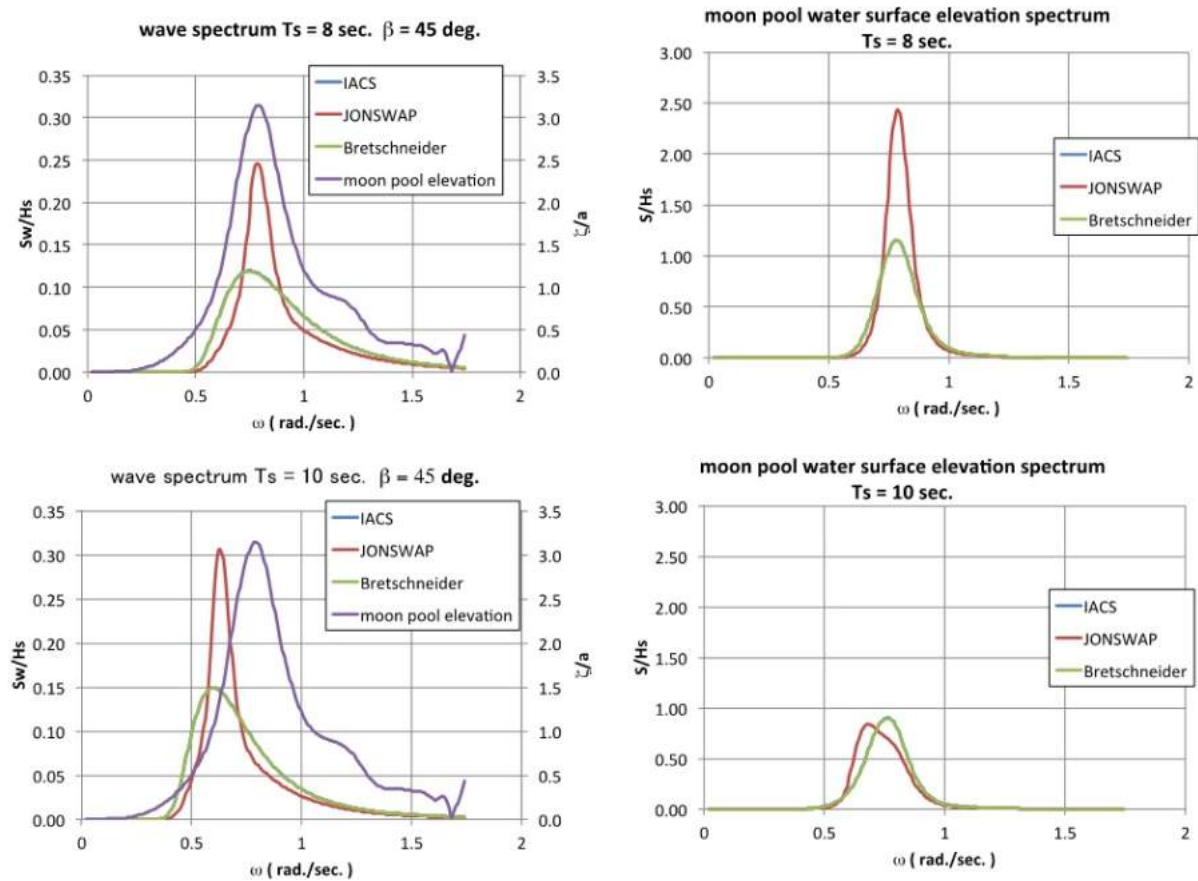


Source: Michima and Kawabe (2014b)

Using a hydrodynamic calculation module, the response of the ship in the essential aspects that allow judging the above-mentioned situations of drill ship operation were obtained: moon pool internal water oscillation amplitude, relative motion of the hull to the water, vertical bending momentum at midship and average drift power. The

calculation was done for the wave spectra: IACS, JONSWAP and Bretschneider. Then a comparison of the effects of the wave spectra on the water surface elevation spectrum (figure 21) was made, from which JONSWAP was chosen for having the biggest effect, thus predicting the worse situation to assess safety.

Figure 21: Effect of wave spectra on water surface elevation spectrum inside moon pool, with incidence angle $\beta = 45^\circ$. Left hand charts: wave spectra and moon pool water elevation, IACS coincide with Bretschneider. Upper with significant wave height $T_s = 8s$, nearly coincident with the moon pool's natural frequency (the peaks of non-dimensional amplitude of moon pool elevation and wave spectra are approximately coincident). Bottom with with significant wave height $T_s = 10s$, different from the moon pool's natural frequency. Right hand charts: moon pool water surface elevation spectra in response to the correspondent wave spectra on the left, IACS coincide with Bretschneider.



Source: Michima and Kawabe (2014b)

The threshold significant wave heights considering probabilities of a certain number of peaks to happen for each safety criterion were then calculated for different significant wave periods, as shown in figure 20. The calculation formulae is presented in more details in section 4.2 of the assessment formulae for the criteria, since they were used also in this work.

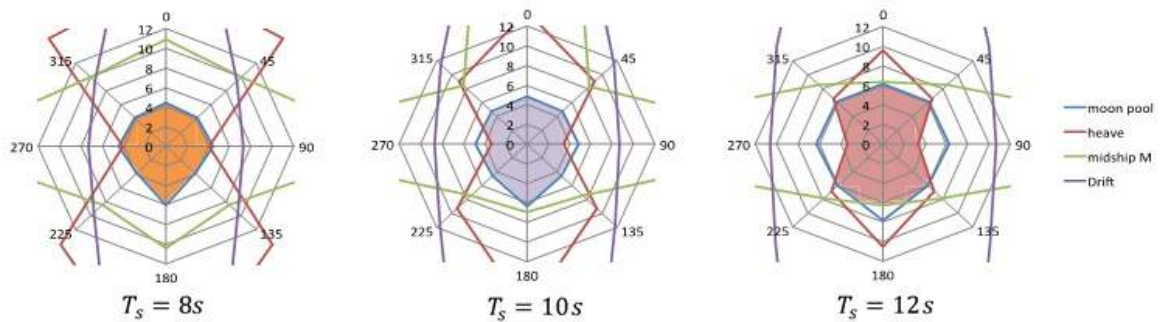
In each criterion chart there are several lines, for each angle of incidence, from $\beta = 0^\circ$ to $\beta = 180^\circ$, in which the value of the threshold significant wave height wave

height is plotted for each significant period. The chart is symmetrical from $\beta = 180^\circ$ to $\beta = 360^\circ$. There is a limiting dashed line that limits the wave slope to the domain of the linear theory. It can be identified that for the moon pool overflow criterion, the biggest restriction is imposed to the significant wave height around $H_s \cong 4\text{m}$ and $T_s \cong 8\text{s}$, because this is when the overflow will start to happen in $\beta = 135^\circ$. In a similar way, heave compensator stroke criterion would have the biggest restriction by $\beta = 90^\circ$, around $H_s \cong 3.5\text{ m}$ and $T_s \cong 10\text{s}$ to 12s . Midship vertical bending moment would be restricted by both $\beta = 0^\circ$ and $\beta = 180^\circ$ in $H_s \cong 6.2\text{m}$ and $T_s \cong 12\text{s}$, and the y -direction drift force restricted by $\beta = 90^\circ$, around $H_s \cong 7\text{m}$ and $T_s \cong 7\text{s}$.

From those charts, the most limiting significant wave period values were selected to generate the operability charts including the four criteria, presented in figure 22. Each line color shows the limit above which the corresponding criterion is not satisfied. The region between the two symmetric lines of that criterion define their operability region. Colour-filled areas highlight the intersection area of all criteria in all different incidence angles β . That region varies with period for each shape and area, as can be seen in the figure. The wider the coloured region is, bigger will be the possibility of staying operable for the input sea state conditions, thus smaller will be the chances of downtime in comparison to others with more restricted areas.

It is also noted that either from the charts in figure 20 or in figure 22, depending on the significant wave height, the predominance of operability limiting will be defined by different sets of criteria. So, for the present example, for the significant wave periods $T_s = 8\text{s}$ and $T_s = 10\text{s}$, the moon pool water overflow and heave compensator stroke are the most restrictive parameters, and for bigger values of T_s the dominance of restriction by moon pool overflow starts to be more evenly shared with the other criteria as heave and midship vertical bending moment.

Figure 22: Radar charts of threshold wave heights for specific significant periods: $T_s = 8\text{s}$, $T_s = 10\text{s}$ and $T_s = 12\text{s}$. The highlighted area including the origin is the clearance space at which all the criteria are attended.



Source: Michima and Kawabe (2014b).

Some of those most restricting significant wave periods might not happen in the

operation area, so the correspondent restrictions might not be of interest for analysis. If it is assumed that the characteristic sea states profile of the operation regions is known, the characteristic periods can be chosen specifically to make a collection of the threshold wave heights of all the criteria.

Özüm, Şener and Yilmaz (2011) tried adoption of seakeeping analyses as an integral part of ship design applied to fast ships in conceptual design stage. Among other conclusions, it was found that variation of main dimensions would be more effective in vertical plane oscillations mitigation than form parameters. Also, Approaching of LCB to the aft reduces heave amplitudes, but has no effect on pitch motion. However, they concluded that interpretation of the output provided by seakeeping design method is possible in qualitative terms, but it is not always going to be straightforward in quantitative terms.

This work proposes an analysis that uses quantitative results as a means to evaluate fitness. For that matter, not only is it necessary to be “well” operable, but “how much of operability” does it have, too. So, the most convenient value that can be used to attribute a quantitative judgement of operability was found to be the area inside the intersection of limit lines.

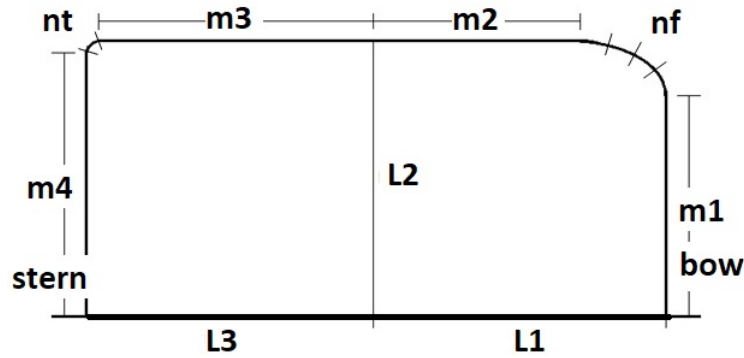
From the sample ship described above, when focusing on design stage, a question may arise of “how would it be possible to find the most suitable moon pool shape that provides the smallest downtime risk for a given operation area (*i.e.* given sea states)?”. Knowing from the already studied works referenced in the section 2, of the literature survey, that the performance of the moon pool is directly related to its shape and dimensions, an investigation was started to search the shapes what would provide better performance from operability point of view, without the need to use extra appendages. Also, to make the best use of the space, the clearance area should neither have restrictions in the inner part, nor “invade” storage or other useful spaces on its external side other than that of the access to seabed. Hence, it should have only vertical walls, *i.e.*, be prismatic.

The figure 23 shows geometric parameters used for the optimization, as implemented in Cavalcante (2015).

The parameters involved in the definition of the configuration for the MP mesh generation are:

- L1 - longitudinal half-length, argument parameter;
- L2 - transversal half-length, argument parameter;
- m1 - transversal coordinate of the fore corner polygon, dependent parameter;
- m2 - longitudinal coordinate of the fore corner polygon, dependent parameter;
- m3 - longitudinal coordinate of the aft corner polygon, dependent parameter;

Figure 23: Parameters of the moon pool contour. It is symmetric about the longitudinal centre line. The fore points towards to the right, and aft to the left.



Source: adapted from Cavalcante (2015)

- **m4** - transversal coordinate of the aft corner polygon, dependent parameter;
- **nf** - number of segments of the fore corner polygon, independent non-argument parameter;
- **nt** - number of segments of the aft corner polygon, independent non-argument parameter;

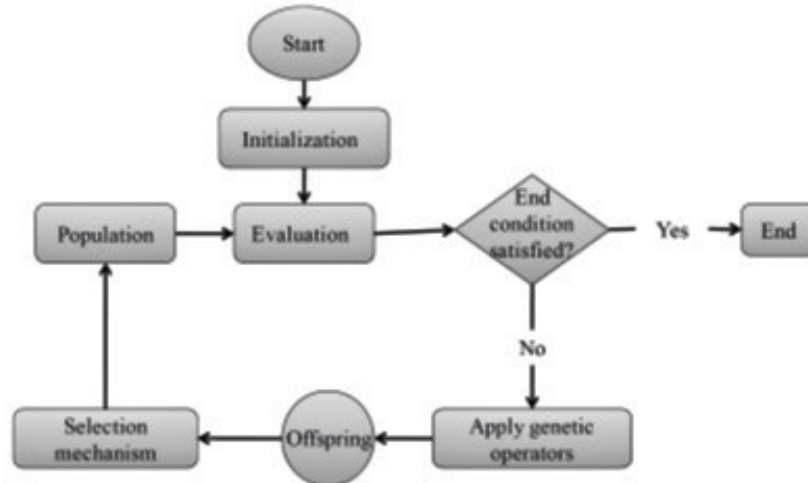
The corners are polygons composed of straight lines that match at ends belonging to a quarter of ellipse. The parameters that are not shown in the figure above, **nf** and **nt** define the amount of segments. The smaller **nf** and **nt** are, more chamfer-like the corners become and the bigger the parameters **m1**, **m2**, **m3** and **m4** are, more square-like the shape becomes. Among terms of the parameters used to vary the configuration, some assume values independently, defining the main dimensions, and some are function of those, establishing the shapes.

To assure a better refinement of the combinations of variables, the argument parameters were approached in a different way to force a complete scanning of dimensions, since from literature it has been continuously learned that the main dimensions and form coefficients that indicate proportions of them have a big influence on the performance of the system. For those argument parameters, **L1** and **L2**, a silly sort was applied, subdividing the search in a $k = a \times b$ independent searches, where **a** and **b** are respectively the numbers of values that **L1** and **L2** can assume. Among the **k** best solutions obtained, finally the global best of all solutions is found.

The search approach was decided to be an evolutionary algorithm, specifically based on the genetic algorithm (see flowchart in figure 24): a set of candidate solutions, called individuals, can be randomly generated by varying the values of each parameter to which we call “gene” and the objective function can be used as a means of measuring how the individuals perform in the problem domain. In other words, applied to the case in the present study, by randomly varying the values that define the shape and dimensions,

an individual is defined and a ship with a moon pool attached to an external hull mesh obtained from input is created with those characteristics. Its fitness is then assessed in terms of operability, and a group of best solutions is selected to seed the next generation by applying recombination and/or mutation on them.

Figure 24: Generic flowchart of a genetic algorithm.



Source: Bagheri and Ghassemi (2014)

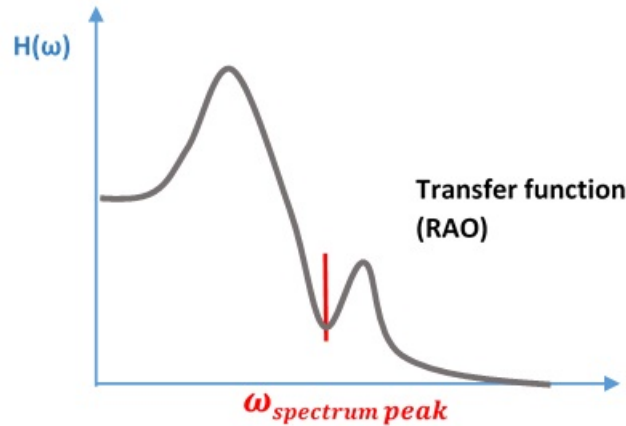
A recombination operator, known as crossover, generates new individuals from two or more selected “parents” of the previous population, by matching parts of their parameter values. To guarantee that the obtained optimal solution is a global maximum performance, and not a local one, some mutations are introduced to those breeds. The mutation consists in changing randomly some of the values of the parameters of the individuals, pushing the search to anywhere in the solution space outside of the evolution gradient. If the individuals deriving from mutation have a fitness grade higher than the others, a new optimal solution area is explored. This procedure can be iterated until a quitting criterion is satisfied. The use of this procedure improves the fitness values for the next generation.

Original concepts of genetic algorithm indicate that the next population is formed by creating an intermediate offspring by crossover in 1 point only of the string of genes, and applying a random probability of mutation on each member that will finally result in the next population.

If we simplify the problem studied in this work for just a matter of adjusting the moon pool configuration in such a way that the spectrum peak of the chosen sea state doesn’t coincide with the natural frequencies of the moon pool in any mode and for any response, a raw illustration of that search would be like the sketch shown in the figure 25.

The horizontal axis is the frequency and vertical axis is the oscillation amplitude.

Figure 25: Sketch of moon pool RAO. The horizontal axis is the frequency and vertical axis is the oscillation amplitude. If the search counts too much on gradient search with a small rate of mutation, it can get “trapped” in the trough instead of finding better configurations at frequencies smaller than the left peak or bigger than the right peak.



Source: Author

If the search counts too much on gradient search with a small rate of mutation, it can get “trapped” in the trough instead of finding better configurations at frequencies smaller than the left peak or bigger than the right peak. The search would get trapped if falling into a region where small change in the moon pool configuration would result in very bad performance and this would lead the search to redirect to the opposite direction, that would also be bad, despite of some small probability of mutation would have already been applied.

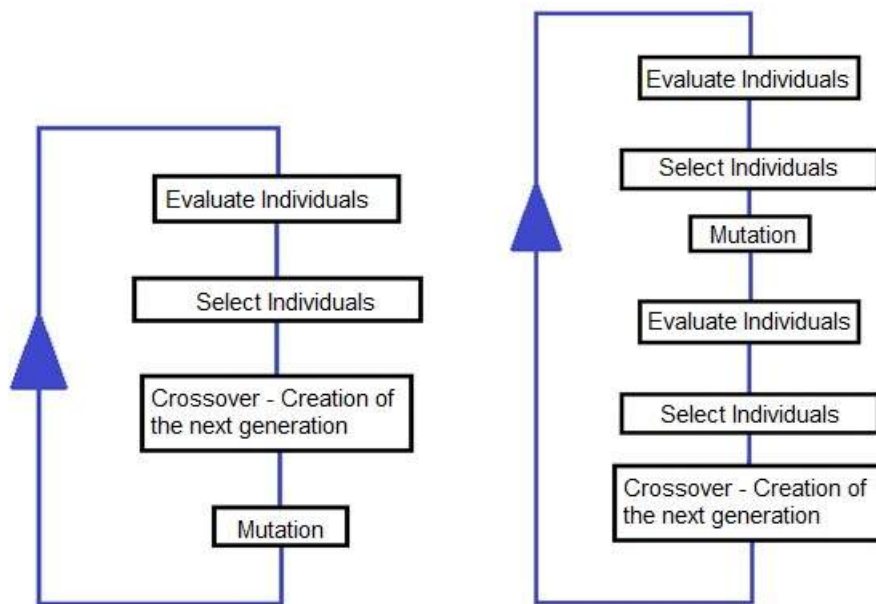
To increase the chances of skipping to other possible areas to explore, a modification to the original genetic algorithm was done. Inspired in the multimembers evolutionary strategies cited by Schwefel (1981), the mutation is induced with a probability to all the individuals, after a selection. Then, among originals and mutants, there is a new test and selection of the ones to which the crossover will be applied and finally result in the next population. A comparison can be done with the figure 26.

The modified algorithm can still be classified as genetic for using crossover as a tool for evolution. As a reference to the fiction histories from *Marvel Comics*® in which several times, mutants appeared after explosion to gamma radiation, this modified algorithm was named Gamma (CAVALCANTE, 2015). An overall view of the composition of the Gamma algorithm is given in figure 27.

A general file flowchart of the whole tool with the optimization module coupled to a hydrodynamic simulation module presented by Fonseca (2016) is illustrated in figure 28.

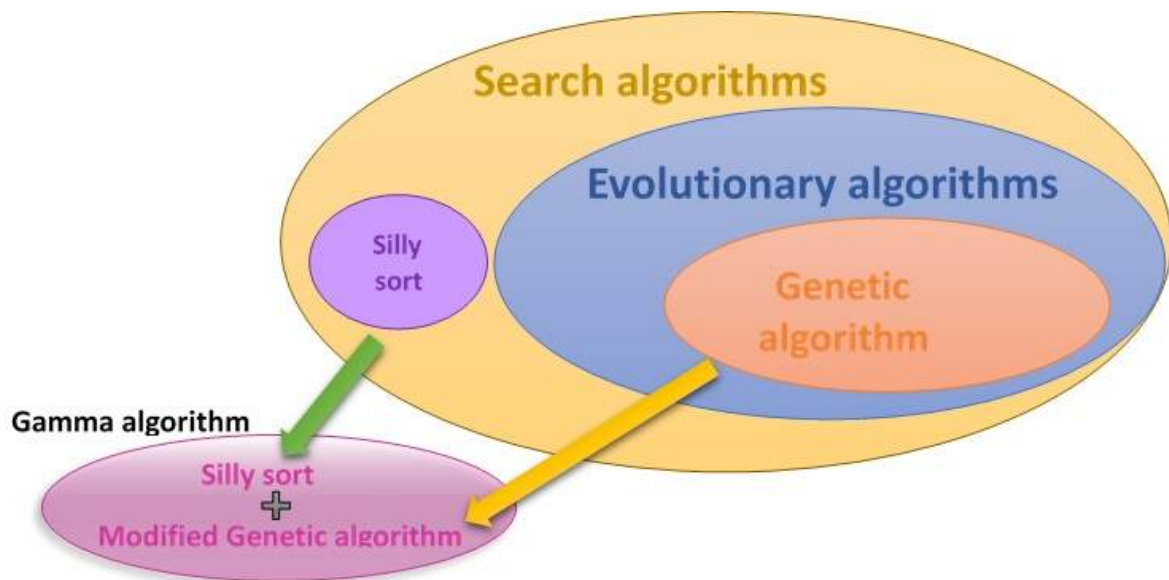
The input from the user is the mesh of the hull without previous opening for the

Figure 26: Flowcharts of the algorithms. Left: original genetic algorithm; Right: modified algorithm.



Source: adapted from Cavalcante (2015)

Figure 27: Overall view of the composition of the Gamma algorithm.

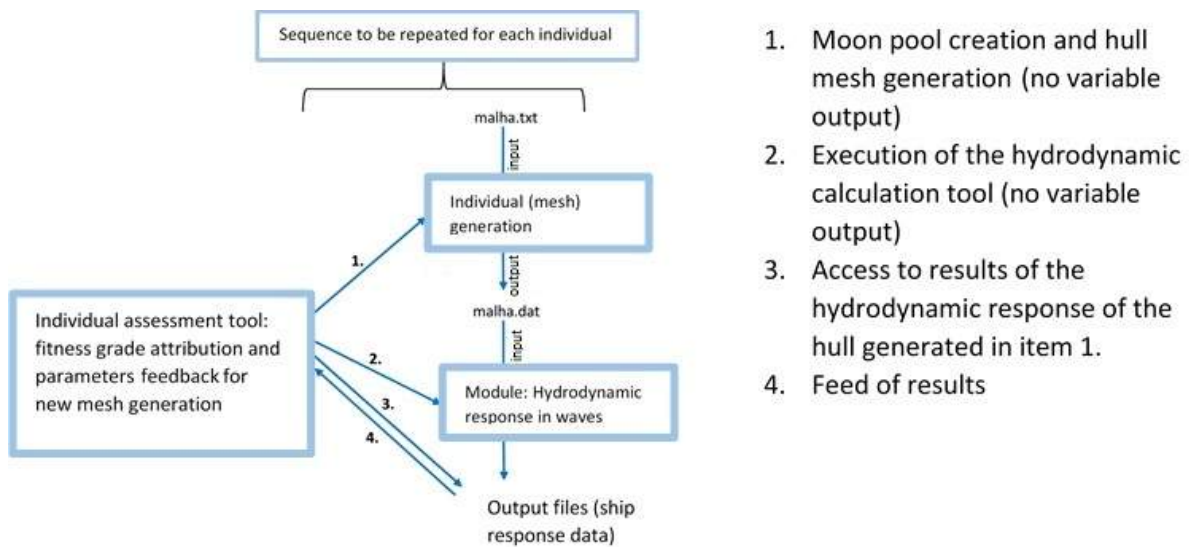


Source: Author.

moon pool, and the settings are done about:

- Size of the divisions of the moon pool mesh in the z direction. By default, it should be same as the spacing of the hull mesh to keep the uniformity of the shapes of the elements;

Figure 28: General file flowchart of the optimization tool interacting with the hydrodynamic calculation module.



Source: Adapted from Fonseca (2016)

- Spectrum types to be used for the response analysis: JONSWAP, IACS and/or Bretschneider;
- Significant wave periods to be considered for the sea state. Depending on the operation area, the typical sea state is defined to assess the response of the ship, as in the example shown in figure 22.
- Type of analysis: long crested or short crested wave analysis, respectively for more conservative analysis or less conservative analysis. Usually it is recognized that long crested irregular waves give the most severe ship responses comparing to short crested waves (TAKEZAWA et al., 1993). Since the short-crested waves are those of not fully-developed seas, there is the directional amplitude coefficient that distributes the wave height in each direction, and therefore the resultant heights in each direction are shorter than for fully developed seas. By considering short crests, the designer assumes that a not-so-big wave condition will determine the operation environment, hence designs the system assuming that smaller safety coefficients are needed.

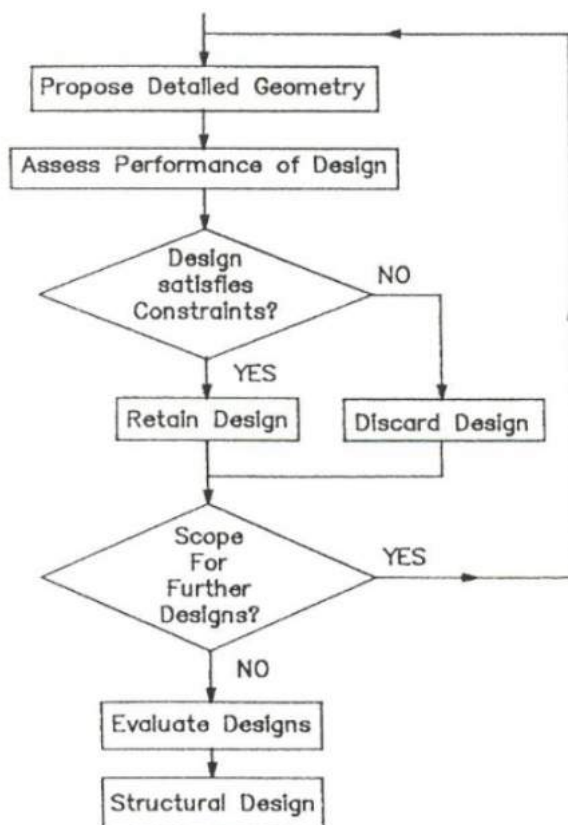
3 Theoretical foundation

“All entities move and nothing remains still.”

— Heraclitus, quoted by Plato, *Cratylus*, 401d

This section describes the concepts upon which the models used in the present work were constructed. The search algorithm, parametrization and assessment strategies are similar to the ones presented on the previous section 2.3 of the detailed review. As explained by Day (1990), the selection of the geometry is best carried out using an iterative approach, as suggested in the flowchart in figure 29.

Figure 29: Detailed moon pool geometry flow diagram.



Source: Day (1990)

According to the author, the tasks involved in the iteration are:

1. Propose a detailed geometry, setting out basic geometry and any additional structure deemed necessary;
2. Assess performance of design;
3. Assess whether the design is a potential solution, satisfying the imposed constraints, and retain the ones that satisfy;

4. Examine the scope for further geometries to be considered, and in affirmative case, propose another geometry;
5. Evaluate designs which satisfied all the imposed constraints and select the most suitable geometry, considering also the detailed structural design;
6. If it proves impossible to produce a design satisfying the constraints and the structural design, then the problem must be reassessed. This process may involve the relaxation of one or more constraints, modification of some of the input data (for example, vessel hull form) or, in an extreme case, abandonment of the project as infeasible. In some cases, the reassessment of the problem requires examining several scenarios with varying design constraints.

The present work provides the assessment tool considering the criteria justified previously in the section 4.2 of the assessment formulae but can be adapted to include as many restrictions as desired. The designer can take the results and proceed directly to the step number 5, for the evaluation of feasibility of the structural design.

In the following subsections more detailed information about the concepts used to approach the search for the optimal solution are presented: first concepts are found in section 3.1, of the wave condition response of a ship with moon pool, where the mathematical modelling used for the hydrodynamic response calculation tool are described, and the following concepts in section 4.1, of the performance and fitness grading, are the basis of the search algorithm used for the optimal solution search.

3.1 Ship response in waves

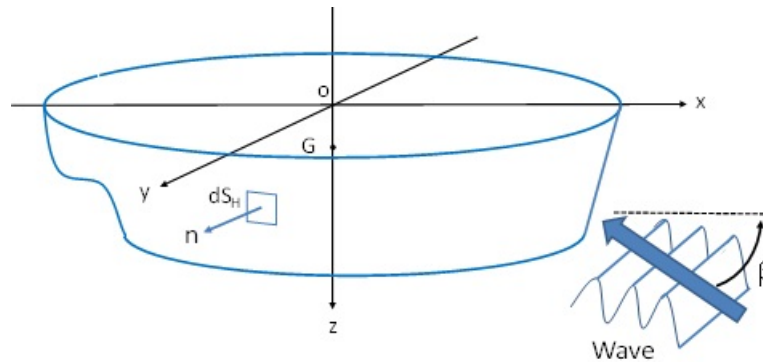
This subsection covers the main concepts used for the mathematical modelling of the motion of a ship with a moon pool inside. The presented development starts with the definition of the coordinate system on which the references are taken, and details the general equation of motion, The velocity potential modelling is done, allowing the calculation of the first order forces, followed by the drift force.

By linear modelling, it is possible to separate the origin of the excitation force in several independent components, and to determine the resultant hydrodynamic force acting on the hull and pressure fluctuations of the water inside the moon pool. The specific equation of motion is then presented in the frequency domain from which the regular wave response is obtained, followed by the time domain where the irregular wave response calculation is done.

3.1.1 Coordinate system

Defining the coordinate system is very important, since the position of the centre of gravity related to the origin can simplify or increase the complexity of the equations. The adopted coordinate system is illustrated below in figure 30.

Figure 30: Coordinate system.



Source: Hiroshi Kawabe's notes, edited by author.

The origin is positioned at the longitudinal centre line of the ship, assumed to be the x -axis. The positive counting is towards to the bow. The y -axis is the transversal line that coincides with the midship, positive at east board. It crosses the x -axis at the waterline, and hence the z -axis points downwards in the same direction as the gravity acceleration. The centre of gravity G of the ship is located in the z -axis, at a positive distance (OG_z) from the origin.

Incident waves reach the hull with an inclination β related to the x -axis positive side. The normal vector is defined always pointing from the considered surfaces into the fluid domain. Based on this system, the following subsections will present the mathematical developments to obtain the equation of motion for a standard ship.

3.1.2 General equation of motion

Analysing the ship response to waves requires establishing the relationship between the fluid motion and the floating body through the wetted surface interface. The action of the water on the ship is performed by pressure, and its fluctuation results in the so-called hydrodynamic interaction, which can be expressed in terms of hydrodynamic loads (forces). The wave reaches the ship with independent frequency and height, and this is the start point of the excitation and response chain.

The ship motion is expressed in terms of its 6 degrees of freedom positioning x in a coordinate system, and the variations of x are obtained as function of the water pressure. In a general form, the pressure is obtained from the velocity distribution field,

and in the case of potential flows model to be derived in section 3.1.3, the pressure is obtained from the velocity potential derivative. This is how the calculation in this work was made, starting from the general equation of motion presented as follows.

From Newton's second law, we can generally describe the motion of the floating body in the six degrees of freedom as:

$$M\ddot{x}(t) = F(t) \quad (3.1)$$

in which the motion displacement is expressed as a time-derivative. The mass term M here described in general terms expresses the inertia, which for a coordinate system defined as in the previous subsection 3.1.1 is given by:

$$M_{ij} = \begin{bmatrix} m & 0 & 0 & 0 & w & 0 \\ 0 & m & 0 & -w & 0 & 0 \\ 0 & 0 & m & 0 & 0 & 0 \\ 0 & -w & 0 & I_{xx} & 0 & 0 \\ w & 0 & 0 & 0 & I_{yy} & 0 \\ 0 & 0 & 0 & 0 & 0 & I_{zz} \end{bmatrix}$$

Where $w = m \cdot (OG_z)$, the product between the mass of the system and the distance between the centre of gravity G located at $(0, 0, z)$ and the origin $O = (0, 0, 0)$. The inertia momentum terms of the angular motions around each axis x, y and z are the last three terms of the main diagonal line in the matrix. It might at first sight seem to be inconvenient to set the origin out of the centre of gravity, since each response output calculated relative to G needs to be corrected to the offset system, but this choice is done because it would be even more complex to adjust the equations for the surface wave model.

If a rigorous and absolutely precise analysis should be taken, the exciting force F of the right-hand side member would be represented by interdependent components of force that would be very complex to be treated separately. Although it would be more realistic, such complexity would either lead to a time expensive numerical calculation or provide a low cost-benefit performance in terms of increase of precision at the present time, with the present available tools in this research. Thus, a linear model is adopted, to allow the separation of those components and superposition of effects.

From the next subsection on, the modelling presented is all developed in the Linear Theory.

3.1.3 Linear theory model

As stated in DNV (2011), a linear analysis will usually be sufficiently accurate for prediction of global wave frequency loads. The concept of linearity is based on some premises that simplify flow conditions so that second order terms in the mathematical model of the phenomena are negligible, variations are smooth and wave steepness is small. Consequently, there is no wave breaking and the fluid dynamic pressure and the resulting loads are proportional to the wave amplitude. Also, the effects of waves and other motions, such as loads from individual waves in an arbitrary sea state can be simply superimposed.

Only the wetted area of the floater up to the mean water line is considered. The analysis gives first order excitation forces, hydrostatics, potential wave damping, added mass, first order motions in rigid body degrees of freedom and the mean drift forces/moments. The mean wave drift force and moments are of second order, but depend on first order quantities only.

The decomposition of the exciting force follows a standard division. There is the incoming wave force F_0 , that is responsible for the start and maintenance of the ship motion. As the wave meets the hull, it will induce an effect that, as described in (DNV, 2011), within a linear analysis, defines a hydrodynamic problem that is usually divided into two sub-problems:

- Diffraction problem: the structure is restrained from motions and is excited by incident waves. The resulting loads are wave excitation loads. The part of the wave excitation loads that is given by the undisturbed pressure in the incoming wave is called the Froude-Krylov forces/moments, F_0 . The remaining part is called diffraction forces/moments, F_D .
- Radiation problem: considers that the body is forced to oscillate with the wave frequency in a rigid body motion mode with no incident waves. Actually, this is the response motion, that leads to generation of progressive waves advancing away from the body and transferring kinetic energy from the floating body to the water. The resulting damping load is called radiation force F_R . In addition to this dynamic component, since the submerged volume varies with the oscillation of the body, the restoration force by the buoyancy should also be considered, as a static force F_s .

The right-hand side of Newton's second law equation can be thus replaced by the summation of those components:

$$F = F_0 + F_D + F_R + F_s \quad (3.2)$$

By making use of the concepts presented here, the following subsections will show the work on specifying the equation of the second law of Newton in terms of velocity potential that describes the velocity field of the fluid domain and thus permits predicting the ship behaviour in wave condition.

3.1.4 Linear equation of motion

When the floating body without motion restrictions is excited by an incoming wave, it moves in each degree of freedom. The motion due to the excitation is called response. From the previous section 3.1.3 of the linear modelling, where the decomposition of the external force is done, if one should divide the components into active and reactive terms, the incident wave and its diffraction would be the active ones, that do not depend on the body's motion x , and the others would be reaction. The reaction has three components, two from wave radiation phenomenon and one from restoration. One of them affects acceleration as a damping, therefore it is proportional to inertia, referred to as added mass. The other term is a velocity damping term, and the last is the hydrostatic reaction, based on Archimedes' principle.

$$M\ddot{x} = (F_0 + F_D)_{active} + (F_{R\propto\ddot{x}} + F_{R\propto\dot{x}} + F_s)_{reactive} \quad (3.3)$$

where

M is the mass of the body, $F_{R\propto\ddot{x}}$ is the force related to the added mass, and $F_{R\propto\dot{x}}$ is the force related to damping.

If the equation is re-arranged to have motion-dependent terms on the left-hand member and motion-independent terms on the right-hand member, the equation of motion becomes:

$$(M + A)\ddot{x} + B\dot{x} + Cx = E \quad (3.4)$$

Where:

- M is the mass of the body;
- A is called added mass, because is one of the terms of the wave radiation damping and has inertia unit;
- B is the coefficient of wave radiation damping proportional to velocity;
- C is the restoration coefficient;
- E is the wave exciting force.

Since the 3D motion analysis accounts for the six degrees of freedom, each motion mode is referred to by the indexes 1, 2, 3, 4, 5, 6, respectively: surge, sway, heave,

roll, pitch and yaw. The equation of motion regarding those modes is a summation of them:

$$\sum_{j=1}^6 [(M_{ij} + A_{ij}) \ddot{x}_j + B_{ij} \dot{x}_j + C_{ij} x_j] = E_i \quad (3.5)$$

where i is the incident wave excitation mode and j is the response mode of the body. The expression accounts also for the existence of crossed responses. In other words, the body will be excited in several degrees of freedom j even if the excitation is given in one mode i only.

If it is considered that the flow is incompressible, inviscid and irrotational, it is possible to work in the Linear Theory, and use of a scalar mathematical entity, the velocity potential Φ . The directional derivation $\partial/\partial r$ of that potential results in the directional velocity component $\frac{\partial \Phi}{\partial r} = \vec{v} \cdot \hat{n}_r = v_r$. Furthermore, the velocity potential, which is a function of position and time, can be written as $\Phi_j(x, y, z : t) = \Phi_j(P : t)$.

Hydrodynamic forces acting on a body are results of pressure fluctuation distribution along its surface of interaction, *i.e.* the wetted surface. From the linearised Bernoulli equation, the pressure p is expressed in potential term as $p = \rho \frac{\partial \Phi}{\partial t}$, and the velocity potential is obtained from the boundary value problem solution. In the same fashion as in equation 3.2, we can also divide the velocity potential into the respective components:

$$\Phi = \Phi_0 + \Phi_D + \Phi_R + \Phi_S \quad (3.6)$$

where

Φ_0 is the velocity potential of the incident wave, Φ_D is the velocity potential of the diffracted wave, Φ_R is the velocity potential of the radiated waves, and Φ_S is the velocity potential due the static restoration.

The response of the body to wave excitation can be calculated using the velocity potential applied to the equation of motion, which in turn, depends on the domain where the analysis will be performed: in frequency or in time.

3.1.5 Ship response model

Day, Lee and Kuo (1989) explain that two basic approaches may be adopted. The problem may be solved in the full non-linear form using a time domain approach; alternatively, the force equation may be linearised and a frequency domain solution implemented. As in the case of the water column oscillation, each approach has drawbacks and advantages; the time domain approach involves fewer approximations,

but takes significantly longer to solve, whilst the frequency domain approach is efficient in solution but may suffer inaccuracies due to the linearisation required.

The following subsections contain the description of each of the terms above in either approaches with which the ship response can be obtained. As the time domain calculation uses results from frequency domain, it will be the second one to be presented.

3.1.5.1 Frequency domain

Taking the advantage of the linear analysis, one can predict the responses of a system subjected to several individual regular waves of different periods/frequencies, and superimpose them. As described in DNV (2011), analysing a large volume structure in regular incident waves is called a frequency domain analysis.

The motion in frequency domain is expressed by $X_j(t) = X_j e^{i\omega t}$ where actually only the real part of the complex value has a physical meaning. Using the exponential expression turns to be convenient when using differential operations. Then the velocity potential at point P in a given instant t is defined as $\Phi_j(P : t) = \phi_j(P) e^{i\omega t}$. Since the instant information does not influence in the frequency domain analysis, the time-independent part $\phi_j(P)$ is used. Nonetheless, taking the time-derivative of the motion, $\dot{X}_j = i\omega X_j e^{i\omega t}$, given that the direction derivative of the potential is the direction velocity component, the velocity amplitude $i\omega X_j$ can be taken separately from the velocity potential. By doing so, it is possible to work on the velocity potential by unit motion, $\varphi_j(P) : \phi_j(P) = i\omega X_j \varphi_j(P)$. If φ_j is solved, then the equation of motion can be calculated to find the motion X_j . For the sake of keeping a logical sequence of the main development, the boundary value problem approach to model φ_j is described in section 3.2 of the boundary value problem without moon pool.

Recalling the equation of motion 3.5 from the subsection 3.1.4, since the time derivation of the exponential term of the motion ends up turning to a proportion to itself, the left-hand side member in that equation can be written as a coefficient of X_j :

$$\sum_{j=1}^6 \left[-\omega^2 (M_{ij} + A_{ij}) + i\omega B_{ij} + C_{ij} \right] X_j e^{i\omega t} = E_i(\omega) e^{i\omega t} \quad (3.7)$$

Given that the added mass and damping term are the wave radiation force components, their origin is obtained from the wave radiation pressure distribution integral over the wetted surface. In terms of velocity potential, this force can be expressed by:

$$\begin{aligned}
F_{Ri} &= F_{Ri}(\omega) e^{i\omega t} = \sum_{i=1}^6 \left[-\omega^2 A_{ij} + i\omega B_{ij} \right] X_j e^{i\omega t} \\
&= - \int_S p_{Rj} n_i dS = - \int_S -\rho \frac{\partial \Phi_j^R}{\partial t} n_i dS
\end{aligned} \tag{3.8}$$

The pressure p_R signal is negative because pressure on surface is positive into the surface, which it is opposite to the normal vector convention adopted in the present system. The velocity potential used should still be the time-function one, since the Bernoulli linearised equation for the pressure requires the time derivation. The unit vector that is normal to the vector surface is \hat{n} , so the n_i term is the modulus of the component of \hat{n} in i direction. The last integral expression results in a complex expression of which, by comparison, the real part corresponds to $-\omega^2 A_{ij}$ and the imaginary part corresponds to $i\omega B_{ij}$. Applying the derivative to the Φ_j^R potential, results in:

$$F_{Ri}(\omega) e^{i\omega t} = e^{i\omega t} \int_S \rho i\omega \sum_{j=1}^6 i\omega X_j \varphi_j n_i dS \tag{3.9}$$

which can be re-arranged to

$$F_{Ri}(\omega) e^{i\omega t} = -\rho\omega^2 e^{i\omega t} \sum_{j=1}^6 X_j \int_S \varphi_j n_i dS \tag{3.10}$$

since the velocity potential in this development is a complex entity, for convenience it can be written as

$$F_{Ri}(\omega) e^{i\omega t} = -\omega^2 e^{i\omega t} \sum_{j=1}^6 \left[\text{Re} \left(\rho \int_S \varphi_j n_i dS \right) + i \text{Im} \left(\rho \int_S \varphi_j n_i dS \right) \right] X_j \tag{3.11}$$

Keeping the previous equation 3.11 for a later reference, now recalling from 3.8, the equation can be rearranged for comparison as:

$$F_{Ri}(\omega) e^{i\omega t} = -\omega^2 e^{i\omega t} \sum_{i=1}^6 \left[A_{ij} - \frac{i}{\omega} B_{ij} \right] X_j \tag{3.12}$$

therefore, from 3.8 and 3.11,

$$\begin{cases} A_{ij} = \rho \text{Re} \left[\int_S \varphi_j n_i dS \right] \\ B_{ij} = -\omega \rho \text{Im} \left[\int_S \varphi_j n_i dS \right] \end{cases} \tag{3.13}$$

In the same manner, the origin of E_i exciting force is the summation of the incident wave (Froude-Krylov) pressure p_0 and diffracted wave pressure fluctuations.

$$E_i(\omega) e^{i\omega t} = - \int_S [p_0(t, \omega) + p_7(t, \omega)] n_i dS \quad (3.14)$$

where the negative signal of the integral means that the signal of the normal component in the kernel of the integral (that indicate the direction of the pressure outward the fluid domain into the ship) is opposite to the convention of our fluid domain calculation where the normal vector points into the fluid. The incident wave and scattered wave pressures are defined by:

$$p_0(t, \omega) = -\rho \frac{1}{g} \frac{\partial}{\partial t} \Phi_0(t, \omega) \quad (3.15)$$

$$p_7(t, \omega) = -\rho \frac{1}{g} \frac{\partial}{\partial t} \Phi_7(t, \omega) \quad (3.16)$$

Since the wave potentials are given by:

$$\Phi_0(t, \omega) = \frac{ag}{i\omega} \varphi_0(\omega) e^{i\omega t} \quad (3.17)$$

$$\Phi_7(t, \omega) = \frac{ag}{i\omega} \varphi_7(\omega) e^{i\omega t} \quad (3.18)$$

where a is the wave amplitude. Then, the excitation force can be rewritten:

$$E_i(t, \omega) = \frac{\rho}{g} \int_{S_h} \frac{\partial}{\partial t} \{\Phi_0(\omega) + \Phi_7(\omega)\} n_i dS \quad (3.19)$$

$$E_i(t, \omega) = E_{0i}(\omega) e^{i\omega t} = \frac{\rho a}{i\omega} \int_{S_h} \frac{\partial}{\partial t} \{\varphi_0(\omega) + \varphi_7(\omega)\} e^{i\omega t} n_i dS \quad (3.20)$$

$$E_{0i}(\omega) e^{i\omega t} = \rho a \int_{S_h} \{\varphi_0(\omega) + \varphi_7(\omega)\} n_i dS \quad (3.21)$$

As a convention, because the radiated waves' indexes go from 1 to 6 and the incident wave, which is the origin of the motion, is identified with the index 0, the index of the diffracted wave is 7. The restoration coefficient C_{ij} depends exclusively on the submerged part geometry of the floating body, thus there is no previous calculation involving the velocity potential.

On the hull surface, two boundary conditions can be applied: for the incident wave and scattering velocity potentials, and for the radiated waves velocity potential, as below:

$$\frac{\partial}{\partial n} \{ \varphi_0(\omega) + \varphi_7(\omega) \} = 0 \text{ on } S_h \text{ (incident and scattered waves)} \quad (3.22)$$

$$\frac{\partial}{\partial n} \varphi_i = n_i \quad \text{on } S_h \text{ (radiated waves)} \quad (3.23)$$

If these boundary conditions are applied, the wave exciting force can be rewritten as:

$$\begin{aligned} E_{0i}(\omega) &= \int_{S_h} \{ \varphi_0(\omega) + \varphi_7(\omega) \} n_i dS \\ &= \int_{S_h} \{ \varphi_0(\omega) + \varphi_7(\omega) \} \frac{\partial}{\partial n} \varphi_i(\omega) dS \\ &= \int_{S_h} \left\{ \varphi_0(\omega) \frac{\partial \varphi_i(\omega)}{\partial n} + \varphi_7(\omega) \frac{\partial \varphi_i(\omega)}{\partial n} \right\} dS \end{aligned} \quad (3.24)$$

Using the artifice of adding $+a - a = 0$ to the expression, it is possible to manipulate:

$$\begin{aligned} E_{0i}(\omega) &= \\ &= \int_{S_h} \left\{ \varphi_0(\omega) \frac{\partial \varphi_i(\omega)}{\partial n} - \varphi_i(\omega) \frac{\partial \varphi_0(\omega)}{\partial n} + \varphi_i(\omega) \frac{\partial \varphi_0(\omega)}{\partial n} + \varphi_7(\omega) \frac{\partial \varphi_i(\omega)}{\partial n} \right\} dS \\ &= \int_{S_h} \left\{ \varphi_0(\omega) \frac{\partial \varphi_i(\omega)}{\partial n} - \varphi_i(\omega) \frac{\partial \varphi_0(\omega)}{\partial n} \right\} dS + \int_{S_h} \left\{ \varphi_i(\omega) \frac{\partial \varphi_0(\omega)}{\partial n} + \varphi_7(\omega) \frac{\partial \varphi_i(\omega)}{\partial n} \right\} dS \\ &= \int_{S_h} \left\{ \varphi_0(\omega) \frac{\partial \varphi_i(\omega)}{\partial n} - \varphi_i(\omega) \frac{\partial \varphi_0(\omega)}{\partial n} \right\} dS + \int_{S_h} \left\{ \varphi_i(\omega) \frac{-\partial \varphi_7(\omega)}{\partial n} + \varphi_7(\omega) \frac{\partial \varphi_i(\omega)}{\partial n} \right\} dS \end{aligned} \quad (3.25)$$

Since $\nabla^2 \varphi_7(\omega) = \nabla^2 \varphi_0(\omega) = 0$ in the fluid domain V , from the Green's second theorem, the second integral of the right-side member becomes zero:

$$\begin{aligned} &\int_{S_h} \left\{ -\varphi_i(\omega) \frac{\partial \varphi_7(\omega)}{\partial n} + \varphi_7(\omega) \frac{\partial \varphi_i(\omega)}{\partial n} \right\} dS = \\ &= \int_V \left\{ \varphi_i(\omega) \nabla^2 \varphi_7(\omega) - \varphi_7(\omega) \nabla^2 \varphi_i(\omega) \right\} dV = 0 \end{aligned} \quad (3.26)$$

Thus, the wave exciting force can be calculated using the radiation and incident velocity potentials only, which is the so-called Haskind theorem:

$$E_{0i}(\omega) = \int_{S_h} \left\{ \varphi_0(\omega) \frac{\partial \varphi_i(\omega)}{\partial n} - \varphi_i(\omega) \frac{\partial \varphi_0(\omega)}{\partial n} \right\} dS \quad (3.27)$$

Back to the equation of motion, once the coefficients of added mass, damping, restoration and excitation force above are calculated, that equation can be solved for X_j assuming different values of regular wave excitation frequency. Since the calculation is done for a unit motion potential, inside the Linear Theory, the response of a wave excitation of any amplitude ς is obtained by simply multiplying the calculated response by ς^2 . If the response is calculated several times, each of them for a frequency value belonging to a range, one obtains a discrete chart of the unit amplitude wave excitation response of the body “versus” frequency, which is the so-called Response Amplitude Operator (RAO). This operator is used as a transfer function where the input is the regular wave amplitude and frequency, and the output is the ship response to that wave, *i.e.*, how much that input wave is amplified or reduced when becomes response motion, as shown in figure 31.

Figure 31: Ship as a transfer function between incident wave and response to its excitation.



Source: Author.

The ship response spectrum in regular waves is obtained if the transfer function is done for all the wave spectrum frequency range, as illustrated in figure 8 from section 2.1.1 of the water oscillation mechanism inside a moon pool.

3.1.5.2 Time domain

Although the frequency domain calculation is convenient for fast calculations, some information is lost, such as phase lag between the components of the irregular wave time series. Nonetheless, the memory effect of the damping term is also lost, since the time-dependent term is neglected.

Mathematically modelling in time domain does not allow the expression simplification that was made in the equation of motion 3.11 for frequency domain, and the differential terms of the motion must be kept. However, calculating the response in time steps provide more precise information for irregular wave response. The equation of motion in time domain is given by

$$\sum_{j=1}^6 \left\{ [M_{ij} + m_{ij}(\infty)] \ddot{X}_j(t) + \int_0^t L_{ij}(t - \tau) \dot{X}_j(\tau) d\tau + C_{ij} X_j(t) \right\} = E_i(t) \quad (3.28)$$

where the added mass term $m_{ij}(\infty)$ is the added mass term from frequency domain A_{ij} calculated for $\omega = \infty$. From the physical point of view of the way how the added mass term varies with the frequency, an infinite frequency is so high that, considering for example the dispersion relation of the wave in deep water $2\pi g = \omega^2 \lambda = \text{constant}$, if ω goes to infinite, the wavelength goes to zero, and Linear Theory forces the wave height to be also small to keep a small steepness. This situation thus becomes equivalent to nearly no radiated wave height.

To obtain the added mass, thus, reference should be done to equation 3.13, the real part of the complex velocity potential φ_j should be obtained. The detailed development of the boundary value problem is described on the section 3.2, of the boundary value problem without moon pool, where a Green function should be proposed. The Green function should have the shape:

$$G = \frac{1}{4\pi} \left(\frac{1}{r} + \frac{1}{r_1} \right) + \widetilde{G}_W \quad (3.29)$$

where the first parcel is the source Green function and \widetilde{G}_W is the wave-related complex term. Since for $\omega \rightarrow \infty$, there will be nearly no radiated wave height, this term is assumed to be zero. Therefore, only the source term is left, and thus the Green function has only the real part, so

$$m_{ij}(\omega) = \rho \int_S \varphi_j(P : \omega = \infty) n_i dS \quad (3.30)$$

The velocity-proportional damping term includes a memory effect expressed by the convolution of the damping coefficient with the velocity. It works as an echo function of the previous wave heights effects. The damping coefficient L_{ij} is also calculated using the frequency domain damping coefficient, by the relation below:

$$L_{ij} = \frac{1}{2\pi} \int_0^\infty B_{ij}(\omega) e^{i\omega t} d\omega \quad (3.31)$$

When the integral calculation is applied to the numerical simulation, the integral from zero to infinity is infeasible. Then, the strategy used is either to monitor the ratio of variation of the B_{ij} value as ω increases, and impose a stop criterion to assume that the value is constant, or to adjust a trend to the $B \times \omega$ curve and predict the final constant value.

Finally, the excitation force is given by the convolution of the impulse response function and the wave:

$$E_i(t) = \int_0^t h_i(t - \tau) \varsigma(\tau) d\tau \quad (3.32)$$

where the wave function is given as a time series history. The impulse response function is also calculated from the frequency domain excitation force:

$$h_i(\tau) = \frac{1}{2\pi} \int_0^\infty E_i(\omega) e^{-i\omega\tau} d\omega \quad (3.33)$$

3.2 Boundary value problem without moon pool

A hydrodynamic problem is defined by a governing equation limited by specific restrictions of the flow being studied. In potential flows, the governing equation is the Laplacian equation with boundary value specifications of the fluid domain that define the hydrodynamic problem for a mathematical modelling. That equation remains always the same, since it is derived from the continuity equation in an incompressible flow, $\text{div } \vec{v} = 0$ (div free condition), applied to a $\nabla\varphi = \vec{v}$ gradient velocity field: $\nabla^2\varphi = 0$.

Considering a regular ship without a moon pool, keeping the same coordinate system as presented in the subsection 3.1.1 of the coordinate system, the closed domain fluid surrounding it is composed by four surfaces, as illustrated in figure 30 of the coordinate system: The hull surface S_H , the bottom surface at the seabed S_B , the free surface S_F in the interface between air and water and the imaginary ring-like surrounding surface at a far distance from the hull S_∞ . The boundary conditions are:

$$\frac{\partial\varphi_j}{\partial n} = n_j \quad \text{on } S_H \quad (3.34)$$

means that there is no detaching of the particles from the hull surface, they can only slide parallel to it.

$$\left(-\omega^2 + g \frac{\partial}{\partial z}\right) \varphi_j = 0 \quad \text{on } S_F \quad (3.35)$$

implies that the height assumed by the particles at the free surface coincide with the wave curve in the interface with the air.

$$\frac{\partial\varphi_j}{\partial n} = 0 \quad \text{on } S_B \quad (3.36)$$

is equivalent to saying that there is no detaching of the particles from the seabed they can only slide parallel to it.

$$\varphi_j \rightarrow 0 \quad \text{on } S_\infty \quad (3.37)$$

means that the perturbation is only local, and vanishes for far distances from its origin, *i.e.*, vanishes in far field.

By using Green's second identity, the integral equation of the velocity potential in a given location P of the fluid domain is given by

$$\varphi_j(P) = \int_S \left(\frac{\partial \varphi_j}{\partial n} G - \varphi_j \frac{\partial G}{\partial n} \right) dS = \int_S N dS \quad (3.38)$$

where the surface S is composed by all the surfaces that define the closed fluid domain. G is the Green function that assumes different shapes according to the flow type (with or without wave, with or without current, etc.), that satisfies $\nabla^2 G = 0$. The integral expression then can be calculated separately in each surface:

$$\varphi_j(P) = \int_S N dS = \int_{S_H} N dS + \int_{S_B} N dS + \int_{S_F} N dS + \int_{S_\infty} N dS \quad (3.39)$$

and for each nucleus N apply the respective boundary value. To solve the above equation and obtain the potential $\varphi_j(P)$, a specific Green function which simultaneously satisfies the boundary condition on the free surface S_F with wave, on the bottom S_B and on the imaginary far distance lateral frontier S_∞ should be chosen. It should assume the Dirac delta function value at the singularity point. More specifically,

$$\nabla^2 G = \delta(x - \xi)\delta(y - \eta)\delta(z - \zeta) \quad (3.40)$$

$$\frac{\partial G}{\partial z} + (K - i\mu)G = 0 \quad \text{on } S_F \quad (3.41)$$

$$\frac{\partial G}{\partial n} = 0 \quad \text{on } S_B \quad (3.42)$$

$$\varphi_j \rightarrow 0 \quad \text{on } S_\infty \quad (3.43)$$

The first covers the singularity of the $G(P, Q)$ function when the points $P(x, y, z)$ on the hull and $G(\xi, \eta, \zeta)$ on S_a (as in figure 32) coincide, that its value assume the delta function for each coordinate. The development of the Green function that attends the free surface boundary condition considers a velocity potential with the shape (NEWMAN, 1977).

$$\Phi(x, t) = \text{Re} \left[\phi(x) e^{i(\omega - i\epsilon)t} \right] \quad (3.44)$$

It differs from the conventional $\phi(x) e^{i\omega t}$ by the $-i\epsilon$ adjustment. This adjustment causes the potential for $t \rightarrow -\infty$ to be zero¹, i.e. by making the initial motion equal to zero, the initial impulse delta function that contains all the frequencies is suppressed

¹ $e^{i\omega t} = \cos(\omega t) + i \sin(\omega t)$
 $e^{i(\omega - i\epsilon)t} = e^{i\omega t} e^{\epsilon t} = \text{limited function} * e^{\epsilon t} \implies t \rightarrow 0: \text{limited function} * 0 = 0$

and the isolation of 1 frequency only for analysis is allowed. The wavenumber for deep sea case results:

$$\tilde{K} = \frac{(\omega - i\epsilon)^2}{g} = \frac{\omega^2 - 2i\omega\epsilon - \epsilon^2}{g} \quad (3.45)$$

As the order of ϵ is too small, the squared term is negligible, and it can be assumed that

$$\tilde{K} \cong \frac{\omega^2}{g} - i\mu, \quad \mu = \frac{2\omega\epsilon}{g} \quad (3.46)$$

This term is for a sort of a damping term, as if there was a virtual viscosity. Since the modelling assumption is of an ideal fluid, this term has to be reduced to zero. According to Wehausen and Laitone (1960), the Green function expression is:

$$G(P, Q) = -\frac{1}{4\pi} \left(\frac{1}{r} + \frac{1}{r_1} \right) - \frac{K}{2\pi} \hat{G}(R, z_P + z_Q) \quad (3.47)$$

where

$$r = \sqrt{(x_P - x_Q)^2 + (y_P - y_Q)^2 + (z_P - z_Q)^2} \equiv \sqrt{R^2 + (z_P - z_Q)^2}, \text{ and} \\ r_1 = \sqrt{(x_P - x_Q)^2 + (y_P - y_Q)^2 + (z_P + z_Q)^2} \equiv \sqrt{R^2 + (z_P + z_Q)^2}$$

The first term becomes zero as the distances r and r_1 go to infinite. The second term depends on the derivation of $\hat{G}(R, z + \varsigma)$, where R is the finite distance between the point P and the point Q in the azimuthal plan.

$$\hat{G}(R, z_P + z_Q) \equiv \lim_{\mu \rightarrow 0} \int_0^\infty \frac{e^{-k(z_P + z_Q)} J_0(kR)}{k - (K - i\mu)} dk \\ = \oint_0^\infty \frac{e^{-k(z_P + z_Q)} J_0(kR)}{k - K} dk - i\pi e^{-K(z_P + z_Q)} J_0(KR) \quad (3.48)$$

In the last expression, the integral is a Cauchy integral and becomes zero. The wavenumber K differs from k because it is the simplified wavenumber for deep water. In the case where $k = K$, there is a singularity on the integral definition, and the numerical solution should be found in other references, such as Newman (1984). The J_0 Bessel function is given by:

$$J_\nu(z) = \sqrt{\frac{2}{\pi z}} \cos\left(z - \frac{2\nu + 1}{4}\pi\right) \text{ in this case, } \nu = 0, \text{ so} \quad (3.49)$$

$$J_0(KR) = \sqrt{\frac{2}{\pi KR}} \cos\left(KR - \frac{1}{4}\pi\right) = \sqrt{\frac{2}{\pi KR}} \operatorname{Re} \left[e^{-iKR + \frac{\pi}{4}i} \right] \text{ hence,} \quad (3.50)$$

$$G(P, Q) = -\frac{1}{4\pi} \left(\frac{1}{r} + \frac{1}{r_1} \right) - \frac{K}{2\pi} \left(-i\pi e^{-K(z_P + z_Q)} \sqrt{\frac{2}{\pi KR}} \operatorname{Re} \left[e^{-iKR + \frac{\pi}{4}i} \right] \right) \quad (3.51)$$

and as $r, r_1 \rightarrow \infty$,

$$G \rightarrow \frac{K}{2\pi} i\pi e^{-K(z_P + z_Q)} \sqrt{\frac{2}{\pi KR}} \operatorname{Re} \left[e^{-iKR + \frac{\pi}{4}i} \right] \quad (3.52)$$

Applying the boundary values at each integral term of the equation (A.1) results that some of them becomes zero, and then:

$$\varphi_j(P) = \int_S N dS = \int_{S_H} N dS + \int_{S_F} N dS \quad (3.53)$$

Also, if the above Green function is used, *i.e.*, if the Green function attends the requirement that $(-\omega^2 + g \frac{\partial}{\partial Z})G = 0$ on the free surface S_F , then the integral term on the free surface becomes zero and

$$\varphi_j(P) = \int_{S_H} N dS = \int_{S_H} \left(\frac{\partial \varphi_j}{\partial n} G - \varphi_j \frac{\partial G}{\partial n} \right) dS \quad (3.54)$$

This can be written as a matrix equation and solved numerically as described in appendix 10.

3.2.1 Wave drift force

Although the drift force is a second order phenomenon, it depends only on linear quantities, so it is possible to calculate using the velocity potential. The force can be decomposed in 2 components, x and y . The development is done for x , and can be used in the same fashion for y .

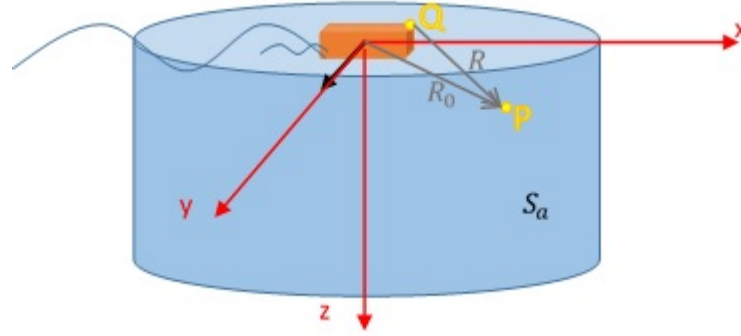
The mean drift force is given by

$$\bar{F}_x = \rho \int_{S_a} \left\{ \frac{\partial \Phi}{\partial n} \frac{\partial \Phi}{\partial x} - \frac{\partial \Phi}{\partial t} n_x - \frac{n_x}{2} \left[\left(\frac{\partial \Phi}{\partial x} \right)^2 + \left(\frac{\partial \Phi}{\partial y} \right)^2 + \left(\frac{\partial \Phi}{\partial z} \right)^2 \right] - g z n_x \right\} ds \quad (3.55)$$

where the first term is the previous instant pressure, and the last 3 terms come from the Bernoulli equation. Since there are second order terms, it is easier to calculate the

force using the far field approach, based on the momentum conservation. The integral is taken over the whole surrounding region S_a at a finite distance far away from the ship, as shown in the figure 32. The surrounding surface radius R_0 is defined, where the reference points P are used for calculation. From the wave dispersion relation $2\pi g = \omega^2 \lambda$ for deep water, it is easy to understand that for different frequencies there are different wavelengths. Therefore, just to state that R_0 is big is not enough to assure that it will be considerably big for all wavelengths. Thus, to impose that R_0 is a sufficiently far away distance, it should be stated that the amount of wave lengths is also big, so a far-field condition $KR \rightarrow \infty$ in $z = 0$ is used.

Figure 32: Short and long waves and coordinate system, P far away from the hull, contained in the volume defined by S_a and Q on the hull surface.



Source: Author.

From the second identity of Green on the surface of the hull, the integral equation of the potential is given by:

$$\Phi(P) = \int_{S_H} \left(\Phi \frac{\partial}{\partial n} - \frac{\partial \Phi}{\partial n} \right) G(P, Q) dS_H \quad (3.56)$$

Since the far field approach is being used, it is assumed that $r, r_1 \rightarrow \infty$. Replacing $G = \frac{K}{2\pi} i\pi e^{-K(z_P+z_Q)} \sqrt{\frac{2}{\pi KR}} Re \left[e^{-iKR+\frac{\pi}{4}i} \right]$ equation 3.52, and $z_P + z_Q = z + \zeta$ from becomes:

$$\Phi(P) = \frac{iK}{2} \int_{S_H} \left(\Phi \frac{\partial}{\partial n} - \frac{\partial \Phi}{\partial n} \right) e^{-K(z+\zeta)} \sqrt{\frac{2}{\pi KR}} e^{-iKR+\frac{\pi}{4}i} dS_H \quad (3.57)$$

The Green function in point P depends on the distance between it and the other points of the domain. Due to this concept of distance described as R , it is more convenient if the above expression is used in the polar coordinates. The distance R from P to Q can be rewritten in terms of $R_0 = [x_P^2 + y_P^2]^{1/2}$.

$$R = \left[(x_P - x_Q)^2 + (y_P - y_Q)^2 \right]^{\frac{1}{2}} = \left[(R_0 \cos \beta - x_Q)^2 + (R_0 \sin \beta - y_Q)^2 \right]^{\frac{1}{2}} \quad (3.58)$$

$$R = \left[(R_0^2 \cos^2 \beta - 2R_0 x_Q \cos \beta + x_Q^2) + (R_0^2 \sin^2 \beta - 2R_0 y_Q \sin \beta + y_Q^2) \right]^{\frac{1}{2}} \quad (3.59)$$

Rearranging and expanding, approximately

$$R \approx R_0 - (x_Q \cos \beta + y_Q \sin \beta) \quad (3.60)$$

Resuming the velocity potential

$$\begin{aligned} \Phi(P) = & \frac{iK}{2} \int_{S_H} \left(\Phi \frac{\partial}{\partial n} - \frac{\partial \Phi}{\partial n} \right) e^{-K(z+\zeta)} \\ & \sqrt{\frac{2}{\pi K [R_0 - (x_Q \cos \beta + y_Q \sin \beta)]}} e^{-iK[R_0 - (x_Q \cos \beta + y_Q \sin \beta)] + \frac{\pi}{4}i} dS_H \end{aligned} \quad (3.61)$$

Then, as $e^{\pi/4i} = \cos \frac{\pi}{4} + i \sin \frac{\pi}{4} = \frac{1}{\sqrt{2}}(1 + i)$ is a constant value, it represents only an offset in the velocity potential value, and can be discarded because the calculation of interest is done upon a unit motion.

$$\begin{aligned} \Phi(P) = & \frac{iK}{2} \int_{S_H} \left(\Phi \frac{\partial}{\partial n} - \frac{\partial \Phi}{\partial n} \right) e^{-K(z+\zeta)} \\ & \sqrt{\frac{2}{\pi K [R_0 - (x_Q \cos \beta + y_Q \sin \beta)]}} e^{-iK[R_0 - (x_Q \cos \beta + y_Q \sin \beta)]} dS_H \end{aligned} \quad (3.62)$$

So, for $R_0 \gg (x_Q \cos \beta + y_Q \sin \beta)$, the distance of the point Q to the origin is negligible, and the term in the square root is simplified.

$$\Phi(P) = \frac{iK}{2} e^{-Kz - iKR_0} \sqrt{\frac{2}{\pi K R_0}} \int_{S_H} \left(\Phi \frac{\partial}{\partial n} - \frac{\partial \Phi}{\partial n} \right) \left[e^{-K\zeta + iK(x_Q \cos \beta + y_Q \sin \beta)} \right] dS_H \quad (3.63)$$

The exponential term with $(x_Q \cos \beta + y_Q \sin \beta)$ cannot be neglected because it is a harmonic function:

$$(x_Q \cos \beta + y_Q \sin \beta) = (\cos K)(x_Q \cos \beta + y_Q \sin \beta) + (\sin K)(x_Q \cos \beta + y_Q \sin \beta) \quad (3.64)$$

Then, as $H(K, \beta)$ is the Kochin function:

$$H(K, \beta) = \int_{S_H} \left(\Phi \frac{\partial}{\partial n} - \frac{\partial \Phi}{\partial n} \right) \left[e^{-K\zeta + iK(x_Q \cos \beta + y_Q \sin \beta)} \right] dS_H \quad (3.65)$$

hence

$$\Phi(P) = \frac{iK}{2} e^{-Kz - iKR_0} \sqrt{\frac{2}{\pi K R_0}} H(K, \beta) \quad (3.66)$$

Changing the coordinate system of the velocity potential Φ from Cartesian to polar brings the need of also converting the coordinate system of the force \bar{F}_x from expression 3.55.

$$\bar{F}_x = \rho \int_{-\pi}^{\pi} R \cos \theta \left[-\frac{1}{4K} \left(\frac{\partial \Phi}{\partial R} \right)^2 + \frac{1}{4K} \left(\frac{\partial \Phi}{\partial z} \right)^2 - \frac{1}{2g} \left(\frac{\partial \Phi}{\partial t} \right)^2 \right] d\theta \quad (3.67)$$

The time average is then manipulated, becoming:

$$\begin{aligned} \bar{F}_x &= \rho \int_{-\pi}^{\pi} R \cos \theta \left[-\frac{1}{8K} \Phi_R \Phi_R^* - \frac{\omega^2}{4g} \Phi \Phi^* \right] d\theta \\ &= -\frac{\rho K}{8} \int_{-\pi}^{\pi} R \cos \theta \left[\frac{1}{K^2} \Phi_R \Phi_R^* + 2\Phi \Phi^* \right] d\theta \end{aligned} \quad (3.68)$$

where the potential Φ is complex and has its conjugate Φ^* for each component of excitation mode. Φ is composed by the following expressions due to the incident wave Φ_0 and to the radiated wave Φ_r :

$$\begin{aligned} \Phi_0 &= \frac{iga}{\omega} e^{-iKR \cos(\theta - \beta)}, \quad \beta \text{ is the encounter angle and} \\ \Phi_r &= \left(\frac{iK}{2} \sqrt{\frac{2}{\pi K R}} e^{-iKR + \frac{i\pi}{4}} \right) H_r(K, \theta). \end{aligned}$$

the R-derivative terms are:

$$\begin{aligned} \Phi_R &= \frac{iK}{2} \sqrt{\frac{2}{\pi K}} \left[-\frac{1}{2} \frac{1}{R^{\frac{3}{2}}} e^{-iKR + \frac{i\pi}{4}} - \frac{iK}{\sqrt{R}} e^{-iKR + \frac{i\pi}{4}} \right] \\ &H_r(K, \theta) + \frac{iga}{\omega} \left[-iK \cos(\theta - \beta) e^{-iKR \cos(\theta - \beta)} \right] = \\ &\sqrt{\frac{K}{2\pi}} \left[-\frac{1}{2} \frac{1}{R^{\frac{3}{2}}} - \frac{iK}{\sqrt{R}} \right] e^{-iKR + \frac{i\pi}{4}} H_r(K, \theta) + \frac{gaK}{\omega} \cos(\theta - \beta) e^{-iKR \cos(\theta - \beta)} \end{aligned} \quad (3.69)$$

$$\Phi_R^* = \sqrt{\frac{K}{2\pi}} \left[-\frac{1}{2} \frac{1}{R^{\frac{3}{2}}} + \frac{iK}{\sqrt{R}} \right] e^{iKR - \frac{i\pi}{4}} H_r^*(K, \theta) + \frac{gaK}{\omega} \cos(\theta - \beta) e^{iKR \cos(\theta - \beta)} \quad (3.70)$$

so that their product $\Phi_R \Phi_R^*$ will be

$$\begin{aligned} \Phi_R \Phi_R^* = & \frac{K}{2\pi} \left\{ \left[\frac{1}{4} \frac{1}{R^3} + \frac{K^2}{R} \right] H_r(K, \theta) H_r^*(K, \theta) \right\} + \left[-\frac{1}{2} \frac{1}{R^{\frac{3}{2}}} - \frac{iK}{\sqrt{R}} \right] \\ & e^{-iKR + \frac{i\pi}{4}} H_r(K, \theta) \frac{gaK}{\omega} \cos(\theta - \beta) e^{iKR} \\ & + \left[-\frac{1}{2} \frac{1}{R^{\frac{3}{2}}} + \frac{iK}{\sqrt{R}} \right] e^{iKR - \frac{i\pi}{4}} H_r^*(K, \theta) \frac{gaK}{\omega} \cos(\theta - \beta) e^{-iKR \cos(\theta - \beta)} \\ & + \frac{g^2 a^2 K^2}{\omega^2} \cos^2(\theta - \beta) \end{aligned} \quad (3.71)$$

After applying those expressions back to the equation 3.63, results that

$$\bar{F}_x = -\frac{\rho K^2}{8\pi} \int_{-\pi}^{\pi} H_r H_r^* \cos \theta d\theta - \frac{\rho K}{8} \sqrt{\frac{KR}{2\pi}} \frac{ga}{\omega} (I_1 + I_2) \quad (3.72)$$

where I_1 and I_2 are given by

$$I_1 = \int_{-\pi}^{\pi} \cos \theta [\cos(\theta - \beta) + 1] H_r^* e^{iKR[\cos(\theta - \beta) - 1] + \frac{i\pi}{4}} d\theta \quad (3.73)$$

$$I_2 = \int_{-\pi}^{\pi} \cos \theta [\cos(\theta - \beta) + 1] H_r e^{-iKR[\cos(\theta - \beta) - 1] - \frac{i\pi}{4}} d\theta \quad (3.74)$$

The incident wave direction is β , and since the drift direction is the same as the incident wave, so $\beta = \theta$. The second term of 3.72 is now rearranged to become

$$-\frac{Kga}{4\omega} (H_r + H_r^*)_{\theta=\beta} = \frac{K^2}{8\pi} \int_{-\pi}^{\pi} H_r H_r^* d\theta \quad (3.75)$$

hence the force in direction x will be

$$\bar{F}_x = \frac{\rho K^2}{8\pi} \int_{-\pi}^{\pi} H_r H_r^* (\cos \beta - \cos \alpha) d\alpha = \frac{\rho K^2}{8\pi} \int_{-\pi}^{\pi} |H_r|^2 (\cos \beta - \cos \alpha) d\alpha \quad (3.76)$$

where α is the integral variable of the round surface and β is the incident wave angle. The symbol θ was replaced by α to avoid mixing different variables with the same name. It should be noted that the Kochin function above is composed by the radiation and diffraction terms

$$H_r = \sum_{i=1}^6 i\omega \xi_i H_i + \frac{iga}{\omega} H_7 \quad (3.77)$$

In the same fashion, the y component is obtained

$$\bar{F}_y = \frac{\rho K^2}{8\pi} \int_{-\pi}^{\pi} H_r H_r^* (\sin \beta - \sin \alpha) d\alpha \quad (3.78)$$

Finally, the mean drift force D is obtained by vector addition of the two components,

$$\bar{D} = \sqrt{\bar{F}_x^2 + \bar{F}_y^2} \quad (3.79)$$

The steady drift force in a regular wave is a function of the square of wave amplitude, a^2 . The mean steady drift force in an irregular wave condition is calculated by

$$\overline{D(H_s^2, T_s, \beta)} = 2 \int_0^\infty F_D(\omega, \beta) S_w(\omega; H_s, T_s) d\omega \quad (3.80)$$

Yields that the mean steady drift power by incident wave, $P_D(H_s^2, T_s, \beta)$, is

$$P_D(H_s^2, T_s, \beta) = \overline{D(H_s^2, T_s, \beta)} \times U = \overline{D(H_s^2, T_s, \beta)} \frac{2\pi H_s}{T_s} \quad (3.81)$$

where $U = \frac{2\pi H_s}{T_s}$ is the equivalent wave particle speed. Since the drift force is function of the square of wave amplitude and the speed is function of the wave amplitude as well, the power will be function of the cube of the wave amplitude.

3.2.2 Vertical bending momentum

If we consider the whole ship as a beam, the bending moment at a specific section x is given by the integral of the moments caused by the shear acting in each section from the ends to S . The shear force applied to the ship is composed by a resultant of inertia, buoyancy and hydrodynamic load. The wave induced loads at section x , $V_i(x)$, are calculated by the following equations (TAKAGI; ARAI, 1996).

$$V_i(x) = I_i(x) - \int_{AP}^x p n_i dS \quad (3.82)$$

where I_i is the inertia force for the i^{th} degree of freedom, and p is the dynamic pressure. The inertia for the vertical bending moment is I_5 :

$$I_5(t) = \int_{AP}^{x_0} m(x)(x_0 - x) \{ \ddot{X}_3(t) - x \ddot{X}_5(t) \} dx + \int_{AP}^{x_0} m(x) \overline{z(x)} \ddot{X}_1(t) dx \quad (3.83)$$

$$I_5(x) = \int_{AP}^{x_0} m(\xi) \{ \ddot{X}_3 - \xi \ddot{X}_5 + \overline{x_G(\xi)} \ddot{X}_1 \} d\xi \quad (3.84)$$

where $m(\xi)$ is the mass of the section, X_i and \ddot{X}_i are respectively the motions and accelerations in the i^{th} motion mode and $\overline{Z_G}(\xi)$ is the approximate height of the centre of gravity of the section. As described in the following equation, in the case of the vertical bending moment, the dynamic pressure will be the resultant of the balance between the motion in each of the 6 modes (first term), corrected for each location of the ship section (second term) and the buoyancy response, accounting the incident and diffracted waves (last term).

$$p = \rho \omega^2 \sum_{j=1}^6 X_j \varphi_j + \rho g (X_3 + yX_4 - xX_5) - \rho g a (\varphi_0 + \varphi_7) \quad (3.85)$$

here, ρ is the water density and φ_i are the velocity potentials of each mode. The indexes 0 and 7 are for incident wave and diffracted wave.

3.3 Boundary value problem with moon pool

One of the main problems of the drill ship operability issue is the moon pool free surface height response in comparison to its wall free board. The MP consists on an opening in the bottom of the hull around which a surrounding wall is attached from bottom to nearly the same height of the outside hull. The water fills in the inner space limited by this wall, and in calm water with no advance speed nor ship motion, it reaches the same height as the sea water level. This free surface however will assume different behaviour from the outside water when ship motion exists, not only because the ship motion generates wave both inside the MP and outside it, but also because it is a restricted area.

The generated progressive waves outside the hull travel from the ship's location towards to the unlimited surrounding space until they vanish. In the case of the waves inside the MP, they meet the opposite wall and reflect, in self-superposition. The overlap of those waves in addition to the ship squatting due to its wave response motion may cause such a constructive interference that the resultant wave heights become too high in comparison to the free board of the moon pool and cause overflow. This phenomenon is investigated through velocity potential calculation to find the main motion frequency at which the overflow might happen.

Although the incoming wave is independent from the existence of the ship, all the other resultant phenomena such as the ship motion itself and the waves resulting from the whole interaction are interdependent. Thus, the water motion inside the moon pool of the drill ship also depends on the ship response, and a Response Amplitude Operator (RAO) can be calculated.

The boundary value problem for a regular hull standard modelling description is presented in the section 3.2 of the boundary value problem without moon pool. When the hull has a moon pool opening, additional information should be used. For a potential flow model, the governing equation is the Laplacian, $\nabla^2 \Phi = 0$. The boundary conditions for the ordinary hull are:

$$\frac{\partial \varphi_i}{\partial n} = n_j \quad \text{on} \quad S_H \quad (3.86)$$

$$\left(-\omega^2 + g \frac{\partial}{\partial z} \right) \varphi_j = 0 \quad \text{on} \quad S_F \quad (3.87)$$

$$\frac{\partial \varphi_j}{\partial n} = 0 \quad \text{on} \quad S_B \quad (3.88)$$

$$\varphi_j \rightarrow 0 \quad \text{on} \quad S_\infty \quad (3.89)$$

When there is a moon pool, due to the additional moon pool wall surface S_M and its inner water free surface S_{MF} , two additional boundary conditions are imposed. The first is:

$$\frac{\partial \varphi_i}{\partial n} = n_j \quad \text{on} \quad S_M, \quad (3.90)$$

which has the same meaning as the outside hull surface condition, that there will be no particles detaching, and they are allowed only to slide along the solid surface. The second condition is the free surface condition on S_{MF} . For this last one, if a boundary condition is assumed to be the same as the one for S_F , the height response would be too exaggerated, which does not correspond to reality. This happens because the only dissipation of energy happens through radiated waves in potential model (AALBERS, 1984), (FALTINSEN; ROGNEBAKKE; TIMOKHA, 2007). Due to this fact, the so-called Rayleigh damping term is used (more details in the section 3.2 of the boundary value problem without moon pool, from where the damping term μ from equation 3.46 is kept), and the wavenumber K from the free surface S_F boundary condition is replaced by $\tilde{K} \approx \omega^2/g - i\mu$. The final boundary condition becomes:

$$\left(-\omega^2 + g \frac{\partial}{\partial z} \right) \varphi_j + i\mu \varphi_j = 0 \quad \text{on} \quad S_{MF} \quad (3.91)$$

The Rayleigh damping coefficient μ value is adjusted using experimental data. Applying the above boundary conditions with the appropriate Green function G that satisfies simultaneously the boundary conditions: at the free surface with waves, at the

sea bottom surface and far away from the body at the infinite surrounding surface, the velocity potential derived from Green's second identity is given by

$$\varphi_j(P) = \int_S \left(\frac{\partial \varphi_j}{\partial n} G - \varphi_j \frac{\partial G}{\partial n} \right) dS = \int_S N dS = \int_{S_H+S_M} N dS + \int_{S_{MF}} N dS \quad (3.92)$$

Since the moon pool walls belongs to the hull, with the same boundary conditions, the integral term is calculated on those surfaces together.

Making a more detailed observation of the conditions at the free surface inside the MP, the normal vector to the element surface points to the seabed, which coincides with the z -axis. Also, as the Rayleigh damping is experimentally adjusted, the value can be set with other scales, such as g , for convenience. The wavenumber $K = \omega^2/g$ differs from k because it is the simplified wavenumber for deep water:

$$\left(-\omega^2 + g \frac{\partial}{\partial n} \right) \varphi_j + i\mu \varphi_j = 0 = \left(-\omega^2 + g \frac{\partial}{\partial z} \right) \varphi_j + i\mu \varphi_j \quad (3.93)$$

$$\frac{\partial \varphi_j}{\partial n} = \frac{-i\mu \varphi_j + \omega^2 \varphi_j}{g} = (K - i\mu^*) \varphi_j \quad \text{on } S_{MF} \quad (3.94)$$

Replacing the potential derivatives by the correspondent boundary values, results:

$$\varphi_j = \int_{S_H+S_M} \left(n_j G - \varphi_j \frac{\partial G}{\partial n} \right) dS + \int_{S_{MF}} \left[(K - i\mu^*) G - \frac{\partial G}{\partial z} \right] \varphi_j dS \quad (3.95)$$

From this point, a matrix equation is solved to obtain φ_j as shown in appendix 10, of the matrix-shaped equation of the potential expression.

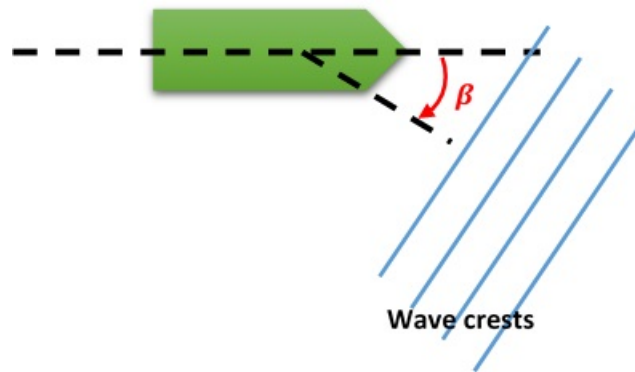
3.4 Effect of MP on motion RAO

An optimal mesh of hull was defined as described in section 5.1, and the hydrodynamic response module was used to calculate the motion RAO of the drill ship for 7 wave incidence angles. The angle of incidence is defined between the longitudinal centreline of the hull and the propagation velocity of the wave train, as shown in figure 33.

Table 5: Units of the motion RAOs

Description	Motion	Variable	unit
Translation x -axis	Surge	X_1/a	m/m
Translation y -axis	Sway	X_2/a	m/m
Translation z -axis	Heave	X_3/a	m/m
Rotation x -axis	Roll	X_4/a	deg./m
Rotation y -axis	Pitch	X_5/a	deg./m
Rotation z -axis	Yaw	X_6/a	deg./m
Lateral drift force		$\bar{F}_y/\rho g a^3$	m
Vertical bending moment amidship		M/a	ton-m/m
Oscillation of free surface inside MP		ζ/a	m/m
Abscissa axis		ω	rad/s

Source: Author

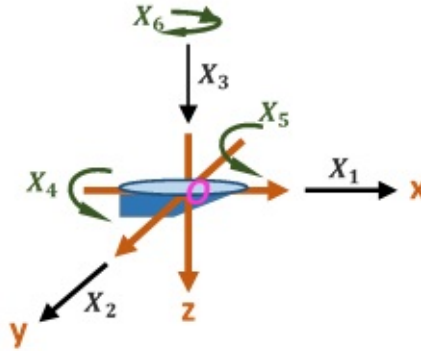
Figure 33: Incident angle β 

Source : Author.

As explained in subsection 2.1.1, a Response Amplitude Operator (RAO) for a given motion mode is a transfer function that determines the amplification of the reaction of the system to the excitation of waves with unit height. Since it is a linear response calculation, one can simply multiply the non-unit amplitude of the input wave by the response amplitude from RAO to obtain the actual output of the response to wave excitation. For each excitation frequency, the amplitude of the response motion has a value, and with the collection of those response amplitudes for a range of regular frequencies, a chart is obtained. Usually the RAOs are expressed in nondimensional units. Because of the way how the RAO will be used, the presented values are provided in units as shown in table 5. The calculated irregular wave responses use linear superposition between RAO and irregular wave spectrum $S(\omega)/H$, and are only divided by significant wave height. Hence the standard deviations of the irregular response are divided by significant wave height, R/H and the threshold wave heights can be easily obtained from equation 4.8 of section 4.2.

The figures 35 to 40 present the charts of motion RAO of the drill ship hull with and without moon pool for different incident wave angles in each degree of freedom (illustrated in figure 34).

Figure 34: Degrees of freedom in ship motions.



Source : Author.

First a discussion about the hull RAO without moon pool in the (a)-figures, and after a discussion about the influence of the presence of the opening is done in comparison with the RAO for the hull with rectangular moon pool in the (b)-figures.

The chart in figure 35(a) shows the response to waves in the X_1 mode of motion (surge), that is the oscillating translation in the x -axis direction. The incident angles $\beta = 0^\circ$ and $\beta = 180^\circ$ - respectively corresponding to head and following seas coincide in the chart, and are the ones to which the response is the biggest, with almost the same amplitude as the excitation, since they are parallel to the analysed motion direction. The same happens to the response in X_2 (sway), shown in figure 36(a) for the incident angle of 90° , which is beam sea: since it is the direction parallel to the analysed motion: y -axis oscillating translation, it is the one with the biggest response, that is almost the same as the incident wave amplitude. In both cases, as the angles get farther from the ones in which the peak happens, the response becomes gradually smaller until it is minimal at right angles of incidence to the direction of the motion in study. Furthermore, the bigger responses are located in a range of lower frequencies, usually lower than $\omega = 0.9$ rad/s.

In the figure 37(a), the chart of the heave response, X_3 , starts in the lower frequencies where the vertical oscillation response has the same amplitude as the incident wave, regardless the incidence angle. It is easy to imagine that, since the small frequencies would vary the height in such a slow motion, its effect would be the same as if it were a swell. On the other hand, for higher frequencies, above $\omega = 1.2$ rad/sec., because the wave amplitudes become very small, the excitation is negligible in comparison to the order of the ship's inertia.

Inside the range between those extreme values, as the frequency increases, the

response decreases in most incident angles, in a proportion as the projected area of the ship perpendicular to the incidence decreases. Exceptions happen to the response to the wave excitation with incident angle $\beta = 90^\circ$ (beam sea). The response evolves to values higher than the excitation, characterizing a resonant behaviour with a maximum of $X_3/a \cong 1.5$ in $\omega \cong 0.7$ rad/sec. Other smaller peaks happen for the other incident angles around $\omega \cong 0.75$ rad/sec., that follow the trend of bigger response than the neighbour frequency values as what happens with $\beta = 90^\circ$, but keeping the amplitude smaller without resonance.

The drill ship has approximately no damping in angular motion around the longitudinal axis, X_4 (roll), even though viscous roll damping is considered in this model. Its hull has a bit rounded transversal section symmetric about the Oxz -plane and no bilge keels or other appendages to increase the damping. Furthermore, the righting momentum is small due to low water plane inertia momentum relative to the x -axis. As can be seen in figure 38(a), all the wave incident angles lead to a resonant peak around $\omega = 0.4$ rad/sec. and, as would be expected, among those the highest amplification is for the beam sea (perpendicular to the rotation axis) with the bigger amplitude responses happening in a low-frequency range.

When observing the responses in rotation motions, the same behaviour is identified in all the charts: figure 38(a) of roll motion, and the other motions around the y -axis (pitch) and z -axis (yaw), respectively X_5 and X_6 , shown in the figures 39(a) and 40(a). For $\omega \rightarrow \pm\infty$, the amplification tends to zero. In lower frequencies, since the wavelength of the exciting waves would be big in comparison to the ship's length, the effect would be the same as in heave, as if it were a swell situation, causing vertical motion but almost no inclination in any axis. In higher frequencies, the wavelength would be too short in comparison to the length of the ship, that would in average cause no discrepancy in elevation between the extremes in each main axis.

In the pitch motion RAO of figure 39(a), all the incidence angles present a peak in $0.75 < \omega < 0.85$, where the angles $\beta = 60^\circ$ and $\beta = 120^\circ$ result in resonant behaviour. Except for when the angle of incidence is perpendicular to the plane of rotation Oxz , *i.e.*, $\beta = 90^\circ$ (marked with dots in the chart), all the remaining curves present a trend to have an increasing response leading to a peak around $\omega \cong 0.5$.

The chart of yaw RAO (X_6), shown in figure 40(a), is the oscillatory rotation motion response around the z -axis. As expected, the head and following seas provoke no effect in those motions. A very simplified explanation, neglecting 3D-effects is that, the resultant momentum to the projected plan of the ship in Oyz would be symmetric about the z -axis. For the same reason, the yaw response for $\beta = 90^\circ$ is small since the projected plan of the ship in Oxz -plane would be nearly symmetric about the z -axis, when considering that the difference between bow and stern in comparison to the

parallel middle body is small.

In both cases of pitch and yaw, the curves of the responses nearly coincide in pairs for the angles that are symmetric about the Oyz -plane. They are not exactly coincident as in the roll case, because the ship is not symmetric about that plane. A noticeable discrepancy in the trend of the charts happens at all non-zero curves in $\omega \cong 0.4$ rad/sec because of the influence of roll resonance that can be identified in the figure 38(a). Due to the symmetry of the ship about the vertical plane Oxz , there is no coupling between the roll and the motions in the vertical plane motions (heave, pitch, and surge). If there was no symmetry, the coupling would happen between them as well.

In the yaw chart, for each pair, in the frequency $\omega \cong 0.4$ rad/sec the local peaks have opposite directions: for $\beta \leq 90^\circ$ there is a crest peak, and for $\beta > 90^\circ$ there is a trough peak. The difference has to do with the phase difference between the yaw and roll responses, that in the first case are constructive and in the latter case are destructive in the composition of the amplitude. Although not resonant, the responses in yaw where the biggest peak values are located correspond to the same values of incident wave angles as in pitch: $\beta = 60^\circ$ and $\beta = 120^\circ$, because they present the biggest unbalance between the two parts (fore and aft) relative to the centre of gravity G .

The influence of the existence of an opening as the moon pool can be observed in the charts from figure 35(b) to figure 40(b), where the RAO curves described above are compared to the RAO of the same hull with opening. The simple rectangular moon pool was included in the previously examined hull, as described in section 5.1 (case 4), positioned at midship and with length and width respectively 20.32m and 11.188m.

Figure 35: Drill ship RAO : surge, X_1 for various incidence angles. (a) without MP, and (b) with MP.

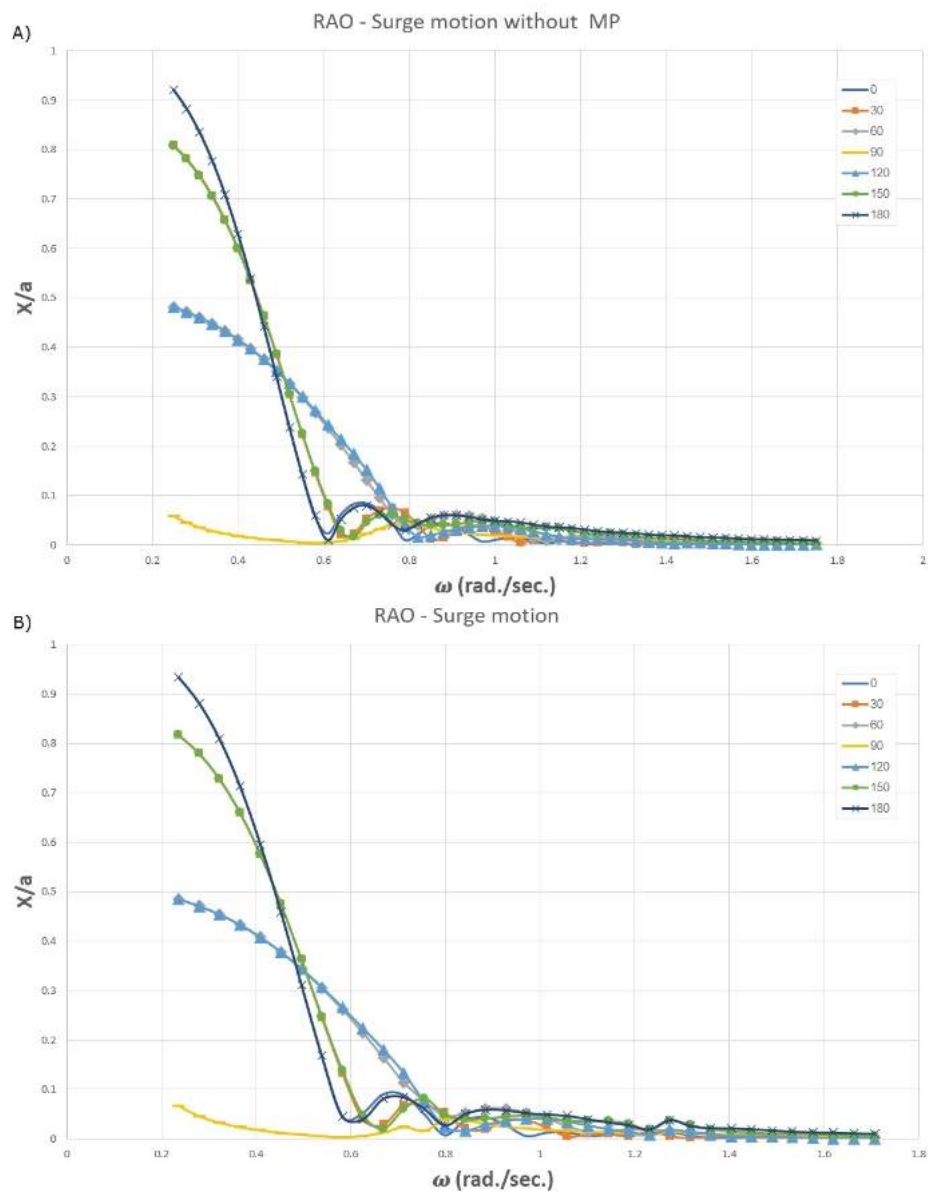


Figure 36: Drill ship RAO: sway, X_2 for various incidence angles. (a) without MP, and (b) with MP.

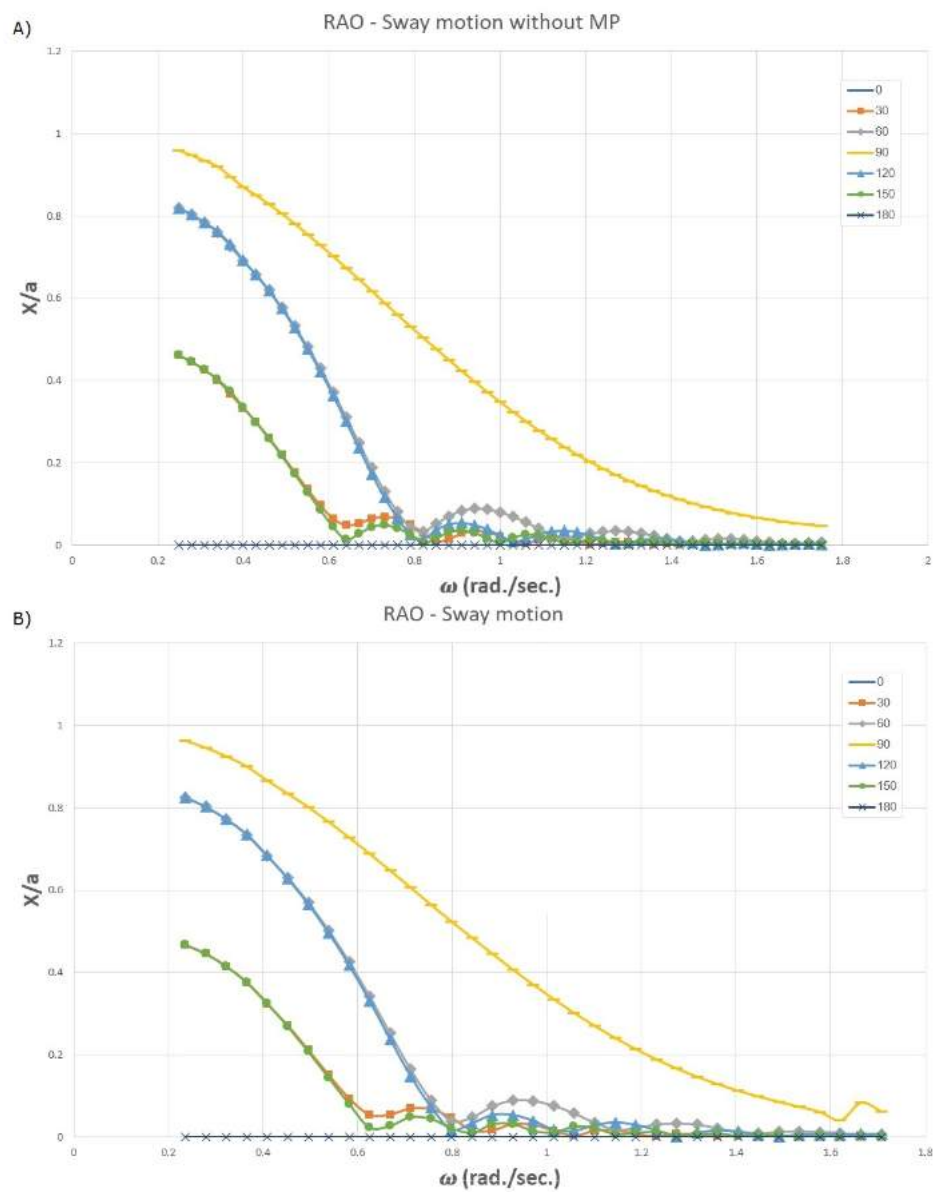
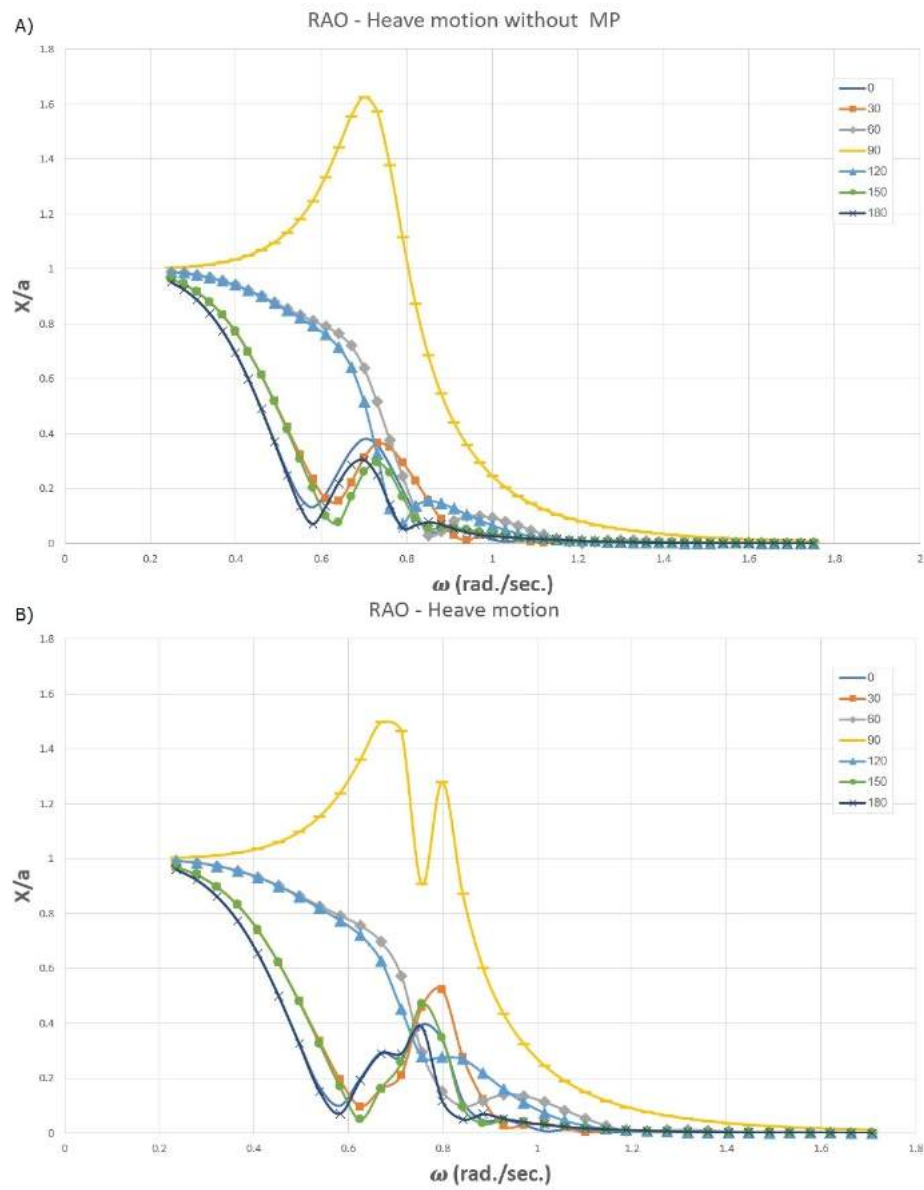
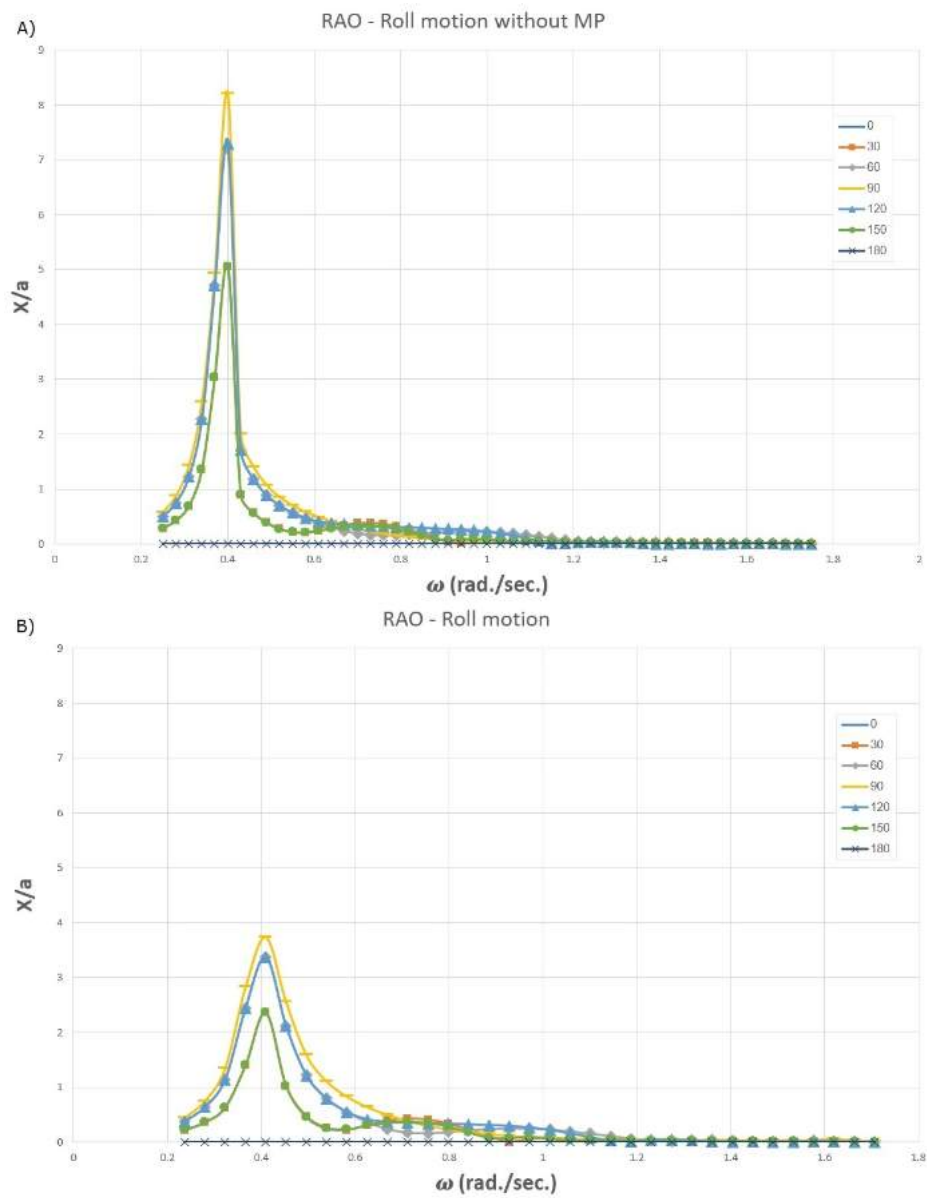


Figure 37: Drill ship RAO: heave, X_3 for various incidence angles. (a) without MP, and (b) with MP.



Source : Author.

Figure 38: Drill ship RAO: roll, X_4 for various incidence angles. (a) without MP, and (b) with MP.



Source : Author.

Figure 39: Drill ship RAO: pitch, X_5 for various incidence angles. (a) without MP, and (b) with MP.

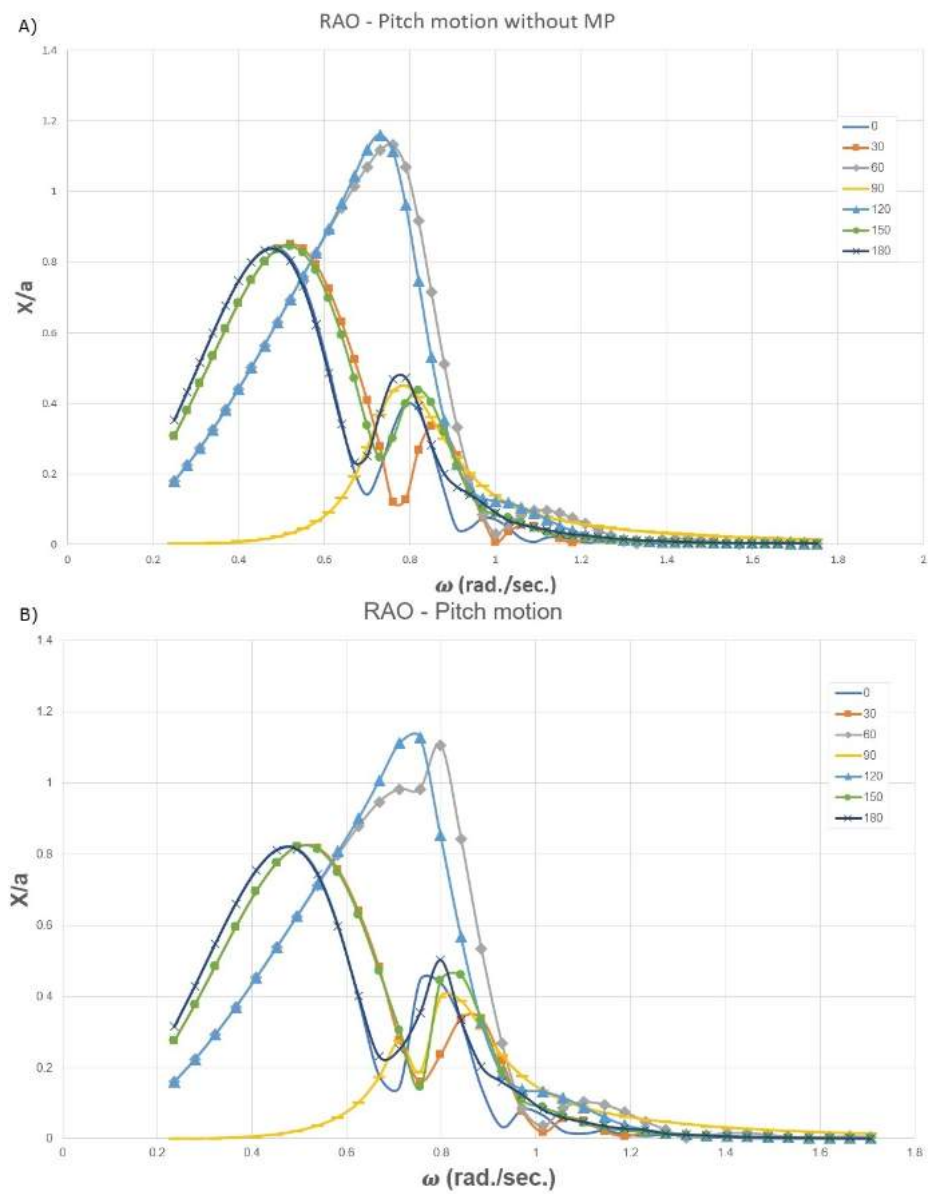
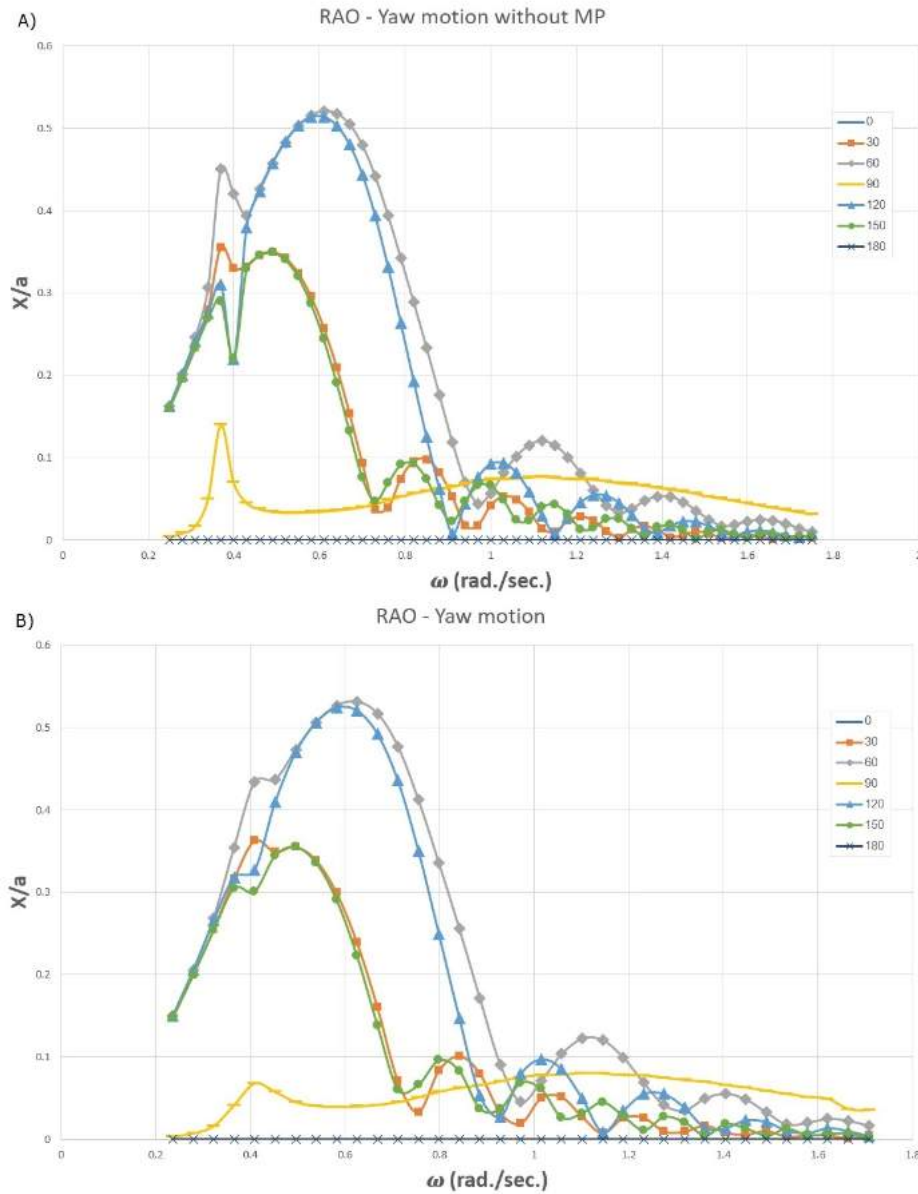


Figure 40: Drill ship RAO: yaw, X_6 for various incidence angles. (a) without MP, and (b) with MP.

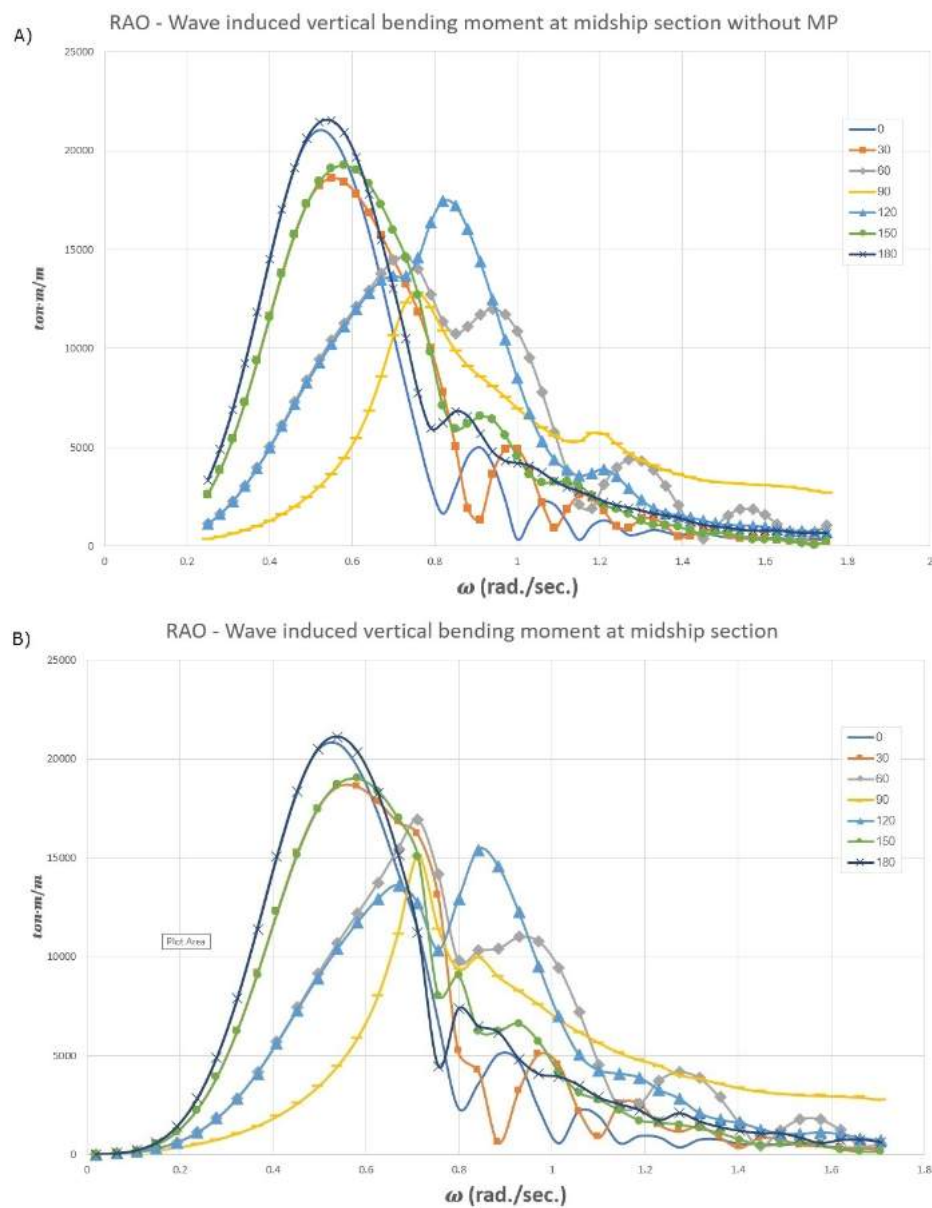


Source : Author.

It is observed that among the modes of motion present there are almost no changes in response when there is the moon pool, except for heave, roll and yaw, respectively X_3 , X_4 and X_6 , and the differences are only around the resonance frequency. In both cases the roll resonance is identified in the region around $\omega = 0.4$ rad/sec. The existence of a moon pool results in a considerable reduction of the peak modulus for roll, which reflects also in the yaw mode response, as a damping due to counterphase with the moon pool's internal water motion. The natural frequency for heave motion is around $\omega = 0.7$ rad/sec., after which (in a slightly higher frequency) where there is a sudden decrease when there is the moon pool, probably due to the influence of the

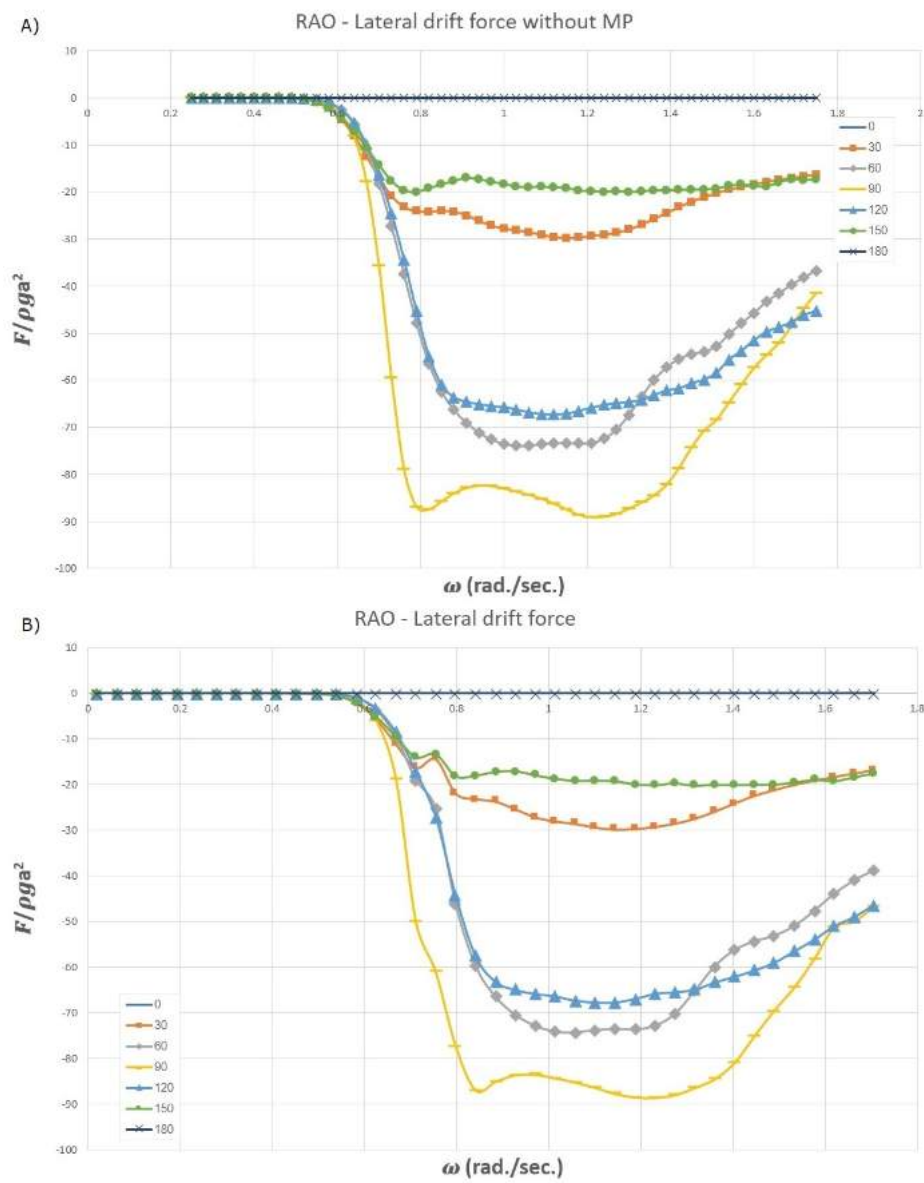
internal water action with a damping effect. From the point of view of the wave effects considered in the present work, besides the heave motion there are the lateral drift force and vertical bending moment, that is evaluated at the midship section. The RAO charts are shown in figures 42 and 41 with and without moon pool, followed by the RAO of the MP internal water at mid of the opening in figure 43. The natural frequency of the piston oscillation mode of the MP internal water is around 0.76 rad/sec., close to the heave motion natural frequency. The amplification of free surface motion is due to its combination with the radiation velocity due to vertical motion of the ship. The sloshing resonance can be found around a higher value, around 1.6 rad/sec., which is a range to which the influence to heave motion will be negligibly small. The presence of the opening is almost not changed for the drift force response, of which the range around 0.76 rad/sec. that is the peak of resonance of the MP internal water, the response is a bit damped for the case with opening in the incidence angles $\beta = 30^\circ$ and $\beta = 150^\circ$. This shows that the operability will be more dependent of the hull itself than of the interaction with its moon pool, from the point of view of station keeping. Due to reduction of the section modulus, the vertical bending moment response at the mid section of the hull presents some changes. Among them, the most significant are around the frequency $\omega = 0.71 \text{ rad/sec.}$ at incidence angles $\beta = 60^\circ$ and $\beta = 90^\circ$.

Figure 41: Drill ship RAO: vertical bending moment at midship section for various incidence angles. (a) without MP, and (b) with MP.



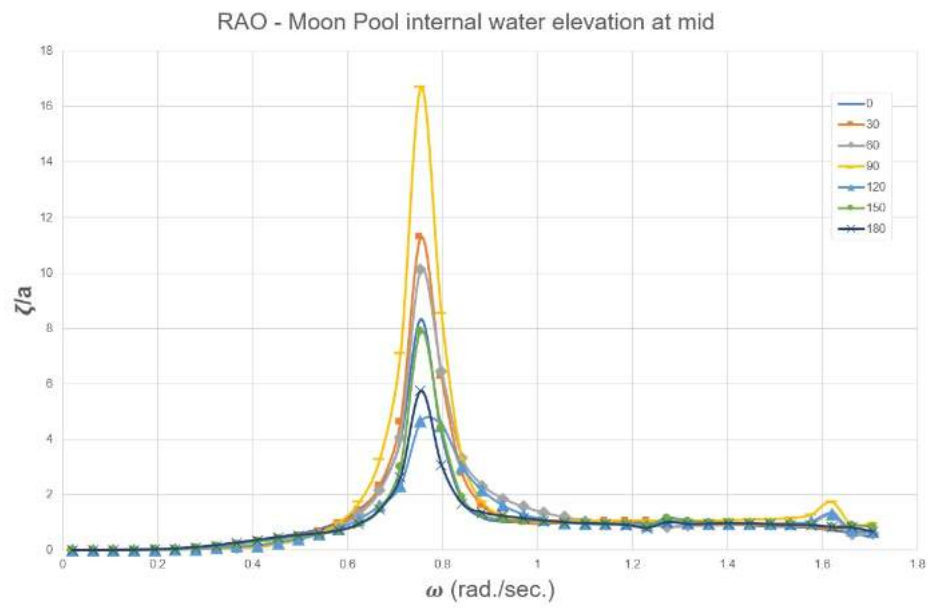
Source : Author.

Figure 42: Drill ship RAO: lateral drift for various incidence angles. (a) without MP, and (b) with MP.



Source : Author.

Figure 43: Drill ship RAO: MP water motion at mid for various incidence angles.



Source : Author.

4 Methodology

There are two outputs from the proposed objectives: the tool that will define the optimum geometry and dimensions of the moon pool, and the operability chart. Hull mesh, ranges of significant wave period, spectrum models and analysis, and moon pool dimension limitations, as well as evolutionary algorithm parameters, are chosen by the user.

The operability of the ship is judged under different criteria. For each of them, the threshold wave heights that divide the global performance into operable or inoperable are calculated for each value of the significant wave periods range. The calculation was carried out through numerical simulation of the seakeeping behaviour using a hydrodynamic calculation module, developed in Fortran language (KAWABE, 2017). Modules related to the search algorithm were developed by the author in Matlab.

Evaluation criteria and limits were elaborated considering the piston mode of oscillation of the water plug as recommended by DNV (2011). The responses used were the ones from time domain calculation, varying the angle of incidence of the wave.

The summary of all the limits of operability per criterion define the most limited operable zone for that moon pool. The fitness grade to be maximized will be the area of operable zone, which in turn is directly related to shape, dimensions and location (DAY, 1990)

Since the moon pool will be prismatic, the search will be done by evolutionary strategy simply upon variations of configuration of the section parallel to the waterline. The contour lines are sectioned and associated to parameters that allow those variations. The description of the MP can be then replaced by the set of parameter values, and these will be the “genes” of an individual for the evolutionary strategy.

In the following subsections the search strategy for optimum solution is summarized based on what was already presented in the detailed review of section 2.3. The assessment values for the criteria are presented subsequently.

4.1 Performance and fitness grading

As presented by Day (1990), ideally, in a typical usage of the design performance analysis of moon pools, a detailed operational model should be established, including details of the expected duration for each operation stage, limiting factors that could delay or impeach it, and a predefined protocol indicating points in which the operation could be resumed if interrupted on each stage. It is also necessary to know the statistics of

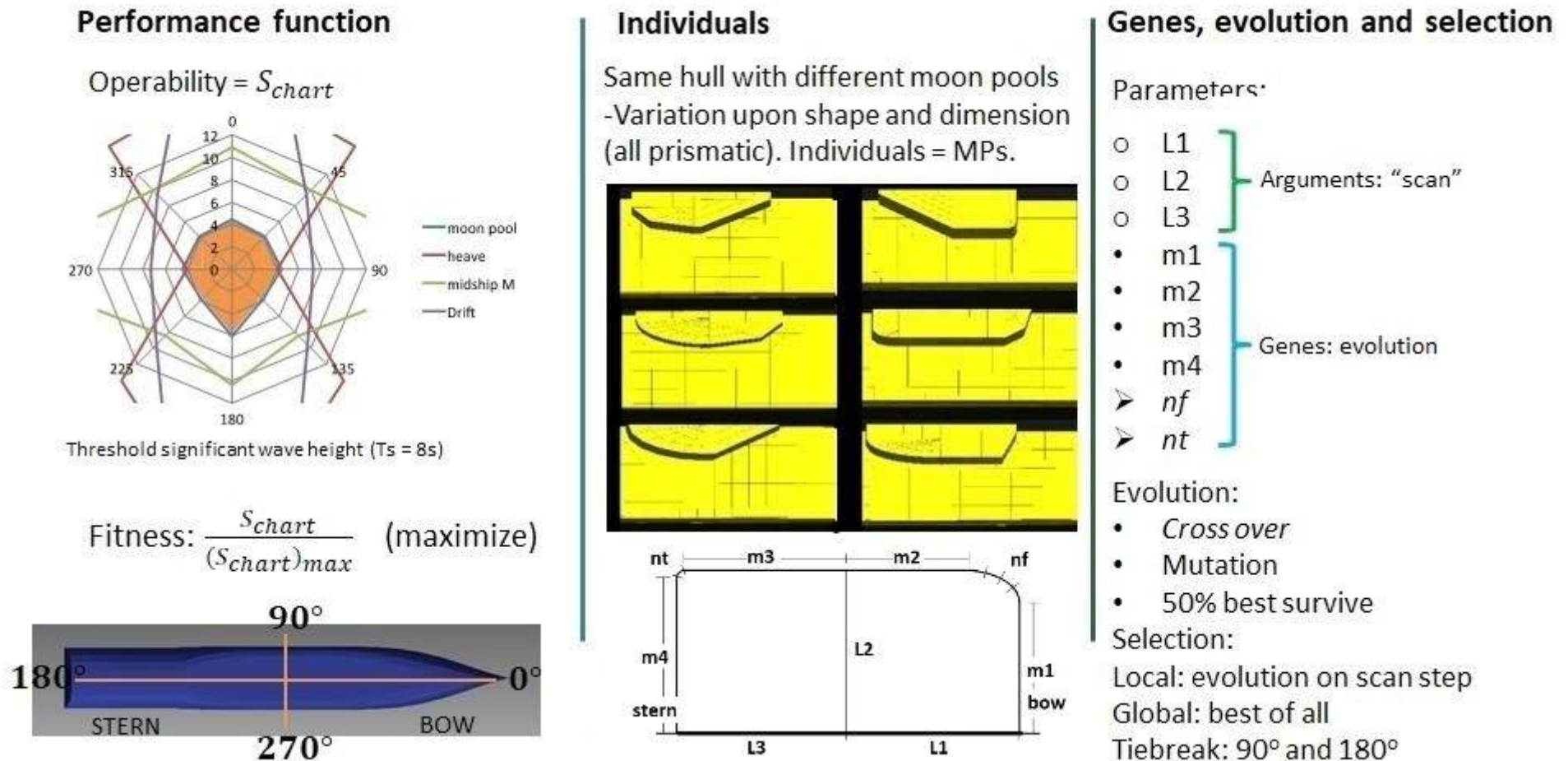
occurring of different sea states and the probability of transitions between them in the operation area. Thus, the sea state would be treated as a Markov process, changing values in regular intervals (e.g., each 4 hours), and a series of long-term events (e.g., 1 month) generated. For each event, the operational model would be used to calculate the downtime of the system; once an enough amount is simulated, the average downtime can be calculated as the simple average of the individual values. The annual predicted time would be then obtained by adding the individual periods, regarding the frequency of work execution.

There are some design methods for use in DNV (2012) that would be suitable to the approach described above: Load and Resistance Factor Design (LRFD), Permissible Stress Method, and Probabilistic method, besides the design assisted by testing. The first two are commonly used in design, but in this work the latter was targeted. According to the code, in Probabilistic design method:

- The evaluation of safety may be based on probabilistic methods, in which calculations are made to determine the probability of failures making use of a probabilistic description of the joint occurrence of the relevant parameters involved, considering the true nature of the failure domain. All relevant failure modes shall be considered.
- All parameters that are essential in the analysis of a failure criterion shall be described as stochastic variables. Such parameters are loads and materials' strength, geometry, imperfections, uncertainties in the failure criterion model used, etc.
- Probabilistic analyses may be directly used as a design method or it may be used in combination with another method. A benefit of this method may be achieved for the determination of partial factors, to be used in dynamic problems, associated with the determination of design loads for floating and compliant structures.
- In probabilistic design analyses the design criteria are normally the calculated probabilities of failure and shall not exceed specified target probabilities.
- The target probability of failure for an individual structural element shall never be higher than the target value for the total system to be met.

The performance analysis of the moon pool in the drill ship used in the present work is based on the strategy described in the detailed review of section 2.3 to meet as much as possible the above-listed conditions. An illustration of the strategy is shown in figure 44.

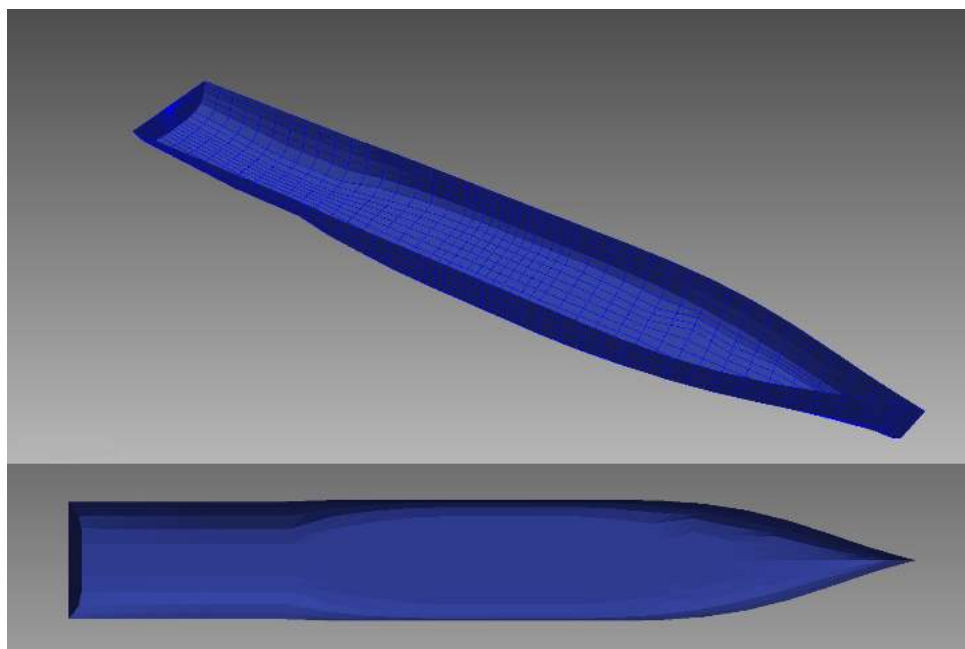
Figure 44: Overview of the strategy used for optimization



Source: Author

If the criteria are all evaluated using the same measure, which was defined to be the Threshold significant Wave Height (TWH), the operable zone will be the result of intersection of the individual radar charts of TWH values in each wave incidence angle per criterion superposed. Its area represents how much operable in general sense that a moon pool can be. The fitness grade was chosen to be the area of that zone, that should be maximized. An individual is the input hull to which a moon pool is generated and coupled. Figure 45 shows the mesh of the hull without opening used as input in the present work. The coupling is done by creating the opening with the shape of the moon pool at the bottom of the hull and attaching a wall to it. This wall consists in the perpendicular prismatic extension of the opening, as if the opening was extruded.

Figure 45: Mesh of the hull without opening used as input in the present work

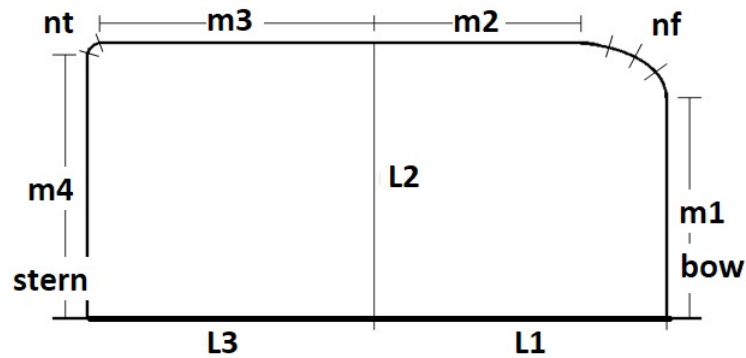


Source: Author

Among the individuals, the difference are the moon pool shapes that, in turn, are defined by values of the dimension and shape parameters. The parameters used in this work are similar to the presented in section 2.3 of the detailed review, but with some modifications. A new dimension parameter $L3$ was added for an independent longitudinal length of the aft part of the moon pool. This might displace a bit the position of the centre of the MP relative to the longitudinal centre of gravity of the ship, LCG. This might not be any problem as long as LCG is kept inside the moon pool region to assure less angular motion effects of the internal water. Figure 46 shows the new parameter configuration. More discussion about the segments of the border can be found in section 2.3 or in the original text by Cavalcante (2015).

The parameters are:

Figure 46: Border parameters of the moon pool, symmetric about the longitudinal centre line. The fore points towards to the right, and aft to the left.



Source: Adapted from Cavalcante (2015)

- L1: longitudinal fore-length, argument parameter;
- L2: transversal half-length, argument parameter;
- L3: longitudinal aft-length, argument parameter;
- m1: transversal coordinate of the fore corner polygon, dependent parameter;
- m2: longitudinal coordinate of the fore corner polygon, dependent parameter;
- m3: longitudinal coordinate of the aft corner polygon, dependent parameter;
- m4: transversal coordinate of the aft corner polygon, dependent parameter;
- nf: number of segments of the fore corner polygon, independent non-argument parameter;
- nt: number of segments of the aft corner polygon, independent non-argument parameter;

For the optimization, thus, the genes are those parameters. The dimensions and centring position relative to the longitudinal centre of gravity (LCG) represented by the “L” parameters are varied within a silly sort, hence scanned at each combination of possible values, and the remaining “m” and “n” parameters are varied within the genetic algorithm. In the optimization process, the generations are evolved through crossover, mutation and selection of the best 50 percent of the individuals. In each combination of values inside the silly sort, the best individual is selected and stored with its grades as local best, for final comparison among those that will result in the global best. If there is a tie, the biggest threshold significant wave height of the operable zone at 90° and 180° are respectively the first and second tie-breaks.

4.2 Assessment formulae for the criteria

To allow ranking different projects in a rational way, Day (1990) says that one has to choose a basis on which the performance will be judged. A criterion that should

be mandatory to consider in any engineering project is the downtime in long term. In the case of moon pool, the downtime problem may have several origins: inadequate structural design, constructive shortcoming, accidental damage or excessive oscillation of the water column. The latter can be considered an appropriate criterion by which the design performance can be judged: The shorter it is, the better will the performance be. Given a suitable analysis model for the hull / moon pool / submerged system, the prediction of downtime can be done by operability analysis.

In the case of a drill ship, it is considered that the time in operation does not require a long term analysis, hence the development was all done focusing in short term, but in case of platforms or other structures that stay in the same place for longer periods, such analysis is required. Comments and development for long term can be found in the appendix 10.

As presented in the introduction of this section, criteria are used for assessment of the candidate solutions to obtain an optimal design. The number of criteria used in this research can be further increased by including as many other criteria as wanted, just regarding that the measurement parameter should be the same as the previous ones, for matters of compatibility with the variable used in the operability chart and fitness evaluation. Michima and Kawabe (2014b) describe the strategy used to define the limits to all the involved criteria as function of the same parameter, explained as follows.

All the problems that happen to a system in terms of seakeeping are related to the sea state characteristics (the significant wave height H_s , significant wave period T_s and their distribution, expressed by the spectra). The choice of a common parameter to use as limit of operability naturally should be done among them. The causes of downtime are loss of balance between the hardware capabilities to compensate or cope loads or dimensions and the exceeding energy of the waves that were expressed in any way such as drift, heave, wave height causing green water, high accelerations in the vertical plane, etc. The wave energy in transit is identified by the wave height: the higher waves carry bigger energy. In this sense, one identifies in an irregular wave spectrum which are the frequencies of regular wave components that would excite the system with more intensity.

Defined as the average of the third part of the biggest wave heights registered in a given sea state, the significant wave height is understood as the expected value of the highest crests in that sea state, and represents a big part of the energy loads that excite the system, and it is the parameter to assess each criterion: there shall be a limit value of significant wave height at which the above-mentioned loss of balance will happen. This limit we call “threshold significant wave height”, or simply “threshold wave height” (TWH).

For a Gaussian sea state, the significant wave height is related to the standard deviation of the wave elevation:

$$H_s \approx 4\sigma \quad (4.1)$$

Nonetheless, the amplitude $a_n = H/2$, where H is the wave height, is Rayleigh distributed.

For the ship, the response amplitude operator, R.A.O. in a regular wave condition, $H(\omega, \beta)$ was defined as a function of the incident wave circular frequency ω with direction β . In an irregular sea state, where the incident wave spectrum is characterized by the significant wave height $H_s(m)$, significant wave period $T_s(s)$ and angle between the ship and wave direction β , the ship response spectrum can be calculated by the following equation:

$$S(\omega: H_s, T_s, \beta) = |H(\omega, \beta)|^2 S_w(\omega: H_s, T_s) \quad (4.2)$$

where $S_w(\omega: H_s, T)$ is the wave spectrum.

Generally, as the response spectrum can be understood as a narrow-banded (Gaussian) spectrum, the statistical distribution of the response value, x , is described by the Rayleigh distribution with parameter R .

$$p(x: H_s, T_s, \beta) = \frac{x}{R(H_s, T_s, \beta)^2} \exp \left\{ -\frac{x^2}{2R(H_s, T_s, \beta)^2} \right\} \quad (4.3)$$

where $R(H_s, T_s, \beta)^2 = \int_0^\infty S(\omega: H_s, T_s, \beta) d\omega = m_0$

To find the significant wave height that makes the response of the system exceed the limit of operability, it is necessary to establish the permissible number of times that the wave height exceedance may happen, above which the operability is no further assured. The expected number of encountered peaks in a sea state characterized by (H_s, T_s) during the time interval of m hours is obtained by finding how many times the period T_s fits in m . It is needed to convert m to the same unity (seconds):

$$N = \frac{m \times 60 \times 60}{T_s} \quad (4.4)$$

The evaluation applied in this work assumes that there is a permissive periodicity of exceedance of the hardware limits. This means that the search is done in order to find the threshold significant wave height that happens at that periodicity. In terms of

statistic calculation, if it is allowed that a specific value x_Q is exceeded n times in m hours, this probability is expressed as:

$$p(x > x_Q) = 1/N \approx \frac{1}{n} \exp\left(-(x_Q)^2 / 2m_0\right) \quad (4.5)$$

Hence,

$$x_Q = R(H_s, T_s, \beta) \sqrt{2 \times \ln\left(\frac{N}{n}\right)} \quad (4.6)$$

This expression can be applied to the moon pool free surface height, exceeding heave motion and wave induced loads. The RAO is linearly proportional to the incident wave height, *i.e.*

$$R(x, T_s, \beta) = x \times R(H_s = 1, T_s, \beta) \quad (4.7)$$

Since linearity allows calculating the RAO for unit significant wave height and just multiply it by the convenient amplitude, granting the simplification of calculation processes, it is not needed to re-calculate the RAO each time that a new significant wave height is being investigated. Resuming the last two equations 4.6 and 4.7, if x is the significant wave height that makes the response of the system exceed the limit of operability x_Q , then

$$H_{s-threshold} = \frac{x_Q}{R(H_s = 1, T_s, \beta) \sqrt{2 \times \ln\left(\frac{N}{n}\right)}} \quad (4.8)$$

This is the threshold significant wave height for short term analysis. If a long term analysis should be applied, some considerations must be made, as described in appendix 10. In the next subsections, the attribution of the threshold value for each criterion is presented.

4.2.1 Moon pool water surface elevation

The moon pool water surface elevation can bring problems if there is an overflow caused by exaggerated elevation that surpasses the deck level. When it happens, there is the risk to the safety of crew and to the equipments surrounding it. The limit value $x_Q = 4\text{m}$ is then chosen to be the minimum free border height, that is the minimum distance from design water level to the deck that can be acceptable. Then, $R(H_s = 1, T_s, \beta)$ is the variance of the RAO for the relative wave height between the water free surface of the moon pool and the centre of the ship at water line. The piston mode only was chosen in the present work due to the recommendations by DNV (2011).

The observation period is $m = 3\text{h}$, as recommended by ITTC (2002). Since no reference with an effective value suggested for moon pool exceedance was found, the probability of green water (overflow of sea water into the ship) from the moon pool in the related criterion was assumed to be 0.05.

4.2.2 Ship motion

The perforating tool consists of a riser with a drill on its end. There is a risk of failure if the vertical motion of the top of that riser causes a big bending on it, so a heave compensator equipment is installed to diminish that amplitude of motion. As the distance from the keel to the seabed increases by heave motion, the heave compensator pushes the top of the riser as to keep its constant draft, but there is a limit of stroke for this equipment to compensate. Also, if the heave compensation equipment is positioned in a level below the deck height and there is an exaggerated elevation of the water level inside the MP, there might be damage of the equipment by the impact of the water on it.

The problem hence has two approaches of analysis: the limit of stroke and the resultant relative positions of the heave compensator equipment and the moon pool water surface level. In this work, the first approach is used for the analysis of operability. The second approach is left for future works.

If the heave compensator stroke is exceeded by the ship motion, the drilling devices might be damaged immediately at the first occurrence, so it is assumed that there is no sense in considering a probability of more than one exceedance at a simulation period. On the other hand, although it might not be informed by the manufacturer, the nominal limit value for stroke of the heave compensator is probably shorter than the actual value, due to an engineering safety coefficient applied for warranty. Considering this, although a precise value could not be inferred for the present work, an increasing factor of the limit stroke value is used in order not to be too conservative. The values used for x_Q and $R(H_s = 1, T_s, \beta)$ are, respectively, the limit stroke value of the heave compensator and the variance of the RAO for the ship motion in heave mode.

As explained above, the probability of stroke exceedance is 1 in any time, since 1 exceedance only would already cause damage and prevent operation, so the acceptable probability of occurrence adopted was 1/10000. According to the recommendations of ITTC (2002), the specified duration of random simulations is 3 hours for modelling a full storm, which is most often used in offshore engineering tests. The design allowable maximum stroke is 3.5m, defined by the maker. In a less conservative analysis, it could be assumed that this value has already a 1.5 safety factor for example, applied to the actual maximum stroke, therefore the compensator would only have malfunction problems at the actual maximum of $3.5 * 1.5 = 5,25$ meters.

4.2.3 Station keeping problem

The effect of occurrence of drift power at an intensity that the Dynamic Positioning System cannot compensate shall not be a matter of safety, however cannot be neglected. If the ship is pushed away from the desired place, especially in the case of a drill ship, the location of the end of the drill would be deflected from the place where it should be positioned to drill the seabed.

If the allowable mean drift force power is given as P_{D0} , the threshold significant wave height considering drift force is given by Maruo (1960):

$$H_{s-drift-y} = \left\{ \frac{P_{D0}}{D(H_s^2 = 1, T_s, \beta) \frac{2\pi}{T_s}} \right\}^{\frac{1}{3}} \quad (4.9)$$

The limit value of drift power used as threshold in this work was extracted from the specifications of the equipment used in the ship “Chikyu” Murata, Nagase and Ozawa (2006): 34.260 metric horsepower.

4.2.4 Structural problems

Hydrodynamic loads due to the water oscillation inside MP can lead to problems of two orders: local order and global order.

The local order problems are related to the equipment inside or surrounding it, that can get damaged by the collision with either a big volume of water at once or other neighbour solid, that can be another device or the wall of the moon pool itself. In this last case, there is also the risk that repeated hit damages or even open a hole in the wall, flooding a chamber.

The global order problem is the one to which bigger concerns shall be addressed, due to the catastrophic failure that might result from it. If not considered in design, the interaction between the water column oscillation, the external waves and the ship motion might eventually contribute to amplify the ship response with a high occurrence of critical wave induced vertical bending moment, causing serious damage to the global structure of the ship, especially at mid section.

Due to reduction of the section module of inertia in the region where there is the moon pool, structural strength is also reduced. Although there might be an increase of strength in lateral regions, if the moon pool walls can be seen as a double hull at a given section, vertical bending moment stresses assume the biggest values at the upper deck transversal line and at the bottom transversal line, where there is a discontinuity due to the opening. It could also get worse with free surface effects in flooded chambers

or tanks that would contribute to amplify the oscillations with, e.g., added torsional moments.

The IACS regulations for structural strength to wave loads provide reference values to be used for deck design. The designer should choose structural elements and distributions that minimize the stress and assure that the ship can cope with those calculated critical values of loads.

In equation 4.8 (reproduced below), the Rayleigh argument will be the probability of happening a peak of V_i .

$$H_{s-threshold} = \frac{x_Q}{R(H_s = 1, T_s, \beta) \sqrt{2 \times \ln \left(\frac{N}{n} \right)}}$$

where x_Q is the limit value allowed for the momentum, which will be described later, $R(H_s = 1, T_s, \beta)$ is the Rayleigh distribution parameter (probability of happening the peak for $V_i(x)$), which is given by $R(H_s, T_s, \beta)^2 = \int_0^\infty S(\omega; H_s, T_s, \beta) d\omega$.

Due to the large amount of information involved in data treatment, the maximum bending moment to be assessed was chosen to be only at the midship section, where the module is usually the biggest, and since the drill ship has a large opening in that location, it would be the most critical region where a failure might happen. The specific value is the IACS (2010) wave induced bending moment, which is defined considering a designed service life of 25 years for which the probability of exceedance is $M_{IACS} = 10^{-8}$, based on the long-term analysis.

The standard cited above gives requirements to design wave load and global strength of seagoing steel ships above 90m. As the intention of the present assessment is to estimate the threshold significant wave height for short-term wave condition, the IACS bending moment probability of exceedance, M_{IACS} , was converted from 25 years maximum to one-month maximum value assuming that the long-term distribution of the wave induced bending moment is a logarithmic probability distribution. The applied equation is shown below (IACS, 2010).

$$n = M_{IACS} \times \frac{\ln \left(\frac{10^8}{25 \times 12} \right)}{\ln(10^8)} = 10^{-8} \times \frac{3.33 \times 10^5}{\ln(10^8)} = 6.9 \times 10^{-9} \quad (4.10)$$

Given a sea state (H_s, T_s) , the adopted value for the expected number of peaks N is 1 month, converted in $m = 720$ hours, using the equation 4.4:

$$N = \frac{m \times 60 \times 60}{T_s}$$

Based also in that regulation, the threshold bending moment used as limit for assessment of the threshold significant wave height was also based on the design wave load formulation, reproduced below (IACS, 2010).

$$M_w = +190 * M * C * L^2 * B * C_b * 10^{-3} \text{ (kN*m) for positive moment}$$

$$M_w = -110 * M * C * L^2 * B * (C_b + 0.7) * 10^{-3} \text{ (kN*m) for negative moment}$$

$$C = \begin{cases} 10.75 - \left[\frac{300-L}{100} \right]^{1.5} & \text{for } 90 \leq L \leq 300 \\ 10.75 & \text{for } 300 \leq L \leq 350 \\ 10.75 - \left[\frac{L-350}{150} \right]^{1.5} & \text{for } 350 \leq L \leq 500 \end{cases}$$

Where:

- M: distribution factor according to the position along the hull. For midship, it is 1.
- L: Length of the ship (m)
- B: Greatest moulded breadth (m)
- C_b : Block coefficient

Once the values for positive and negative moment for the midship section are calculated, the limit x_Q value is chosen to be the minimum of those.

4.2.5 Crew safety, comfort, and workability problems

It is naturally understood that the global order problem described in the subsection 4.2.4 of the structural problems would result in risks to safety of the crew if a structural failure happens. In smaller scale of danger, but still big financial impact, there would be loss of workability due to vibrations causing difficulties in handling machines, and kinetosis, among other problems.

Green water is also another problem that, depending on the amount and frequency of occurrence, would risk safety (for slamming a person to floor). Lack of comfort or workability are caused by insecurity of a personnel to execute an activity with precision of movements or by psychological reasons caused by fear.

The crew comfort is a criterion to be considered as well as the previous ones already described, but was not included in this first version of the program due to schedule issues, so this subsection is dedicated to present a short description of the crew comfort criterion meaning and how it can be expressed in engineering terms.

The presence of the moon pool will affect the amplitude of motion of the hull, and influence the accelerations to which the individuals would be subjected, thus might be a limiting criterion to the operability.

Table 6: General operability limiting criteria for ships

General Operability Limiting Criteria for Ships (NORDFORSK, 1987)			
Description	Merchant Ships	Navy Vessels	Fast Small Craft
RMS of vert. acc. at FP	0.275 g ($L \leq 100$ m) 0.050 g ($L \geq 330$ m)	0.275 g	0.65 g
RMS of vert. acc. at Bridge	0.15 g	0.20 g	0.275 g
RMS of lat. acc. at Bridge	0.12 g	0.10 g	0.10 g
RMS of Roll	6.0 deg	4.0 deg	4.0 deg
Probability of Slamming	0.03 ($L \leq 100$ m) 0.01 ($L \geq 300$ m)	0.03	0.03
Probability of Deck Wetness	0.05	0.05	0.05

Source: NORDFORSK (1987)

Unlike the other applied criteria in which an objective measure is explicit at the establishment of a rule to define a critical value, comfort is a concept that might sound subjective, especially for not expressing effects on machinery or on the floating system. On the other hand, disregarding the existence of the effects of the system's behaviour on the human body presumes that all operation can be crew-less, *i.e.*, even if there is no operator in health conditions to execute the activities, all of them are kept, hence the comfort of the crew does not affect the operability. Since drilling operations require human supervision and drill ships are not autonomous machines, this criterion should be included in a future version of the program.

There is a regulation to be followed when assessing the operability from the crew comfort viewpoint, that is the ISO (1997), by the International Organization for Standardization, Mechanical vibration and shock. It addresses evaluation of human exposure to whole body vibration. The assessment shall be done starting from the accelerations in several positions of the vessel, and comparing them at critical areas where members of the crew might be positioned to the recommended limits of health and operability keeping. The table 6 from NORDFORSK (1987), has a set of limits of different acceleration criteria. Other references of criteria for survivability and operability in rough weather for different classes of ships can be found in the reports from the 19th ITTC, 1971 and Kishev(1974) among others.

5 Calibration

One of the inputs of the optimization program is the closed hull mesh, *i.e.*, without any opening for moon pool. The input mesh is assumed to have acceptable size for the hydrodynamic response calculations. This means that the user shall have already tested several mesh sizes for obtaining the RAOs of the main modes of ship response and assured that the one used as input for the optimization program provides an acceptable precision, so that its size variation to a smaller one would not bring in significant improvements on the seakeeping calculation results. In the next subsection, the particular case of hull mesh used in the present work is used as an example of mesh calibration.

5.1 Discussion about the mesh for moon pool

Preliminary results of the hydrodynamic response module applied to a Series 60 hull mesh with 126 elements were used for assessing the optimization algorithm integration in Fonseca (2016). Since it was not the goal of that work (the focus was code integration), a study to check whether the number of elements and the quality of the mesh was appropriate for reliable results was not done. In this work, a special attention is given to check the mesh refinement and its impact on the calculation results.

A more extensive and detailed description of the moon pool mesh calibration is presented in the appendix 10. It is assumed that the original hull without the opening that will be used as input to the optimization code has a sufficiently fine, regular and harmoniously distributed mesh that will not negatively interfere in the hydrodynamic results. It is preferable to have a quadrangular mesh around the moon pool region with some triangles if needed.

The practical guidelines for ship CFD applications by ITTC (2011) recommend at least 40 grid points per wavelength on the free surface. Considering that the waves that have biggest influence on a system are those of about its length - in this case 203.4m -, the number of grids should be around $203.4/40 \approx 5.08$ m. The grid has 46 longitudinal divisions, resulting in average 4.42m of element size ΔS_H , so its resolution is suitable according to the recommendation.

A collection of RAO data of the motions of a fixed drill ship shape with a rectangular moon pool of length to breadth ratio of 2 : 1 was generated. The RAOs used for the assessment criteria (heave, drift, vertical bending moment at midship and moon pool water elevation) were obtained for each mesh size presented in the table 7.

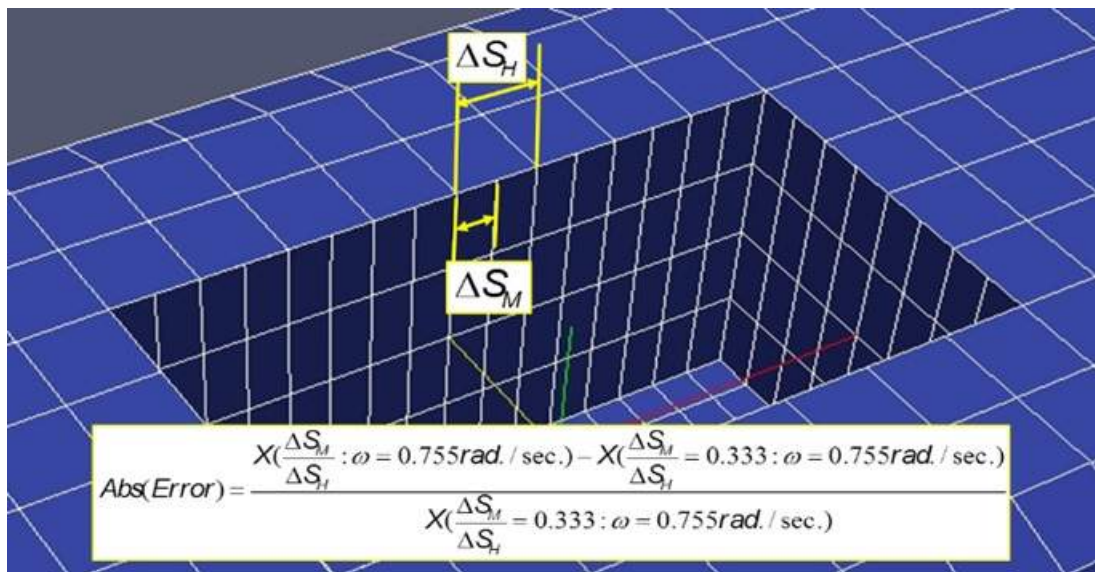
Table 7: Length ratio of the element lengths: hull's to moon pool's

	Longitudinal length ratio between the MP elements and hull elements	Equivalent to
CASE 1	1.00	1:1
CASE 2	0.67	2:3
CASE 3	0.50	1:2
CASE 4	0.40	2:5
CASE 5	0.33	1:3

Source: Author

Data were generated for 5 cases, starting from a proportion of element lengths of the hull to moon pool, respectively, ΔS_H to ΔS_M , equivalent to 1 : 1, 2 : 3, 1 : 2, 2 : 5 and 1 : 3. The parameter ratio of the element size was taken upon the longitudinal size, as illustrated in figure 47.

Figure 47: Illustration of size ratio dimensions used to calculate the modulus of the variation in RAO results. The image represents the case 3.



Source: Author.

From each RAO, the points equivalent to the piston-type resonance frequency, where the most critical values happen in some of the criteria are taken as example to analyse the variation of the module from case to case. The stability of results in each criterion converged to the maximum of 1.9% of variation from case 4 to case 5 in drift force, as can be seen in Table 8. Based on those results, the size ratio of the elements of the moon pool to the hull elements for the present example of hull dimensions can be chosen to be 0.4, as in case 4.

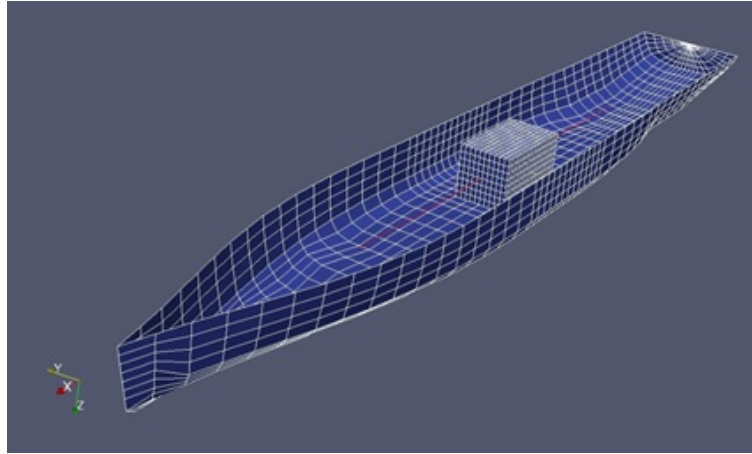
Table 8: Variation of the results for each case taking as reference the case 5

Absolute error in	CASE 1	CASE 2	CASE 3	CASE 4	CASE 5
RAO of Heave $\beta = 90$ deg. $\omega = 0.755$ rad./sec	11.1%	2.8%	1.0%	0.3%	0.0%
Drift y-force $\beta = 90$ deg. $\omega = 0.755$ rad./sec	37.6%	13.2%	5.4%	1.9%	0.0%
Midship Vertical Bending Moment $\beta = 0$ deg. $\omega = 0.755$ rad./sec	22.9%	7.5%	3.1%	1.1%	0.0%
Moonpool water surface elevation at mid $\beta = 0$ deg. $\omega = 0.755$ rad./sec	10.8%	2.1%	0.6%	0.2%	0.0%

Source: Author

Finally, the best version of the hull mesh is illustrated in figure 48. It has some refinements of the mesh in the midship region, and the number of elements is 1748 for the rectangular moon pool shape. From this pattern, as a default, the number of divisions in x -axis direction and number of divisions in y -axis direction, as well as the z -axis direction of the half-breadth for the whole mesh of the free surface is defined, respectively, as 16, 4 and 8.

Figure 48: Drill ship mesh with 1748 elements.



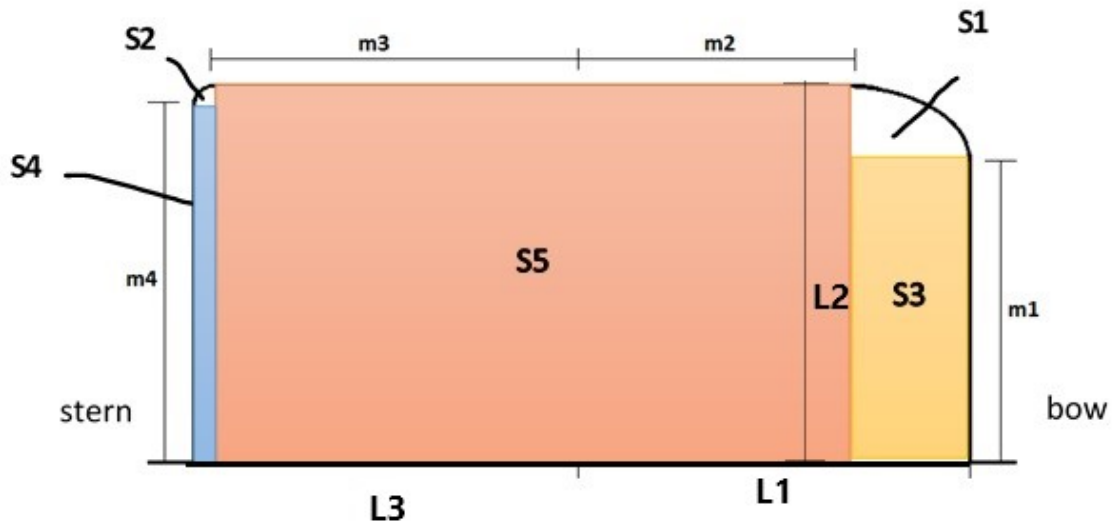
Source: Author.

In the case of variable dimensions and shapes of moon pool, the grid of the free surface of the internal water must be generated based on the values of the parameters that define them, shown in figure 46. In this work, the mesh is created based in rectangular and ellipsoidal sectors of the shape, what may lead sometimes to a heterogeneous matching of the grid in some regions of interface between the sectors. A general division of the free surface mesh is illustrated in figure 49.

For a better distribution of size of the elements, it is recommended that the parameters $L1$, $L2$ and $L3$ vary in a step with the same size of the element dimensions of the hull. The elliptical corners indicated on figure 49 as $S1$ and $S2$ are meshed with quadrangle elements defined between the frontier of the moon pool wall, and the free surface and its offsets. The last elements that have the centre of the ellipse in common are triangle elements, following the same pattern of divisions of the other offsets. An example of a mesh generated in gmsh¹ is shown in figure 50. In the gmsh software it indicates with two colors the two faces of the elements, which is useful to identify whether the normal vectors of each element are pointing to the same direction or not. In our case, the normal vector is pointing inwards to the water. The sides of the surfaces that will interact with the water thus should be coloured in yellow lines and the inner side of the hull should be coloured in black lines.

¹ Free mesh generation software, available for download on internet. Refer to (GEUZAIN; REMACLE, 2009)

Figure 49: Free surface mesh regions used for element generation order.



Source: Author.

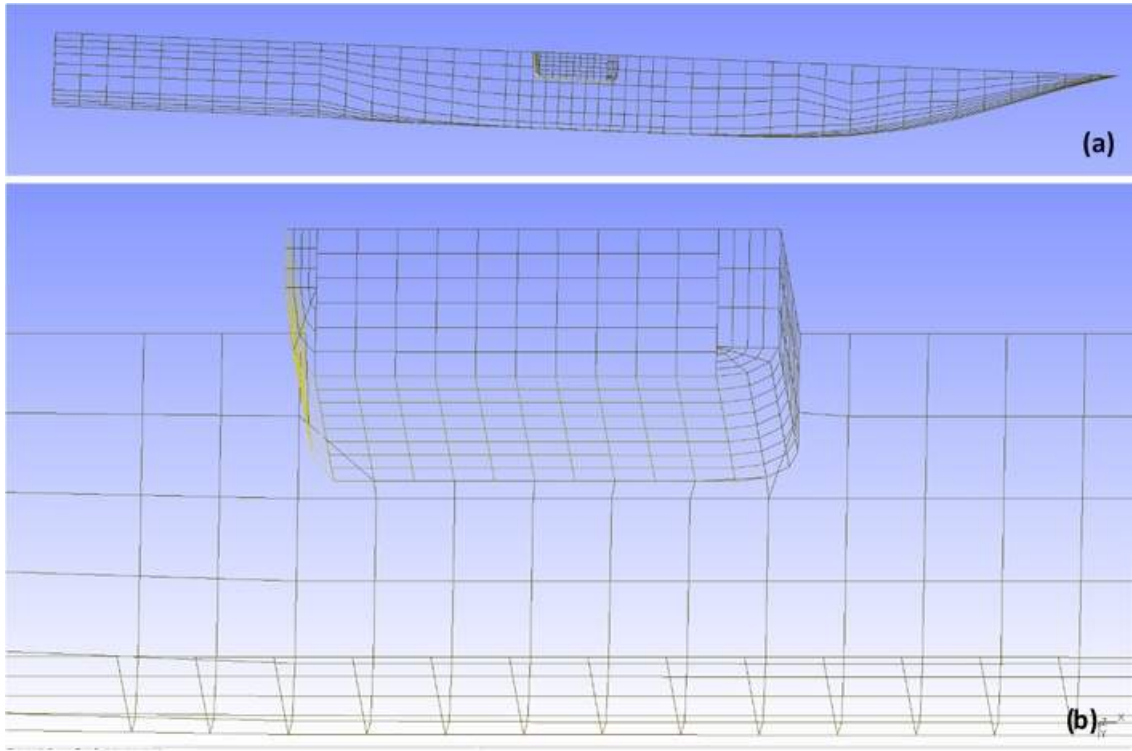
The scheme of mesh generation of the MP as well as its coupling to the hull was completely reformulated to improve the approaches used in Cavalcante (2015) and Fonseca (2016). The previous versions had some pre-selected grid numbers that would be adjusted accordingly to the main sizes of the MP, which means that the respective code was dependent on the specific hull being input.

In the new approach, a scanning is run through all the elements and treats each one of those regarding their status (*e.g.* completely inside, partially inside, with at least one grid contained in the frontier between hull and moon pool wall, etc.). This brings to the program a total flexibility to treat any mesh of any closed hull (without moon pool) input. On the other hand, there still are some adjustments that can be done for the next steps. As it can be seen on the zoomed image, in some of the elements that are intercepted by the moon pool's wall, there are seldom elements in which a small area is missing on the hull outside the moon pool wall, or are lasting inside the moon pool wall corners. Those are due to the limitation of using only quadrangle and triangle elements of almost the same area, without creating polygons of more vertices. It is being assumed that the areas of those imperfections are too small in comparison to the total area of the neighbour elements, so that the error can be neglected in this first stage of the project development.

5.2 Rayleigh damping coefficient adjustment

As was explained in section 3.3 about the boundary value problem with moon pool, in the case of the free surface of the internal water in MP, if a boundary condition is

Figure 50: Example of hull mesh in gmsh visualization: (a) total hull; (b) zoom at the moon pool region.

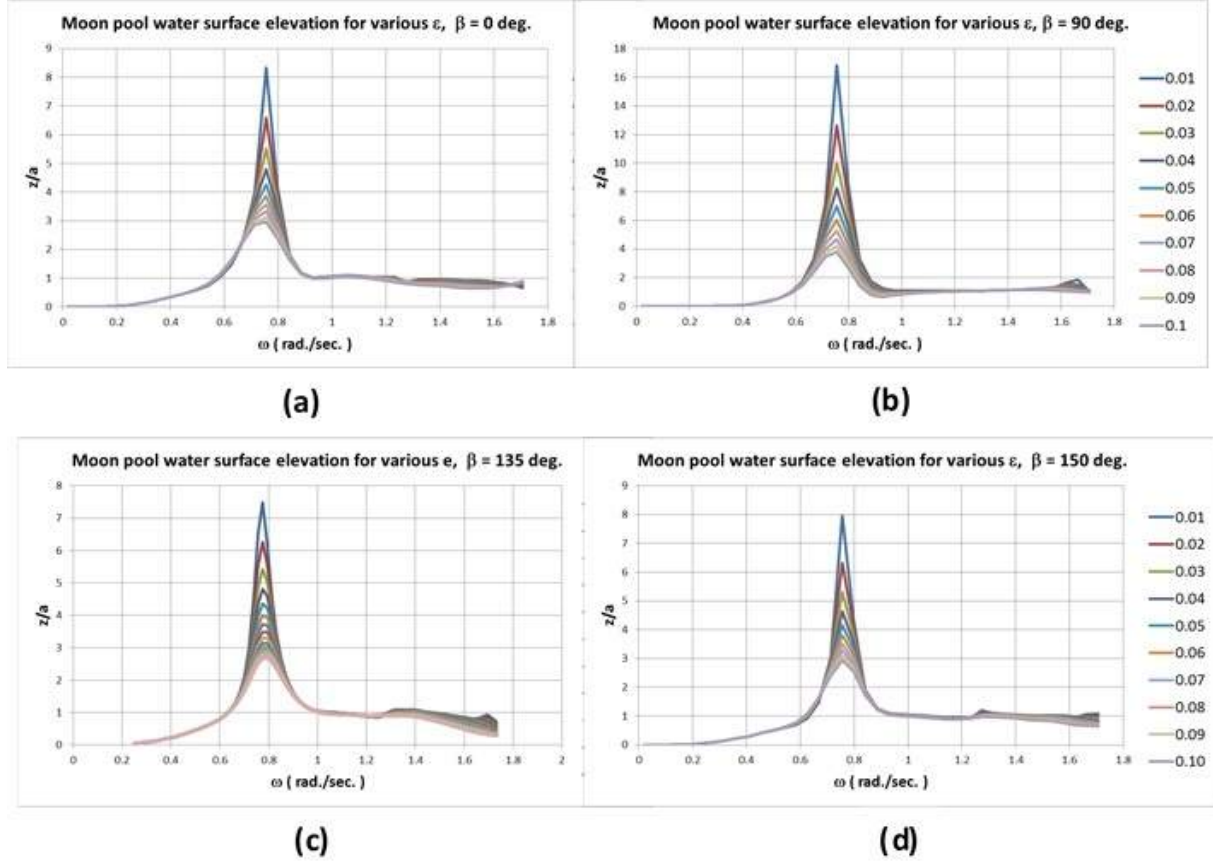


Source: Author.

assumed to be the same as the one for S_F , the height response would be overpredicted. Due to this fact, the viscous term of second order, so-called Rayleigh damping, is used. Its derivation can be found in Newman (1977), and comments are also found in the section 3.2 about the boundary value problem without moon pool.

The value of this coefficient can be adjusted by comparing with experimental data, as can be found in Kawabe et al. (2010). In that work, the model test of free floating ship with moon pool was performed at the Maritime and Ocean Engineering Research Institute (MOERI) Basin in Korea. It was found that the RAO of the ship is nearly not affected by the damping factor, *i.e.*, except for the frequency ranges where the resonance peaks for piston and sloshing modes are located, thus the only concern is related to the resonance peak values. Furthermore, it is explained that at different wave incidence directions the same tendencies are found for the relation between the damping factor and the piston mode resonance amplitude in moon pool, which allows taking the results of any direction. Those facts can be observed in the following figure 51, where the resonance peaks of the centre of the moon pool are shown for various damping coefficients in four incidence angles $\beta = [0 \ 90 \ 135 \ 150]$ degrees. For (a), (b), (d), $0.01 < \varepsilon < 0.10$ and for (c) $0.02 < \varepsilon < 0.15$ due to the set of simulations ran for comparison with the literature.

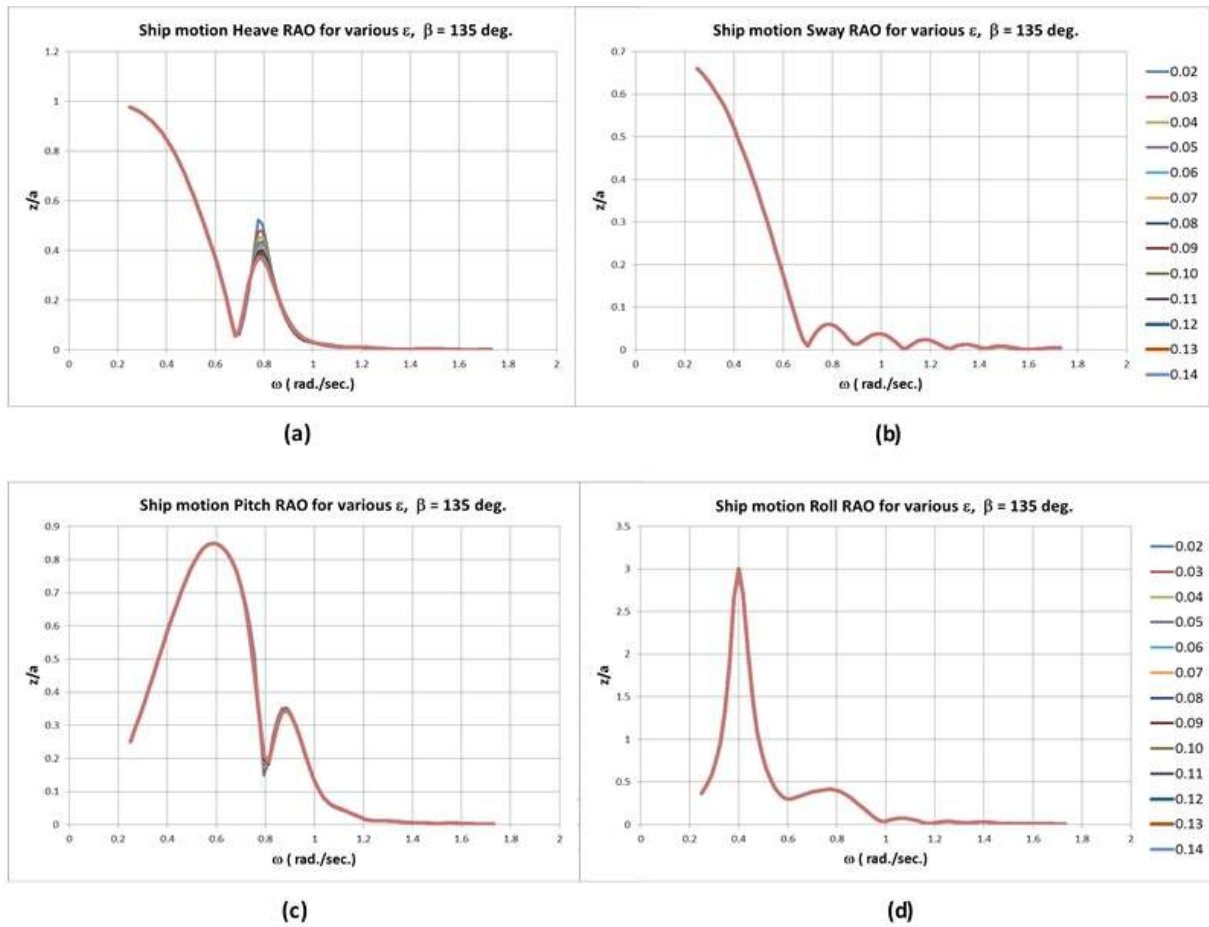
Figure 51: Resonance peaks of the centre of the moon pool at different incidence angles β , for various damping coefficients ε . (a) $\beta = 0^\circ$, (b) $\beta = 90^\circ$, (c) $\beta = 135^\circ$, (d) $\beta = 150^\circ$. For (a), (b), (d), $0.01 < \varepsilon < 0.10$ and for (c) $0.02 < \varepsilon < 0.15$ due to the set of simulations ran for comparison with the literature.



Source: Author.

In the graphs, resonance areas can be identified in $0.7 < \omega < 0.86$ rad/s for piston mode, and some separations of the curves at $\omega > 1.5$ rad/s related to sloshing mode. It is easily observed that in frequencies outside the resonance areas, there is no difference in the relative elevation regardless the value of the damping coefficient, and the shape of the curves inside the resonance regions evolve in the same fashion as the damping coefficient value increases. The graphs in figure 52 show the ship motion RAO for various damping coefficients under the incidence angle of $\beta = 135^\circ$, in heave, sway, pitch and roll.

Figure 52: Ship motion RAO for various values of Rayleigh damping coefficient under the incidence angle $\beta = 135^\circ$ (a) Heave, (b) Sway, (c) Pitch, (d) Roll



Source: Author.

The ship motion is unaffected by the change in the damping factor, except for the heave and pitch responses - respectively, figures 52(a) and 52(c) - in the resonance peak frequency ($\omega = 0.775$ rad/s), since they are directly related with the effects of exaggerated motion of the moon pool water.

Besides those facts, there are also some results from water tank experiments published by Faltinsen, Rognabakke and Timokha (2007), Sandvik (2007), Kristiansen and Faltinsen (2008) and Kawabe et al. (2010), in which the relative water surface amplitude at the piston mode resonance frequency, z/a , are between 3.0 to 4.5 even though the experiment model sizes are different.

The decision of the Rayleigh damping coefficient value for the present work was done by simulating the response of the drill ship with principal dimensions similar to the model used by Kawabe et al. (2010). It was not the same because the hull planes were not available, so balances of weight and geometry that need to be kept in consideration led to small differences. Values of the principal dimensions are shown in the table 9.

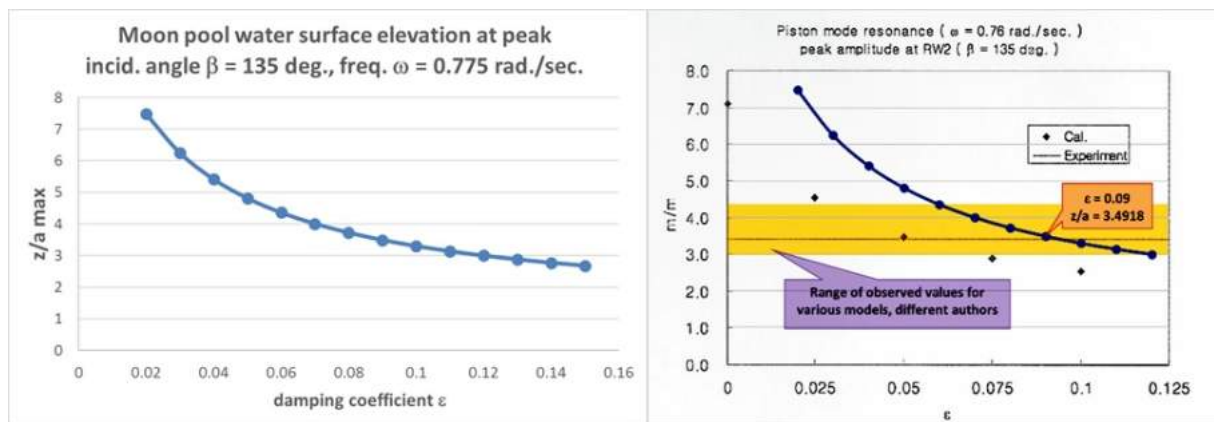
Table 9: Principal dimensions of the models used for comparison

Principal Dimensions	Tested by Kawabe et al. (2010)	Present Work
LBP (m)	208.0	203.4
B (m)	32.2	29.0
TAP (m)	12.0	11.6
TFP (m)	12.0	11.6
GMT (m)	1.0	1.8
Kxx (m)	13.6	10.1
Troll (s)	30.9	16

Source: Author

From the outputs of water surface RAO at mid position of the MP opening, the curves were plotted for different Rayleigh damping coefficient (ε) values, from 0.02 to 0.15 (figure 53, left), and compared for the same angle of attack.

Figure 53: Piston mode resonance peak amplitude for each Rayleigh damping coefficient. The left figure shows the values in the hydrodynamic module simulation, and the right figure is adapted from the original in Kawabe et al. (2010), and shows the comparison of those calculated values to their results.



Source: Author.

The curve does not match with the calculation used for their model, but shows the same trend along the x -axis. The peak or moon pool water surface elevation for the drill ship of the present work happens at around the same frequency band, so it is being assumed that the damping would be similar to the obtained in the experimental test. The value 0.09 was adopted because it is the one at which the closest peak value response is obtained.

6 Validation

The hydrodynamic response calculation module used in this work was written in Fortran (KAWABE, 2017) and provides frequency and time domain responses (RAO) and spectra. The optimization module developed in this work is open source developed in MatLab® and is suitable to other modules.

Simulations were run for validation of the hydrodynamic response module, to make sure that the outputs of that calculation are reliable and correspondent to empirical data. Unfortunately, there were no financial possibilities to run physical tests on the Drill ship hull studied in this work, so the following strategy was adopted.

It was considered that if the outputs of hydrodynamic behaviour simulation for different examples of hulls fit satisfactorily to published results of empirical tests, then the module is suitable for the drill ship as well.

The validation was based on two different hulls with moon pools to reproduce the examples published by Faltinsen, Rognebakke and Timokha (2007), Zhang and Yeung (2016), Torres (2007) and Kang (2018)(to be published). On the next sections, the results and comparison with each of those two studies are presented separately, followed by the qualitative analysis of the Drill ship hull response obtained by the same hydrodynamic response calculation module.

6.1 Rectangular 2D model

The example presented by Faltinsen, Rognebakke and Timokha (2007) is based on a 2D model of a rectangular hull with rectangular moon pool where the piston-like motion is investigated. The schematic drawing shown in figure 54 illustrates the configuration of the model and draft of the tank.

Table 10: Experiment parameters.

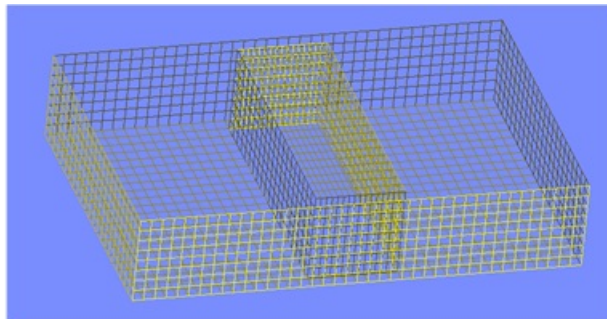
Length of the hull	0.6
Width of the moonpool (L_1)	0.18
Width of each hull (B)	0.36
Width overall ($B + L_1 + B$)	0.9
Water depth in the tank (h)	1.03
Ship draft (d)	0.18
Non-dimensional heave amplitude 1	0.0025
Non-dimensional heave amplitude 2	0.005

Source: Faltinsen, Rognebakke and Timokha (2007)

In that work, the experiments were done in a tank with $1.03m$ water depth to check their proposed theoretical prediction. In the present work, a numerical simulation was done to compare those results for the configuration listed in table 10.

Due to limitations of the code, the configuration of the model used in the present work is similar in main dimensions, but the configuration differs by having continuous mesh at bow and stern instead of being two separated hulls as in the literature. An illustration of the mesh is presented in figure 55.

Figure 55: Mesh of the model used for validation.



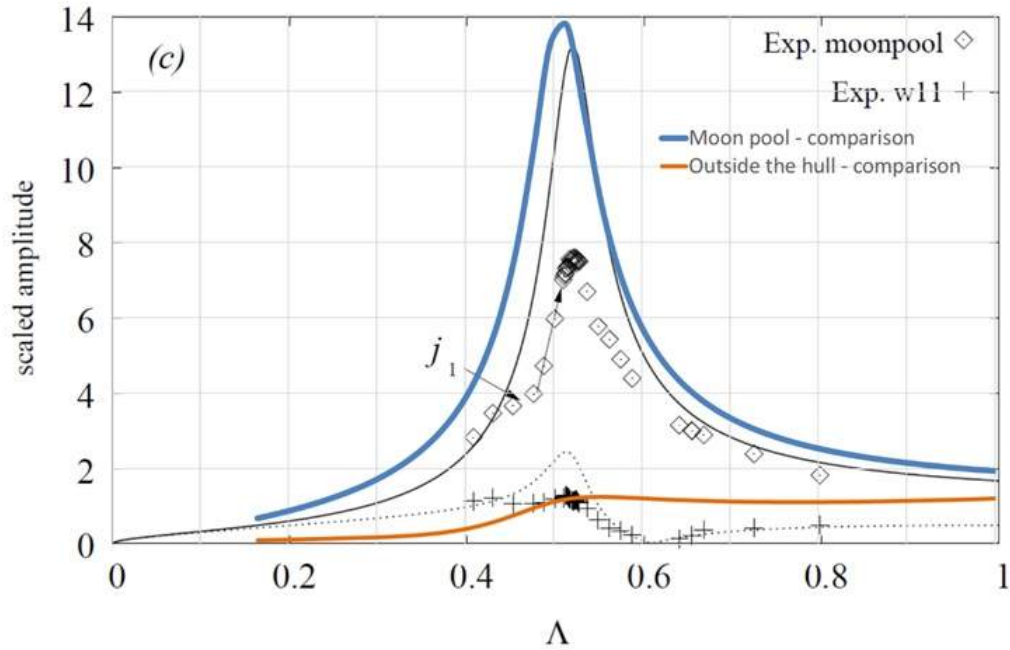
Source: Author.

According to Faltinsen and Timokha (2009), “Faltinsen, Rognebakke and Timokha (2007) pp 106, were not able to get satisfactory agreement between experimental linear theoretical resonant free-surface amplitudes in the moon pool for forced heave motions. Kristiansen and Faltinsen (2008) improved the correlation between theory and experiments by accounting for vortex shedding at the sharp edges of the hull section, inclusion of free-surface nonlinearities, and estimates of experimental bias errors due to wave reflection from the wave beach and the wave generator.”

The objective of the comparison was to try an adjustment of the numerical results, since the vortex shedding and nonlinearities are also neglected in the hydrodynamic module used in the present work. The response inside the moon pool and outside the

hull (at 700mm from the side border, see W11 instrumentation drawing in figure 56) were measured and compared to the theoretical predictions.

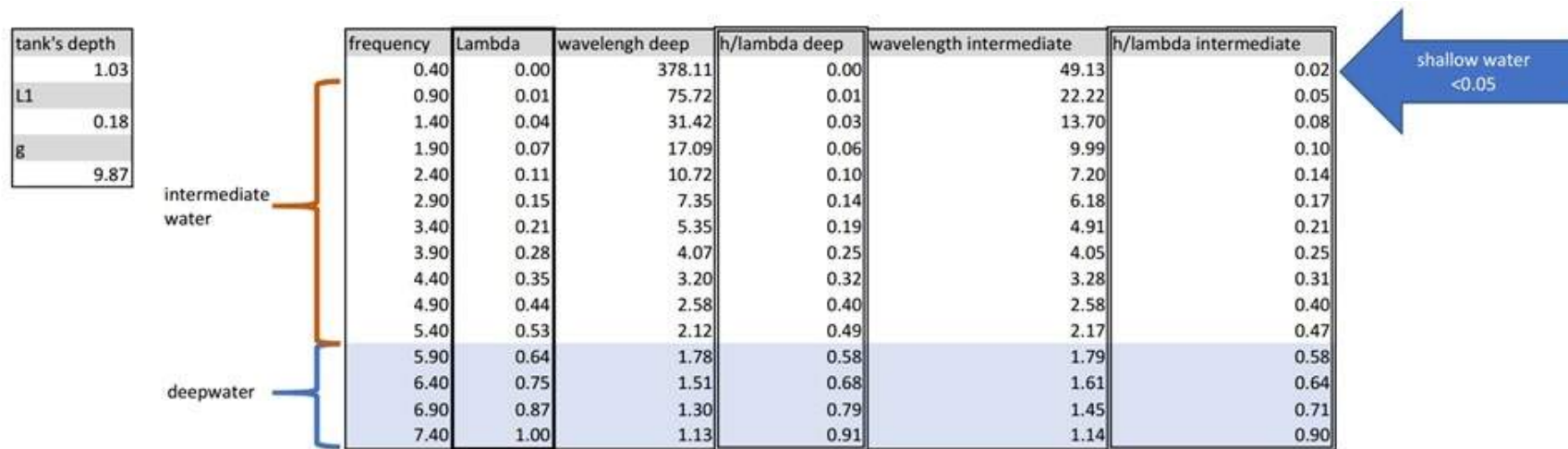
Figure 56: Responses inside and outside MP: comparison between literature and calculation.



Source: adapted from Faltinsen, Rognbakke and Timokha (2007)

There is an agreement of the shape of the curve for the moon pool response between the two theoretical predictions. On the other hand, the trend indicated in the experimental data was not obtained in the position outside the hull. There were differences because the conditions of the experiment could not be totally reproduced in the numerical simulation: some error inputs may have happened when using the simulation modulus for a different scale order, because the frequencies in which the calculation is done for the model are much higher than the range used for the full-scale Drill Ship. The modulus of the incident wave should have at least 1m height to perform a precise calculation. Converting the used frequency value $\Lambda = \frac{\sigma^2 L_1}{g}$ defined by the authors, the range is from ≈ 0.9 to ≈ 7.4 rad/s, configuring intermediate depth for most frequency values up to $\Lambda \cong 0.64$.

Figure 57: Comparison of the predicted response of the rectangular hull with moon pool. The solid and dotted black lines are respectively the numerical predictions by the authors of the amplitude inside the moon pool and outside the hull in W11 position (see figure 54), and the blue and orange line were obtained with the hydrodynamic response module used in this work. The points plotted with squares and crosses are experimental data.



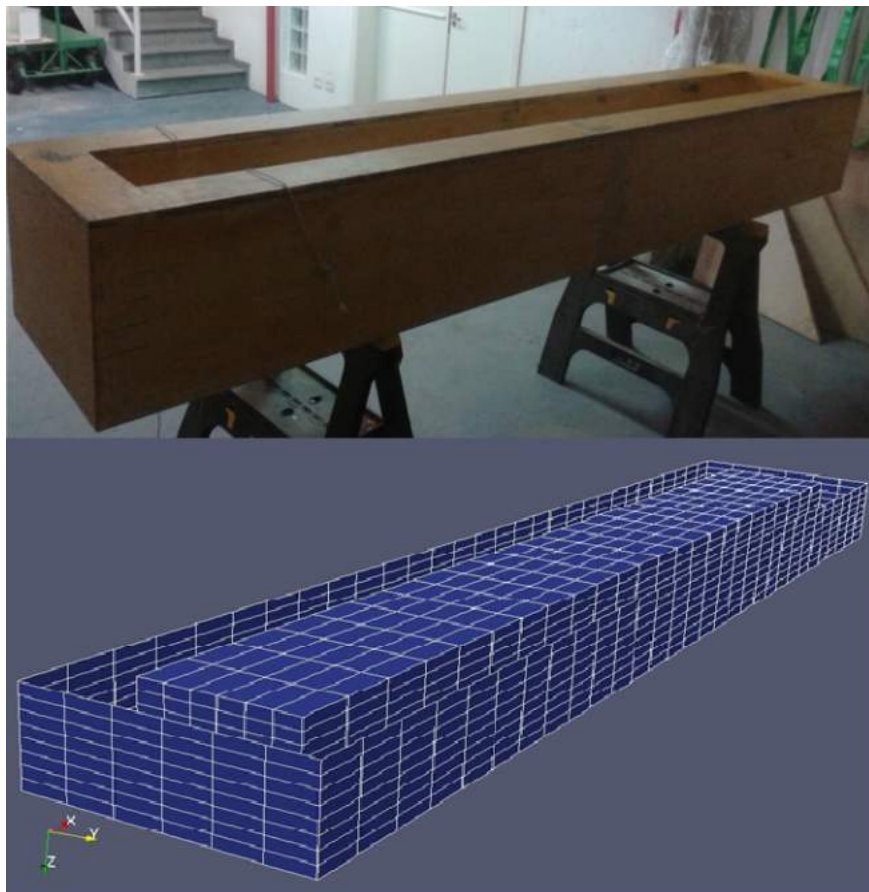
Source: Author

The limitation of use of the mesh for the simulation led to the need of keeping the moon pool restricted by four walls instead of two done in the empirical test, bringing restriction of water volume and 3D effects, what may be reflected in the chart as the smoother shape of the curve after the resonance frequency.

6.2 FPSO model

Experimental data from tests ran at the University of São Paulo by Kang (2018)(to be published) were used for comparison to the prediction by the module developed in the present work. The hull is a rectangular box with a moon pool which principal dimensions are the same order as the hull. The picture of the hull and its mesh are shown in figure 58.

Figure 58: Rectangular hull with moon pool used for empirical data acquisition: picture (left) and mesh (right).



Source of the picture: Kang (2018) (to be published), Source of the mesh: Author.

The dimensions are listed in table 11.

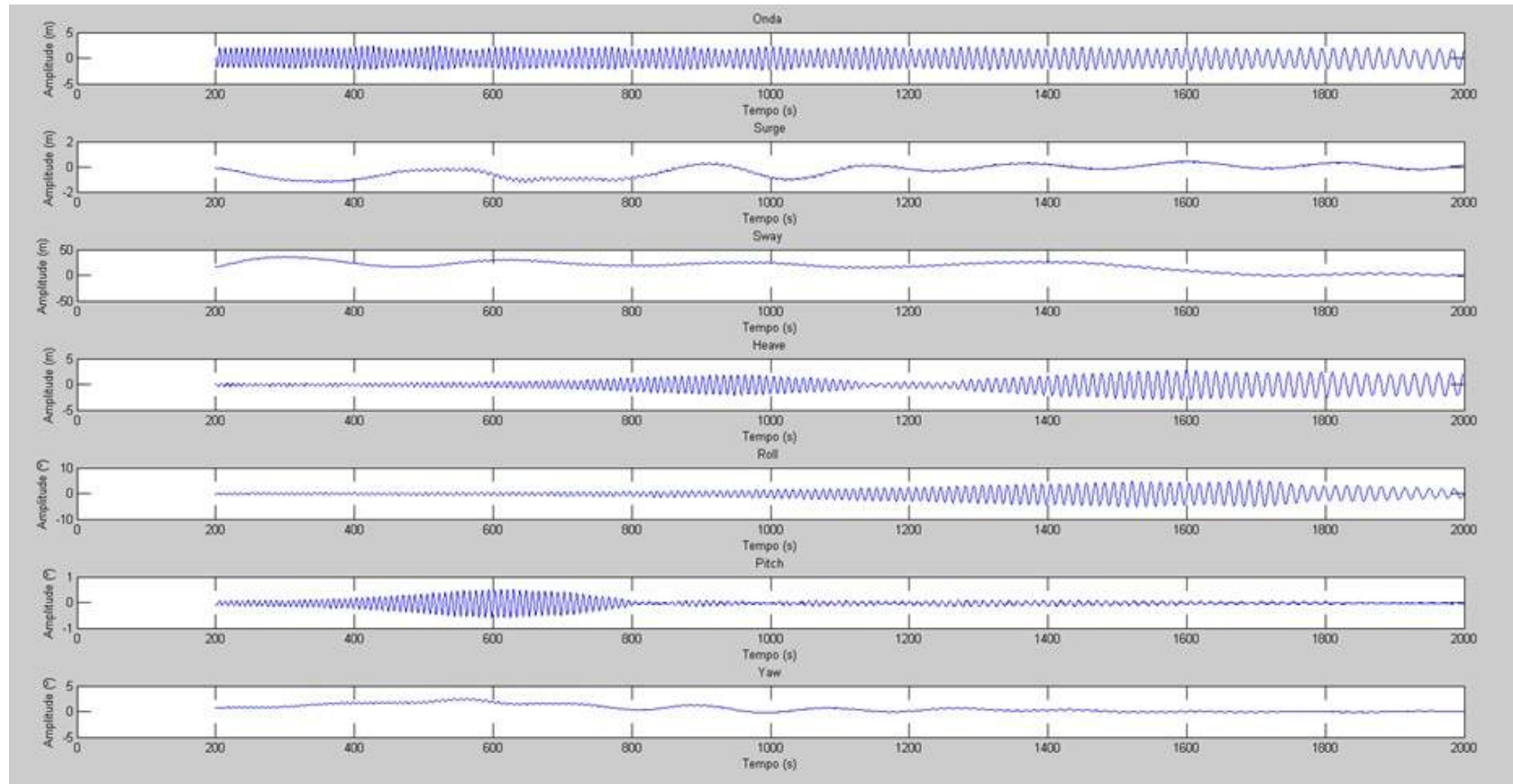
Table 11: Dimensions of the model

Model Scale		
Dimension	Value	Unit
L	295	cm
B	55	cm
D	40	cm
L moonpool	271	cm
B moonpool	31	cm
Thickness of the material	16	mm
ρ material	0.55	g/cm^3
Draft	22.5	cm
R_{xx}	19.4	cm
R_{yy}	70.8	cm
R_{zz}	70.8	cm
Displacement	169.7	kg

Source: Kang (2018) (to be published)

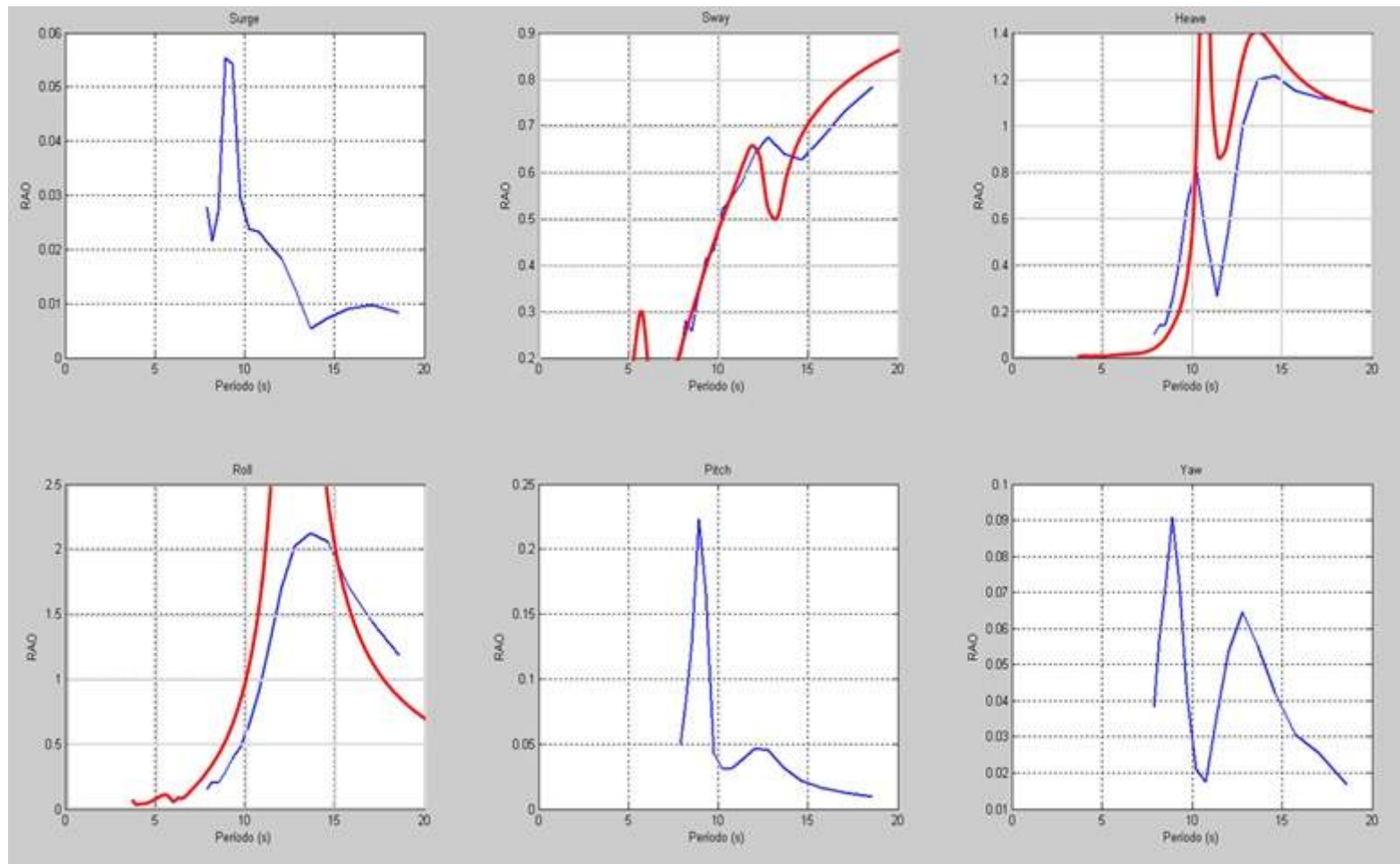
The response to a transient wave excitation was recorded as shown in figure 59, and the RAO was plotted for each motion mode, which was used for comparison to the output of the hydrodynamic module. Figure 60 shows in blue lines the original RAO and in red lines the numerically simulated data.

Figure 59: Time history records of the exciting transient wave and the responses in each motion mode. The first signal corresponds to the wave, followed by surge, sway, heave, roll, pitch and yaw motions.



Source: Kang (2018) (to be published)

Figure 60: RAO in each motion mode: blue line was obtained from the transient wave experimental test with incidence angle 90° . Red line is the result numerically calculated by the hydrodynamic module. The first line are surge, sway and heave, and second line are roll, pitch and yaw. Surge, pitch, and yaw response orders are small, thus neglected.

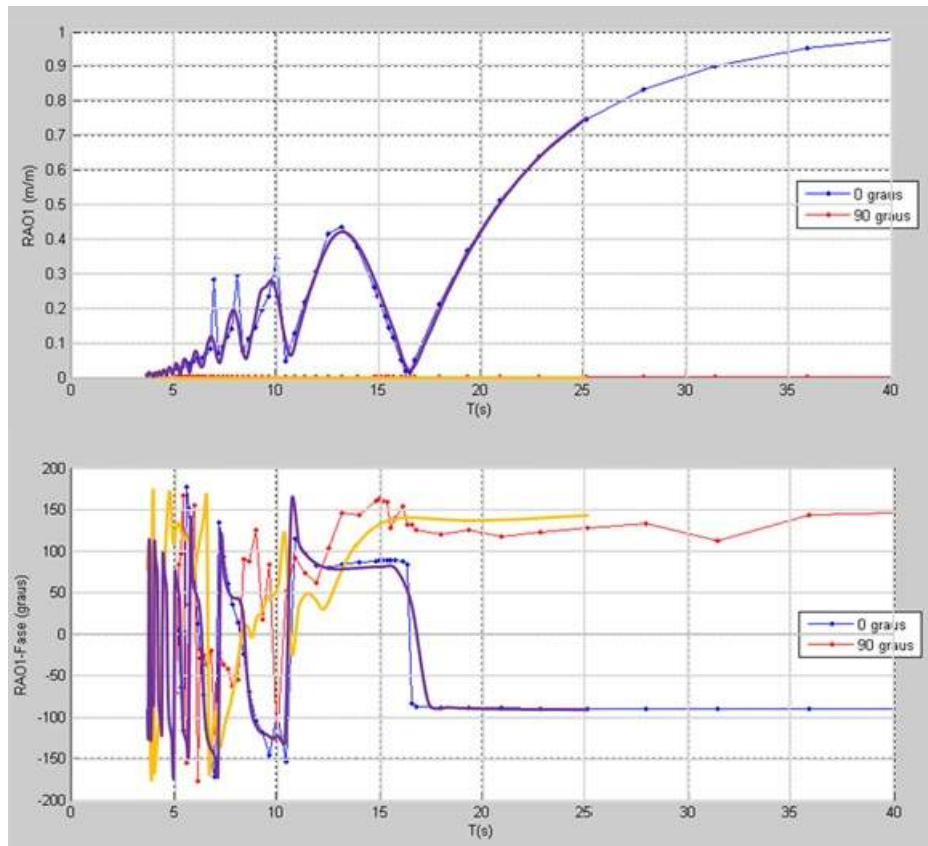


Source: Adapted from Kang (2018) (to be published)

Except for the resonance peak region where there is a damping difference in response probably due to viscous effects, the behaviour predictions agree for sway, heave, and roll motions. The order of the responses in surge, pitch, and yaw are small, thus neglected. An additional comparison was made to the predictions obtained with the software WAMIT[®], shown on figures 61 to 66.

At the incidence angle of 90° , the numerically predicted response amplitude is zero, which agrees with the negligibly small response acquired in the experimental time history. A good agreement between WAMIT[®] and hydrodynamic module calculations can be observed in the response to 0° incident wave excitation.

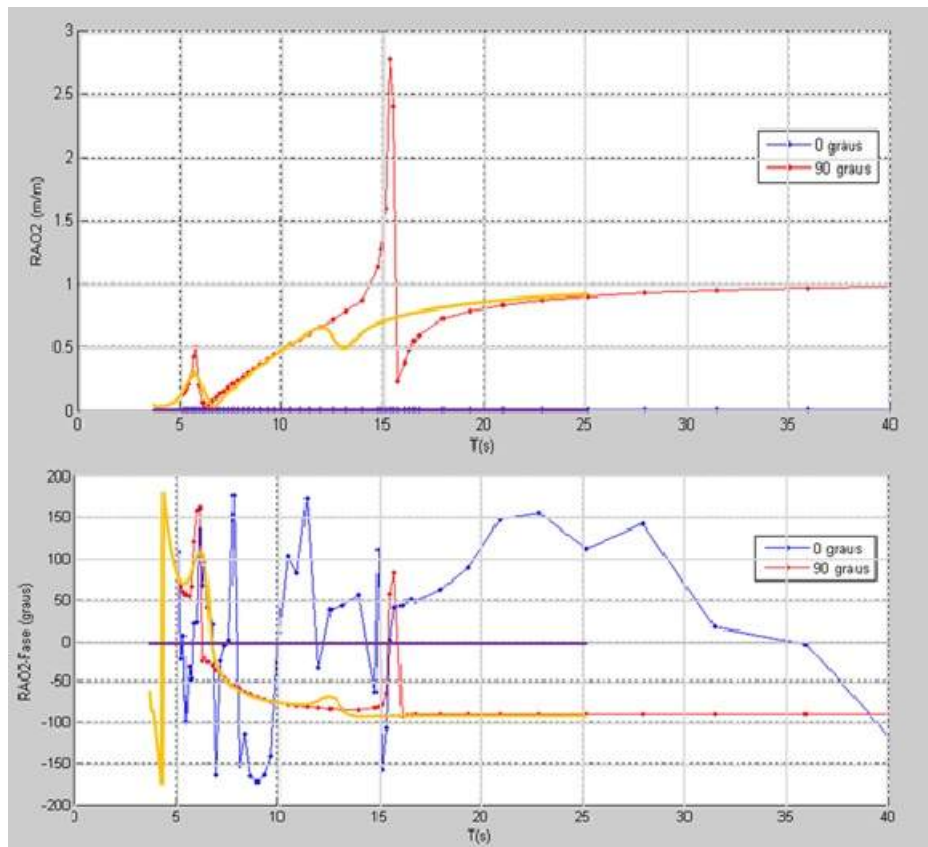
Figure 61: Surge RAO at incidences 0° and 90° , comparison between calculations by WAMIT[®] (respectively, blue and red lines) and hydrodynamic module used in the present work (respectively, purple and yellow lines). Top: amplitude, bottom: phase.



Source: Adapted from Kang (2018) (to be published)

The RAO for sway, as noticed in Figure 4 of the experimental data, had a peak of around 0.7 in the resonance region, which was overestimated by output of the numerical output by WAMIT[®] but nearly reached by the hydrodynamic module.

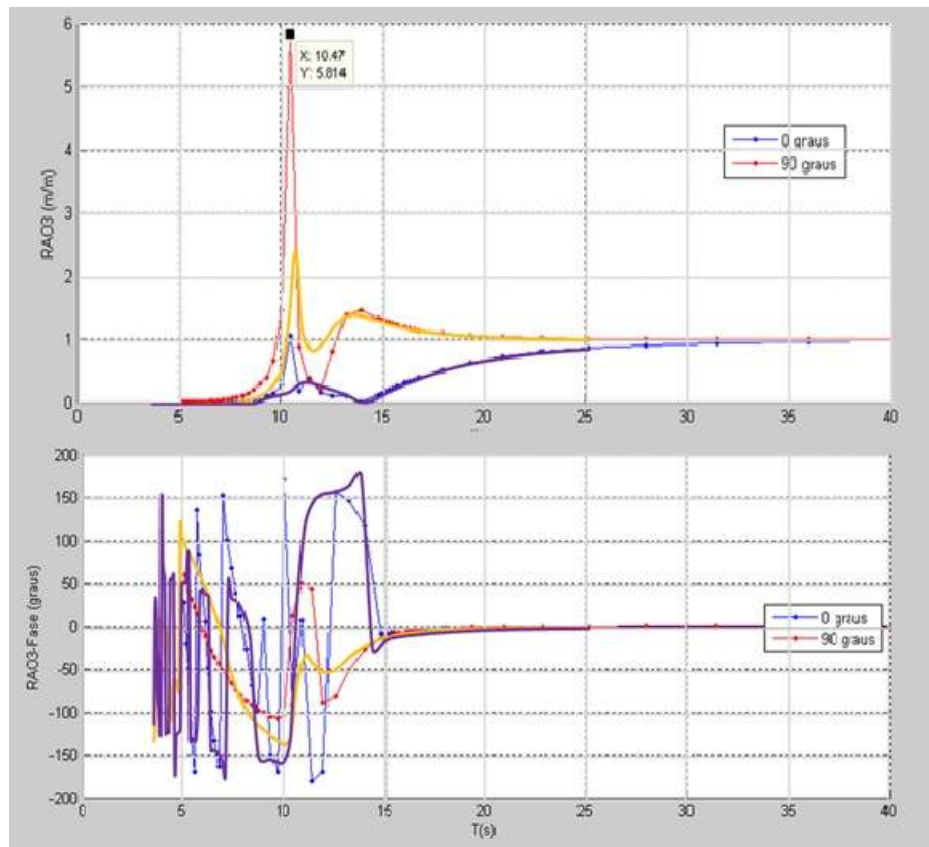
Figure 62: Sway RAO at incidences 0° and 90° , comparison between calculations by WAMIT[®] (respectively, blue and red lines) and hydrodynamic module used in the present work (respectively, purple and yellow lines). Top: amplitude, Bottom: phase.



Source: Adapted from Kang (2018) (to be published)

In the same fashion, the heave response predicted by WAMIT[®] has a very high peak at the resonance region. Although the observed in the experimental data had amplitude was about 1.4 (much smaller than the calculated by WAMIT[®]), it was still overestimated by the hydrodynamic module, although not so exaggerated.

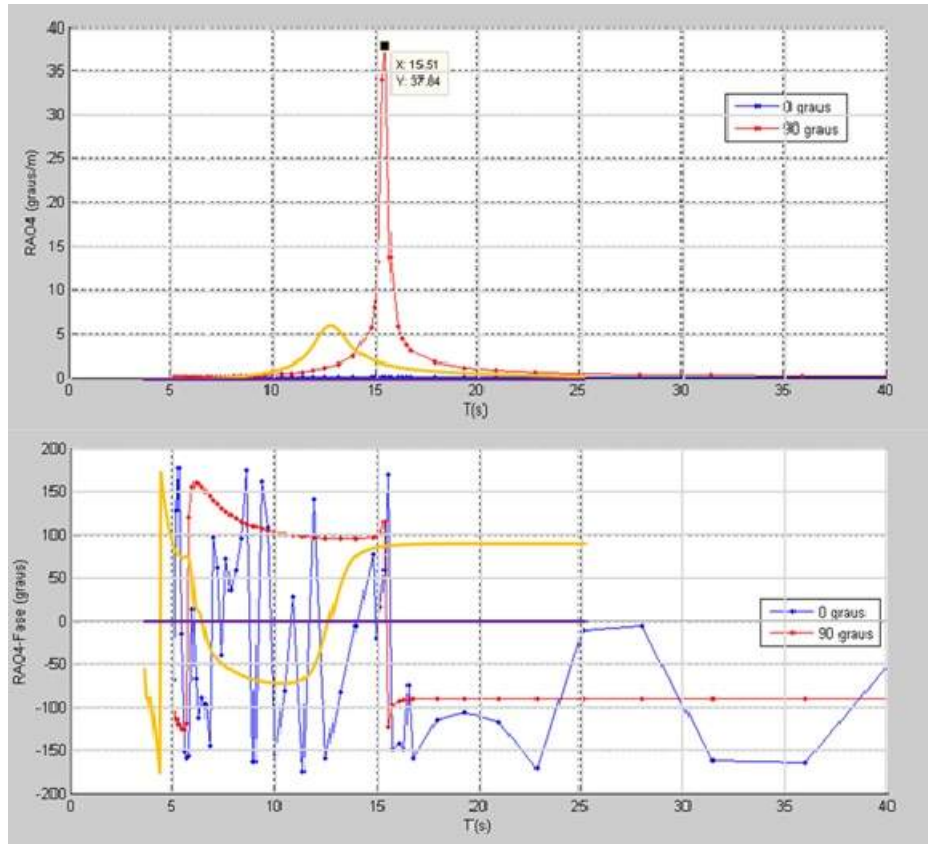
Figure 63: Heave RAO at incidences 0° and 90° , comparison between calculations by WAMIT[®] (respectively, blue and red lines) and hydrodynamic module used in the present work (respectively, purple and yellow lines). Top: amplitude, Bottom: phase.



Source: Adapted from Kang (2018) (to be published)

The experimental peak value at the resonance region was about 2.1 for roll motion, what was overestimated by both numerical methods, in different proportions. The hydrodynamic module predicts around twice the actual value due to non-viscous premises. In addition, the resonance period is more accurate in the prediction by the hydrodynamic module simulation. There is a discrepancy in phase because of lack of data about the metacentric height, that was not informed.

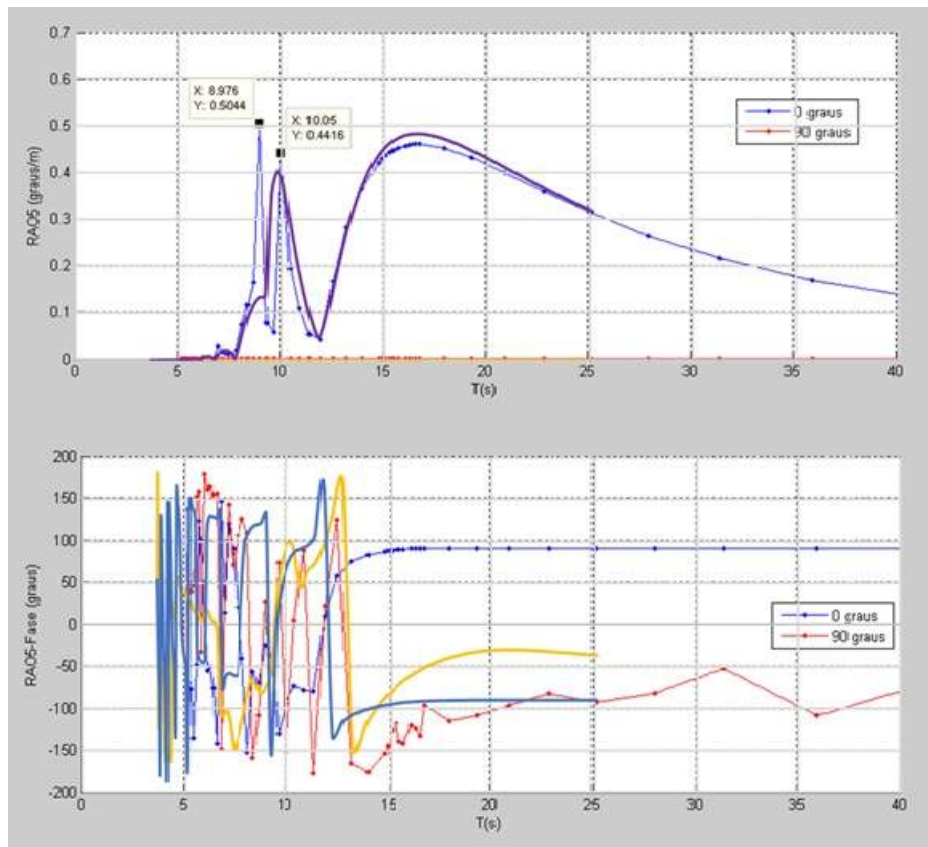
Figure 64: Roll RAO at incidences 0° and 90° , comparison between calculations by WAMIT[®] (respectively, blue and red lines) and hydrodynamic module used in the present work (respectively, purple and yellow lines). Top: amplitude, Bottom: phase.



Source: Adapted from Kang (2018) (to be published)

Same as for surge, pitch RAO response at beam wave is supposed to be negligible, and the output of the numerical calculation by the hydrodynamic module has a good agreement with that by WAMIT[®] at head waves.

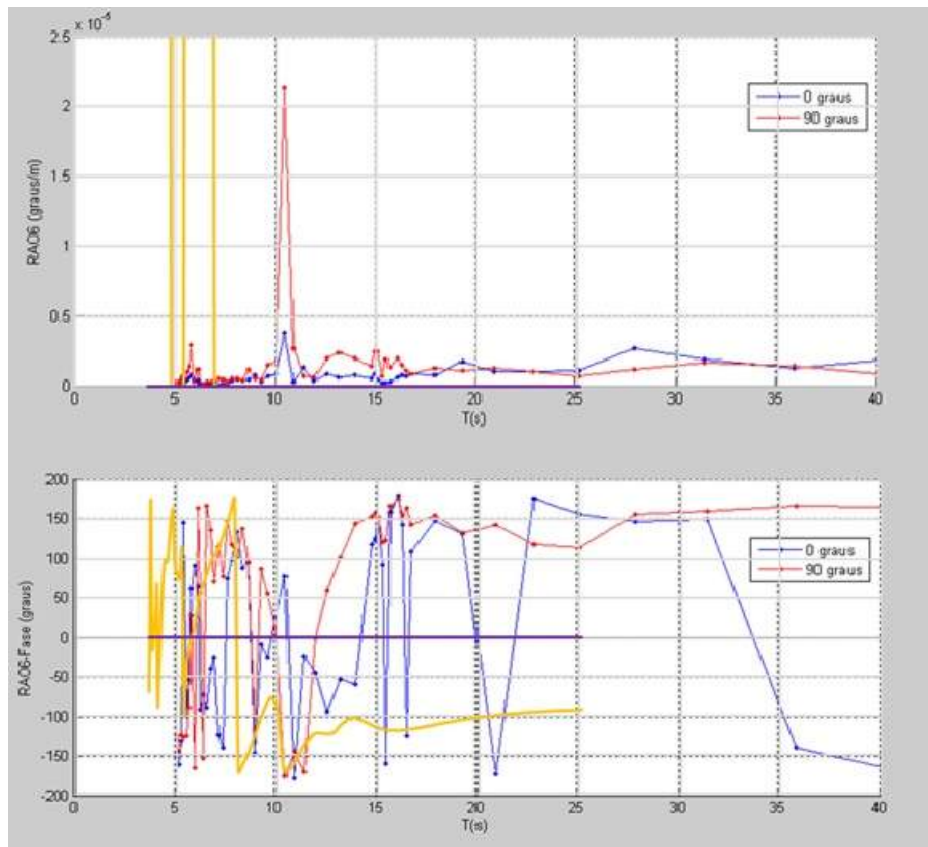
Figure 65: Pitch RAO at incidences 0° and 90° , comparison between calculations by WAMIT[®] (respectively, blue and red lines) and hydrodynamic module used in the present work (respectively, purple and yellow lines). Top: amplitude, bottom: phase.



Source: Adapted from Kang (2018) (to be published)

The yaw RAO is negligibly small as could be noticed from the experimental data in figure 60, although we can see a huge peak expressed in the calculation by WAMIT[®] around the resonance region. The peaks also found on yellow line (for 90°) in the output from the hydrodynamic module are due to lack of information of yaw damping factor.

Figure 66: Yaw RAO at incidences 0° and 90° , comparison between calculations by WAMIT[®] (respectively, blue and red lines) and hydrodynamic module used in the present work (respectively, purple and yellow lines). Top: amplitude, bottom: phase.



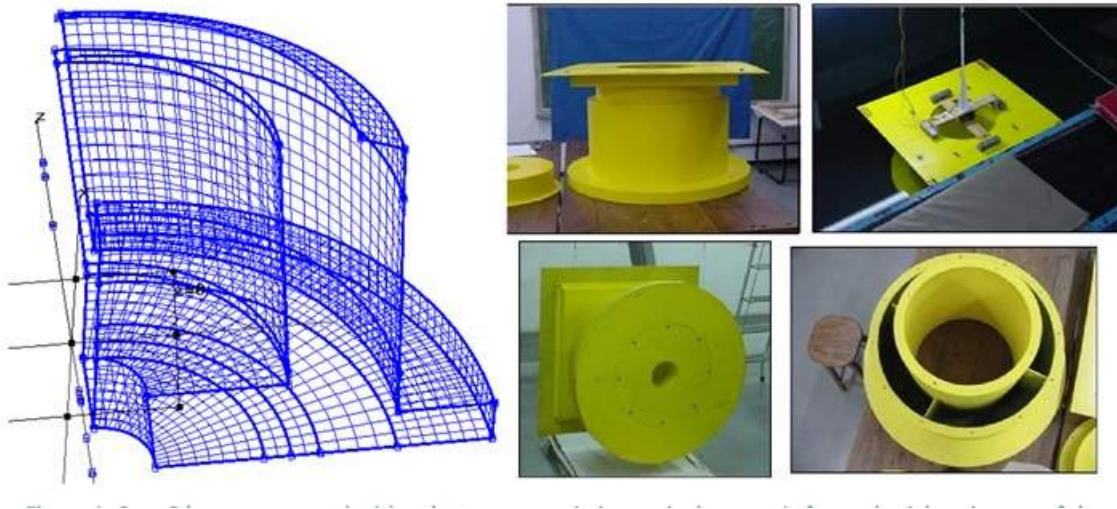
Source: Adapted from Kang (2018) (to be published)

From the above discussed results, the output generated by the hydrodynamic module calculation can be considered reliable for such shape of hull.

6.3 Single column with skirt

An example from Torres (2007) was used for additional validation. The hull shape is a single column platform with a larger diameter portion on its bottom region, called skirt, and inside its moon pool there is a duct-type restriction. A mesh illustration is shown in figure 67 and on table 12 there are the dimensions and properties of the mesh used for calculation.

Figure 67: Case 2: cylinder platform with a moon pool with a duct-type restriction on its bottom. Left: mesh, right: pictures of the model used for experiment.



Source : Torres (2007)

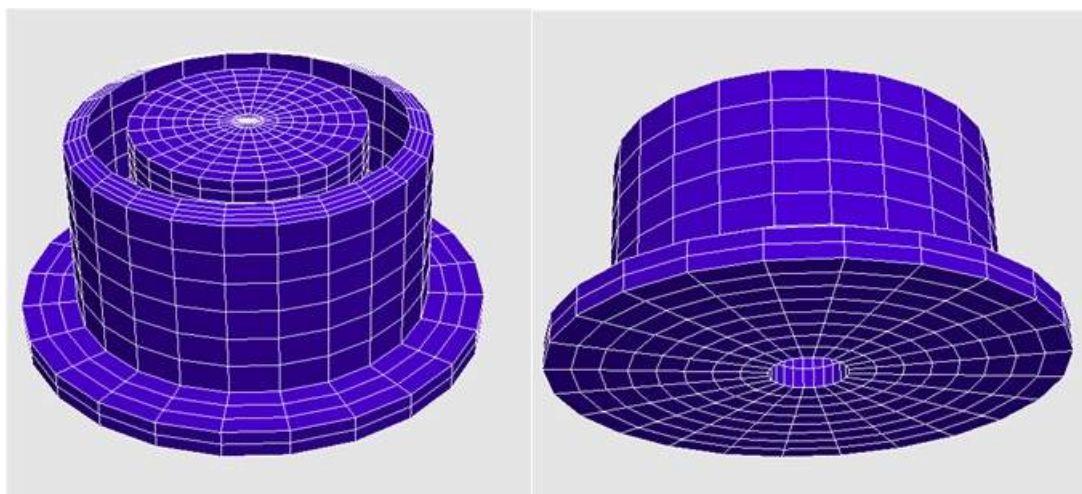
Table 12: Details of the tested models for validation: dimensions and element divisions.

Description	Case 2
Moon pool's internal radius	20.65
Draft	38.40
Radius on top of the beach	27.75
Height of the beach	1.50
Radius of the main body	31.75
Height of the main body	32.00
Radius of the skirt	41.75
Height of the skirt	5.00
Radius of the restriction	6.50
Height of the restriction	10.00
Kxx	28.23
Kyy	28.23
Kzz	29.30
Generatrix curve divisions	
Beach	4
Main body's vertical	6
Skirt's superior surface	3
Skirt's vertical	2
Bottom of the platform	8
Restriction's vertical	3
Restriction's horizontal	3
Rayleigh Damping	0.1

Source : Torres (2007).

The mesh used for calculation is shown in figure 68.

Figure 68: Mesh used for calculation in the hydrodynamic module.



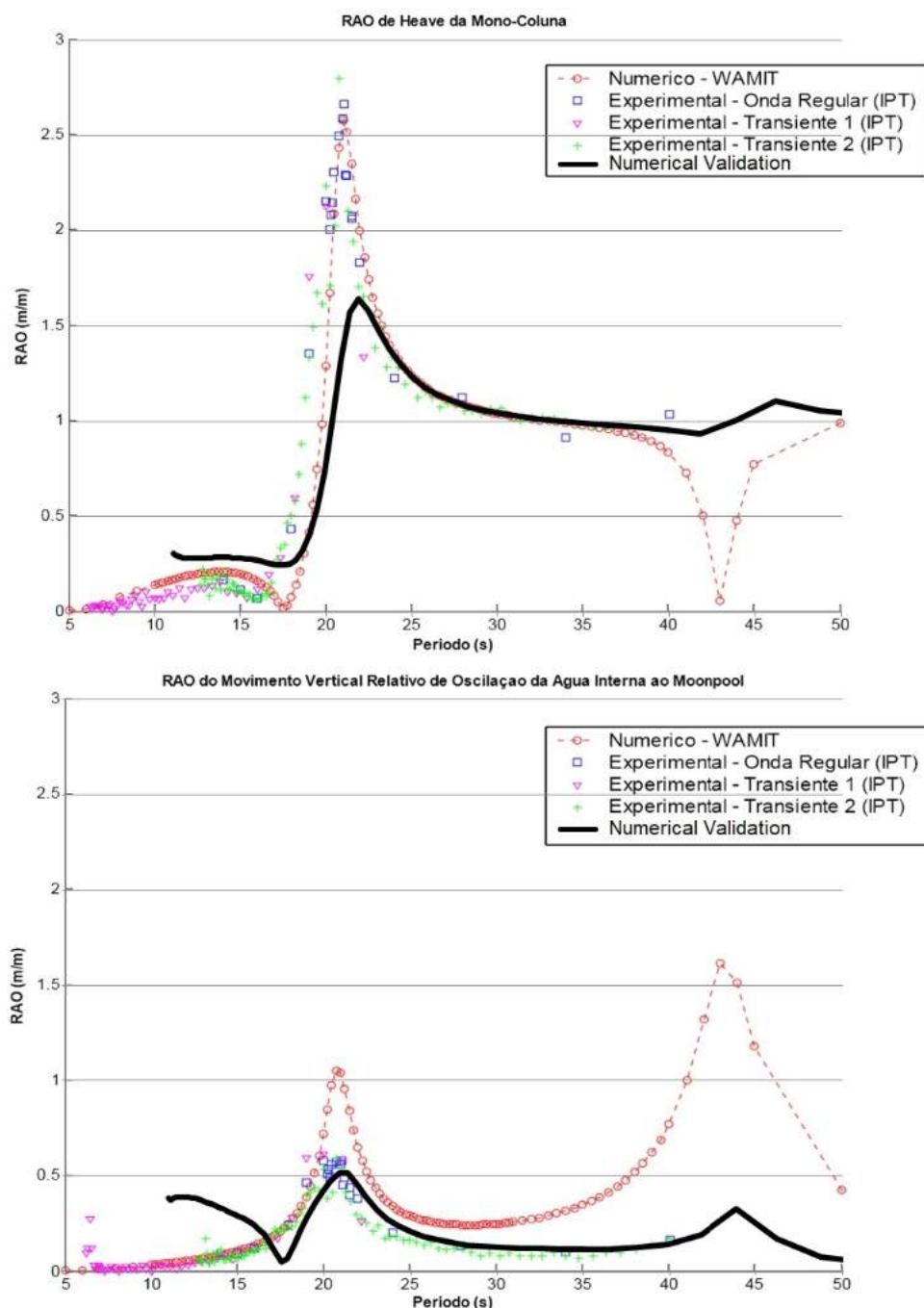
Source : Author

According to the author, the experiment was run in a towing tank at IPT¹. The test was run for regular waves and transient waves, and the model was lashed in horizontal plane with spring-connection steel cables at 60°, 180° and 300° relative to the wave propagation direction. The heave RAOs of the hull and of the water relative vertical oscillation of the MP by measured and calculated data were plotted for the hull and moon pool separately as shown in figure 69.

The experiment condition and numerical calculation by Torres (2007) are limited to only one degree of freedom of motion, that is the heave mode, and the moon pool water motion is also considered the piston mode only. However, the present calculations allow the six degrees of freedom, as well as vertical and horizontal motions of the water inside the moon pool, *i.e.* piston and sloshing mode.

¹ Instituto de Pesquisas Tecnológicas de São Paulo. Its towing tank has 280m length, 6m breadth and 4m depth.

Figure 69: Comparison between numerical and experimental data obtained by Torres (2007) and the calculation by the hydrodynamic module used in the present work (the latter is in solid black line). Top: Heave RAO of the hull, and bottom: RAO of the relative heave oscillation of the water inside the MP.



Source : Adapted from Torres (2007)

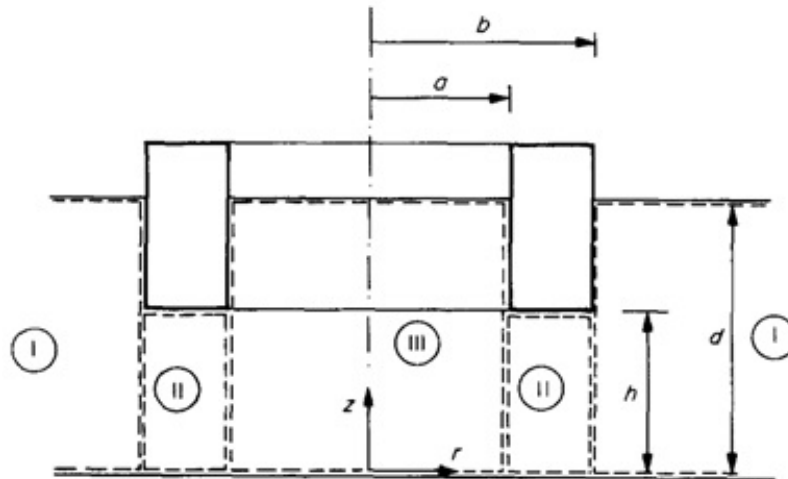
The results calculated with the hydrodynamic module used in this work were plotted on black solid line in both charts. There is a good agreement of this last to the experimental data curves in periods between 17s and 50s, except for the resonance peak in hull motion chart. Since the referred study is only on piston mode with restrictions

on other modes, there is a difference between the responses because the numerical calculation by the hydrodynamic module includes sloshing – which resonance peak is identified around 10s and the six degrees of freedom.

6.4 Cylindrical model

The added mass and damping coefficients of a cylindrical hull with moon pool were obtained by Mavrakos (1988). The configuration used in that work is shown in figure 70.

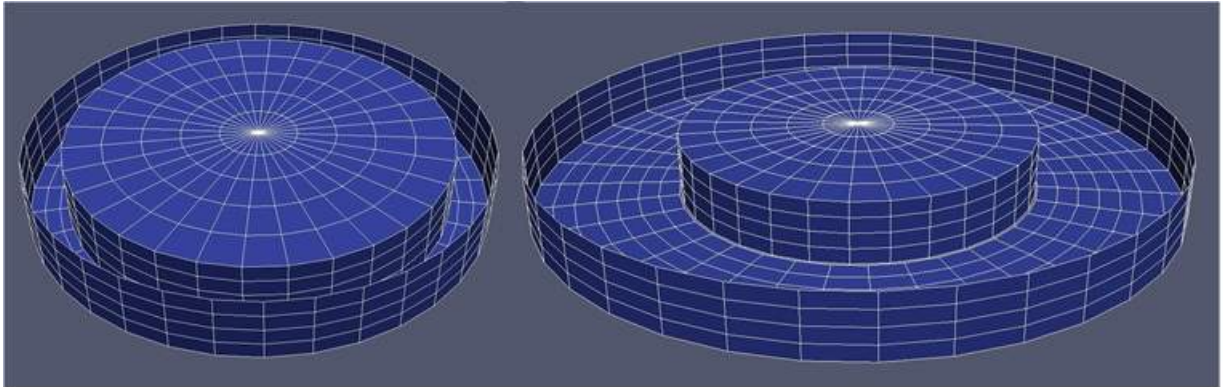
Figure 70: Configuration of the floating ring used by Mavrakos (1988). The dashed rectangles indicate the domains where the calculation was defined. a and b are respectively the internal and external radii, d and $(d - h)$ are respectively the drafts of the tank and of the floating ring.



Source : Mavrakos (1988)

Using the hydrodynamic simulation module, the same geometry was generated, with $a = 30\text{m}$ and $h = 5\text{m}$. The simulation was done for $b/a = 1.2$ and $b/a = 1.8$. The respective meshes are shown in figure 71.

Figure 71: Meshes of hull with free surface inside moon pool of the simulated floating rings. Left: $\frac{b}{a} = 1.2$, right: $\frac{b}{a} = 1.8$



Source : Author.

The obtained charts of the nondimensional added mass and damping coefficients in surge were plotted as superposition of the original ones for comparison. The originals and superpositions are shown in figure 72. A good agreement of the curves for both configurations can be noted in both charts of added mass and of damping coefficients, so the hydrodynamic simulation module shows to be reliable for similar calculations of such coefficients within similar ranges of frequency.

Figure 72: Nondimensional added mass (left) and damping (right) coefficients in surge of the cylinder hull. Top: original charts, and bottom: hydrodynamic simulation module outputs

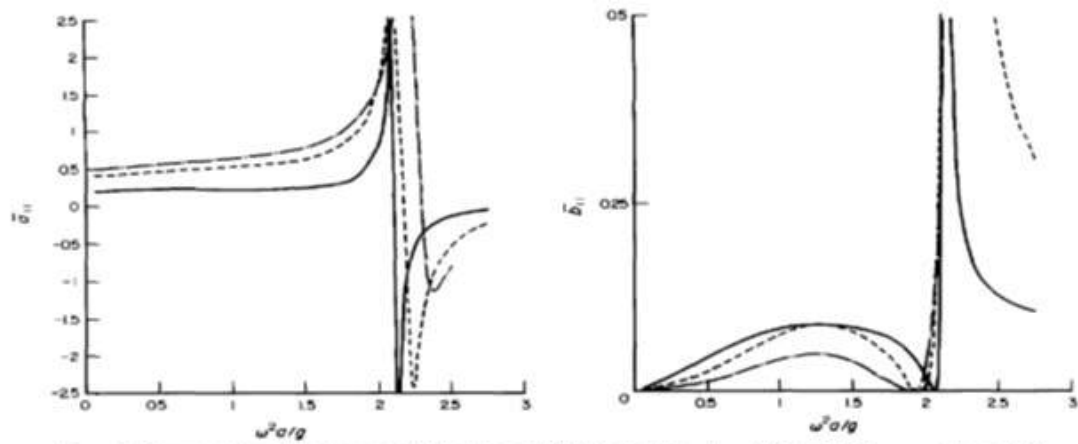
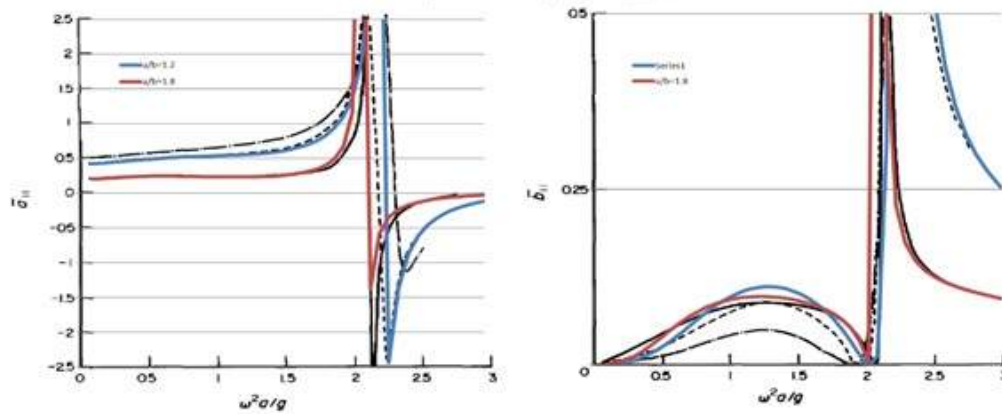


FIG. 3. Dimensionless added mass and damping coefficients in surge. (—) $b/a = 1.8$; (---) $b/a = 1.2$; (- · - · - ·) $b/a = 1.054$.



Source : Adapted from Mavrakos (1988)

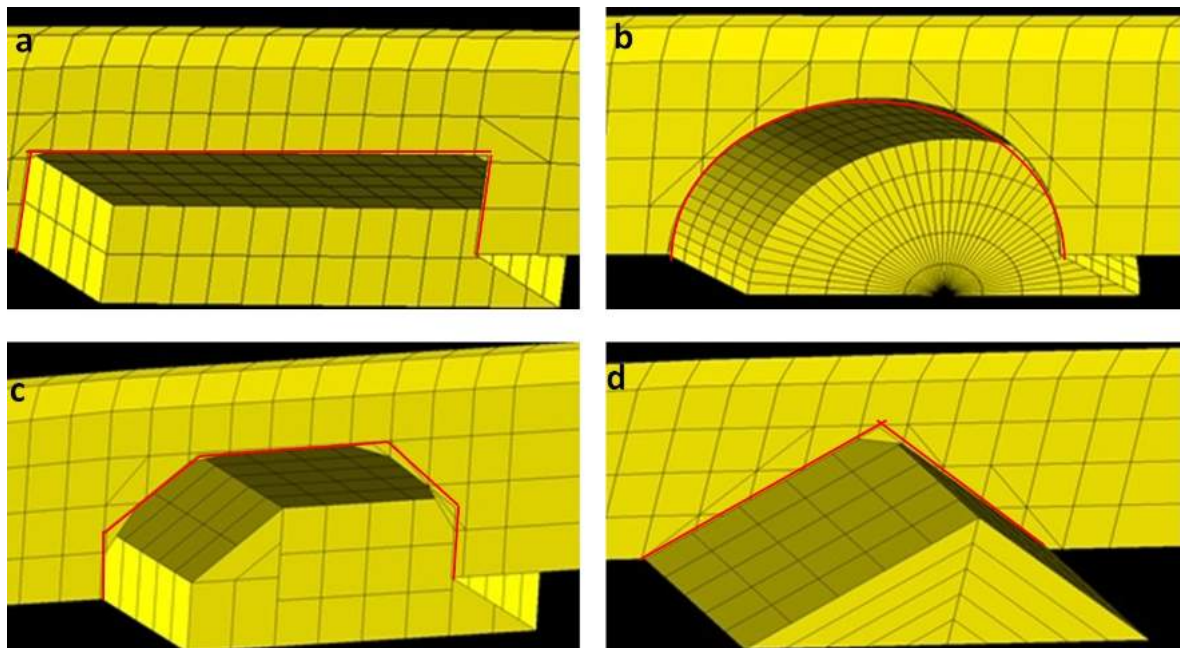
7 Results and discussions

7.1 Characteristics investigations before optimization

The evaluation of operability considering all the criteria and concepts designed in the present work is too complex and does not allow analytical solution neither a precise quantitative judgement, what justifies the need to use numerical calculation and computational simulations instead. To get a qualitative notion of how could the optimum shape tend to look like, a collection of simulations was done to assess the performance of different moon pool configurations and find out if any trend could be identified.

In section 5.1, of the discussion about the mesh for moon pool, it is explained in details how its shape is defined by several parameters: L1, L3 for overall length, L2 for breadth, m1, m4 for rectangle body attached to the longitudinal centre line, m2, m3 for parallel mid body amidship, and nt, nf for corners shape (see fig 46). Two approaches were done, to assess effects of overall length parameters L1, L2, L3 variations and to assess the remaining parameters. The investigated shapes are illustrated in figure 73: rectangle, ellipse, octagon and rhombus.

Figure 73: Basic geometries assessed: rectangle (a), ellipsoid (b), octagon (c) and rhombus (d)



Source: The author.

Each shape was chosen to have a specific characteristic. Rectangles have the

m_i values assuming their superior limit values, what makes nt , nf values negligible (there will not be space for polygon corner other than right angle). The opposite values of m_i , *i.e.* $m1 = m2 = m3 = m4 = 0$ allow ellipse or rhombus, where their difference remain in maximum nf , nt values in ellipse, and minimum nf , nt values in rhombus ($nf = nt = 1$). An intermediate situation between extreme sharp corners as in rhombus and rectangle with right angles was created with the octagon shape.

The first approach consisted in starting from a standard set of main dimensions, and varying them for the same shape parameters in a way that geometry is kept and aspect ratio (length/breadth) is changed. Value setting of those main dimensions was such that the water plane area inside the moon pool would be kept approximately the same for all the samples of the same geometry to assure the same water volume inside them.

The best aspect ratio of each geometry was selected to compare the performance among shapes. This geometry variation assessment was done applying the smallest area value among the selected samples of best performance in each shape.

7.1.1 Aspect ratio variation

The first investigation was carried out with a starting point being the biggest dimensions allowed for the installation of the moon pool on the hull (section 7.2, of the optimization conditions). Those values are approximately the proportional dimensions that are found in the current regular moon pools. In design matters, for the sake of keeping space on the deck it is not recommended to exaggerate those values, but in this assessment, they were exceeded when aspect ratio was changed, to keep the water plane area inside moon pool the same for all samples of that geometry. A set of variations was made by shortening the breadth of the moon pool, and another set was shortening its length. The tables in 13 illustrate the parameter sets used in those trials.

Table 13: Collection of sets of parameters used in each sample of the basic geometries analysed

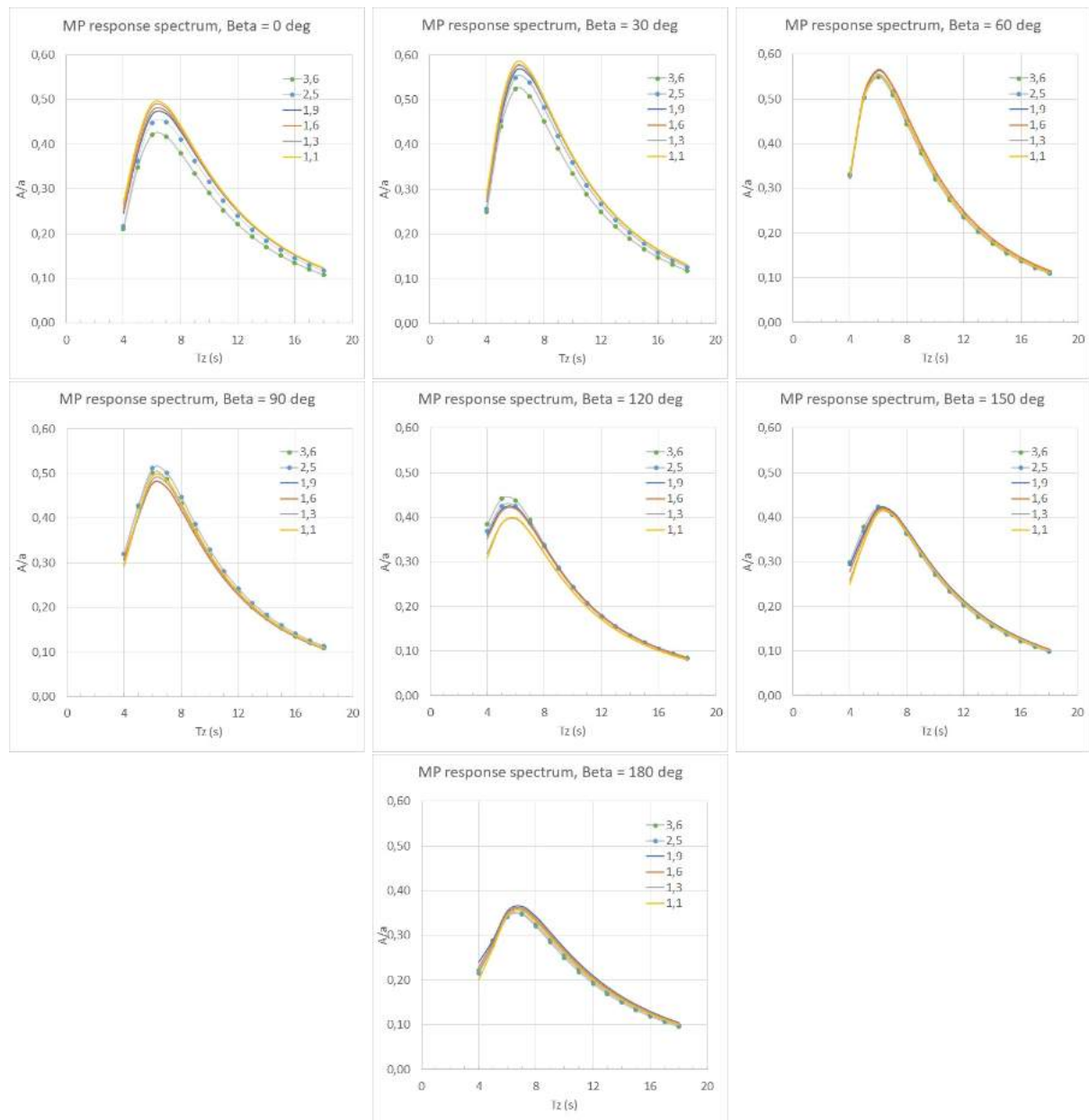
L/B	Rectangle						Ellipse					
	3.65	2.55	1.85	1.6	1.35	1.1	3.65	2.55	1.85	1.6	1.35	1.1
L1	18.200	15.167	13.000	12.000	11.000	10.000	18.195	15.162	13.000	12.000	11.000	10.000
L2	5.000	6.000	7.000	7.583	8.273	9.100	5.000	6.000	7.000	7.576	8.265	9.091
L3	18.200	15.167	13.000	12.000	11.000	10.000	18.195	15.162	13.000	12.000	11.000	10.000
m1	5.000	6.000	7.000	7.583	8.273	9.100	0.000	0.000	0.000	0.000	0.000	0.000
m2	18.200	15.167	13.000	12.000	11.000	10.000	0.000	0.000	0.000	0.000	0.000	0.000
m3	18.200	15.167	13.000	12.000	11.000	10.000	0.000	0.000	0.000	0.000	0.000	0.000
m4	5.000	6.000	7.000	7.583	8.273	9.100	0.000	0.000	0.000	0.000	0.000	0.000
nf	20.000	20.000	20.000	20.000	20.000	20.000	20.000	20.000	20.000	20.000	20.000	20.000
nt	20.000	20.000	20.000	20.000	20.000	20.000	20.000	20.000	20.000	20.000	20.000	20.000

L/B	Octagon						Rhombus					
	3.65	2.55	1.85	1.6	1.35	1.1	3.65	2.55	1.85	1.6	1.35	1.1
L1	18.200	15.167	13.000	12.000	11.000	10.000	18.200	15.167	13.000	12.000	11.000	10.000
L2	5.000	6.000	7.000	7.583	8.273	9.100	5.000	6.000	7.000	7.584	8.273	9.100
L3	18.200	15.167	13.000	12.000	11.000	10.000	18.200	15.167	13.000	12.000	11.000	10.000
m1	2.500	3.000	3.500	3.792	4.136	4.550	0.000	0.000	0.000	0.000	0.000	0.000
m2	9.100	7.583	6.500	6.000	5.500	5.000	0.000	0.000	0.000	0.000	0.000	0.000
m3	9.100	7.583	6.500	6.000	5.500	5.000	0.000	0.000	0.000	0.000	0.000	0.000
m4	2.500	3.000	3.500	3.792	4.136	4.550	0.000	0.000	0.000	0.000	0.000	0.000
nf	1.000	1.000	1.000	1.000	1.000	1.000	1.000	1.000	1.000	1.000	1.000	1.000
nt	1.000	1.000	1.000	1.000	1.000	1.000	1.000	1.000	1.000	1.000	1.000	1.000

Source: Author.

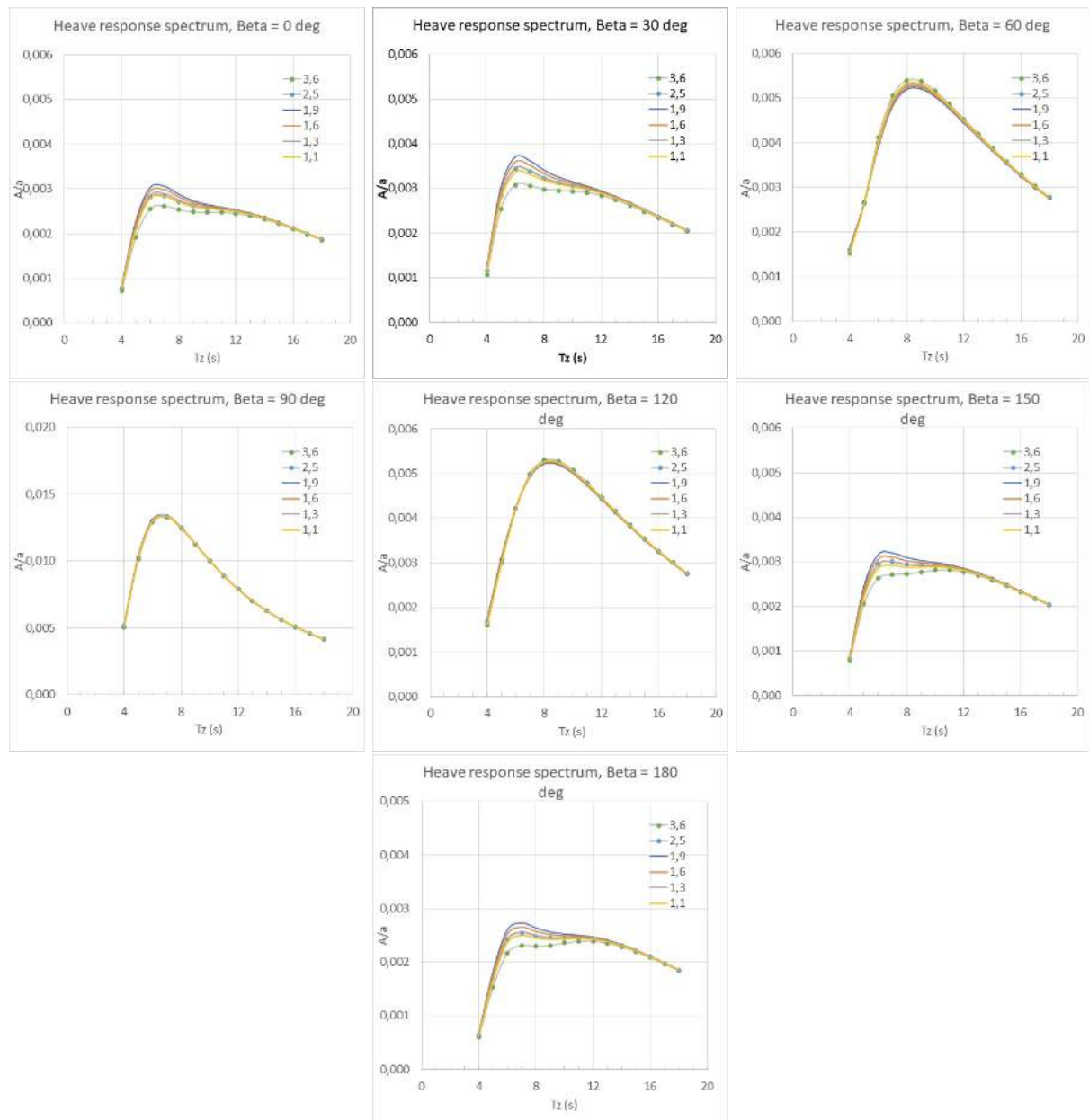
Among all the hydrodynamic behaviour results of the samples tested, an investigation was made to understand the impact of the aspect ratio on the performance of the members of each geometric group, comparing primarily the values of response around the resonance peak, which is the most critical region, and complementing with the overall range outside resonance area. Regarding the scale and units, there is a substantial difference between peak variations in moon pool motion and those in vertical bending momentum, for example. Although in moon pool they are the order of 0.1 m, in bending momentum the scale order is of 100 KN-m. The charts were kept in the original scales for compatibility of comparison with other works. Figures 74 to 89 show the response charts obtained for each shape set: rectangle, ellipse, rhombus and octagon.

Figure 74: Response charts of the moon pool internal water in vertical motion at mid, for several incidence angles β and different aspect ratios: rectangle moon pool



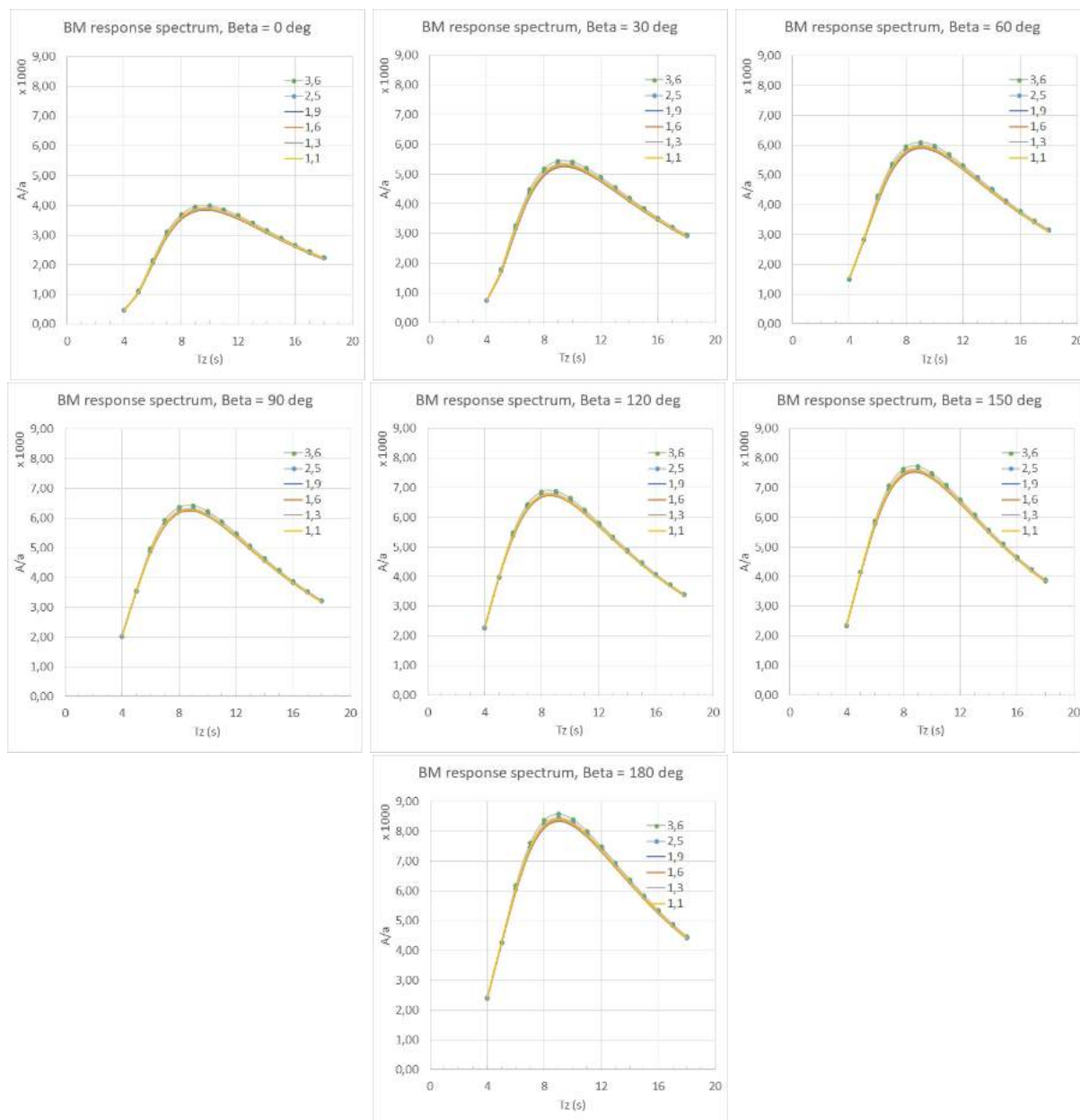
Source: Author.

Figure 75: Response charts of the heave motion, for several incidence angles β and different aspect ratios: rectangle moon pool



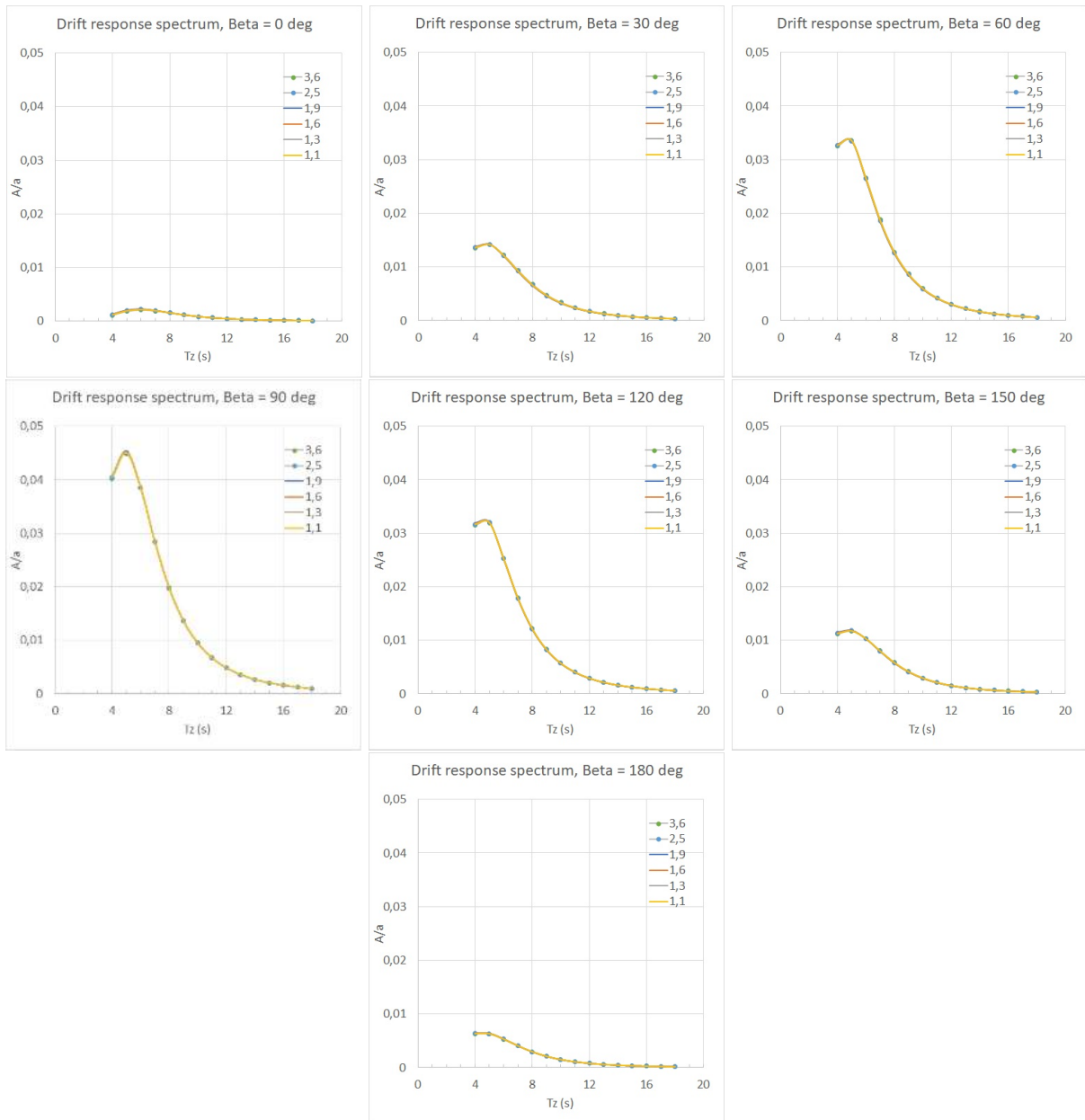
Source: Author.

Figure 76: Response charts of the vertical bending moment amidship, for several incidence angles β and different aspect ratios: rectangle moon pool



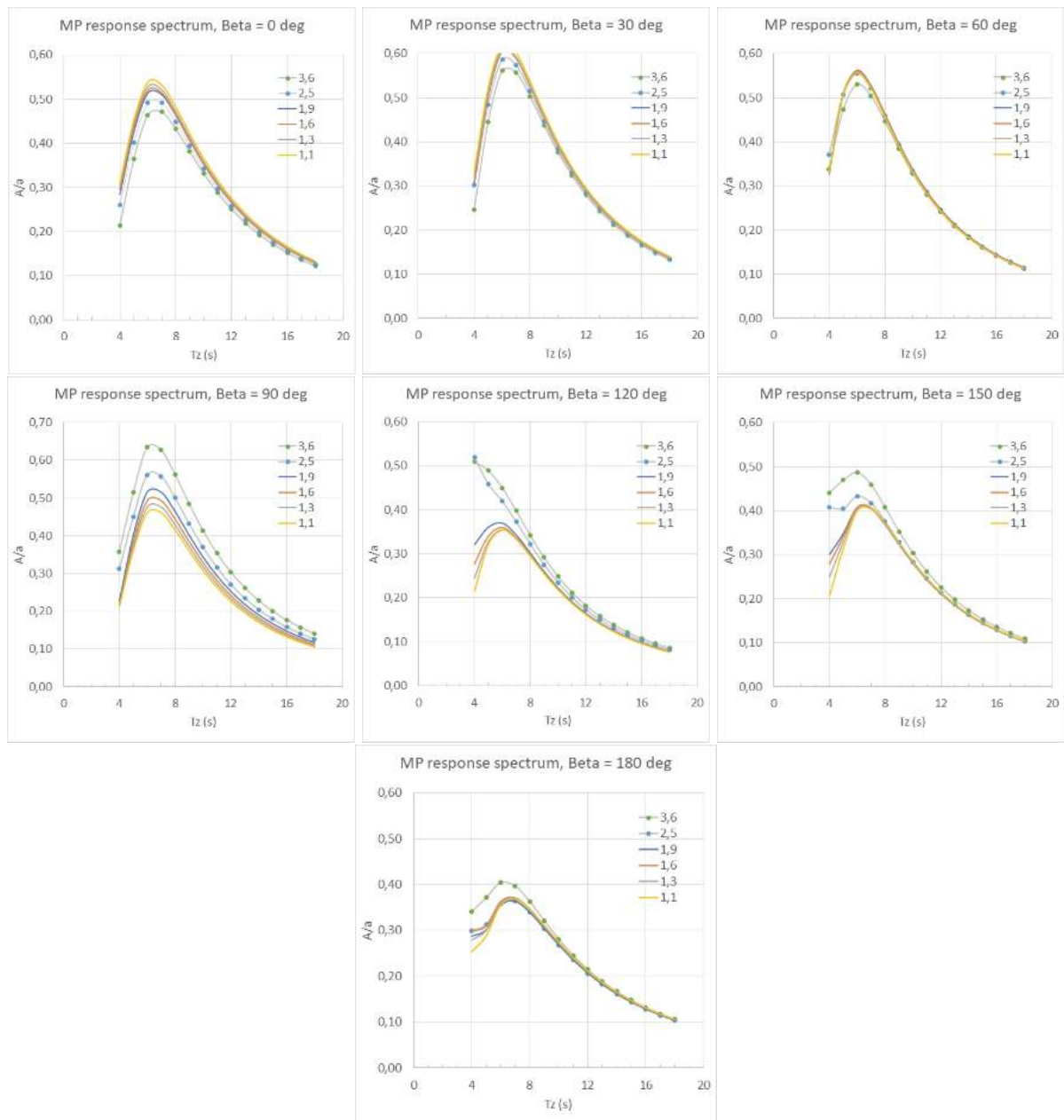
Source: Author.

Figure 77: Response charts of the lateral drift motion, for several incidence angles β and different aspect ratios: rectangle moon pool



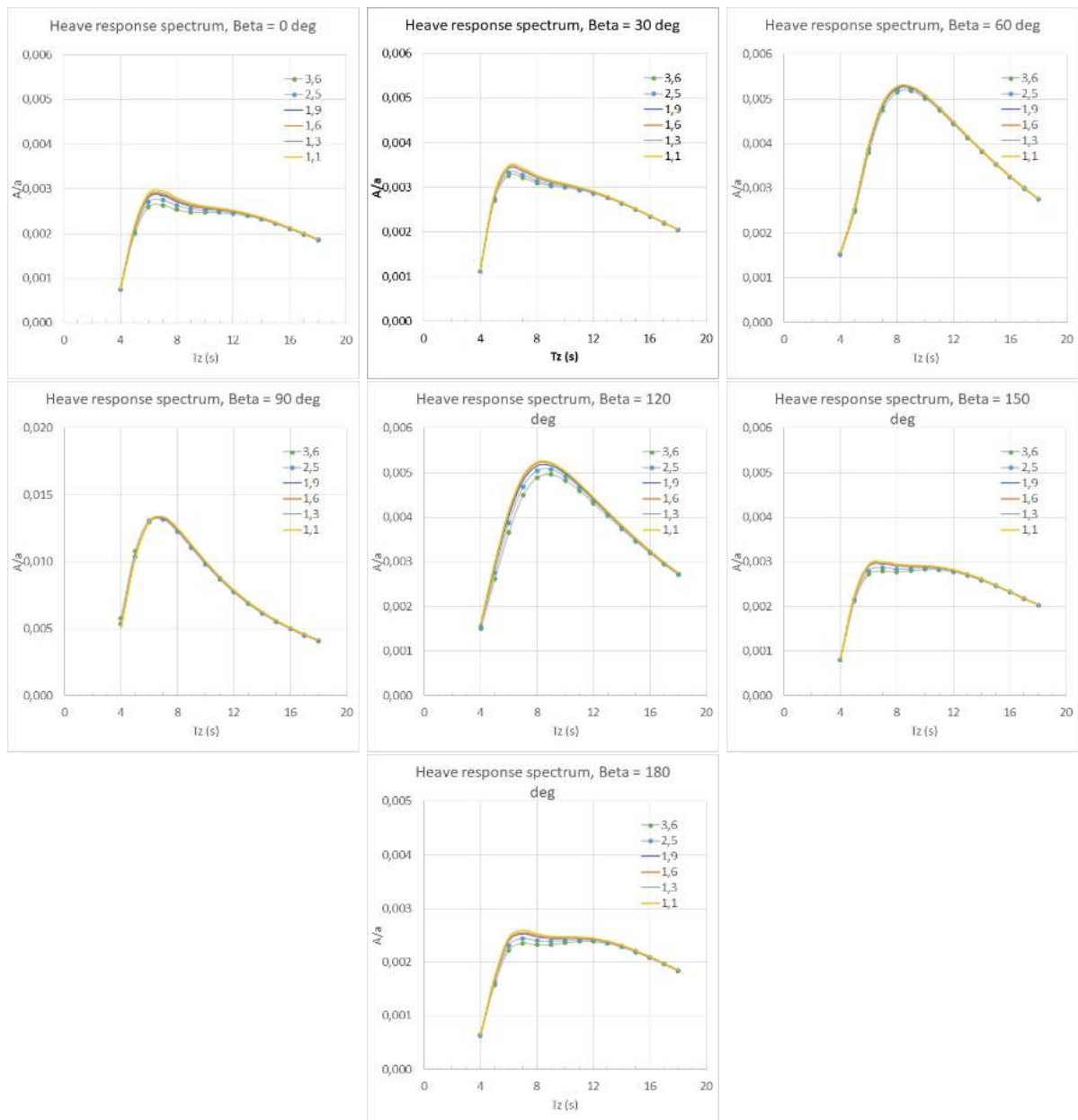
Source: Author.

Figure 78: Response charts of the moon pool internal water in vertical motion at mid, for several incidence angles β and different aspect ratios: ellipse moon pool



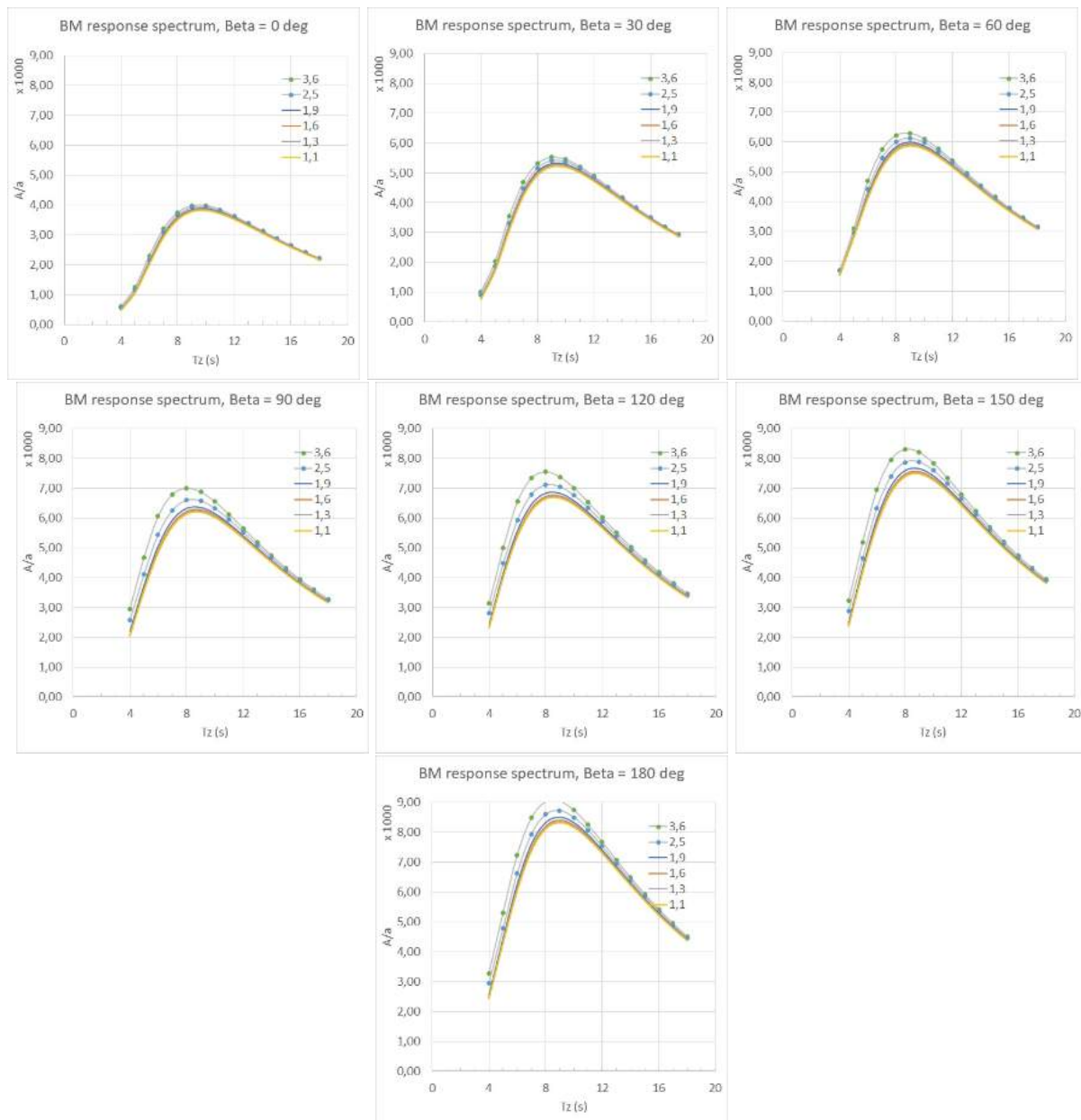
Source: Author.

Figure 79: Response charts of the heave motion, for several incidence angles β and different aspect ratios: ellipse moon pool



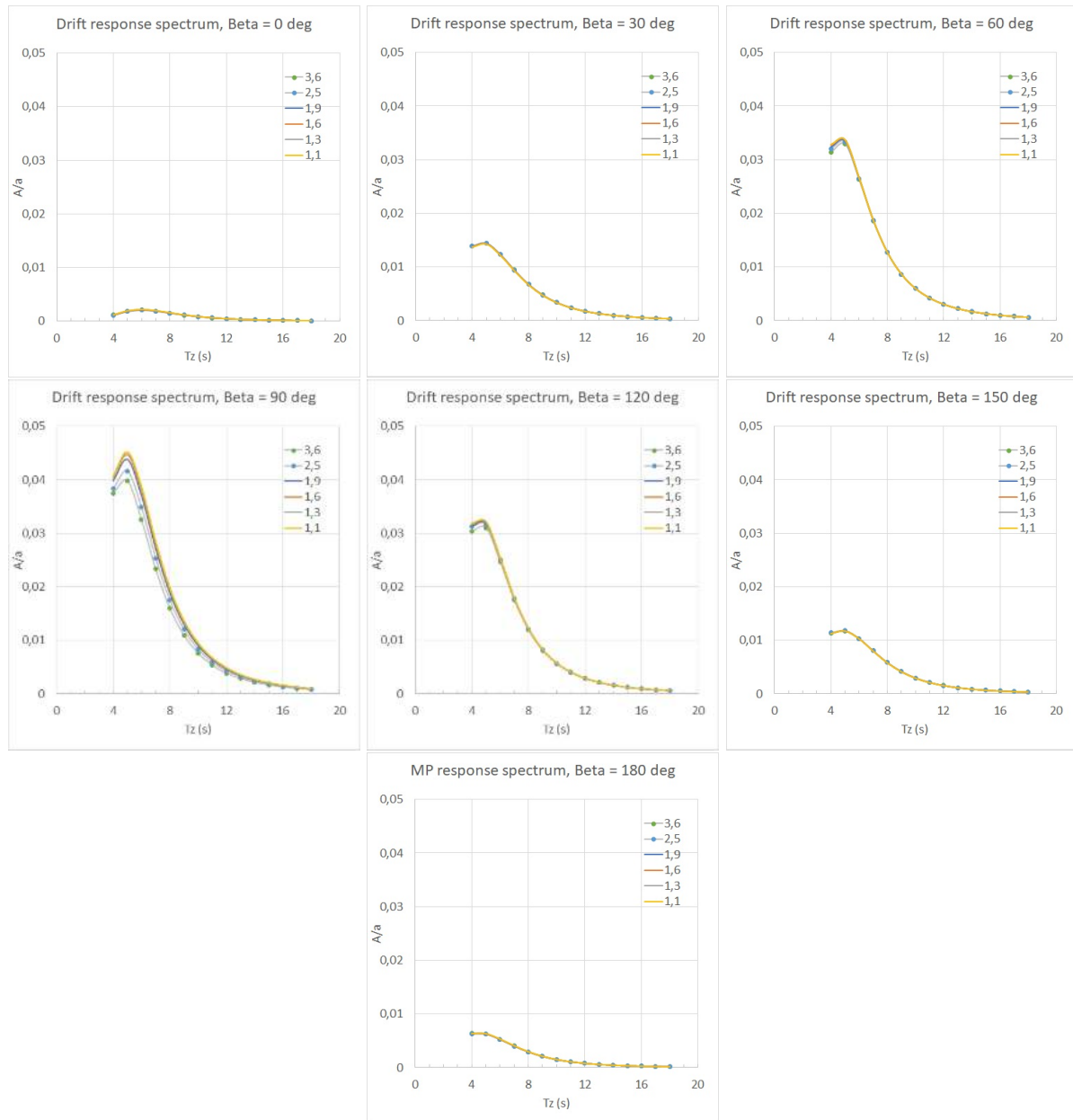
Source: Author.

Figure 80: Response charts of the vertical bending moment amidship, for several incidence angles β and different aspect ratios: ellipse moon pool



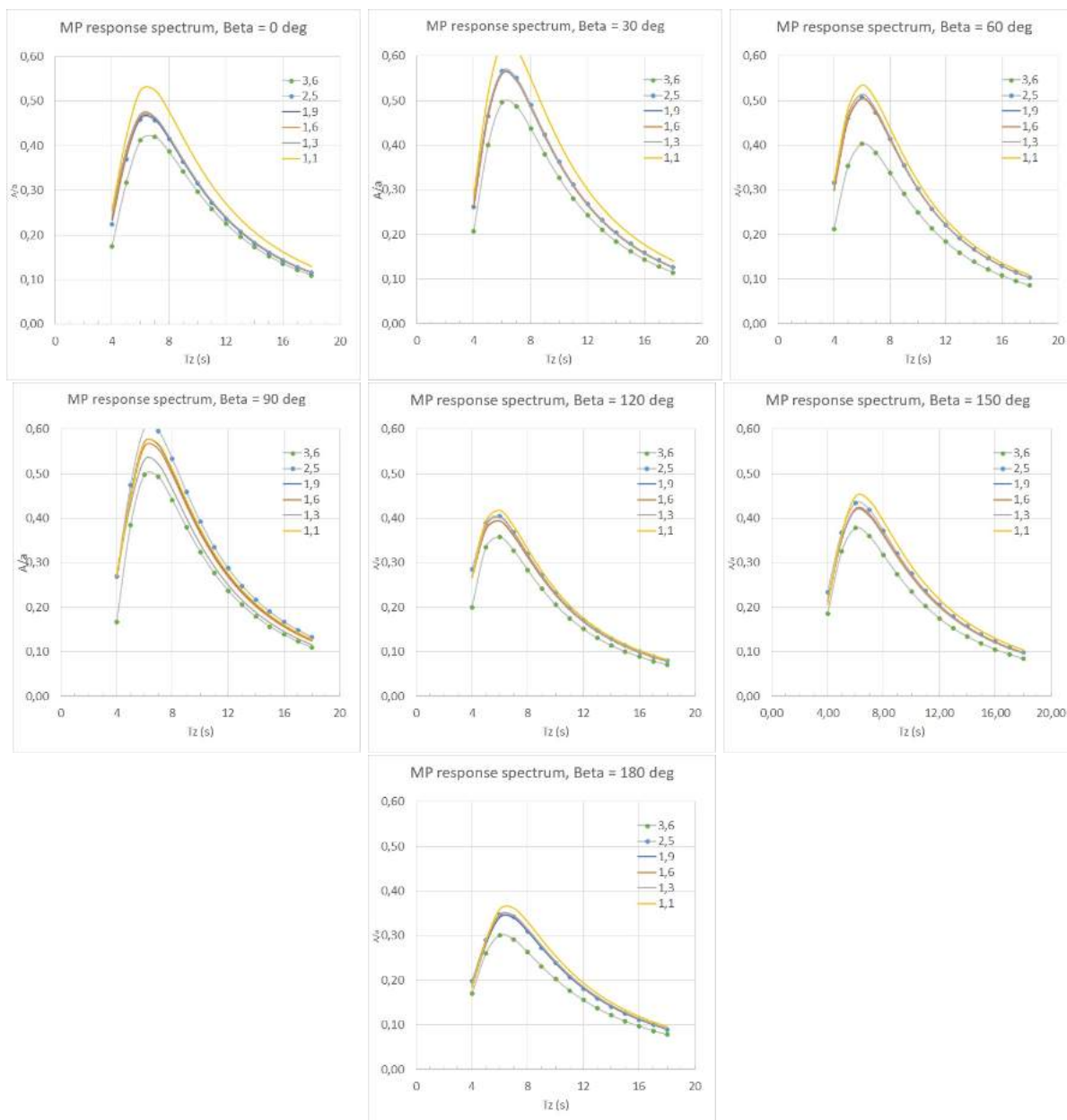
Source: Author.

Figure 81: Response charts of the lateral drift motion, for several incidence angles β and different aspect ratios: ellipse moon pool



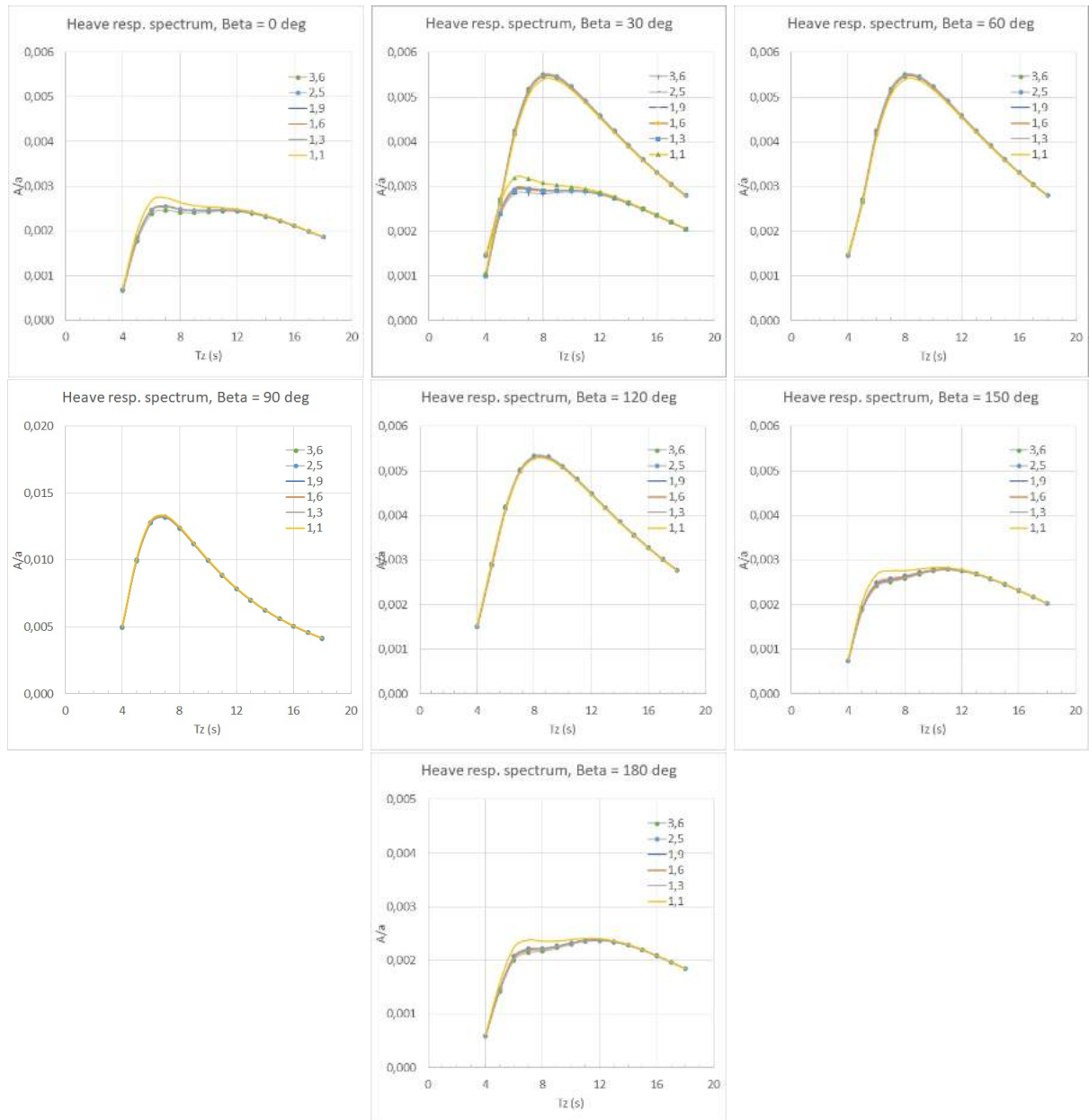
Source: The author.

Figure 82: Response charts of the moon pool internal water in vertical motion at mid, for several incidence angles β and different aspect ratios: rhombus moon pool



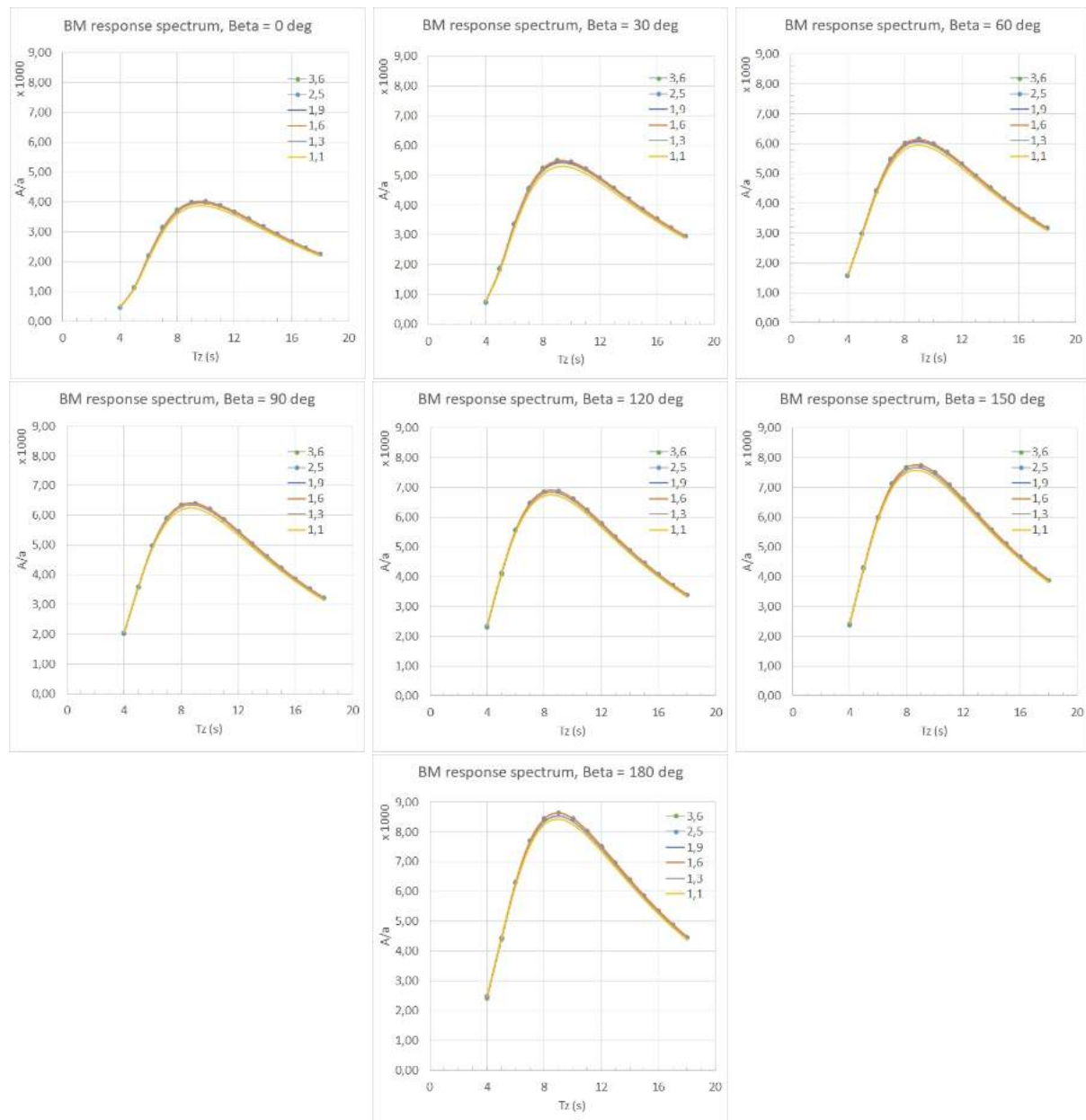
Source: Author.

Figure 83: Response charts of the heave motion, for several incidence angles β and different aspect ratios: rhombus moon pool



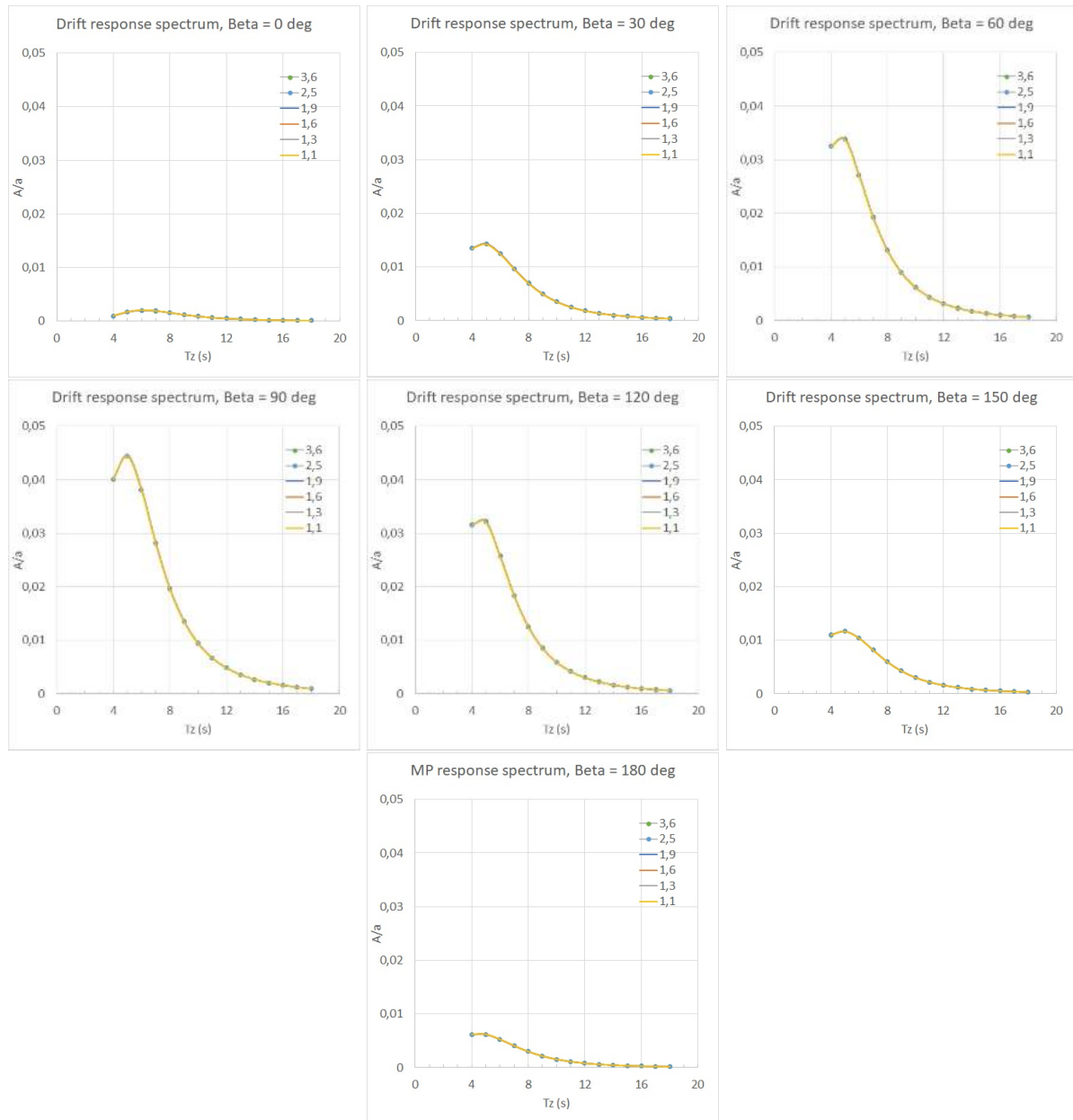
Source: Author.

Figure 84: Response charts of the vertical bending moment amidship, for several incidence angles β and different aspect ratios: rhombus moon pool



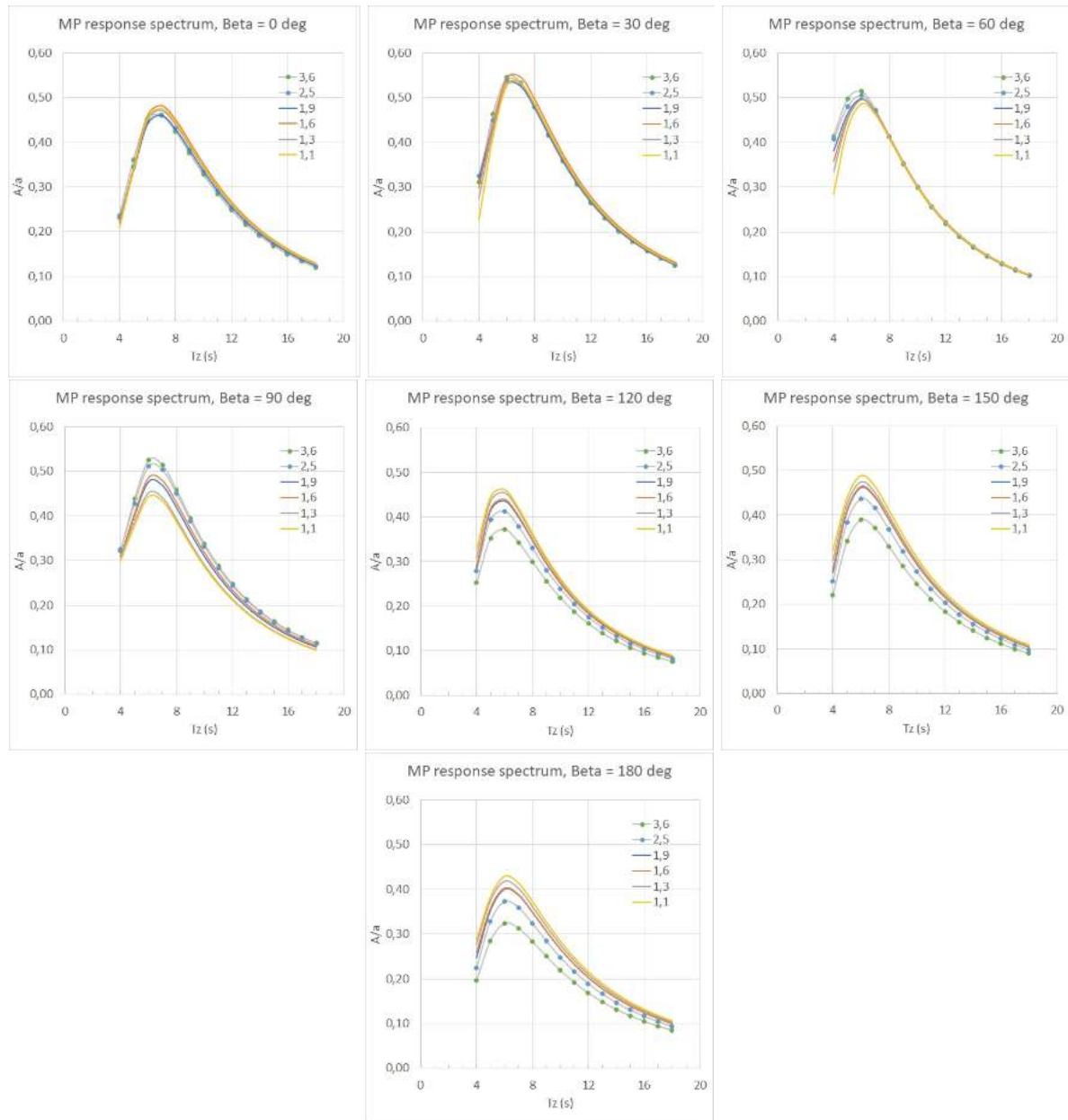
Source: Author.

Figure 85: Response charts of the lateral drift motion, for several incidence angles β and different aspect ratios: rhombus moon pool



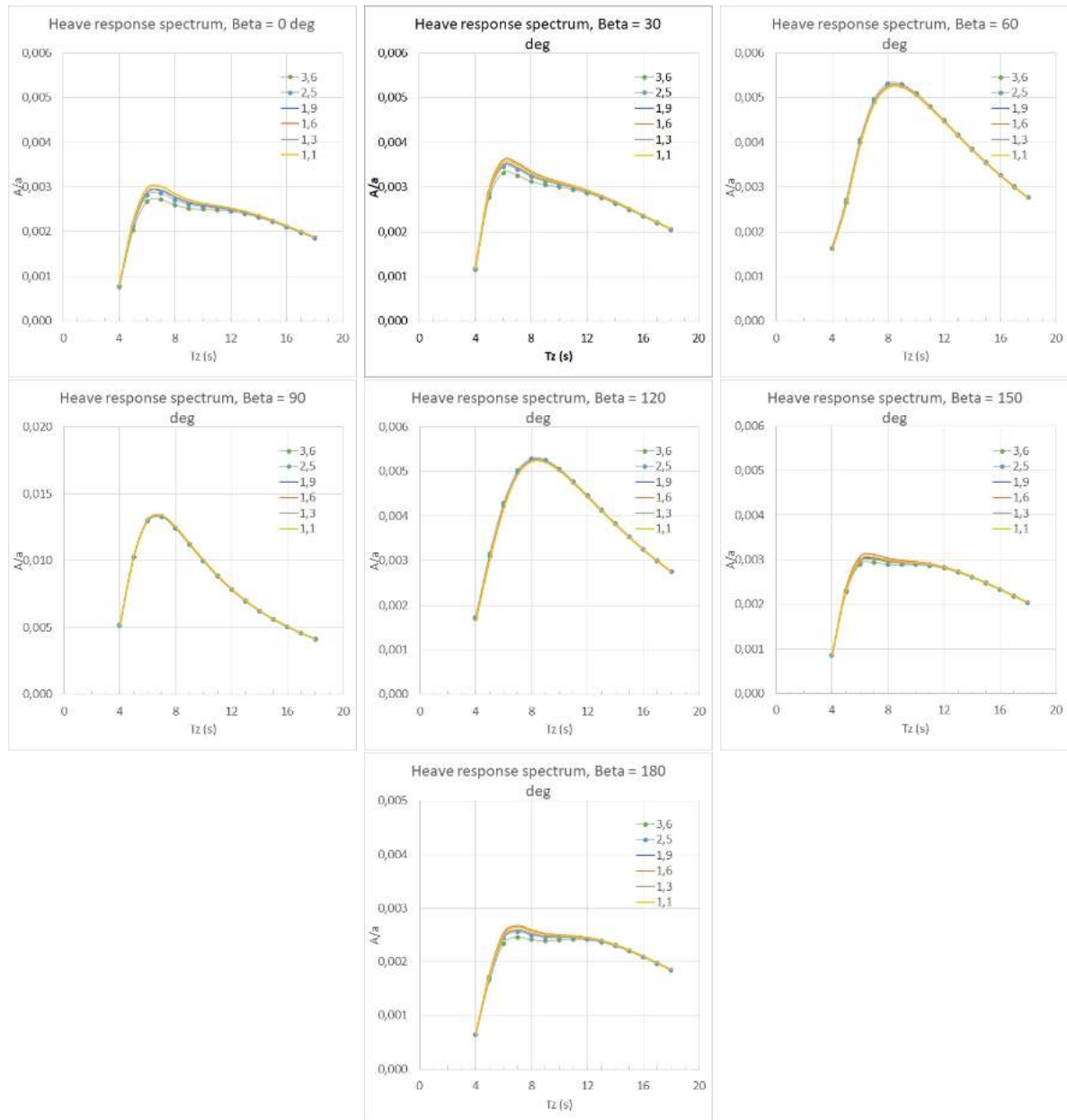
Source: Author.

Figure 86: Response charts of the moon pool internal water in vertical motion at mid, for several incidence angles β and different aspect ratios: octagon moon pool



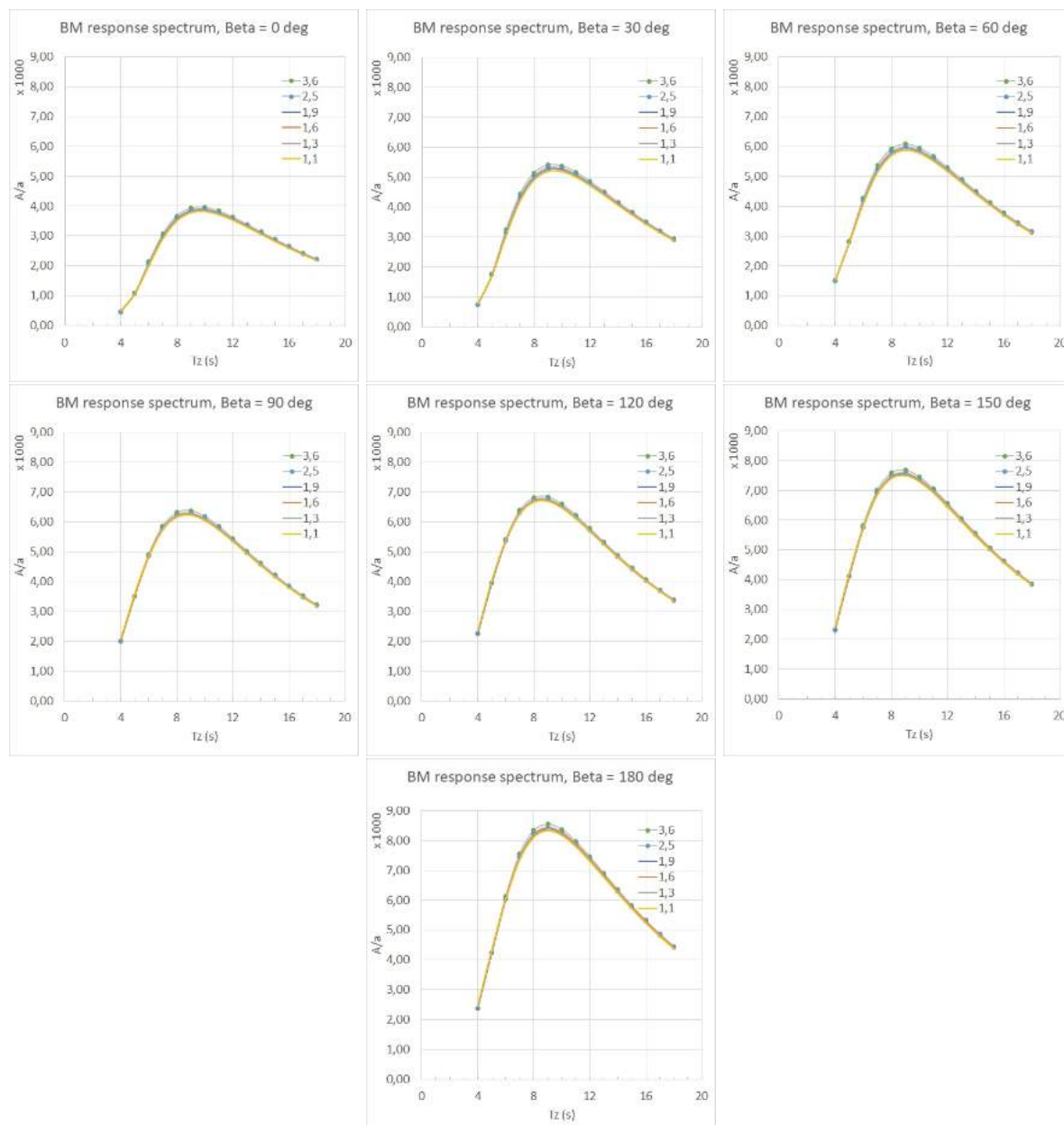
Source: Author.

Figure 87: Response charts of the heave motion, for several incidence angles β and different aspect ratios: octagon moon pool



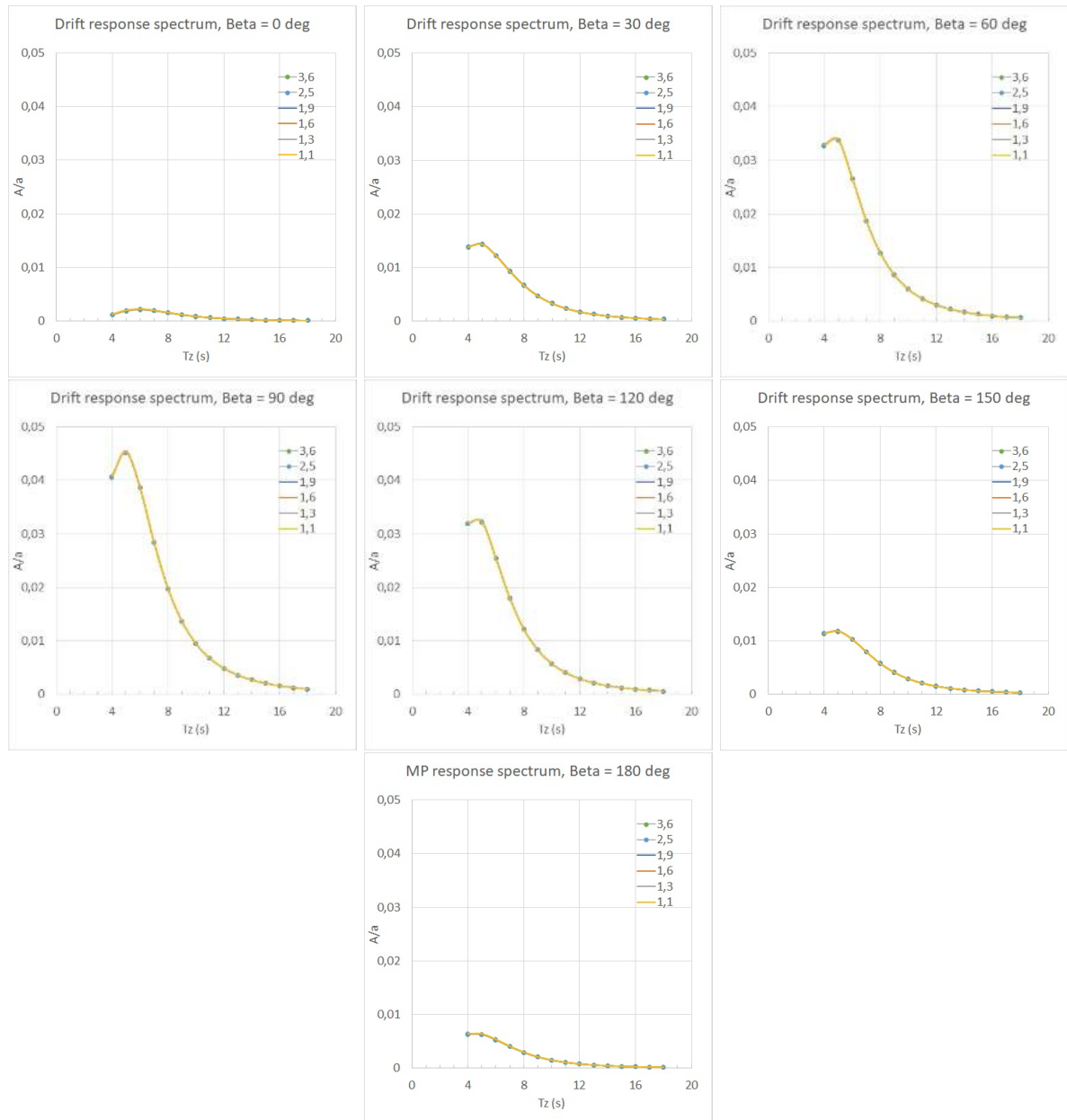
Source: Author.

Figure 88: Response charts of the vertical bending moment amidship, for several incidence angles β and different aspect ratios: octagon moon pool



Source: Author.

Figure 89: Response charts of the lateral drift motion, for several incidence angles β and different aspect ratios: octagon moon pool



Source: Author.

The charts show the drift motion as indifferent to the aspect ratio variation. The responses of hull motion in heave mode have the same nature as the moon pool water motion, but there is a significant difference in scales: moon pool water motion is the order of 10^{-1} while hull motion is the order of 10^{-3} , thus from the point of view of maximum admissible wave height the limitation imposed by hull motion response might be negligible.

Some variation around the peak region are observed in vertical bending moment. Since its scale is the order of 10^3 and of different nature from the other analysed criteria,

nothing can be stated without further analysis. From the respective data, some peak values were collected to understand the relevance of variation of the aspect ratios shown in the charts for each criterion.

It is observed from the charts that the performance of the rectangle in all L/B in moon pool internal water oscillation is better than ellipse for all angles except 120° . The response of rhombus-shaped moon pool samples are specially different from the others in moon pool internal water oscillation from the viewpoint of behaviour variation with L/B value increments. Besides having more clear changes between the response of the samples at each increment, it has a special trend that for beam to aft-shoulder angles (from 90° to 150°), there is a gap from worse performance to best performance, that may be explained by its configuration of congruence of walls in the main directions of flow. The influence of its aspect ratio on the sloshing motion of the water inside moon pool can lead to extreme opposite behaviours depending on the wavelength-beam combination. Such instability in trend with variation of L/B ratio is also observed in heave response at 30° .

Charts of incidence angles that presented the most expressive differences between responses of various L/B values at their peak were used to take the data samples. For each of them, the threshold wave height was calculated at their most limiting situation (peak period), and two kinds of differences were calculated: between highest peak and standard dimensions' peak, and between the extreme peaks (highest and lowest). Standard means the initial configuration (starting point) as described in the beginning of this section. Some of them had both classifications coinciding, resulting in one calculated difference only. Table 14 shows a collection of those data.

For example, in moon pool internal water oscillation there are four sets of data, each corresponding to a different incidence angle of the same geometry set (rectangular). The columns contain the response value read from data ("resp"), the threshold significant wave height calculated according to the peak period shown in the first line of the headings of the table 14, and the last column is the "admittance" increment of wave heights (diff). Except for the third group, all of them have three lines. The upper one is the highest peak value among all aspect ratios of the chart, the shaded line has the value of the peak corresponding to the standard (initial) main dimensions. In some cases, this line coincides with the above-mentioned one, of the lowest value of peak.

The cases with two lines are the third set of moon pool water oscillation, and all sets of ship motion and vertical bending moment. Since the drift response shows to be the same regardless the aspect ratio, for each set, there was only one value to represent the peak of all the samples.

Table 14: Threshold significant wave heights and differences between chosen L/B cases.

T 7		
MP internal water oscillation		
resp	H	diff
0.491	1.792	0.298
0.475	1.852	0.240
0.421	2.090	
0.582	1.512	0.167
0.572	1.538	0.140
0.524	1.679	
0.512	1.718	0.277
0.478	1.840	0.120
0.441	1.995	0.216
0.421	2.090	0.120
0.398	2.210	

T 7		
Ship motion in heave mode		
resp	H	diff
0.00310	198.797	39.759
0.00260	238.556	
0.00370	164.4105	33.096
0.00310	197.506	
0.00539	112.8607	2.351
0.00530	115.212	
0.00539	112.8607	2.351
0.00530	115.212	

T		
Vertical bending moment amidship		
resp	H	diff
6420	23.353	0.635
6250	23.988	
6880	21.792	0.552
6710	22.344	
7710	19.446	0.518
7510	19.964	
8580	17.474	0.374
8400	17.848	

T 5	
Lateral drift motion	
resp	H
0.006	2.756
0.032	1.597
0.034	1.573
0.014	2.090

Source: Author

After bringing those information to comparison based in the same concept of threshold significant wave height (TWH), the most evident variation identified is the moon pool internal water surface. As stated in the previous paragraphs, although a big value of increment is observed in ship motion table, they are over an extremely high range of values of TWH, far from physical feasibility, what means that any wave height would be acceptable, and thus do not represent a suitable limiting criterion for selection based in operability in the present case (fixed internal area of moon pool, same geometry). In the same fashion, vertical bending moment amidship (CrVBM) shows to be too permissive, since wave heights of around 20m or more are not expected to be found. From the point of view of operability, the results observed in moon pool internal water oscillation (CrMPO) and drift motion (CrDFT) are the group that can be considered suitable for using as measure for a judgement of the effects of shape and dimensions in performance, although the second does not itself suffer much changes at variations in shape by the parameters. For these reasons, the following analysis was carried out of moon pool water oscillation responses only.

Among the analysed responses, there are incidence angles at which the performance is almost not influenced by the variation in each approach. For instance, aspect ratio influences on rectangle shapes are observed at incidence angles of 0° , 30° , 90° and 120° for moon pool internal water, whereas for vertical bending moment those incidence angles are 90° , 120° , 150° and 180° . Keeping the focus of finding out which kind of data reduction shall be made to lessen the amount of information for analysis and achievement of the optimal solution, some trends of values or of behaviours were searched. The table below illustrates the incidence angles and observation of better performance variation. It was considered for each sample isolated whether a gap between peaks of the same angle was at least around twice the regular gap found in other angles charts, as well as the existence of differences in non-resonance frequency range, and its highest values in comparison with other different values of incidence angle.

Table 15: Incidence angles at which the impact is more significant

Geometry	0°	30°	60°	90°	120°	150°	180°
<i>L/B</i> Rectangular	X	X		X	X		
<i>L/B</i> Ellipse	X			X	X	X	
<i>L/B</i> Octagon				X	X	X	X
<i>L/B</i> Rhombus		X	X	X			X

Source: Author

Although an overall view of the table suggests that most impact appears to be more expressive from beam to rear angles, such distribution still has a significant

number of incidences in fore angles, and does not allow an assertive affirmation that this should be a path to follow towards the best changes, so an alternative approach was done as described below.

When considering the performance of high L/B ratio in contrast with low L/B ratio, for example, in rectangular and ellipse shapes with same area, bigger L/B present better performance in moon pool water oscillation in frontal (approximately 0 to 30°), and a slightly worse performance in beam seas. In rear angles, rectangular shapes show almost no difference, while ellipse shapes present a significantly worse performance of those with high L/B ratio. Table 16 shows the situation of improvement (O) or worsening (X) of performance of the main criterion for each shape, in each incidence angle.

Table 16: Comparison of highest L/B ratio in each incidence angle for moon pool internal water oscillation response.

Geometry	0°	30°	60°	90°	120°	150°	180°
L/B Rectangular	O	O	-	X	X	-	O
L/B Ellipse	O	O	O	X	X	X	X
L/B Octagon	O	-	X	X	O	O	O
L/B Rhombus	O	O	O	X	X	X	O

Source: Author

From the table 16 the performance of high L/B is better or indifferent most fore incidence angles and worse for beam seas, but there is no statement that can be done for aft angles. So there might be the possibility that lower or moderate L/B have better behaviour than high values. To confirm this hypothesis, the same investigation was carried out for low L/B , shown in table 17.

Table 17: Comparison of lowest L/B ratio in each incidence angle for moon pool internal water oscillation response and vertical bending moment at midship response.

Geometry	0°	30°	60°	90°	120°	150°	180°
L/B Rectangular	X	X	-	X	O	-	O
L/B Ellipse	X	X	-	O	O	O	O
L/B Octagon	-	-	O	O	X	X	X
L/B Rhombus	X	X	X	-	X	X	X

Source: Author

The rectangular MP with lowest L/B ratio present worse behaviour in piston mode, as expected from Fukuda (1977) and van't Veer and Tholen (2008). In fore angles, the lowest L/B ratio (approx 1.1) supports the idea that higher values of the ratio are more likely to have good performance subjected to fore angles. From tables 16 and 17, information of aft incident angles are inconclusive, and regarding that fore angles

and beam seas are opposite in behaviour prediction for highest L/B ratio (approx 3.6), moderate values tend to be the best solution at least for the four shapes proposed without composition of characteristics.

Table 16 shows that moderate L/B ratios have more chance to behave better – and thus more chances to be closer to optimal than extreme (high or low) ones at the resonance period. Considerations still should be kept that this analysis have so far made a conservative approach, since criteria are being treated independently at their worst case, that is the peak at each individual resonance period. If a specific significant period is chosen for all of them combined, that is the situation in the optimization, there might be response values of some criterion that do not coincide with the peak, allowing bigger operable area for that case.

It is important to stress that those observations are only valid for the hull shape used in the present study, and are result of an analysis for the limit values imposed as in section 4.2 of the assessment formulae for the criteria. If the limits are more conservative for bending moment and stroke, for example, the threshold wave heights for those criteria would be smaller, maybe becoming also limits in some incidence angles. If the moon pool's free border would be higher, the threshold wave heights for overflow criterion would be bigger, and in the same manner, with a bigger DPS power, maybe have contribution of criteria other than drift and overflow to define the operable region.

7.1.2 Shape variation

From the previous approach, the sample of each set of geometry that presents the best overall performance in terms of L/B was selected to make a compatible comparison among the shapes. The rhombus shape is the one with smallest internal water plane area value, which should be used as a common value for the other three geometries. Then, the parameters yielded as follows:

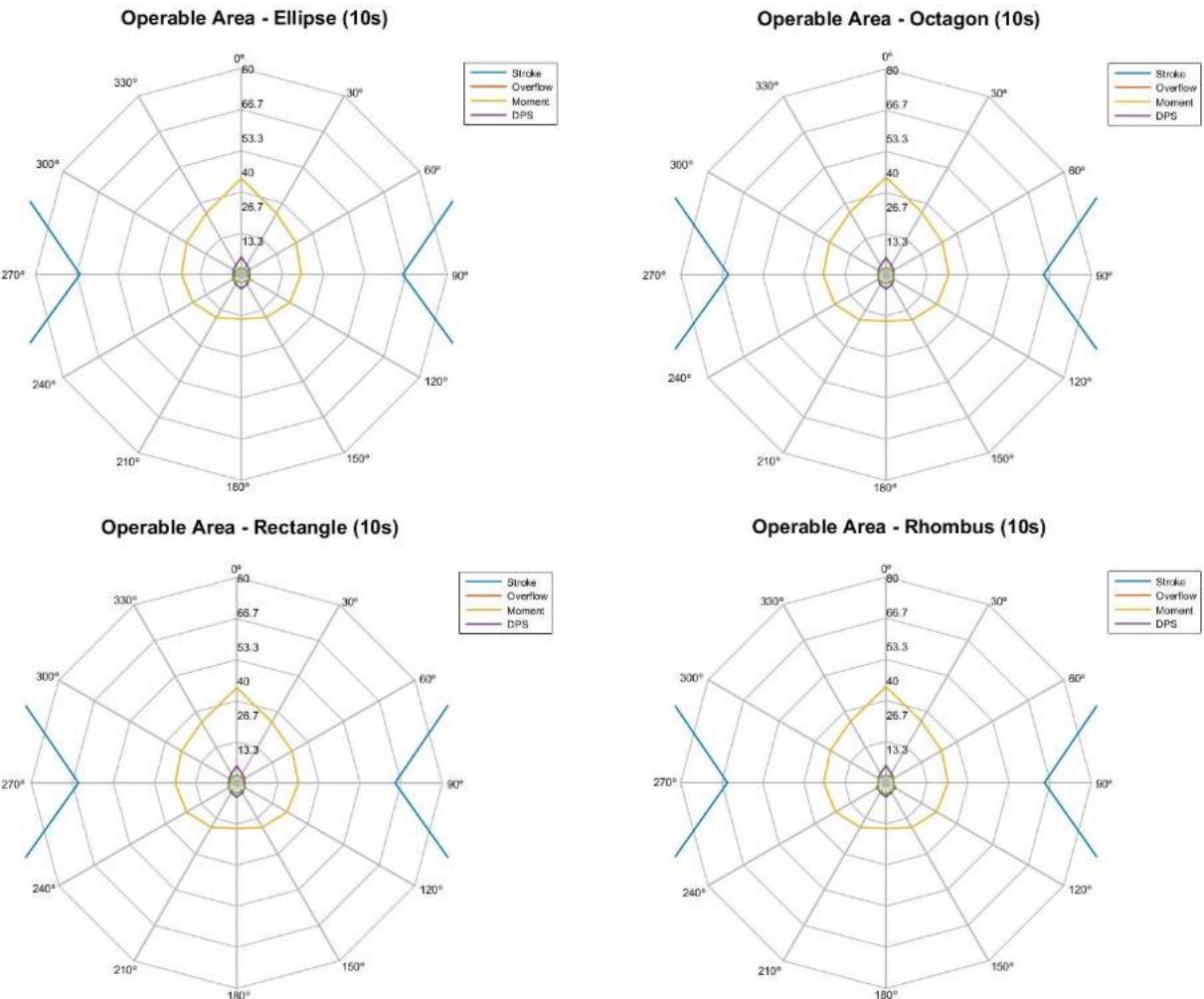
Table 18: Samples of the best L/B in each geometry with the same internal water plane area.

All geometries				
Shape	Ellipse	Rhombus	Octagon	Rectangle
L/B	3.64	3.64	1.10	3.65
L1	14.54	18.20	7.57	12.89
L2	3.99	5.00	6.88	3.53
L3	14.54	18.20	7.57	12.89
m1	0.00	0.00	3.44	3.53
m2	0.00	0.00	3.78	12.89
m3	0.00	0.00	3.78	12.89
m4	0.00	0.00	3.44	3.53
nf	20.00	1.00	1.00	20.00
nt	20.00	1.00	1.00	20.00

Source: Author.

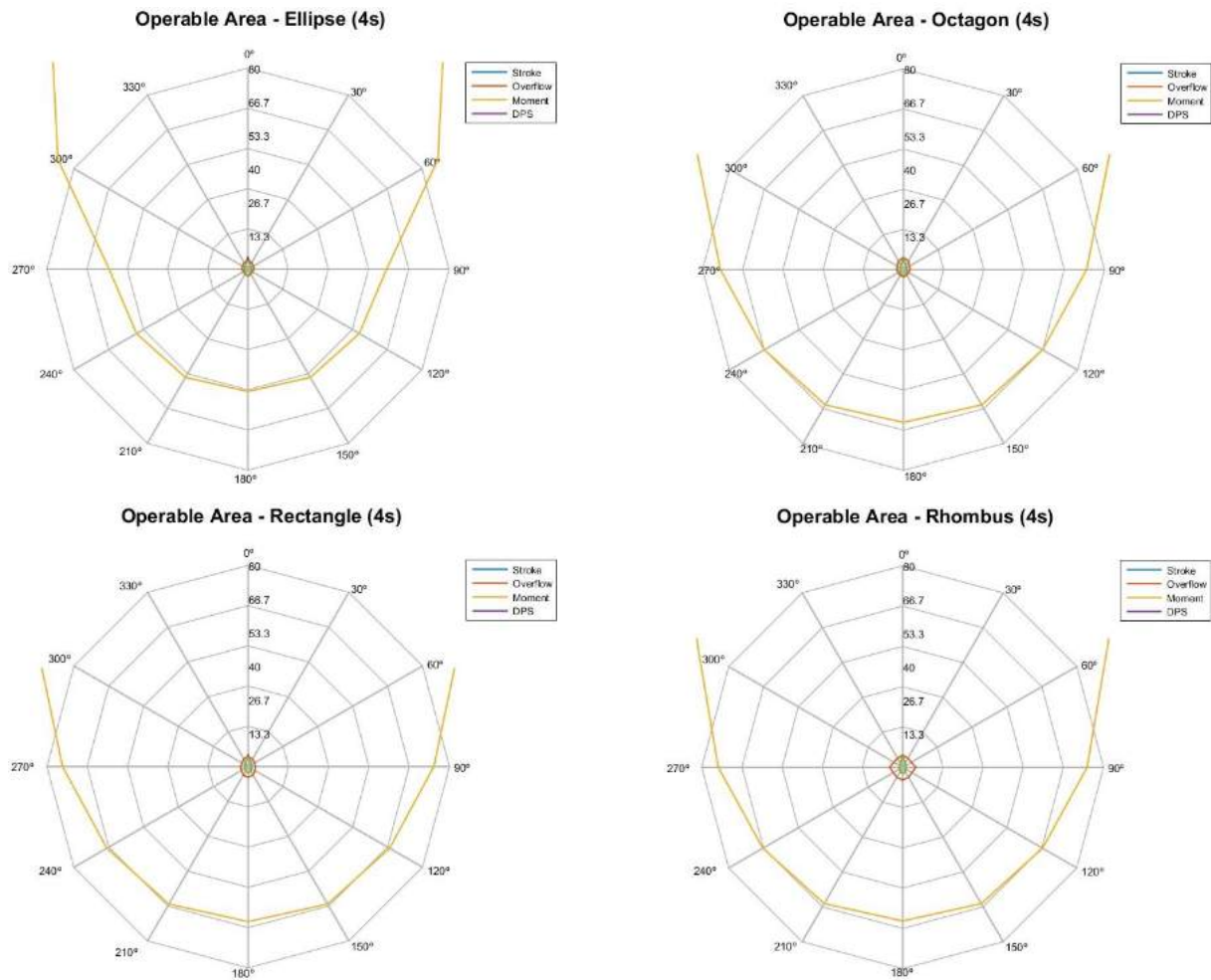
Significant wave period suggested by Cavalcante (2015) $T_s = 10s$, and additional $T_s = 4s$ were chosen as examples to analyse. The latter was decided due to the more evident difference of response among the samples. The radar chart of each configuration is shown in figures 90 and 91. As expected, the curve for stroke has high values, above the grid limits, and thus does not appear in the charts due to scale limitations (otherwise the smaller curves would not be visible). There are five colors in scheme, four of criteria and one of intersection curve. The charts show the CrMPO criterion in red (Overflow), CrVBM in yellow (Moment), CrDFT in purple(DPS), and the operable area that is the resultant internal area of all the intersections, in green.

Figure 90: Operability charts of each sample for period $T_s = 10s$ in big axis range. The green line delimits resultant operable region, representing the intersection of all the criteria's operable regions.



Source:Author.

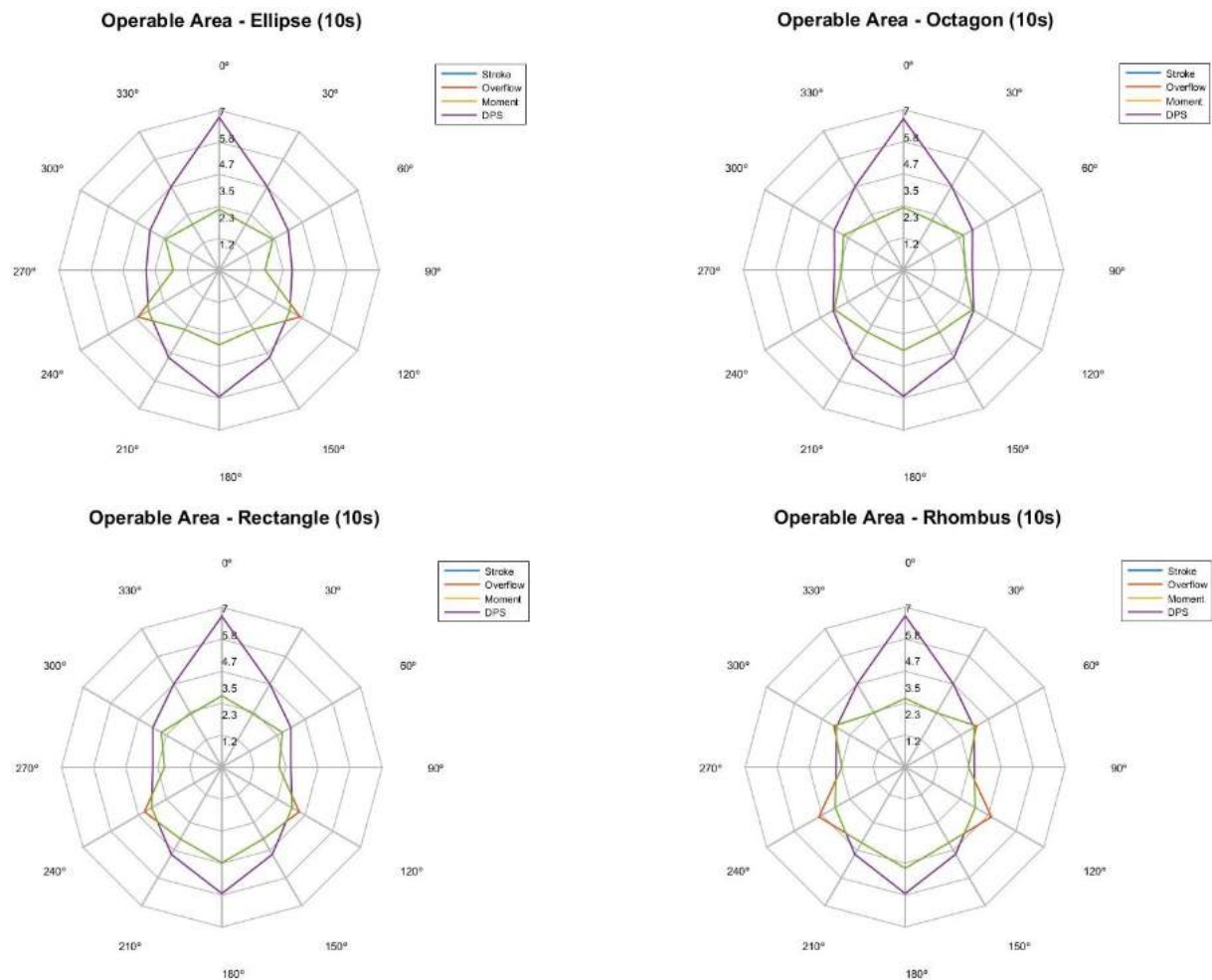
Figure 91: Operability charts of each sample for period $T_s = 4s$ in big axis range. The green line delimits resultant operable region, representing the intersection of all the criteria's operable regions.



Source: Author.

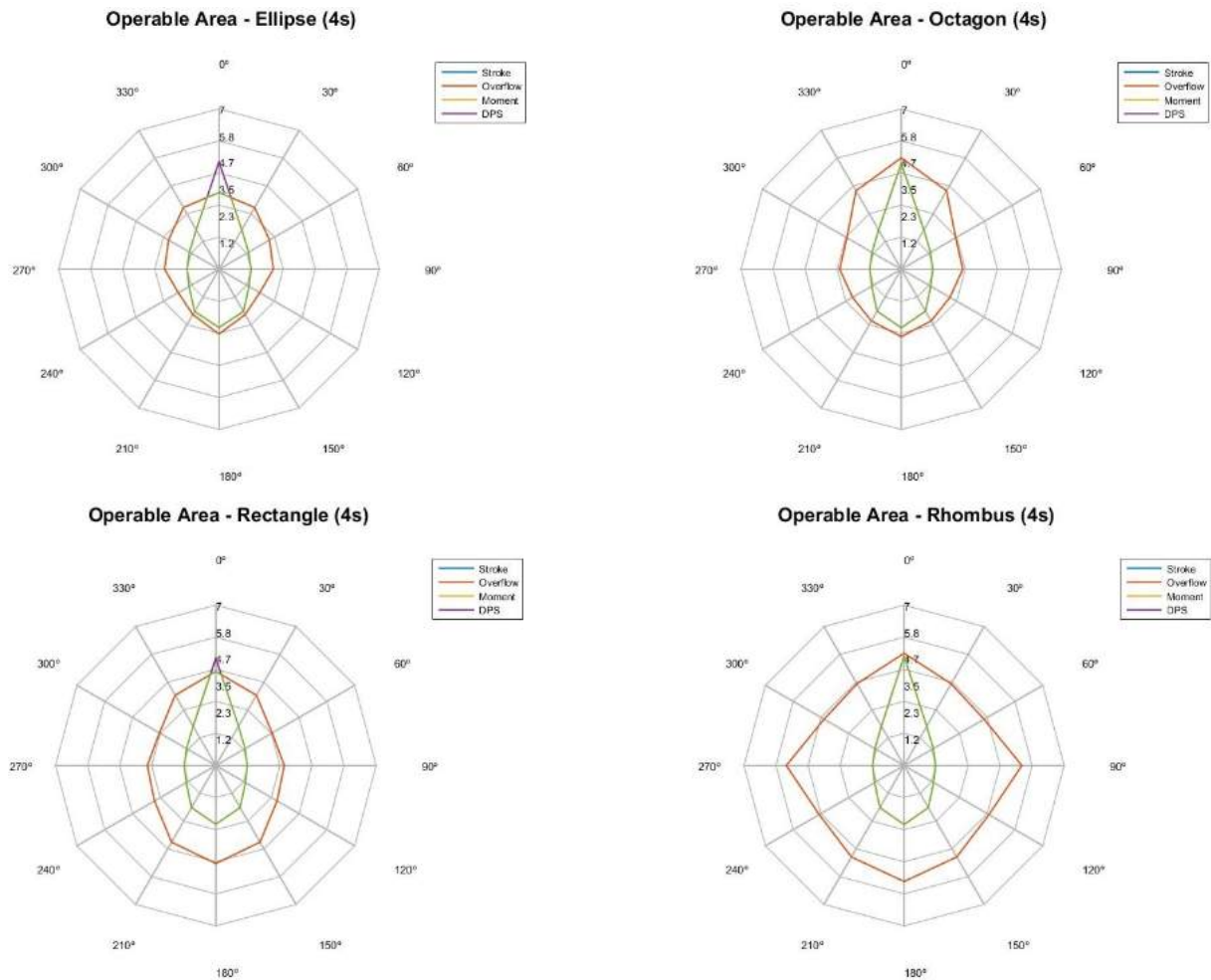
The chart of operable area in big axis range show a bending moment curve of too high order, so the inner curves are almost unreadable. A re-scaling was done to the charts of the results to allow more detailed analysis, since more changes are found between the shapes' performance charts. They are shown in figures 92 and 93.

Figure 92: Operability charts of each sample for period $T_s = 10s$ in small axis range. The green line delimits resultant operable region, representing the intersection of all the criteria's operable regions.



Source: Author.

Figure 93: Operability charts of each sample for period $T_s = 10s$ in small axis range. The green line delimits resultant operable region, representing the intersection of all the criteria's operable regions.

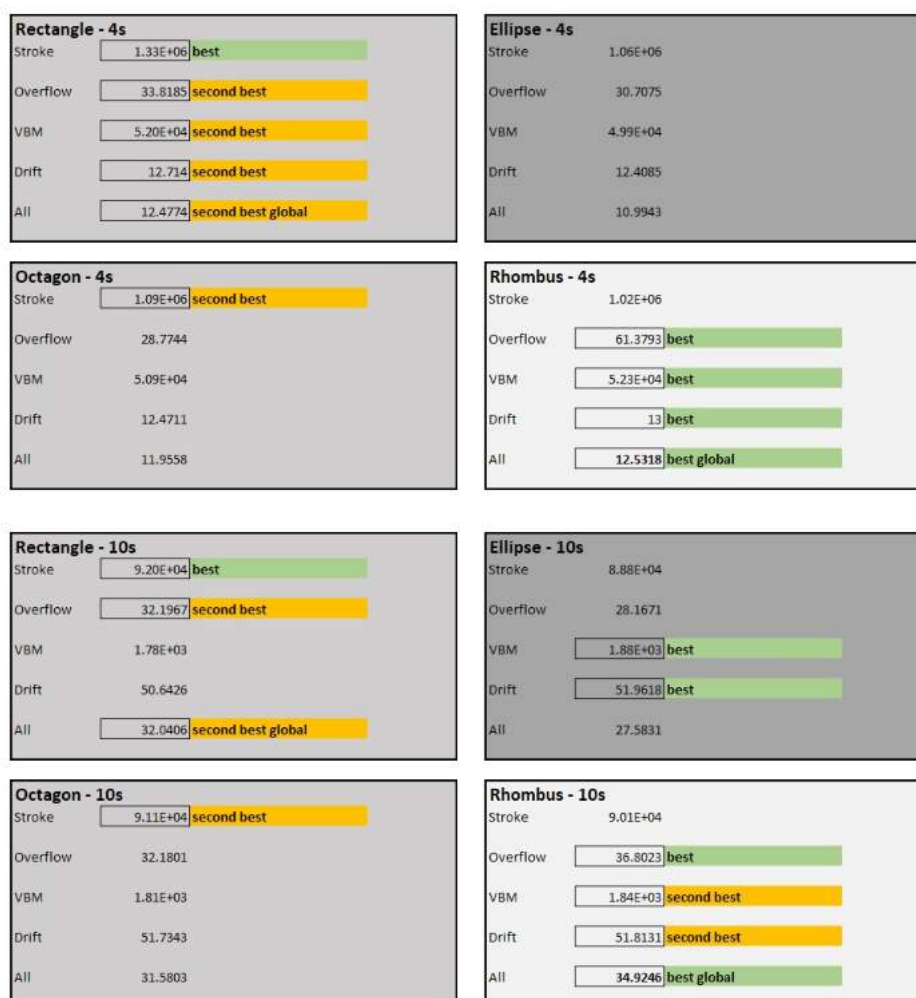


Source: Author.

It is clear from all the charts that the DPS criterion is unchanged with moon pool shape and is also the main limiting factor for beam seas. In addition, a similar response is observed at vertical bending moment in pairs, for those with the characteristic of larger dimension at mid, that narrows to fore and aft. Different from what was observed in the charts of S60 hull from Michima and Kawabe (2014b), the dominance of criteria do not change with the current operability limits and drill ship hull.

In general, for moon pool water overflow, fore-direction incident wave heights have lower TWH values than the other directions, opposite to DPS. From the performance analysis of each geometry, taking the criteria separately and the overall grades, the obtained result was as follows.

Figure 94: Results of the performance analysis of each geometry, taking the criteria separately and the overall grades



Source: Author

It is noticeable from the schemes shown that the global best profile must have a good operability in overflow. Also, regardless of the significant period, rhombus and rectangle shapes are respectively the best and second-best profiles so, probably, for the example of hull geometry of this work, the optimum moon pool should have some characteristics of both: m1 values near zero with m4 values near L2, or vice-versa.

It is not intuitive to imagine the rhombus-shaped moon pool among the best profiles to provide best performance in sea keeping, since one imagines the main streamline directions (as head, beam or following seas) flowing around the hull's bottom and converging somehow towards the corners of the rhombus which not always will be right-angles. The reason is that the present criterion of moon pool internal water oscillation is considering only the free surface height at mid, what attenuates the participation of high sloshing effects on it. Such phenomenon might be unlikely to

be observed in intermediate incidence angles at rectangle moon pools because the shape of the hull would allow redirecting the streamlines along the bottom of the hull, decreasing the deviation.

Nonetheless, it explains why there is a contradictory behaviour between subsequent values of L/B where the highest L/B has the best performance and the second-highest has nearly the worse performance in moon pool overflow criterion at incident wave angles 90° , 120° and 150° (fig 82). Since L/B is changing, the combination of breadth B projected in the direction of flow and the incident threshold wave length may change from destructive interference to constructive interference of the wave crossing back and forth inside the moon pool, resulting in such difference in performance.

Considering that stroke is far from being a potential limiting factor for this geometry and drift is not affected by the moon pool shape variations, some characteristics that could be found from each geometry sets regarding to moon pool internal water oscillation and vertical bending moment amidship are as follows:

- Rectangular MP response charts present a clear correspondence between the parameter L/B increments and curves progressive or regressive shift; Low values of the parameter have good performance in moon pool water oscillation except for head to 30° waves, while bending moment does not have much improvement outside peak region, and improvement in performs are opposite to L/B increment.
- Ellipse shape has a high sensitivity for CrMPO and CrVBM in peak regions, and is moderately affected outside them, keeping coherence in shift of the curves. In moon pool internal water oscillation response, it has a quite unstable change with L/B variation around 120° to 180° of incidence angle with abrupt gaps in low significant periods (figures 78 and 80), for moon pool water and vertical bending moment. It also keeps the coherence in shifting of the curves in the same manner as L/B variations.
- Octagonal moon pools have a high sensitivity to changes in L/B , keeping the correspondence between its increments and its curves, as well as the curves' shapes.
- Rhombus shapes show to be affected by L/B variation in opposite intensity to rectangle, *i.e.*, in incidence angles to which the variation of response to L/B is big for rectangle, it is small to rhombus, and vice-versa.

The above observations are useful for eventual change in dominance of criteria due to changes in limit values or equipment specifications.

7.2 Optimization

The conditions for optimization follow the procedure presented in section 4.2 of the assessment formulae for the criteria, also described in Michima and Kawabe (2014b).

A more detailed description of the way how each parameter defines characteristics of the moon pool's dimensions and shapes is found in section 5.1 of the moon pool mesh calibration. Basically, $L1$, $L2$, $L3$ correspond to the main dimensions in the water plane, respectively length fore, width, length aft. The $m1$, $m2$, $m3$, $m4$ parameters are respectively, percentage of $L2$ at fore, percentage of $L1$, percentage of $L3$ and percentage of $L2$ at aft that will be straight. The shape of the corners is defined by the number of segments that will compose it at fore and aft, respectively nf , nt .

Observations about those variations are presented in the following paragraphs. The analysis was carried out taking as an example the responses to a long-crested wave spectrum by IACS formulation. Table 10 presents the values used in this work.

Table 19: Values used as parameters for the evaluation criteria of operability

Criterion	Dimension	Reference Value	Evaluation
Moon pool overflow	Minimum free board	4m	Probability of deck wetness $N/n = 0.05$
Non-compensated heave	Compensator's stroke	3.5m	Probability of exceeding: 1/1000
Drift	DPS power limit	34 260 PS (metric HP)	Not to exceed the limit. Specification from "Chikyu" (MURATA; NAGASE; OZAWA, 2006)
Max. Midship, vert. bend. moment	Max. probab. value in 1 month	IACS S11, max in 25y with prob. of exceed. 10^{-8} conv. to short term	Probability of exceeding: 1/1000

Source: Author

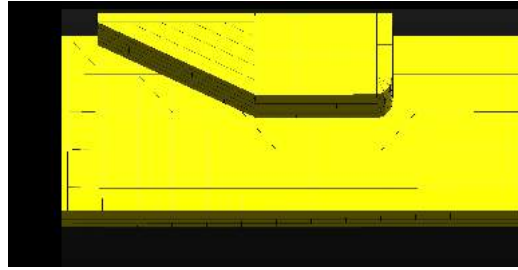
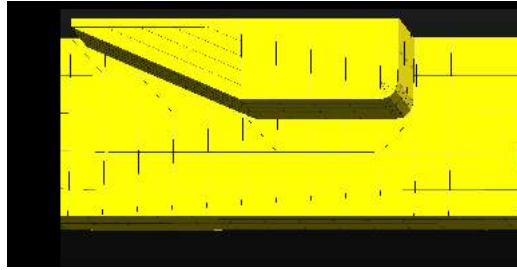
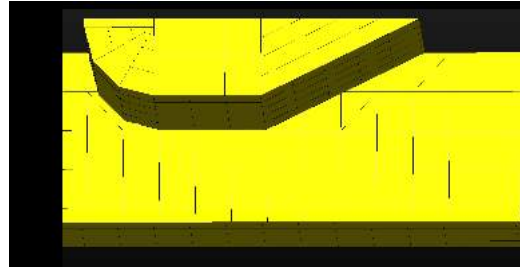
The minimum and maximum values of the parameters that define the shape and dimensions of the moon pool are listed below.

- L1, L3 from 10m to 23m
- L2 from 5m to 7m
- m1, m4 from 0m to L2
- m2, m3 from 0m to L1, L3 respectively
- nf, nt from 1 to the floor of the maximum divisions allowed based on the typical mesh element.

To understand the influence of each imposed criterion on the moon pool shape, an optimization process was run applying only one of them in each time, then find out the trend in geometry of the champions. The optimization time in a commercial model HP EliteDesk 800 G1 SFF (Intel Core i7-4790, 3.6GHz, RAM 16GB DDR3, with SSD) is average 315h (approximately 13 days).

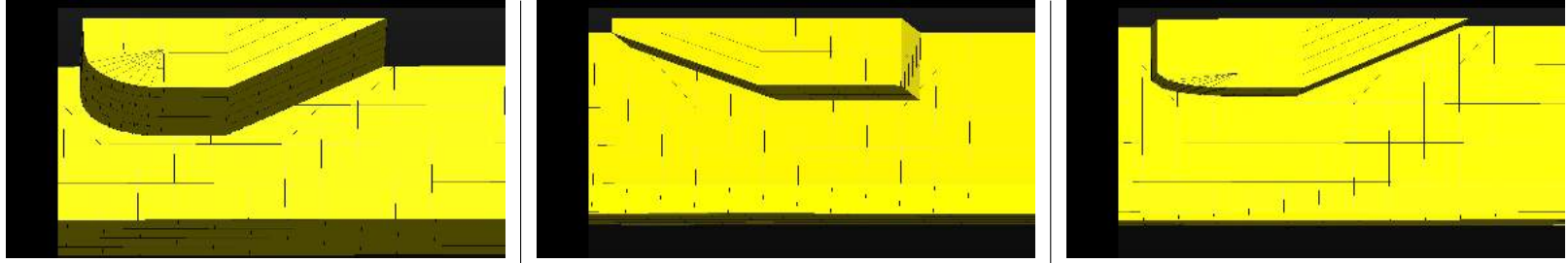
The figures in tables 20 to 22 show the three best performance moon pools, respectively of moon pool water overflow, ship motion, drift and vertical bending moment amidship.

Table 20: Three best configurations of optimization by moon pool water oscillation criterion only: L/B ratio, moon pool profile parameters and operability grade (OGr). The value of $m1 + m3$ indicates length of the mid parallel body.

									
L/B	1.8			2.0			2.1		
L1	10			11.5			12.5		
L2	6			6			5.5		
L3	11.5			12.5			11		
m1	4.6667			4.6667			0		
m2	8.8889	m2 + m3	8.8889	10.2222	m2 + m3	10.2222	1.3889	m2 + m3	7.5
m3	0			0			6.1111		
m4	0.667			0.6667			0.6111		
nf	3			3			1		
nt	1			1			3		
OGr	46.23			39.91			37.15		
Nodes	727			736			707		
Elements	596			603			588		


Source: Author.

Table 21: Three best configurations of optimization by ship motion criterion only: L/B ratio, moon pool profile parameters and operability grade (OGr). The value of $m1 + m3$ indicates length of the mid parallel body.

									
L/B	2.1			2.10			2.2		
L1	10			10.5			12		
L2	5			5			5		
L3	10			11			10.5		
m1	0			4.99			0		
m2	0	m2 + m3	4,4444	1.1667	m2 + m3	1.1667	0	m2 + m3	4.6667
m3	4.4444			0			4.6667		
m4	2,2222			1.1111			3,8889		
nf	1			2			1		
nt	9			1			9		
OGr	1147333.38			1117865.46			1118200.50		
Nodes	718			697			721		
Elements	602			582			601		

Source: Author.

Table 22: Three best configurations of optimization by drift criterion only: L/B ratio, moon pool profile parameters and operability grade (OGr). The value of $m1 + m3$ indicates length of the mid parallel body.

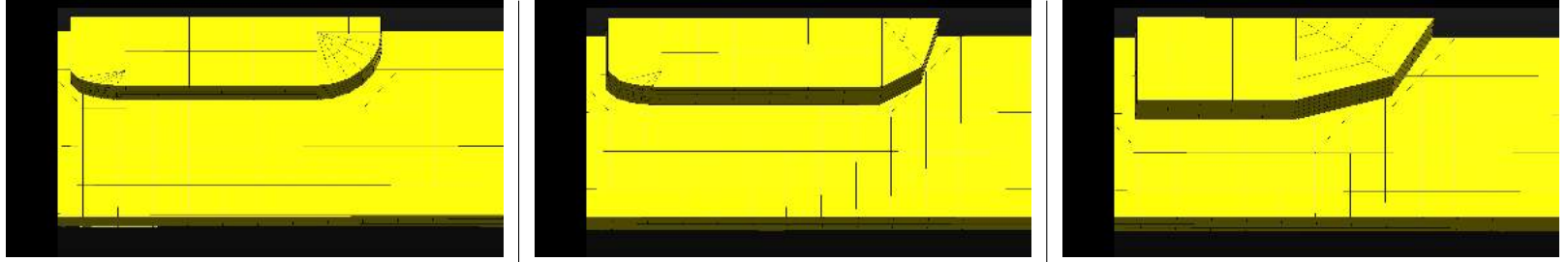
			
L/B	2.2		
L1	11		
L2	5		
L3	11		
m1	1.6667		
m2	0	m2 + m3	0
m3	0		
m4	1.1111		
nf	2		
nt	7		
OGr	12.59		
Nodes	726		
Elements	605		

L/B	2.0		
L1	10		
L2	5		
L3	10		
m1	1.1111		
m2	0	m2 + m3	1.1111
m3	1.1111		
m4	2.2222		
nf	1		
nt	2		
OGr	12.58		
Nodes	694		
Elements	576		

L/B	2.25		
L1	11		
L2	5		
L3	11.5		
m1	0.5556		
m2	1.2222	m2 + m3	1.2222
m3	0		
m4	0.5556		
nf	1		
nt	5		
OGr	12.58		
Nodes	727		
Elements	603		

Source: Author.

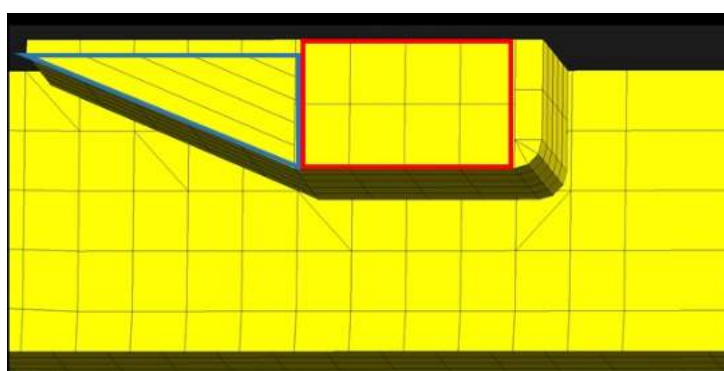
Table 23: Three best configurations of optimization by vertical bending moment amidship criterion only: L/B ratio, moon pool profile parameters and operability grade (OGr). The value of $m1 + m3$ indicates length of the mid parallel body.

									
L/B	2.2			2.4			1.8		
L1	10.5			12.5			10		
L2	5			5			6		
L3	12			11.5			11.5		
m1	1.1112			0			0		
m2	5.8333	m2 + m3	13.8333	8.3333	m2 + m3	16	0	m2 + m3	11.49
m3	8			7.6667			11.49		
m4	3.8889			3.8889			5.99		
nf	6			2			2		
nt	9			9			7		
OGr	1747.32			1740.78			1739.39		
Nodes	769			719			698		
Elements	637			597			580		

Source: Author.

The calculation of TSH is similar for moon pool water oscillation and ship motion in heave, so the shape trend is similar for both. It shows that chamfer in one of the sides of the moon pool and a parallel mid body is always present in the best individuals as in Figure 95. The parallel mid body is always shifted to the side without chamfer, and is shorter for the shapes that yield from stroke optimization than the ones from internal water oscillation optimization. As it was expected, from a range of $L/B = 1.42$ to 2.6, the samples with best performance of moon pool internal water oscillation have moderate values, near the average 2.

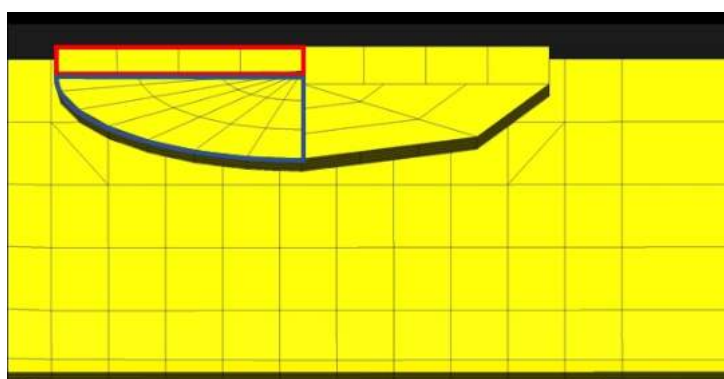
Figure 95: Common characteristic of the champions in moon pool water oscillation and in ship motion criteria: parallel mid body and chamfer



Source: Author.

Optimization by drift criterion leads to a characteristic round corner dominant in longitudinal extension attached to a portion parallel to the longitudinal centre line in one of the sides of the moon pool, as shown in Figure 96. Almost not present parallel body at mid.

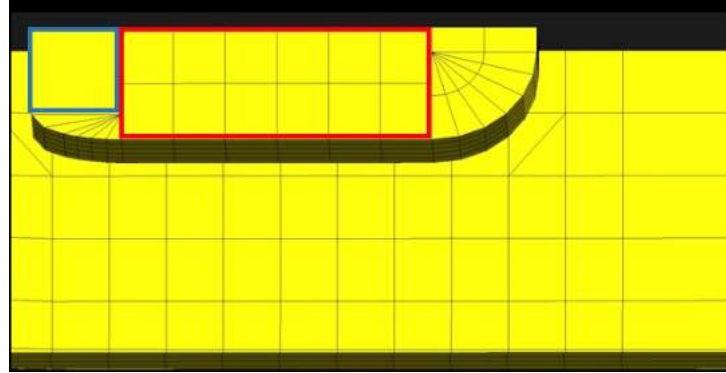
Figure 96: Common characteristic of the champions in drift criterion: round corner dominant in longitudinal extension attached to a portion parallel to the longitudinal centre line in one of the sides of the moon pool.



Source: Author.

The vertical bending moment imposes the existence of a long parallel mid body and one of the sides with a dominant vertical wall in one of the ends, as illustrated in Figure 97.

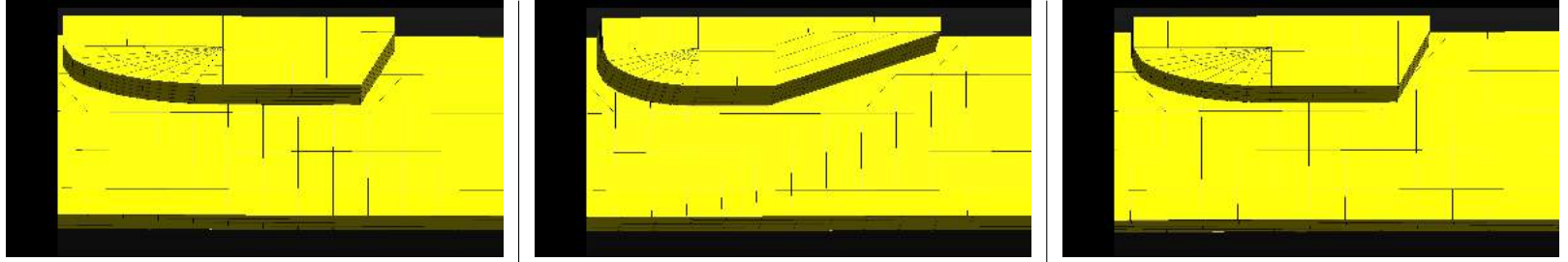
Figure 97: Common characteristic of the champions in vertical bending moment criterion: parallel mid body and one of the sides with a dominant vertical wall in one of the ends



Source: Author.

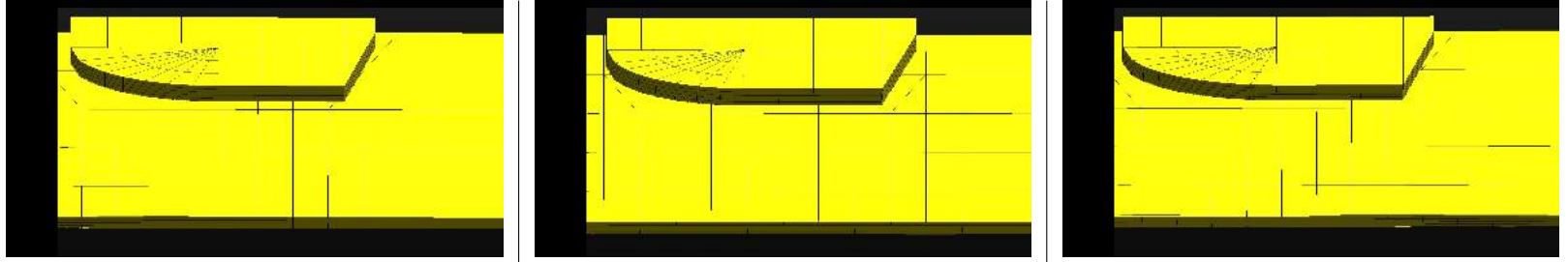
Once defined the main shape characteristics of the most probable candidate to optimum, the size should be investigated. Given the limit values chosen for this work and the drill ship hull geometry used, it was already understood that the only criteria that predominantly participate in the definition of the operable area would be the moon pool water oscillation and drift. An optimization was run using the two criteria to check if the characteristics of the individual optimizations were identified and if the optimization including all the criteria would follow the same trend. Tables 24 to 25 show the three best configurations.

Table 24: Three best configurations of optimization by overflow + drift criteria only: L/B ratio, moon pool profile parameters and operability grade (OGr). The value of $m1 + m3$ indicates length of the mid parallel body.

									
L/B	2.4			2.4			2.1		
L1	11			12			10		
L2	5			5			5		
L3	13			12.5			11		
m1	1.1111			1.1111			1.1111		
m2	8.5556	m2 + m3	10	0	m2 + m3	5.5556	7.7778	m2 + m3	9
m3	1.4444			5.5556			1.222		
m4	2.2222			2.2222			2.2222		
nf	1			1			1		
nt	9			9			9		
OGr	12.49			12.46			12.45		
Nodes	754			763			734		
Elements	626			631			613		

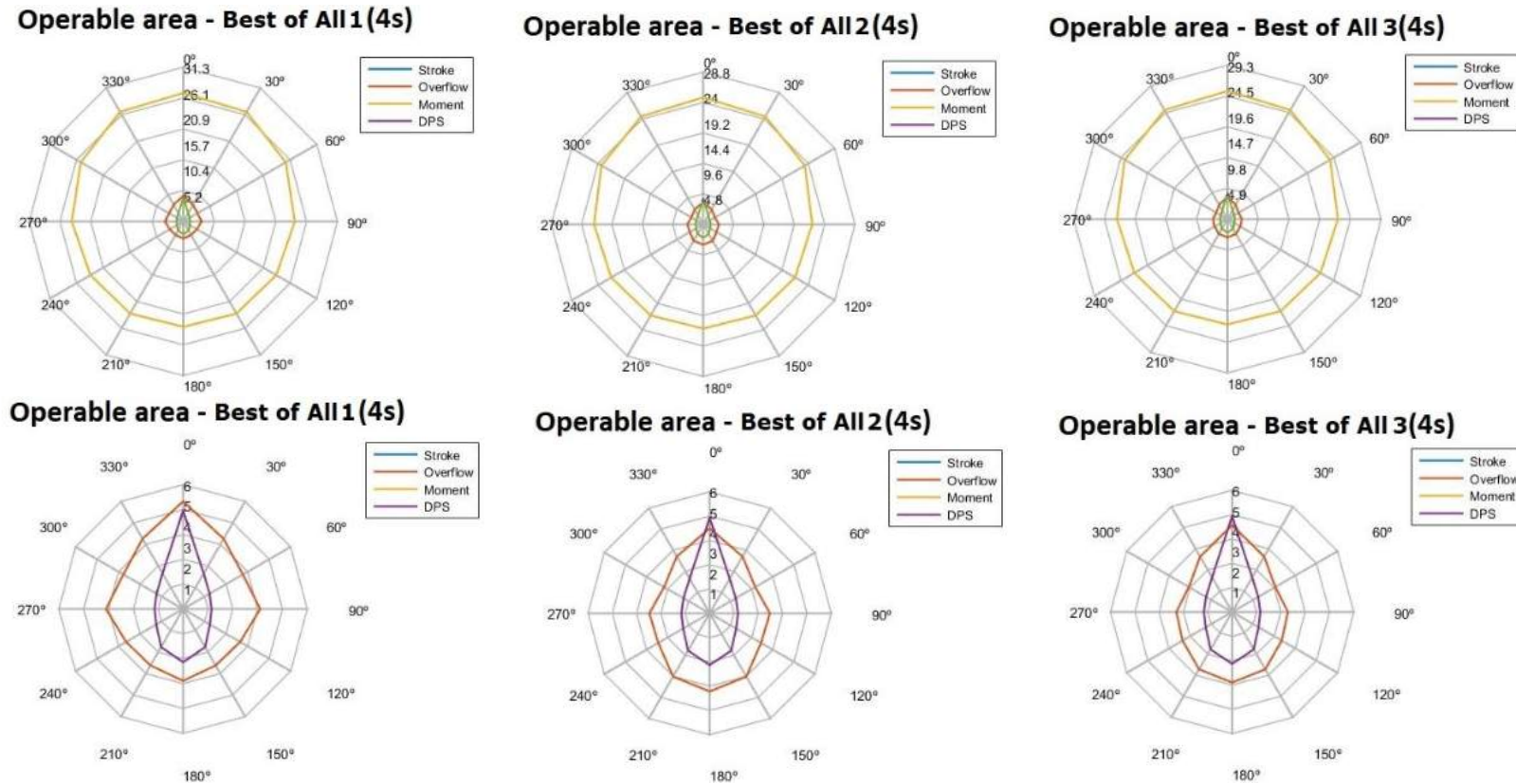
Source: Author.

Table 25: Three best configurations of optimization by all criteria: L/B ratio, moon pool profile parameters and operability grade (OGr). The value of $m1 + m3$ indicates length of the mid parallel body.

									
L/B	2.2			2.2			2.2		
L1	10			11			10		
L2	5			5			5		
L3	12			11			12.5		
m1	1.1111			1.1111			1.1111		
m2	7.7778	m2 + m3	9.1111	8.5556	m2 + m3	9.7778	7.7778	m2 + m3	9.1667
m3	1.3333			1.2222			1.3889		
m4	2.2222			2.2222			2.2222		
nf	1			1			1		
nt	9			9			9		
OGr	12.45			12.44			12.43		
Nodes	735			742			734		
Elements	612			618			612		

Source: Author.

Figure 98: Radar charts of the three best resultant configurations of optimization by all criteria. Top line: radar chart containing all but stroke criteria. Bottom line: “zoomed” radar chart with details of the operable zone delimited by overflow and drift criteria.



Source: Author.

As predicted, the characteristics that were expected to appear in the solutions due to the influence of moon pool internal water oscillation (chamfer and parallel body around mid) and drift criteria (round corner attached to a parallel longitudinal body in one side) are found in the solutions. Previously it was seen that in isolated criteria each of those characteristics is more dominant in the geometry, *i.e.*, represents a big portion of the perimeter of the shape, what is still observed combined in the solutions presented. The second best sample of MP overflow + drift optimization configures an exception in parallel mid body length and centring. Due to the conflicting characteristics of parallel mid body for the two dominant criteria: moon pool water oscillation includes it, while drift has almost no parallel mid body, it is centred towards to the location of the chamfer.

When the optimization includes the four criteria, the results are similar to what was observed in interaction between the two main criteria only, agreeing with the expectation. The L/B ratio were kept moderate values and the parallel mid body length is the order of the one in moon pool internal water oscillation criteria isolated.

There are some variations between the results obtained with two criteria only (moon pool internal water oscillation and drift) and the ones obtained with all the criteria. This can be due to the evolution stop criterion that might still need to be more “strict”, but since higher precision on stop criterion would imply much higher processing cost in time and hardware. The differences involve only longitudinal dimensions ($L1$, $L3$, $m2$, $m3$), while the corner shapes and transversal dimensions had converged to the same value.

8 Conclusions

This research presents results that show that, given a hull and operation conditions such as the sea state of the region where the tasks will be realised, and the operability limit values, it is possible to define the optimum moon pool shape, dimensions and location relative to the centre of gravity.

The evaluation of operability demands establishment of relations between safety parameters and reliable prediction of response in waves by the system. Therefore, it would be no use to define a configuration of moon pool that is better than the standard shapes if there is no good approximation of what the ship will have to undergo in practice. Hence, this work presented a detailed development of the potential model used to describe the ship and free surface motions, proposing a Rayleigh damping term and a boundary condition at the moon pool's free surface, as an improvement to that proposed in Michima and Kawabe (2014b).

A model was proposed also for the elaboration of the formulae that transform the acceptable limit values of each criterion in threshold wave height information. In this way, free surface height, ship motion, hull structure strength and positioning in azimuthal plane are all assessed through that same index.

It was shown that judging operability considering all the criteria and concepts designed in the present work is too complex and does not allow analytical solution neither a precise quantitative evaluation of how should the configuration be changed to attend the requirements. Therefore, the need to use numerical calculation and computational simulations instead is justified. A simple illustration of this fact can be seen in the radar charts from section 7 of the results and discussion: a similar response is observed at MP overflow criterion in pairs, but with different combinations in each significant period, so no pattern of similarity of response among the profiles can be established.

Searching characteristics that would determine the configuration of the optimum prismatic moon pool for a given set of environmental and safety parameters regarding to operation was done using three main approaches:

- Investigating how the proposed criteria would influence the definition of configuration or of operability. The influence depends on the limit values of safety or acceptable limits of loads that the equipment can receive without suffering damage or failure, and on which of them yield threshold wave heights of the same order. Those limits define whether the radar chart of that criterion would be wider or narrower, longer or shorter, and if there would be intersection with other criteria.

Eventually, there may be criteria that allow too high wave heights that end up not influencing in MP shape definition (due to response being too small, it allows any wave height without changing much in its response. It is expressed in the radar chart as a big internal area curve);

- Superposed influences of the dominance of the criteria and the geometric characteristics that they impose to the moon pool profile define the resultant configuration as in linear combination;
- Some criteria are more influenced by external hull characteristics than by moon pool configuration, presenting almost no variation in radar chart shapes, and small variation in operable area, such as drift, whereas others are highly influenced by moon pool configuration and present different shapes of radar chart at each different configuration, such as the MP overflow.
- Varying the L/B ratio to find if extreme values would be more likely to provide optimum performance for the proposed situation;
 - For the present example hull shape, highest L/B values would be advantageous in fore incidence angles, but disadvantageous at beam seas. Aft incidence angles show to be inconclusive for highest and for lowest, therefore moderate L/B values are expected to have better performance, which was confirmed in the simulations.
- Analysing if convergent streamlines in longitudinal ends (fore and aft of the moon pool) would fit better than parallel ones, based on pure geometric shapes (no combinations), like extreme parallel: rectangle, totally convergent sharp: rhombus, extreme convergent round: ellipse, moderate parallel and sharp: octagon.
 - Both extreme characteristics are expected to be present, what was confirmed in the results of simulations: one end of moon pool with a parallel longitudinal body and one end of moon pool with a chamfer and almost negligible parallel longitudinal body;
 - The response of rhombus-shaped moon pool samples are specially different from the others in moon pool internal water oscillation from the viewpoint of behaviour variation with L/B value increments. It is possible that including free surface height near the borders of the moon pool in the optimization might attenuate the chamfer's angle of the longitudinal end profile.

Small differences were found between the benchmark created by the optimization involving only the dominant criteria and the final optimized moon pools, which can be due to computational limitations. The transversal dimensions have already converged, so such variation of longitudinal dimensions is also limited by order of length and L/B .

Those variations though are limited since the transversal dimensions and corner division parameters had converged, and the L/B ratio is kept moderate.

From some sample simulations, it was possible to have some clues of the characteristics of the optimum solution before running optimization, and since it depends only on limits and hull shape by user input, the method can be applied to any floating system in the same situation of operation, if response spectra is provided in the same formatting as required to be readable by the code (see appendix 10).

In terms of construction complexity, the new moon pool shapes don't seem to present any limitations in terms of construction, since they are prismatic, so a bow or a stern shape is much more complex than the moon pool, and from mesh definition, is composed of only flat plates in all its perimeter, demanding no extra work in plate conformation.

It was shown possible to define from user input: hull geometry and limit values for operability, which is the optimum prismatic moon pool configuration maybe very different from the standard rectangle. Furthermore, once the results of the optimization are obtained, since it will be in design stage, it is possible to change characteristics of the ship that would conveniently improve operability in the same fashion as Özüm, Şener and Yilmaz (2011), or as suggested by Day (1990), described in the theoretical foundation at section 3. For example, if the overflow criterion is limiting too much the operability, and if it is feasible, the free border of the moon pool might be increased. In the same manner, other changes could be done in DPS power, etc.

Finally, the output radar chart for the desired significant periods can be used as fast-taking decisions tool during operation.

9 Ongoing and further works

“Theses are like ships: you don’t finish. You just stop and they go away.”

— Paula Michima

The success and safety ensuring of a design will depend on a hydrodynamic comprehensive optimization, including points of assessment for resistance, stability, seakeeping, etc., because optimizing one to the detriment of the others could lead to results that do not match to reality. It might be interesting to continue this research with future studies for the optimization of the moon pool considering both transit and operation situations. In this case, attention should be paid for the evaluation of short term for very high speed condition. As can be found in Takezawa et al. (1993), the encounter wave mean period of directional spectrum wave with wide spreading angle is largely modified comparing to long crested seas, becoming sometimes close to the natural period of ship motion, especially in roll mode.

Besides that, other suggestions for future works are listed below:

- Empirical tests with real drill ship hull data instead of series 60.
- Inclusion of more operability criteria, among which the comfort of the crew based on kinetosis that is already in course.
- the Drift force in the present model is multiplied by the drift velocity to determine the power. Improvements may be done by considering also the yaw momentum together with the currently used translation.
- In addition to the vertical bending momentum amidship, the torsional momentum shall be evaluated as well.
- Inclusion of resultant relative position between the heave compensator equipment and the moon pool internal water surface level at the heave compensator criterion, as described in section 4.2.2.
- Studies using real flow analysis (CFD, for instance) might be done to evaluate the 3D impact of vortex shedding on the damping as the parameters of the moon pool shape vary.
- Varying the geometry of the external hull to investigate the impact on operability charts while fixing the same operation conditions and limit values might give an idea about the variation of dominance of criteria, as suggested by Bales (1980).

- Data of the free surface height near the moon pool wall might be included to analysis to avoid situations in which harsh sloshing is disguised by low oscillation at mid in MP internal water oscillation response, principally in rectangle-like ones as suggested by Vijith, Viswanathan and Panneerselvam (2014). (This is already in course).
- Kawabe et al. (2015) present an analytical strategy of geometry search of a prismatic body that receives a head regular wave train and oscillates in order to absorb theoretically 100% of its energy. The mathematical model is based on the Kochin function and can be evolved to a frequency range. If a device is developed to be coupled to the internal wall of the moon pool, it is possible to obtain energy for the internal operation of the ship. The wave absorption is a damping strategy as well, collaborating to improve its operability conditions.
- Assessment of strength of the hull due to chines and directional loads that the hull is subjected to would also be an important item for a decision upon operability.
- In this work the choice of value for the Rayleigh damping term was extrapolated from experimental data of experiments with other hull. Experimental check of the chosen value is also recommended.

10 Contribution of the present work

Based on the proposed objectives of the present work, the contributions are focused on exploring broader possibilities to keep the operation of a floating system with moon pool for given sea states that happen in the operation area. The innovation comes from determining in design stage the shape of its moon pool as a solution that keeps its clearance as without increasing complexity of the profile, *i.e.* without adding recess and instead of using palliative or holistic solutions, *e.g.* as appendages to reduce the resonance effects of water oscillations inside the opening.

The contributions of this work are summarized as follows.

- Before running optimization:
Identification with fast tests some characteristics that will be present in the optimal solution.
- In design stage:
Determination of the shape of optimum moon pool;
Easy-to-construct solutions;
Identification of characteristics that can be changed to improve the operability of the system.
- During operation:
Chart for fast-taking decisions.
- Optimization:
Mixed algorithms: allows splitting optimization in ranges for ordinary computer usage;
Algorithm with flexibility to use customized hydrodynamic module.
- Modelling:
Potential model proposal of damping term and boundary value to attend the MP's free surface.

REFERENCES

AALBERS, A. The water motions in a moonpool. *Ocean engineering*, Elsevier, v. 11, n. 6, p. 557–579, 1984. Cited 4 times on page 31, 35, 44, and 83.

BAGHERI, H.; GHASSEMI, H. Genetic algorithm applied to optimization of the ship hull form with respect to seakeeping performance. *Transactions of FAMENA*, Fakultet strojarstva i brodogradnje, v. 38, n. 3, p. 45–58, 2014. Cited 2 times on page 47 and 56.

BALES, N. K. *Optimizing the seakeeping performance of destroyer-type hulls*. [S.l.]: David W. Taylor Naval Ship Research and Development Center, 1980. Cited 2 times on page 47 and 190.

BALES, S. L. Practical seakeeping using directional wave spectra. *Johns Hopkins APL Technical Digest*, v. 8, n. 1, 1987. Cited on page 35.

BULL, D. An improved understanding of the natural resonances of moonpools contained within floating rigid-bodies: Theory and application to oscillating water column devices. *Ocean Engineering*, Elsevier, v. 108, p. 799–812, 2015. Cited on page 45.

CAVALCANTE, T. *Ferramentas computacionais para geração e seleção de geometrias de moonpool de drill ship com base na operabilidade*. Dissertação (Bachelor Thesis) — Universidade Federal de Pernambuco, Recife, Brazil, 2015. Cited 8 times on page 54, 55, 57, 58, 102, 103, 116, and 167.

DAY, A. The design of moonpools for subsea operations. *Marine technology*, Society of Naval Architects and Marine Engineers, v. 27, n. 3, p. 167–179, 1990. Cited 9 times on page 9, 21, 33, 36, 37, 60, 99, 103, and 189.

DAY, A.; LEE, B.; KUO, C. The prediction of moonpool response—water column oscillation and hydrodynamic forces. *Royal Institution of Naval Architects Transactions*, v. 131, 1989. Cited 5 times on page 21, 27, 35, 36, and 66.

DAY, A. H.; DOCTORS, L. J. Rapid estimation of near-and far-field wave wake from ships and application to hull form design and optimization. *Journal of ship research*, Society of Naval Architects and Marine Engineers (SNAME), v. 45, n. 1, p. 73–84, 2001. Cited on page 47.

DNV. Modelling and analysis of marine operations. In: DET NORSKE VERITAS. [S.l.], 2011. DNV-RP-H103. Cited 9 times on page 22, 23, 32, 34, 44, 64, 67, 99, and 106.

DNV. *Marine operations, design and fabrication*. [S.l.], 2012. DNV-OS-H102. Cited on page 100.

EIBEN, A. E.; SMITH, J. E. et al. *Introduction to evolutionary computing*. [S.l.]: Springer, 2003. v. 53. Cited 2 times on page 46 and 47.

ENGLISH, J. *A means of reducing the oscillations in drillwells caused by vessels' forward speed*. [S.l.]: NMI, 1976. Cited 2 times on page 31 and 35.

FALTINSEN, O. *Sea loads on ships and offshore structures*. [S.I.]: Cambridge university press, 1993. v. 1. Cited on page 44.

FALTINSEN, O.; TIMOKHA, A. *Sloshing* cambridge university press. *Cambridge, UK*, 2009. Cited 2 times on page 40 and 123.

FALTINSEN, O. M.; ROGNEBAKKE, O. F.; TIMOKHA, A. N. Two-dimensional resonant piston-like sloshing in a moonpool. *Journal of Fluid Mechanics*, Cambridge University Press, v. 575, p. 359–397, 2007. Cited 7 times on page 44, 83, 119, 121, 122, 123, and 124.

FALTINSEN, O. M.; TIMOKHA, A. N. Analytically approximate natural sloshing modes for a spherical tank shape. *Journal of Fluid Mechanics*, Cambridge University Press, v. 703, p. 391–401, 2012. Cited on page 40.

FONSECA, Í. A. *Compatibilização de Códigos Computacionais para a Otimização da Configuração de Moon Pool sob o Ponto de Vista da Operabilidade*. Dissertação (Bachelor Thesis) — Universidade Federal de Pernambuco, Recife, Brazil, 2016. Cited 4 times on page 57, 59, 112, and 116.

FREDRIKSEN, A. G.; KRISTIANSEN, T.; FALTINSEN, O. M. Experimental and numerical investigation of wave resonance in moonpools at low forward speed. *Applied Ocean Research*, Elsevier, v. 47, p. 28–46, 2014. Cited on page 38.

FUKUDA, K. Behavior of water in vertical well with bottom opening of ship, and its effects on ship-motion. *Journal of the Society of Naval Architects of Japan*, The Japan Society of Naval Architects and Ocean Engineers, v. 1977, n. 141, p. 107–122, 1977. Cited 7 times on page 29, 30, 31, 32, 35, 43, and 165.

GAILLARDE, G.; COTTELEER, A. Water motion in moonpools empirical and theoretical approach. *Association Technique Maritime et Aeronautique (ATMA)*, p. 1–14, 2004. Cited 3 times on page 29, 30, and 38.

GEUZAIN, C.; REMACLE, J.-F. Gmsh: A 3-d finite element mesh generator with built-in pre-and post-processing facilities. *International journal for numerical methods in engineering*, Wiley Online Library, v. 79, n. 11, p. 1309–1331, 2009. Cited on page 115.

GINGOLD, R. A.; MONAGHAN, J. J. Smoothed particle hydrodynamics: theory and application to non-spherical stars. *Monthly notices of the royal astronomical society*, Oxford University Press Oxford, UK, v. 181, n. 3, p. 375–389, 1977. Cited on page 38.

HEO, J.-K. et al. Influences of vorticity to vertical motion of two-dimensional moonpool under forced heave motion. *Mathematical Problems in Engineering*, Hindawi Publishing Corporation, v. 2014, 2014. Cited on page 45.

HOGGEN, N.; DACUNHA, N. M. C.; OLLIVER, G. F. *Global Wave Statistics*. [S.I.]: Produced by BMT, published by Unwin Brothers, 1986. Cited 4 times on page 204, 205, 206, and 207.

IACS. Longitudinal strength standard. In: INTERNATIONAL ASSOCIATION OF CLASSIFICATION SOCIETIES. *Unified Requirement of the International Association of Classification Societies*. [S.I.], 2010. IACS UR S11. Cited 2 times on page 109 and 110.

- ISO. *Mechanical vibration and shock-Evaluation of human exposure to whole-body vibration-Part 1: General requirements*. Geneva, 1997. Cited 2 times on page 22 and 111.
- ITTC. *Recommendations of the Waves Committee*. Bergen/Trondheim, 2002. Cited on page 107.
- ITTC. *Recommended Procedures and Guidelines - Practical Guidelines for Ship CFD Application*. [S.l.], 2011. ITTC 7.5 – 03 – 02 – 03. Cited on page 112.
- KANG, K. Y. *Design de plataforma FPSO com Moonpool*. Dissertação (Mestrado) — Universidade de São Paulo, 2018. Cited 11 times on page 121, 126, 127, 128, 129, 130, 131, 132, 133, 134, and 135.
- KAWABE, H. *Three dimensional drill ship motion and moonpool water surface elevation simulation program - Regular and irregular wave version*. [S.l.: s.n.], 2017. Cited 3 times on page 99, 121, and 203.
- KAWABE, H. et al. The numerical and experimental study on moonpool water surface response of a ship inwave condition. In: INTERNATIONAL SOCIETY OF OFFSHORE AND POLAR ENGINEERS. *The Twentieth International Offshore and Polar Engineering Conference*. [S.l.], 2010. Cited 3 times on page 117, 119, and 120.
- KAWABE, H. et al. Numerical calculation method for the optimum wave energy absorption configuration based on the variation of kochin function. *Journal of Marine Science and Technology*, Springer, v. 20, n. 4, p. 617–628, 2015. Cited on page 191.
- KNOTT, G.; FLOWER, J. Measurement of energy losses in oscillatory flow through a pipe exit. *Applied Ocean Research*, Elsevier, v. 2, n. 4, p. 155–164, 1980. Cited on page 45.
- KOSHIZUKA, S.; OKA, Y. Moving-particle semi-implicit method for fragmentation of incompressible fluid. *Nuclear science and engineering*, Taylor & Francis, v. 123, n. 3, p. 421–434, 1996. Cited on page 38.
- KRISTIANSEN, T.; FALTINSEN, O. Application of a vortex tracking method to the piston-like behaviour in a semi-entrained vertical gap. *Applied Ocean Research*, Elsevier, v. 30, n. 1, p. 1–16, 2008. Cited 3 times on page 45, 119, and 123.
- KÜKNER, A.; SARIÖZ, K. High speed hull form optimisation for seakeeping. *Advances in Engineering Software*, Elsevier, v. 22, n. 3, p. 179–189, 1995. Cited on page 47.
- MAISONDIEU, C. et al. Numerical and experimental evaluation of the viscous damping in a wellbay. In: 23rd International Conference on Offshore Mechanics and Arctic Engineering. [S.l.]: American Society of Mechanical Engineers, 2004. p. 423–431. Cited on page 38.
- MALTA, E. B. et al. Numerical moonpool modelling. In: AMERICAN SOCIETY OF MECHANICAL ENGINEERS. *25th International Conference on Offshore Mechanics and Arctic Engineering*. [S.l.], 2006. p. 493–500. Cited 2 times on page 37 and 38.
- MARUO, H. The drift of a body floating in waves. *J Ship Res*, v. 4, p. 1–10, 1960. Cited on page 108.

- MAVRAKOS, S. Hydrodynamic coefficients for a thick-walled bottomless cylindrical body floating in water of finite depth. *Ocean engineering*, Elsevier, v. 15, n. 3, p. 213–229, 1988. Cited 3 times on page 11, 139, and 141.
- MICHIMA, P. S. A.; KAWABE, H. Hybrid approach of mps and bem for modelling moon pool water sloshing. In: AMERICAN SOCIETY OF MECHANICAL ENGINEERS. *ASME 2014 33rd International Conference on Ocean, Offshore and Arctic Engineering*. [S.l.], 2014. Cited on page 38.
- MICHIMA, P. S. A.; KAWABE, H. Preliminary chart of drill ship operability considering moon pool sloshing effects. *Journal of Marine Science and Technology*, Springer, p. 1–12, 2014. Cited 10 times on page 33, 48, 49, 51, 52, 53, 104, 171, 174, and 187.
- MOLIN, B. On the piston mode in moonpools. In: *Proc. 14th Int. Workshop on Water*. [S.l.: s.n.], 1999. Cited on page 44.
- MOLIN, B. On the sloshing modes in moonpools, or the dispersion equation for progressive waves in a channel through the ice sheet. In: *15th Intl. Workshop on Water Waves and Floating Bodies*. [S.l.: s.n.], 2000. p. 122–125. Cited on page 40.
- MOLIN, B. On the piston and sloshing modes in moonpools. *Journal of Fluid Mechanics*, 2001. Cited on page 40.
- MURATA, K.; NAGASE, S.; OZAWA, H. Development of dynamic positioning system of “chikyu”. *Mitsui Zosen Technical Review*, 2006. Cited 2 times on page 108 and 175.
- NESJØ, E. N. *Resistance due to open moonpools on offshore ships*. Dissertação (Mestrado) — NTNU, 2015. Cited 3 times on page 21, 28, and 34.
- NEWMAN, J. An expansion of the oscillatory source potential. *Applied Ocean Research*, Elsevier, v. 6, n. 2, p. 116–117, 1984. Cited on page 75.
- NEWMAN, J. N. *Marine hydrodynamics*. [S.l.]: MIT press, 1977. Cited 2 times on page 74 and 117.
- NORDFORSK. Seakeeping performance of ships. In: *Assessment of a Ship Performance in a Seaway*. [S.l.: s.n.], 1987. Cited on page 111.
- ÖZÜM, S.; ŞENER, B.; YILMAZ, H. A parametric study on seakeeping assessment of fast ships in conceptual design stage. *Ocean Engineering*, Elsevier, v. 38, n. 13, p. 1439–1447, 2011. Cited 3 times on page 47, 54, and 189.
- SANDVIK, P. C. Cosmar moonpool dynamics. In: *SINTEF*. Trondheim: [s.n.], 2007. Cited on page 119.
- SCHWEFEL, H.-P. *Numerical optimization of computer models*. [S.l.]: John Wiley & Sons, Inc., 1981. Cited on page 57.
- TAJIMA, K. (田島清瀬). *Engineering of oscillation - in Japanese (振動の工学)*. [S.l.]: Sangyo Tosho (産業図書), 1972. Cited 3 times on page 40, 41, and 42.
- TAKAGI, M.; ARAI, S. *Sea keeping theory for ships and ocean structures*. [S.l.]: Seizando, 1996. Cited on page 81.

- TAKEZAWA, S. et al. Seakeeping assessment of a displacement type super high speed ship in directional spectrum waves. In: *FAST'93*. Yokohama: [s.n.], 1993. Cited 2 times on page 59 and 190.
- TÖRNBLOM, J.; HAMMARGREN, E. *Effect of the Moonpool on the Total Resistance of a Drillship*. Dissertação (Mestrado) — Chalmers University of Technology, Göteborg, Sweden, 2012. Cited 2 times on page 38 and 39.
- TORRES, F. G. d. S. *Estudo do moonpool como sistema de minimização de movimento em uma plataforma do tipo monocoluna*. Dissertação (Mestrado) — Universidade de São Paulo, 2007. Cited 7 times on page 11, 37, 121, 135, 136, 137, and 138.
- VAN'T VEER, R.; THOLEN, H. J. Added resistance of moonpools in calm water. In: *Proceedings of the ASME 27th International Conference on Offshore Mechanics and Arctic Engineering*. OMAE2008-57246. [S.l.: s.n.], 2008. Cited 5 times on page 23, 28, 29, 31, and 165.
- VIJITH, P.; VISWANATHAN, S.; PANNEERSELVAM, R. Moon pool effects on a floating body. *International Journal of Design and Manufacturing Technology (IJDMT)*, v. 5, n. 13, p. 23–28, 2014. Cited 4 times on page 26, 37, 44, and 191.
- WEHAUSEN, J. V.; LAITONE, E. V. Surface waves. In: *Fluid Dynamics/Strömungsmechanik*. [S.l.]: Springer, 1960. p. 446–778. Cited on page 75.
- ZHANG, X.; YEUNG, R. W. On hydrodynamic behavior of a cylindrical moonpool with an entrapped two-layer fluid. In: *International Workshop on Water Waves and Floating Bodies*. Plymouth: [s.n.], 2016. p. 3–6. Cited on page 121.

Appendix

Appendix A Matrix-shaped equation of the potential expression

For a numerical calculation, the final integral equation of the velocity potential should be discretized. If the calculation strategy is done by the panel method (BEM), because the expression remains only with calculations on the hull surface (meaning the external hull with the moon pool wall) and internal water free surface of the MP, a surface discretizing should be done for both.

The total number of element of the surface is N , from which the elements numbered from 1 to N_1 belong to the hull and the rest, from $N_1 + 1$ to N compose the internal water free surface of the moon pool. It is assumed that the velocity potential value is constant in each element surface, and the calculation is done considering a normal unit vector in the centre point of each element, so that the centre point and normal vector represent the element.

Picking one isolated element P for analysis, the velocity potential on each element is a summation of the influences of all the other Q elements, including itself:

$$\varphi_j(P) = \int_{S_H+S_M+S_{MF}} \left(\frac{\partial \varphi_j(Q)}{\partial n_Q} G(P, Q) - \varphi_j(Q) \frac{\partial G(P, Q)}{\partial n_Q} \right) dS_Q \quad (1)$$

where there is a term in which $\varphi_j(Q) = \varphi_j(P)$.

Adopting a counter l for the chosen element P and a counter k for the other elements Q , the velocity potential in P_l is given by:

$$\varphi_j(P_l) = \sum_{K=1}^N \left[\int_{S_H+S_M+S_{MF}} \frac{\partial \varphi_j(Q_k)}{\partial n_Q} G(P_l, Q_k) - \varphi_j(Q_k) \frac{\partial G(P_l, Q_k)}{\partial n_Q} dS_{Q_k} \right] \quad (2)$$

$$l = 1, 2, \dots, N$$

The boundary condition applied at each element P is then defined:

$$\frac{\partial \varphi_j(Q_k)}{\partial n_Q} = n_j(Q_k) \quad \text{on} \quad S_H + S_M \quad (3)$$

and

$$\left(-K + \frac{\partial}{\partial Z} \right) \varphi_j(Q_k) + i\mu^* \varphi_j(Q_k) = 0 \quad \text{on} \quad S_{MF} \quad (4)$$

Isolating the differential term to replace in the integral equation, becomes:

$$\frac{\partial \varphi_j(Q_k)}{\partial n_Q} = (K - i\mu^*)\varphi_j(Q_k) \quad (5)$$

From this point on, the summation must be applied in two different parts, first for the hull surface, with the elements from 1 to N_1 , and then for the moon pool surface elements, from $N_1 + 1$ to N .

$$\varphi_j(P_l) = \sum_{S_H+S_M} + \sum_{S_{MF}} = \sum_{K=1}^{N_1} + \sum_{K=N_1+1}^N \quad (6)$$

The expression becomes:

$$\begin{aligned} \varphi_j(P_l) = & \sum_{K=1}^{N_1} \left[\int_{S_H+S_M} n_j(Q_k)G(P_l, Q_k) - \varphi_j(Q_k) \frac{\partial G(P_l, Q_k)}{\partial n_Q} dS_{Q_k} \right] \\ & + \sum_{K=N_1+1}^N \left[\int_{S_{MF}} (K - i\mu^*)\varphi_j(Q_k)G(P_l, Q_k) - \varphi_j(Q_k) \frac{\partial G(P_l, Q_k)}{\partial n_Q} dS_{Q_k} \right] \end{aligned} \quad (7)$$

Since the chosen Green function satisfies simultaneously the boundary conditions on the free surface S_F with wave, on the bottom S_B and on the imaginary far distance lateral frontier S_∞ , it is true that $(-K + \frac{\partial}{\partial Z})G = 0$, so the first term of the integral on the water free surface inside the MP can be further simplified:

$$\begin{aligned} (K - i\mu^*)\varphi_j(Q_k)G(P_l, Q_k) - \varphi_j(Q_k) \frac{\partial G(P_l, Q_k)}{\partial n_Q} &= \left(K - \frac{\partial}{\partial n_Q} \right) G(P_l, Q_k) \varphi_j(Q_k) \\ &- i\mu^* \varphi_j(Q_k)G(P_l, Q_k) = 0\varphi_j(Q_k) - i\mu^* \varphi_j(Q_k)G(P_l, Q_k) \end{aligned} \quad (8)$$

Then, the velocity potential expression becomes:

$$\begin{aligned} \varphi_j(P_l) = & \sum_{K=1}^{N_1} \left[\int_{S_H+S_M} n_j(Q_k)G(P_l, Q_k) - \varphi_j(Q_k) \frac{\partial G(P_l, Q_k)}{\partial n_Q} dS_{Q_k} \right] \\ & + \sum_{K=N_1+1}^N \left[\int_{S_{MF}} -i\mu^* \varphi_j(Q_k)G(P_l, Q_k) dS_{Q_k} \right] \end{aligned} \quad (9)$$

In order to have a linear equation system of the shape $A\varphi = B$, it is rewritten as:

$$\begin{aligned}
\varphi_j(P_l) &+ \sum_{K=1}^{N_1} \left[\varphi_j(Q_k) \int_{S_H+S_M} \frac{\partial G(P_l, Q_k)}{\partial n_Q} dS_{Q_k} \right] \\
&+ \sum_{K=N_1+1}^N \left[\varphi_j(Q_k) i\mu^* \int_{S_{MF}} G(P_l, Q_k) dS_{Q_k} \right] \\
&= \sum_{K=1}^{N_1} \left[n_j(Q_k) \int_{S_H+S_M} G(P_l, Q_k) dS_{Q_k} \right] \quad l = 1, 2, \dots, N
\end{aligned} \tag{10}$$

To make the left-hand side term be composed by a single matrix $[A_{lk}]_{N \times N}$, due to the overlap of contribution of the velocity potentials where $\varphi_j(Q_k) = \varphi(P_l)$, the term where $Q_k = P_l$ (i.e., the diagonal terms) becomes $(1 + A_{ll})$. In spatial terms, representing integral terms of the the above equation by the correspondent matrix elements, it is easier to identify the composition of the equation system:

$$\begin{aligned}
\int_{S_H+S_M} \frac{\partial G(P_l, Q_k)}{\partial n_Q} dS_{Q_k} &= [A_{lk}^a]_{N \times N_1}, \\
\int_{S_{MF}} G(P_l, Q_k) dS_{Q_k} &= [A_{lk}^b]_{N \times (N-N_1)}, \\
\int_{S_H+S_M} G(P_l, Q_k) dS_{Q_k} &= [C_{lk}]_{N_1 \times 1},
\end{aligned} \tag{11}$$

where the matrix coefficients $[C_{lk}]_{(N_1 \times 1)}$ and $[A_{lk}^b]_{N \times (N-N_1)}$ are the same function that just differ in the surface where the calculation is done: the hull with moon pool wall $S_H + S_M$ and the free surface inside the moon pool S_{MF} .

The right-hand side of the linear equation is the column matrix $[B_{lk}]_{N \times 1} = [n_j(Q_k) B_{lk}, k = 1, 2, \dots, N]$. For the sake of easy computer code manipulation, since $n_j(Q_k)$ is an already existent matrix, the linear coefficient $[B_{lk}]_{N_1 \times 1}$ can be obtained from the multiplication:

$$\begin{bmatrix} C_{lk} & 0_{N \times (N-1)} \\ 0_{(N-N_1) \times 1} & 0_{(N-N_1) \times (N-N_1)} \end{bmatrix}_{N \times N} [n_j(Q_k), k = 1, 2, \dots, N]_{N \times 1} \tag{12}$$

Finally, the matrix equation in the shape $A\varphi = B$ becomes:

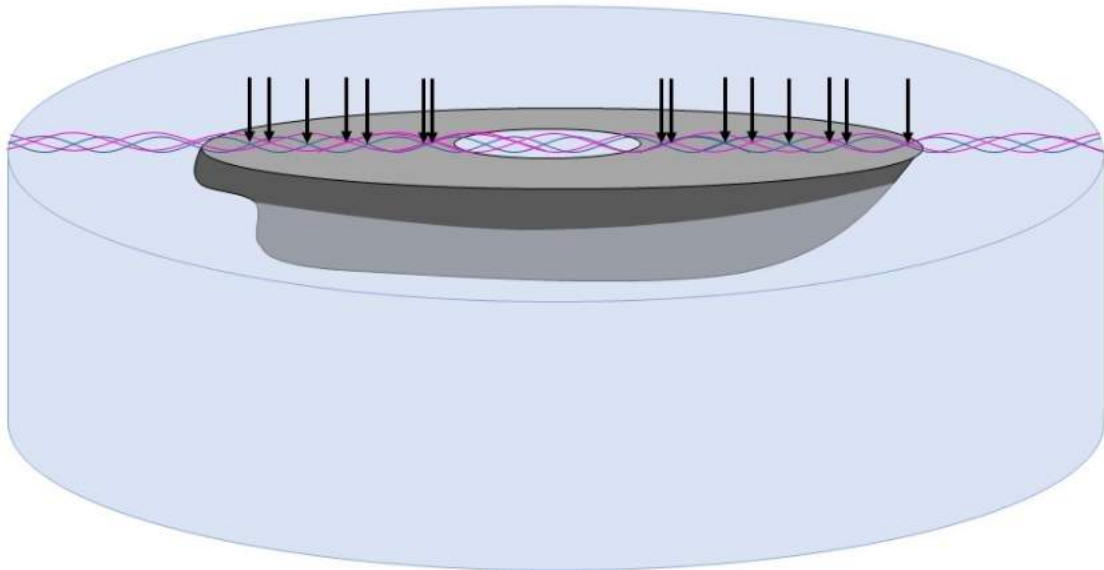
$$[A_{lk}^a \quad \mu A_{lk}^b]_{N \times N} \begin{bmatrix} \varphi_j(Q_k), k = 1, 2, \dots, N_1 \\ \varphi_j(Q_k), k = N_1 + 1, \dots, N \end{bmatrix}_{N \times 1} = [B_{lk}]_{N \times 1} \tag{13}$$

For a ship without moon pool, all the variables cover the range from 1 to N and the equation simplifies to

$$[A_{lk}^a]_{N \times N} [\varphi_j(Q_k), k = 1, 2, \dots, N]_{N \times 1} = [C_{lk}]_{N \times 1}. \tag{14}$$

The solution of the above matrix equation could be obtained by multiplying both sides by the inverse of the matrix A : $[A]^{-1}[A][\varphi] = [A]^{-1}[B]$. There might be, however, some frequencies at which the determinant of A is zero, and the inverse matrix cannot be calculated, resulting in a singularity named “irregular frequency”. Then equation cannot be solved in this way. The physical meaning of this irregular frequency lays on the proposed Green function. If the basic Green function $G = \frac{1}{4\pi} \left(\frac{1}{r} + \frac{1}{r_1} \right)$ where only the mirrored source pairs are used, no velocity exists inside the region delimited by the solid shape and its image shape, including the free surface line. Thus, the wave term $\frac{-K}{2\pi} \hat{G}(R, z_P + z_Q)$ needs to be added to attend the free surface wave condition. Although it makes easier to solve the integral equation, it introduces the existence of waves inside the hull, out of the fluid domain. Even though, it is possible to find velocity potential value equal to zero in that region. The reason is that, for some frequencies, there is one or more of the harmonic nodes in that region, which leads to the value zero of $\det(A)$. The sketch shown in figure 99 illustrates this trend.

Figure 99: Steady waves inside the moon pool originated from the mathematical model of boundary condition at free surface introduce some harmonic nodes to the region outside the fluid domain, inside the hull.



Source: Author

To avoid such problem and assure that the potential is in fact equal to zero regardless the presence of nodes (that means, to force zero amplitude of wave inside the hull, outside the fluid domain), some extra points are added in random positions that do not belong to the fluid domain. In practical terms, the addition of points results in

extra lines in the $[A]$ matrix, related to the left-hand side of the Second identity of Green.

$$\int_S \left[\frac{\partial}{\partial n} G - \frac{\partial G}{\partial n} \right] \varphi dS = \begin{cases} 0 & \text{outside } S, \\ \varphi & \text{at } S \end{cases} \quad (15)$$

where the coordinates of the added points are input for G . Then the matrix $[A]$ turns out to be no longer squared, and extra zeros appear in the $[B]$ column matrix, as a result since they are located outside S . The $[\varphi]$ matrix remains the same, since it is related to the number elements, and no extra element was added (this is expressed by not adding extra normal vectors). The mathematical solution must be done with other approach for non-squared matrices, as the least squares method for example.

$$\begin{bmatrix} A \\ D \end{bmatrix}_{(N+M) \times N} [\varphi]_{N \times 1} = \begin{bmatrix} B \\ 0 \end{bmatrix}_{(N+M) \times 1} \quad (16)$$

Although the added points can be located at any place outside the domain, as above the water line, for example, for to have a physical meaning, the waterline plane inside the hull is chosen. Since the velocity potential at the added points result to be zero, several zero-velocity points randomly distributed at different locations of the waterline plane inside the hull would assure that there was no coincidence of choosing a point located at the node of the resonant wave profile.

This procedure was implemented in Fortran in the hydrodynamic calculation module by Kawabe (2017)

Appendix B Long term operability discussion

The present work took as an example a drill ship that has the characteristic of changing its station. As soon as its drilling activity is accomplished in one location, it heads to the next location and thus does not stay for as much time as one could consider a long term. However, it was stated that the optimization can be run for any system with a moon pool, if given the proper input and limit values, so it is important to consider those cases when platforms and other ocean structures that are kept for long term in the same location.

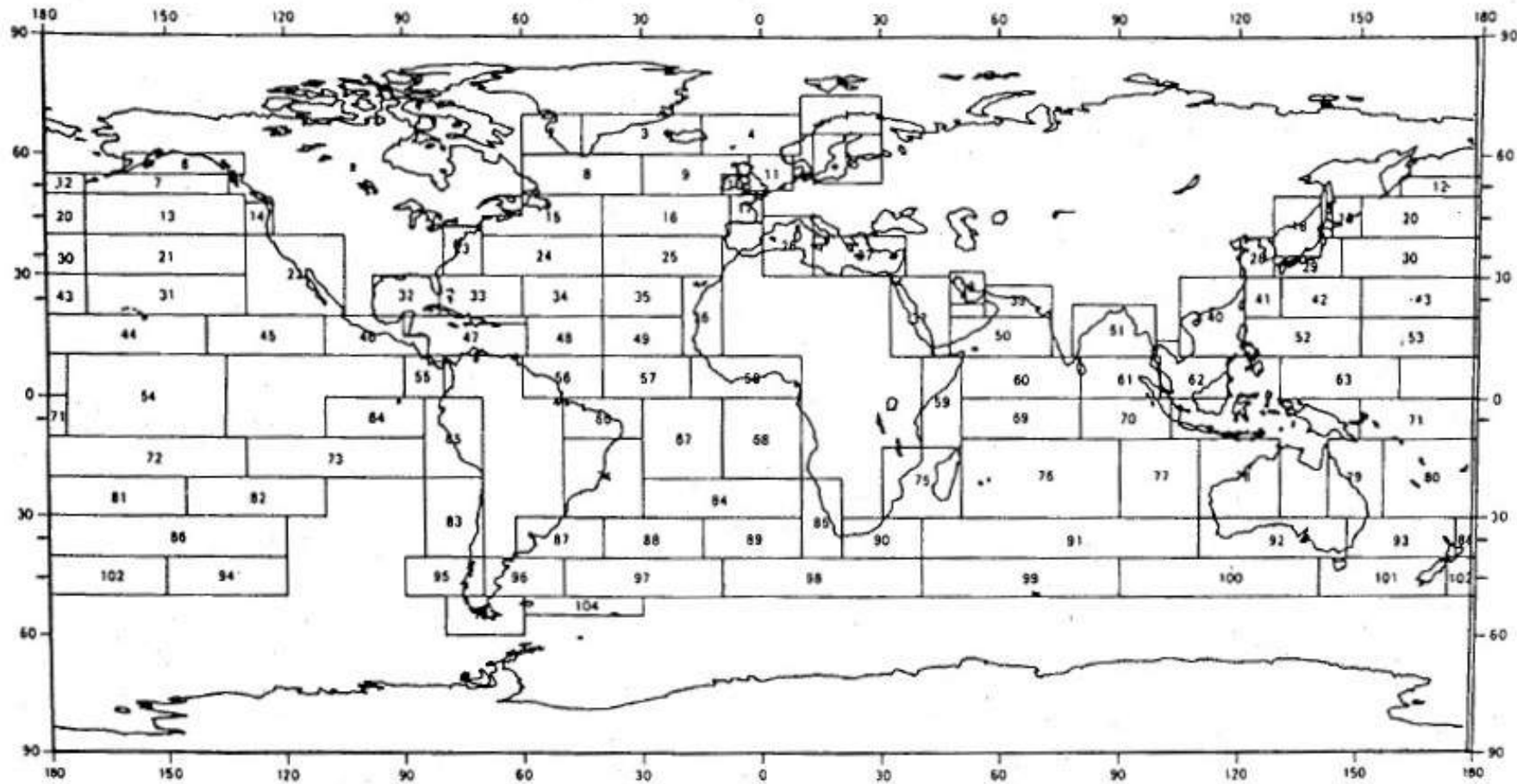
A long term concept involves a sequence of sea states changing along a period within a time span of years. Both the change of sea states and their duration have their probability. Within this situation, second order phenomena and variables become more important.

Among the criteria discussed and derived in this work, drift power is the only criterion involving second order force origin, and is also the only one that does not regard damage or safety risks. During a time span of years, there will be some sea states that will be severe, followed and preceded by some less severe. In drift case, short-term calculation to the most severe ones would be enough if taken for granted that, after the period of severe sea state the system can resume its positioning in azimuthal plane and relative to waves. Moreover, the Rayleigh damping used in the free surface of the internal water of the MP is of second order, experimental data should be used to determine its value for this long term situation.

The other criteria depend on operability in life time, which requires further information. There is a wave statistics data basis of several regions around the world, called Global Wave Statistics (HOGBEN; DACUNHA; OLLIVER, 1986). Those data, with different time history lengths, were acquired in different manners and with different instruments, then treated and adjusted with mathematical models. An illustration of the sector divisions of data around the world is shown in Figure 100.

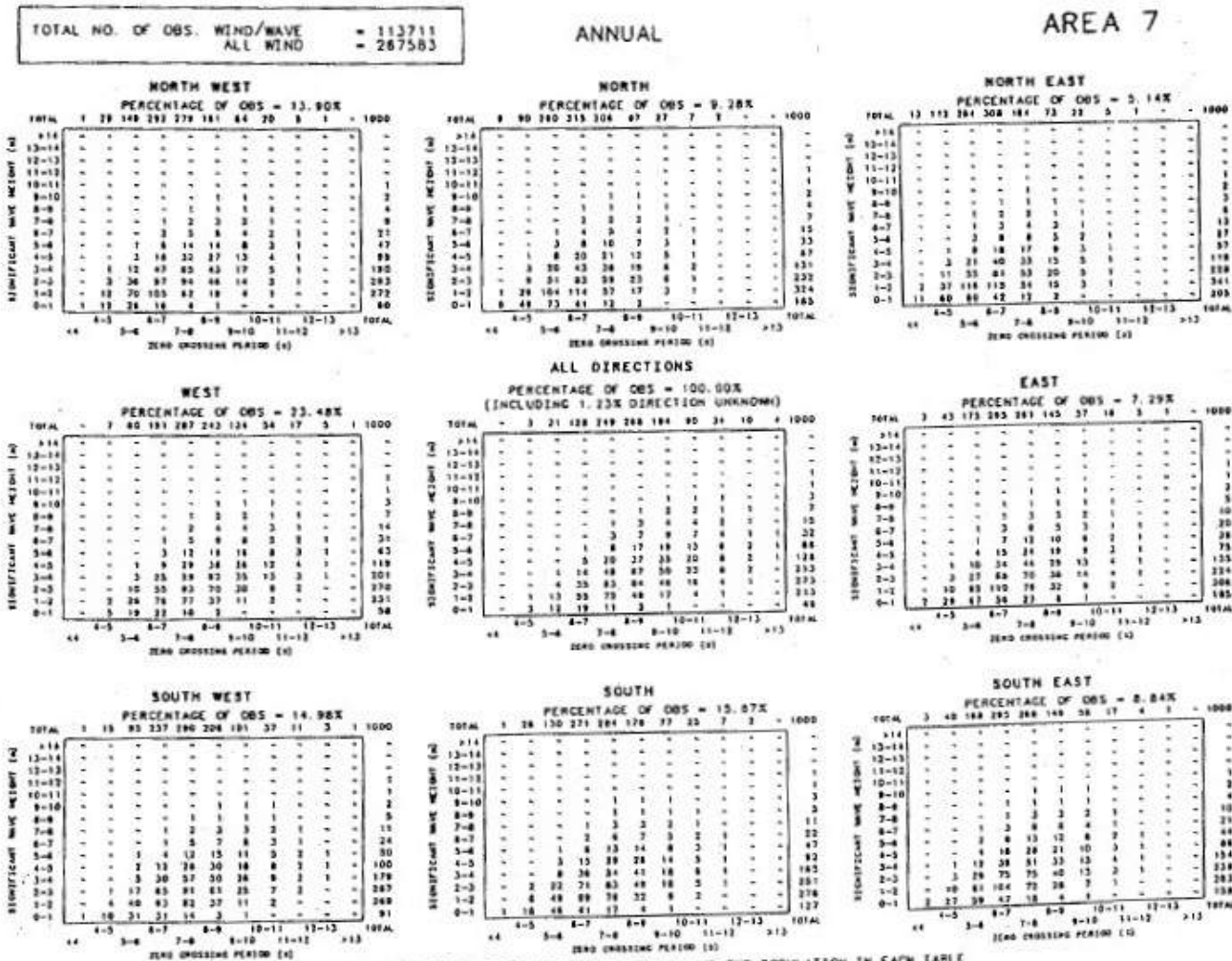
For each section there is a set of tables of joint probability distribution of significant wave heights and zero-crossing periods for each season (winter, spring, summer, autumn) and for an year. Those five sets of tables include data organized in “directions” (north, north west, west, south west, south, south east, east, north east) and “all directions”. An example of a set can be found in Figure 101.

Figure 100: Map of sea areas of the scope of global coverage in the Global Wave Statistics compilation.



Source: Hogben, Dacunha and Olliver (1986)

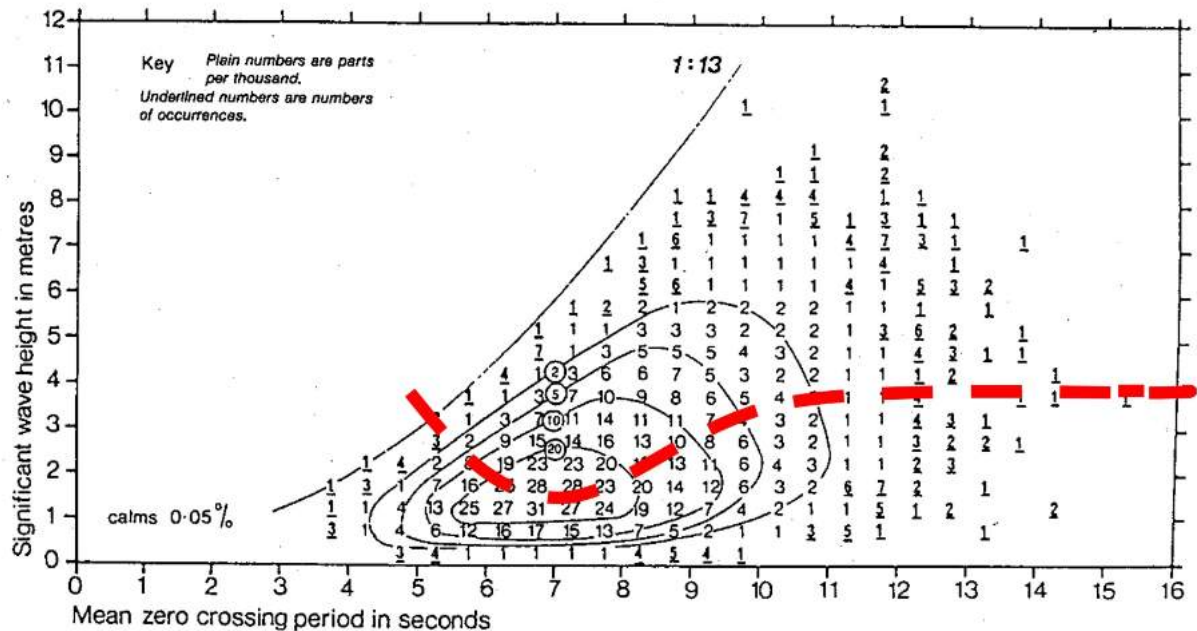
Figure 101: Directional classes of joint probability distribution of wave heights and periods in one season of one of the areas of the Global Wave Statistics compilation.



Source: Hogben, Dacunha and Olliver (1986)

A single chart of those sets is illustrated in figure 102. For each pair of zero-crossing period and significant wave height there is the probability distribution in a total of 1000. So, for example, the probability of a sea state characterized by $(T_z, H_s) = (8.7, 4)$ is 7/1000, and $(T_z, H_s) = (7.3, 2)$ is 28/1000. If the response spectrum of a ship were known and the threshold wave heights in each period of that chart were calculated, a curve could be plotted as the dotted one in the chart. In this example, the resonance period happens around $T_z = 7$ s, so the curve of H_s of the ship assumes its minimum value around that T_z value.

Figure 102: Directional joint probability distribution with curve of threshold significant wave heights of the ship. In this example, the resonance period happens around $T_z = 7$ s, so the curve of H_s of the ship assumes its minimum value around that T_z value.



Source: Hogben, Dacunha and Olliver (1986) adapted by T. Hirayama

There is a limitation, however, that the long term wave statistics currently do not have enough information about the duration of the sea states, so precise calculation shall be kept as a problem to be solved in the future. If such information were obtained, the estimation procedure would be as follows, considering initially that each pair (H_s, T_s) is independent, and that the wave direction is only one, *i.e.*, considering for example that the joint probability distribution used is of the class "all directions" in the annual set of data.

Suppose that the occurrence probability that shows the duration of sea state is, for example over continuous 7 days, defined as $p_7(H_s, T_s)\Delta H\Delta T$, under the given sea condition of $H_s(T_s)$. As said before, ideally that value of p_7 would be available in future. The limiting or critical wave height (TWH) that stops the drilling operation can be given

from the results of the analysis in the present work, where the probability $p(H_s, T_s)$ of happening such wave height value H_s is calculated. Hence the long term probability P_o that the drill ship is subjected to the operable sea condition at the designated position is expressed as:

$$P_o = \sum (H_s = 0 \rightarrow H_{threshold}) \sum (T_s = 0 \rightarrow \infty) p(H_s, T_s) p7(H_s, T_s) \Delta H \Delta T \quad (17)$$

where H_s is a function of the incidence angle β relative to the longitudinal centreline of the system, and of the significant period $H_s = H_s(T_s, \beta)$. If each directional class of waves would be considered, *e.g.* $\beta = 0^\circ : 45^\circ : 360^\circ$ for, *e.g.* North through North East, East, ..., North West, North, then

$$\begin{aligned} P_o = & \sum (\beta = 0^\circ \rightarrow 360^\circ) \\ & \sum (H_s = 0 \rightarrow H_{threshold}) \\ & \sum (T_s = 0 \rightarrow \infty) p(H_s, T_s, \beta) \cdot p7(H_s, T_s, \beta) \Delta H \Delta T \Delta \beta \end{aligned} \quad (18)$$

or, if specific values of periods T_{si} associated to the most restricting significant wave heights are known,

$$P_o = \sum_{\beta=0^\circ}^{360^\circ} \sum_{H_s=0}^{H_s(T_{si})} \sum_i p(H_s, T_{si}, \beta) \cdot p7(H_s, T_{si}, \beta) \Delta H \Delta T \Delta \beta \quad (19)$$

Here, a generic case with β angle variation from 0° to 360° is used because, even though there might be symmetry in the response of the system relative to a certain plane (thus maybe the response spectrum for $\beta = 45^\circ$ is the same as for $\beta = 315^\circ$), the directional class of waves are usually not symmetric at pairs of opposite directions such as North \rightarrow South and South \rightarrow North, so the excitation would have a different profile.

Stopping the drilling operation is very undesirable in short duration, for example, one day or two days, due to cost problems, and the owner expects a long duration of mild sea state. The owner can decide the speculation of the drill ship if the estimation of P_o is given at a desired point in the ocean.

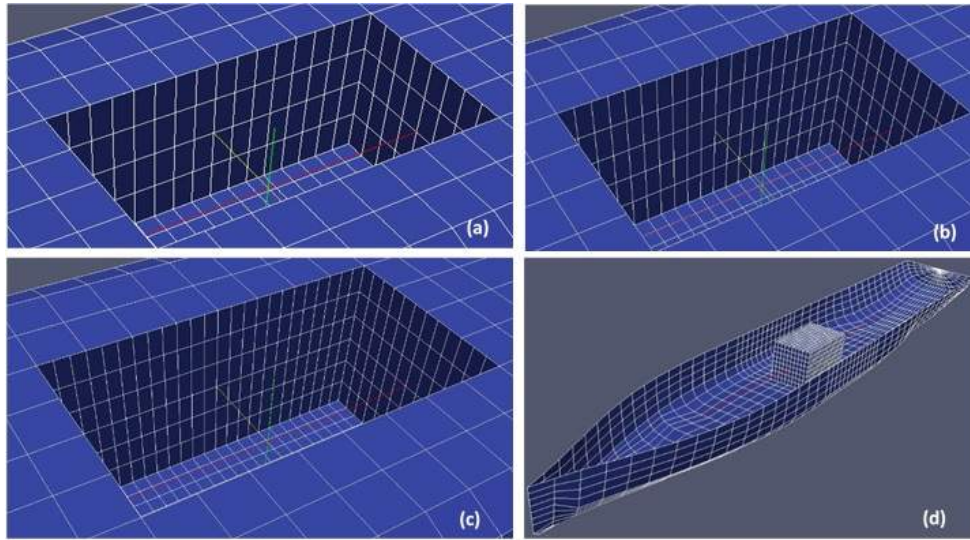
Appendix C Moon pool mesh calibration data

It was assumed that the original hull without the opening that will be used as input to the optimization code has a sufficiently fine, regular, and harmoniously distributed mesh that will not negatively interfere in the hydrodynamic results. A collection of RAO data of the motions of a fixed drill ship shape with rectangular MP of length to breadth ratio of 2 : 1 was generated with each mesh size presented in the table 110.

The variation of the mesh was done by defining the number of elements in a half-breadth of the MP. That parameter was chosen to have an integer number of elements in that dimension because the hull data file is generated for only half of the hull, since it is symmetric about the longitudinal line. The case 1 was generated with 2 elements in half-breadth, and the amount was increased until the case 5 with 6 elements. Since the refinement in the hull mesh was done with increase of elements following the transversal sections (noticeable in figure 103(d), repeated from section 5.1 of the discussion about the mesh for moon pool), the parameter ratio of the element size was taken upon the longitudinal size.

The figure 103 shows the different MP mesh adjusted to the hull opening. The hull mesh remains the same, while the MP meshes change case by case: figure 103(a) is the case 3, with 1 hull element to each pair of MP elements, figure 103(b) is the case 4, in a proportion of 2 : 5 and figure 103(c) is the case 5, with 1 hull element to each 3 MP elements.

Figure 103: Moon pool elements with different size ratio dimensions: (a) case 3, (b) case 4, (c) case 5, (d) complete hull in case 4



Source: Author

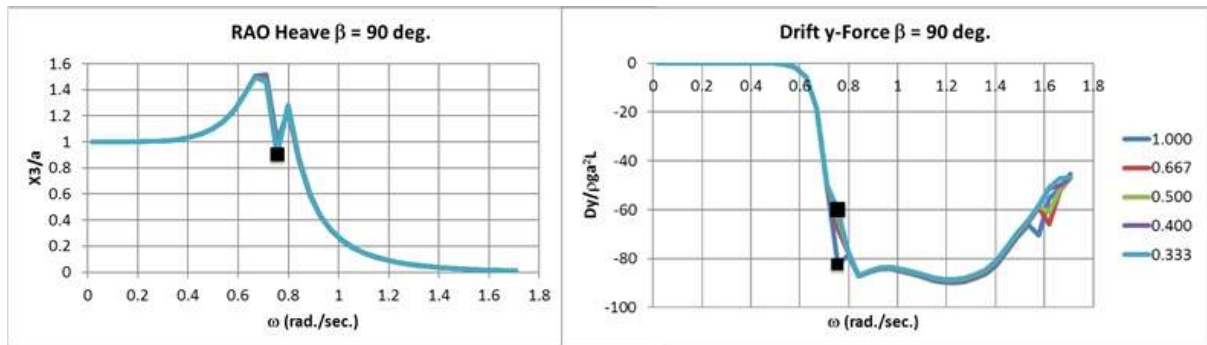
The RAO of the hull with each configuration was calculated for heave, drift force, vertical bending moment at midship and MP water elevation at midpoint. The charts are similar, shown as follows.

- Heave
- Drift
- Vertical bending moment at midship
- MP water elevation at midpoint

The most critical incidence angle that provided the biggest response amplitude among all in each criterion was chosen to make a comparison of the module of the response of the ship in each configuration. For heave and drift the critical curves are at angle $\beta = 90^\circ$, and for vertical bending moment at midship and MP water elevation at midpoint, $\beta = 0^\circ$ was chosen. From the charts, the most remarkable frequency identified was $\omega = 0.755$ rad/s, which corresponds to the resonance peak in the MP water surface elevation at mid. The points correspondent to that frequency were highlighted in each chart, shown in figure 104.

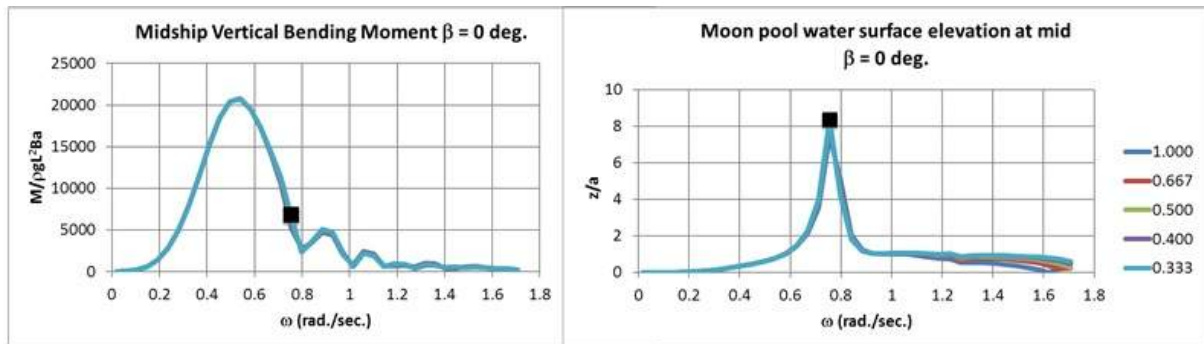
The discussion about the response curve shapes is presented in the section 3.4 of the drill ship response, where the response curves to both the hull without opening and the hull with MP are described and compared. Figure 104 contains the heave and drift charts, both in beam sea situation ($\beta = 90^\circ$). Figure 105 shows the charts of vertical bending moment amidship and the MP water surface elevation at mid, both in head sea situation ($\beta = 0^\circ$).

Figure 104: Heave motion (left) and drift force (right) charts at different moon pool element length ratios, both for $\beta = 90^\circ$



Source: Author

Figure 105: Midship vertical bending moment (left) and moon pool water surface elevation at mid (right) charts with different moon pool element length ratios, both for $\beta = 0^\circ$

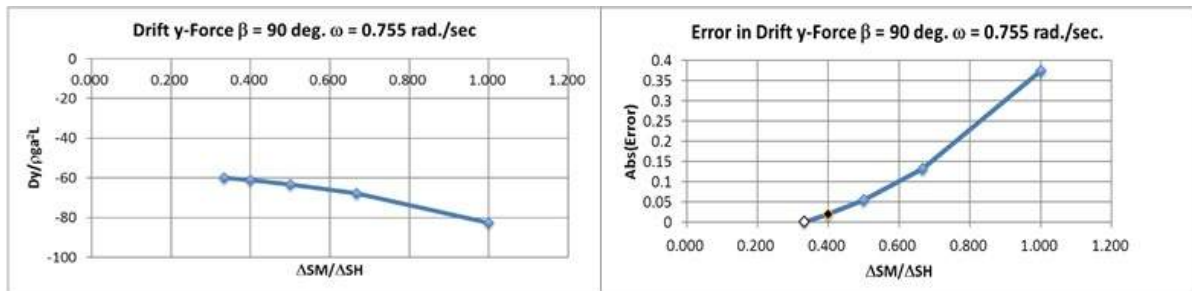


Source: Author

When comparing the values isolated from the identified points at the chosen frequency $\omega = 0.755$ rad/s in each configuration (cases 1 to 5), their difference can be better identified. As the mesh becomes more refined, the length ratio becomes smaller and the variation of the values of response decrease tending to a limit value. It is being considered that a variation of the order of approximately 2% is sufficiently small to consider that the limit was reached. The reason is that refining the mesh too much might imply in a computational cost that is not worthy if compared to the gain in precision.

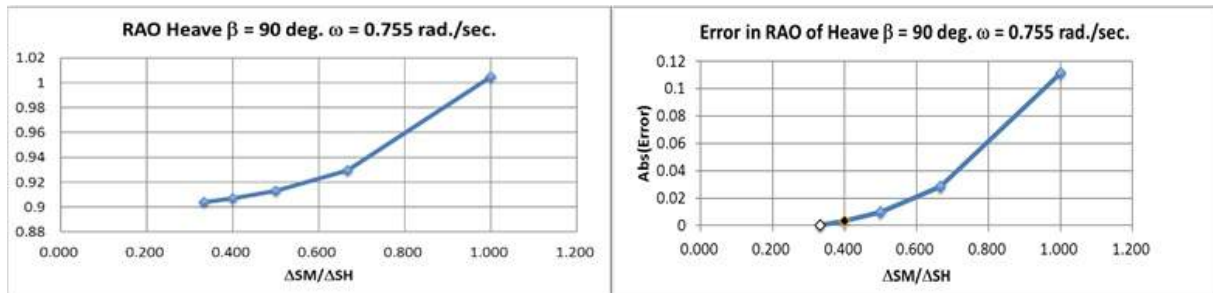
The figures 106 to 109 show pairs of charts for each criterion, where the one on the left shows the response value evolution with length ratio and on the right there is the correspondent error evolution relative to the value of the last case (case 5).

Figure 106: Charts of drift force response value evolution with length ratio: left shows the value, right shows the error relative to case 5 (finest mesh)



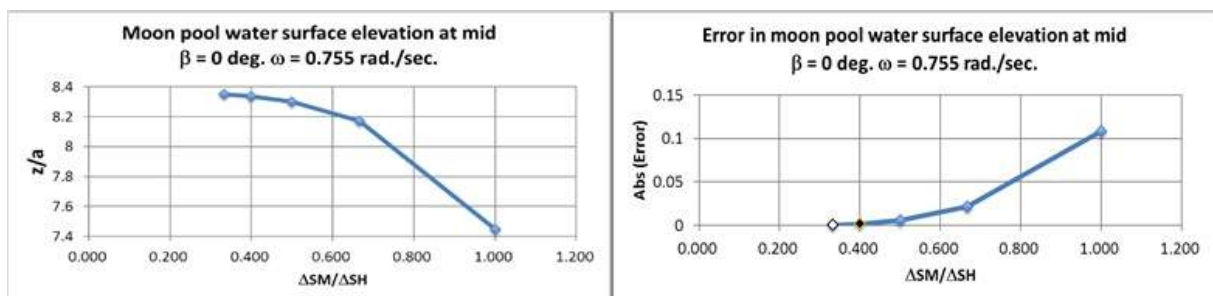
Source: Author

Figure 107: Charts of heave motion response value evolution with length ratio: left shows the value, right shows the error relative to case 5 (finest mesh)



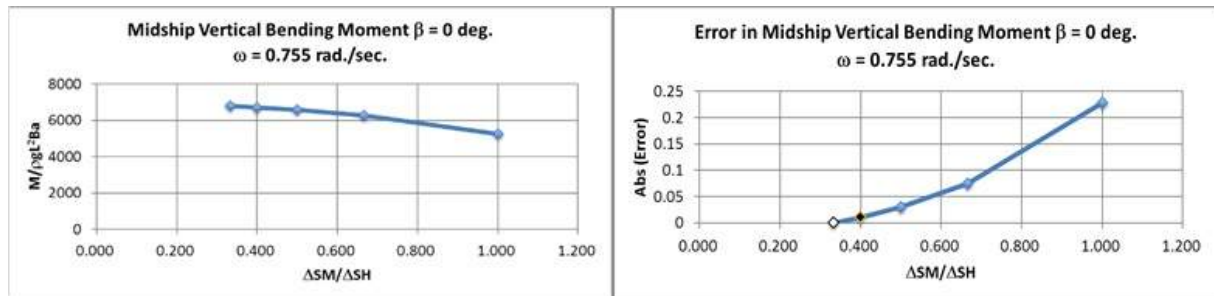
Source: Author

Figure 108: Charts of moon pool water surface elevation at mid response value evolution with length ratio: left shows the value, right shows the error relative to case 5 (finest mesh)



Source: Author

Figure 109: Charts of heave motion response value evolution with length ratio: left shows the value, right shows the error relative to case 5 (finest mesh)



Source: Author

In the error charts, the lowest point is marked in white filling and has always value zero, since they correspond to the error relative to the case 5, that is the error relative to the value itself. Thus, the minimum error values obtained for each criterion are the highlighted ones with black filling and the collection of those values is shown in the figure 111 reproduced from the section 5.1 of the moon pool mesh discussion.

Figure 110: Length ratio of the elements in the MP

	Amount of MP border elements for half-breadth	Length of the MP border element in transversal line	Amount of elements in the longitudinal line (no. of hull elements long.=4*no. of hull elements in half breadth)	Length of the MP border element in longitudinal line	Longitudinal length ratio between the MP elements and hull elements	Equivalent to
	N-WIDE	DELTA SIDE	N-SIDE			
CASE 1	2	2.80	8	2.54	1.00	1:1
CASE 2	3	1.86	12	1.69	0.67	2:3
CASE 3	4	1.40	16	1.27	0.50	1:2
CASE 4	5	1.12	20	1.02	0.40	2:5
CASE 5	6	0.93	24	0.85	0.33	1:3

Source: Author

Figure 111: Length ratio of the elements in the moon pool

Absolute error in	CASE 1	CASE 2	CASE 3	CASE 4	CASE 5
RAO of Heave $\beta = 90$ deg. $\omega = 0.755$ rad./sec	11.1%	2.8%	1.0%	0.3%	0.0%
Drift y-Force $\beta = 90$ deg. $\omega = 0.755$ rad./sec.	37.6%	13.2%	5.4%	1.9%	0.0%
Midship Vertical Bending Moment $\beta = 0$ deg. $\omega = 0.755$ rad./sec.	22.9%	7.5%	3.1%	1.1%	0.0%
Moonpool water surface elevation at mid $\beta = 0$ deg. $\omega = 0.755$ rad./sec.	10.8%	2.1%	0.6%	0.2%	0.0%

Source: Author

Appendix D Input files pictures

The input files presented in this section have the following use:

- Optimization _Parameters.DAT includes the data of acceptable limit values and ranges of the moon pool for the optimization module in Matlab. - input _hull.DAT is the list of grid coordinates and elements of the closed hull mesh. Its first three lines indicate number of grid points, number of elements and Rayleigh damping coefficient value, in this order. This input is used by the optimization module to attach the moon pool. - PANEL.drill-ship.DAT is the input file generated by the optimization module to send to the hydrodynamic response calculation module, and should be used as model for compatibility to the module applied by the user.

It is important that the position of the information coincide with the lines of the example, otherwise the acquisition of information from file by the optimization module may not work properly.

EXAMPLE IMAGES OF THE INPUT FILE *Optimization_Parameters.DAT*

```

1 'Total number of individuals to each evaluation. ni =' 5
2 'Based on the typical MP lenght, set N values for L1 ='
3 10 10.5 11 11.5 12
4 'Based on the typical MP width, set N values for L2 (N same as for L1) ='
5 5
6 'Based on the typical MP lenght, set N values for L3 (N same as for L1) ='
7 11.5
8 'Percentage of the individuals to be selected as the best. p_no =' 0.5
9 'Typical distance between nodes = ' 2.30
10 'data for statistics'
11 'following data is used in Tres_Height'
12 'Wave overflow treshold value xq =' 4
13 'Probability of green water N/n =' 500
14 'Stroke compensation treshold value xq =' 3.5
15 'Stroke compensation exceedance number N/n =' 1000
16 'Bending moment exceedance number N/n =' 0.001
17 'Drift force Dy0 =' 34260
18 'Choose sea states to perform analysis. Binary value.'
19 'IACS LONG CRESTED' 0
20 'IACS SHORT CRESTED' 0
21 'JONSWAP LONG CRESTED' 0
22 'JONSWAP SHORT CRESTED' 1
23 'Bretschneider LONG CRESTED' 0
24 'Bretschneider SHORT CRESTED' 0
25 'Choose significant wave periods to perform analysis. Integer from 4 to 18 seconds, inclusive.'
26 4 10 12
27
28
29

```

Source: Author

EXAMPLE IMAGES OF THE INPUT FILE `input_hull.DAT`

1	572		
2	510		
3	0.09		
4	1 100.600000000	0.000000000	0.000000000
5	2 100.445100000	0.000000000	1.451566667
6	3 100.290200000	0.000000000	2.903133333
7	4 100.135300000	0.000000000	4.354700000
8	5 99.972200000	0.000000000	5.806466667
9	6 99.809100000	0.000000000	7.258233333
10	7 99.646000000	0.000000000	8.710000000
11	8 99.421300000	0.000000000	10.742000000
12	9 98.977766670	0.000000000	11.032233330
13	10 98.534233330	0.000000000	11.322466670
14	11 98.090700000	0.000000000	11.612700000
15	12 95.520000000	1.364000000	0.000000000
16	13 95.520000000	1.313333333	1.451566667
17	14 95.520000000	1.262666667	2.903133333
18	15 95.520000000	1.212000000	4.354700000
19	16 95.520000000	1.155566667	5.806466667
20	17 95.520000000	1.099133333	7.258233333
21	18 95.520000000	1.042700000	8.710000000
22	19 95.520000000	0.850700000	9.726000000
23	20 95.520000000	0.658700000	10.742000000
24	21 95.520000000	0.329350000	11.177350000
25	22 95.520000000	0.000000000	11.612700000
26	23 90.440000000	2.815300000	0.000000000
27	24 90.440000000	2.717300000	2.177350000
28	25 90.440000000	2.619300000	4.354700000
29	26 90.440000000	2.454000000	6.532350000
30	27 90.440000000	2.288700000	8.710000000
31	28 90.440000000	2.018700000	9.387333333
32	29 90.440000000	1.748700000	10.064666670
33	30 90.440000000	1.478700000	10.742000000
34	31 90.440000000	0.985800000	11.032233330
35	32 90.440000000	0.492900000	11.322466670
36	33 90.440000000	0.000000000	11.612700000
37	34 85.360000000	4.499300000	0.000000000
38	35 85.360000000	4.336000000	2.177350000
39	36 85.360000000	4.172700000	4.354700000
40	37 85.360000000	3.911350000	6.532350000
41	38 85.360000000	3.650000000	8.710000000
42	39 85.360000000	3.253100000	9.387333333
43	40 85.360000000	2.856200000	10.064666670
44	41 85.360000000	2.459300000	10.742000000
45	42 85.360000000	1.639533333	11.032233330
46	43 85.360000000	0.819766667	11.322466670
47	44 85.360000000	0.000000000	11.612700000

Source: Author

553	550	-102.600000000	0.000000000	3.045080000
554	551	-102.600000000	2.811340000	0.000000000
555	552	-102.600000000	2.690470000	0.285472153
556	553	-102.600000000	2.569600000	0.570944306
557	554	-102.600000000	2.380130000	0.856455791
558	555	-102.600000000	2.190660000	1.141967277
559	556	-102.600000000	1.577740000	1.408382605
560	557	-102.600000000	1.183340000	1.465461303
561	558	-102.600000000	0.788940000	1.522540000
562	559	-102.600000000	0.525960000	1.522540000
563	560	-102.600000000	0.262980000	1.522540000
564	561	-102.600000000	0.000000000	1.522540000
565	562	-102.600000000	0.000000000	0.000000000
566	563	-102.600000000	0.000000000	0.000000000
567	564	-102.600000000	0.000000000	0.000000000
568	565	-102.600000000	0.000000000	0.000000000
569	566	-102.600000000	0.000000000	0.000000000
570	567	-102.600000000	0.000000000	0.000000000
571	568	-102.600000000	0.000000000	0.000000000
572	569	-102.600000000	0.000000000	0.000000000
573	570	-102.600000000	0.000000000	0.000000000
574	571	-102.600000000	0.000000000	0.000000000
575	572	-102.600000000	0.000000000	0.000000000
576	1 2 1	13 12		
577	2 3 2	14 13		
578	3 4 3	15 14		
579	4 5 4	16 15		
580	5 6 5	17 16		
581	6 7 6	18 17		
582	7 8 7	19 18		
583	8 9 8	20 19		
584	9 10 9	21 20		
585	10 11 10	22 21		
586	11 13 12	24 23		
587	12 14 13	25 24		
588	13 15 14	26 25		
589	14 16 15	27 26		
590	15 17 16	28 27		
591	16 18 17	29 28		
592	17 19 18	30 29		
593	18 20 19	31 30		
594	19 21 20	32 31		
595	20 22 21	33 32		
596	21 24 23	35 34		
597	22 25 24	36 35		
598	23 26 25	37 36		
599	24 27 26	38 37		

Source: Author

1041	466	513	512	524	523
1042	467	514	513	525	524
1043	468	515	514	526	525
1044	469	516	515	527	526
1045	470	517	516	528	527
1046	471	519	518	530	529
1047	472	520	519	531	530
1048	473	521	520	532	531
1049	474	522	521	533	532
1050	475	523	522	534	533
1051	476	524	523	535	534
1052	477	525	524	536	535
1053	478	526	525	537	536
1054	479	527	526	538	537
1055	480	528	527	539	538
1056	481	530	529	541	540
1057	482	531	530	542	541
1058	483	532	531	543	542
1059	484	533	532	544	543
1060	485	534	533	545	544
1061	486	535	534	546	545
1062	487	536	535	547	546
1063	488	537	536	548	547
1064	489	538	537	549	548
1065	490	539	538	550	549
1066	491	541	540	552	551
1067	492	542	541	553	552
1068	493	543	542	554	553
1069	494	544	543	555	554
1070	495	545	544	556	555
1071	496	546	545	557	556
1072	497	547	546	558	557
1073	498	548	547	559	558
1074	499	549	548	560	559
1075	500	550	549	561	560
1076	501	562	552	562	551
1077	502	563	553	563	552
1078	503	564	554	564	553
1079	504	565	555	565	554
1080	505	566	556	566	555
1081	506	567	557	567	556
1082	507	568	558	568	557
1083	508	569	559	569	558
1084	509	570	560	570	559
1085	510	571	561	571	560
1086					

Source: Author

EXAMPLE IMAGES OF THE INPUT FILE PANEL.drill-ship.DAT

```

1 'Panel data '
2 'Opening front x coordinate (m) ' 11.00
3 'Opening aft. x coordinate (m) ' -11.50
4 'Width (half) (m) ' 5.000
5 'Height (m) ' 11.613
6 'Total Grid ' 721 43 573
7 'Total Panel & Free surface panel ' 596 22
8 'Moon pool data'
9 'Fore Division ' 2
10 'Side Division ' 9
11 'Height Division ' 5
12 'Rayleigh Damping ' 0.09
13 'Grid coordinate No. x y z (m)'
14 1 100.600000000 0.000000000 0.000000000
15 2 100.445100000 0.000000000 1.451566667
16 3 100.290200000 0.000000000 2.903133333
17 4 100.135300000 0.000000000 4.354700000
18 5 99.972200000 0.000000000 5.806466667
19 6 99.809100000 0.000000000 7.258233333
20 7 99.646000000 0.000000000 8.710000000
21 8 99.421300000 0.000000000 10.742000000
22 9 98.977766670 0.000000000 11.032233330
23 10 98.534233330 0.000000000 11.322466670
24 11 98.090700000 0.000000000 11.612700000
25 12 95.520000000 1.364000000 0.000000000
26 13 95.520000000 1.313333333 1.451566667
27 14 95.520000000 1.262666667 2.903133333
28 15 95.520000000 1.212000000 4.354700000
29 16 95.520000000 1.155566667 5.806466667
30 17 95.520000000 1.099133333 7.258233333
31 18 95.520000000 1.042700000 8.710000000
32 19 95.520000000 0.850700000 9.726000000
33 20 95.520000000 0.658700000 10.742000000
34 21 95.520000000 0.329350000 11.177350000
35 22 95.520000000 0.000000000 11.612700000
36 23 90.440000000 2.815300000 0.000000000
37 24 90.440000000 2.717300000 2.177350000
38 25 90.440000000 2.619300000 4.354700000
39 26 90.440000000 2.454000000 6.532350000
40 27 90.440000000 2.288700000 8.710000000
41 28 90.440000000 2.018700000 9.387333333
42 29 90.440000000 1.748700000 10.064666670
43 30 90.440000000 1.478700000 10.742000000
44 31 90.440000000 0.985800000 11.032233330
45 32 90.440000000 0.492900000 11.322466670
46 33 90.440000000 0.000000000 11.612700000
47 34 85.260000000 4.499200000 0.000000000

```

Source: Author

725	712	-2.622222222	5.000000000	0.000000000
726	713	-5.155555556	0.000000000	0.000000000
727	714	-5.155555556	2.500000000	0.000000000
728	715	-5.155555556	5.000000000	0.000000000
729	716	-7.688888889	0.000000000	0.000000000
730	717	-7.688888889	2.500000000	0.000000000
731	718	-7.688888889	5.000000000	0.000000000
732	719	-10.222222222	0.000000000	0.000000000
733	720	-10.222222222	2.500000000	0.000000000
734	721	-10.222222222	5.000000000	0.000000000
735	1	2	1	13
736	2	3	2	14
737	3	4	3	15
738	4	5	4	16
739	5	6	5	17
740	6	7	6	18
741	7	8	7	19
742	8	9	8	20
743	9	10	9	21
744	10	11	10	22
745	11	13	12	24
746	12	14	13	25
747	13	15	14	26
748	14	16	15	27
749	15	17	16	28
750	16	18	17	29
751	17	19	18	30
752	18	20	19	31
753	19	21	20	32
754	20	22	21	33
755	21	24	23	35
756	22	25	24	36
757	23	26	25	37
758	24	27	26	38
759	25	28	27	39
760	26	29	28	40
761	27	30	29	41
762	28	31	30	42
763	29	32	31	43
764	30	33	32	44
765	31	35	34	46
766	32	36	35	47
767	33	37	36	48
768	34	38	37	49
769	35	39	38	50
770	36	40	39	51
771	37	41	40	52

Source: Author

1286	552	639	640	654	655
1287	553	640	641	655	656
1288	554	641	642	656	657
1289	555	642	643	657	658
1290	556	643	644	658	659
1291	557	644	645	659	660
1292	558	645	646	660	661
1293	559	646	647	661	662
1294	560	647	648	662	663
1295	561	649	650	664	665
1296	562	650	651	665	666
1297	563	651	652	666	667
1298	564	652	653	667	668
1299	565	653	654	668	669
1300	566	654	655	669	670
1301	567	655	656	670	671
1302	568	656	657	671	672
1303	569	657	658	672	673
1304	570	658	659	673	674
1305	571	659	660	674	675
1306	572	660	661	675	676
1307	573	661	662	676	677
1308	574	662	663	677	678
1309	575	679	680	682	683
1310	576	680	681	683	684
1311	577	685	682	683	683
1312	578	685	683	684	684
1313	579	691	686	687	687
1314	580	691	687	688	688
1315	581	691	688	689	689
1316	582	691	689	690	690
1317	583	692	693	694	695
1318	584	694	695	696	697
1319	585	696	697	698	699
1320	586	700	701	702	703
1321	587	704	705	707	708
1322	588	705	706	708	709
1323	589	707	708	710	711
1324	590	708	709	711	712
1325	591	710	711	713	714
1326	592	711	712	714	715
1327	593	713	714	716	717
1328	594	714	715	717	718
1329	595	716	717	719	720
1330	596	717	718	720	721
1331					

Source: Author

Appendix E Output files description

COMMENTS ON THE STRUCTURE OF THE OUTPUT FILE “CYLINDER -DRIFT-FORCE-RAO.DAT”

Colors:

General information description of main objective

Information of local objective

Shape of data presentation

... Continues the same (can be in vertical position also)

General information and parameters of the simulated model

THREE-DIMENSIONAL PANEL METHOD

FOR RADIATION & DIFFRACTION PROBLEMS

OF A FLOATING SHIP WITH ZERO SPEED

SHIP NAME : RING FLOATER MOONPOOL NO.1 30/3/2015

NUMBER OF HULL SURFACE ELEMENTS: NE = 704
 NUMBER OF ADDED ELEMENTS : NADD = 9
 NUMBER OF TOTAL ELEMENTS : NT = 713

LENGTH IN X-AXIS----- (LENGTH) ---= 41.000 m
 LENGTH IN Y-AXIS----- (BREDTH) ---= 41.000 m
 LENGTH IN Z-AXIS----- (DRAFT) ---= 7.000 m

BLOCK COEFFICIENT----- (CB) ---= 0.47860
 WATER PLANE AREA COEFFICIENT---- (CW) ---= 0.47860
 CENTER OF FLOATATION -----= 0.00000 m
 IXX=VOL*(KXX**2);----- (KXX) ---= 23.45000 m
 IYY=VOL*(KYY**2);----- (KYY) ---= 23.45000 m
 IZZ=VOL*(KZZ**2);----- (KZZ) ---= 14.40000 m
 POSITION OF GRAVITY FROM ORIGIN-- (OXG) ---= 0.00000 m
 POSITION OF GRAVITY FROM ORIGIN-- (OYG) ---= 0.00000 m
 POSITION OF GRAVITY FROM KEEL---- (KG) ----= 0.00000 m
 METACENTRIC HEIGHT FOR PITCH ---- (GML) ---= 20.25000 m
 METACENTRIC HEIGHT FOR ROLL ---- (GMB) ---= 20.25000 m

LONG CRESTED IRREGULAR WAVE

Long crested Drift force spectrum for unit significant wave height at each attack angle beta: 30, 60, 90, 120, 150, 180, 210, 240, 270, 300, 330, 360 and each significant wave period, for each of the 5 values of frequency omega. Fixes beta, varies Tz and omega for

each calculation, changes beta, repeats calculation:

Same for short crested, and all calculated for each irregular wave spectrum

```
For (spectrum = IACS, JONSWAP, Bretschneider){
  For (attack angle beta = 0:360deg){
    For (Tz = 4:18){
      For (wavelength = 1:5){
        A - Drift and moment long crested
      }
    }
    B - Mean nondimensional drift and moment long crested
  }
  For (Tz = 4:18){
    C - Mean nondimensional drift and moment short crested
  }
}
```

For IACS spectrum

A - Headings for each wave angle

***** IRREGULAR WAVE RESPONSE SPECTRUM *****

DRIFT FORCE
SIGNIFICANT WAVE HEIGHT 1.0000 (m)

WAVE DIRECTION 0.0000 (deg.)
 MOON POOL DAMPING epsi 0.0000
 WAVE SPECTRUM IACS
 No. OMEGA(rad./sec.) WAVE FX(DIF.) FY(DIF) FX(FREE) FY(FREE) MZ(DIF.) MZ(FREE)

A - First loop: Fixed IACS spectrum, fixed beta = 0, long crested, varying Tz

WAVE DIRECTION 0.000000000000000E+000 DEG.
 WAVE PERIOD TZ 4.000000000000000 SEC.

ID of omega	Incident wave frequency	Period	Drift x-direct fixed hull	Drift y-direct fixed hull	Drift x-direct free hull	Drift y-direct free hull	Momentum fixed hull	Momentum free hull
----------------	----------------------------	--------	------------------------------	------------------------------	-----------------------------	-----------------------------	------------------------	-----------------------

1	0.10000	0.0000E+00	0.0000E+00	0.0000E+00	0.0000E+00	0.0000E+00	0.0000E+00	0.0000E+00
2	0.43000	0.7955E-23	-0.2619E-24	-0.1592E-38	-0.1173E-27	-0.9044E-42	0.2242E-29	0.4244E-30
3	0.76000	0.5735E-02	-0.5965E-03	-0.2130E-17	-0.3933E-02	-0.2804E-16	-0.4064E-09	-0.3721E-08
4	1.09000	0.7978E-01	-0.4650E-01	-0.2533E-15	-0.5204E-01	-0.3292E-15	-0.8882E-07	-0.9060E-07
5	1.42000	0.5210E-01	-0.3253E-01	-0.1922E-15	-0.3117E-01	-0.2607E-15	-0.7902E-07	-0.7852E-07

WAVE DIRECTION 0.000000000000000E+000 DEG.
 WAVE PERIOD TZ 5.000000000000000 SEC.

1	0.10000	0.0000E+00	0.0000E+00	0.0000E+00	0.0000E+00	0.0000E+00	0.0000E+00	0.0000E+00
2	0.43000	0.1114E-08	-0.3668E-10	-0.2230E-24	-0.1643E-13	-0.1267E-27	0.3140E-15	0.5945E-16

3	0.76000	0.7249E-01	-0.7539E-02	-0.2692E-16	-0.4971E-01	-0.3544E-15	-0.5137E-08	-0.4703E-07
4	1.09000	0.7350E-01	-0.4284E-01	-0.2333E-15	-0.4794E-01	-0.3032E-15	-0.8182E-07	-0.8346E-07
5	1.42000	0.2827E-01	-0.1766E-01	-0.1043E-15	-0.1692E-01	-0.1415E-15	-0.4289E-07	-0.4262E-07
.								
.								
.								

B - Non-dimension mean drift force for each Tz=4:18 collected from previous list of results

LONG CRESTED IRREGULAR WAVE CONDITION

WAVE DIRECTION 0.00 DEG.
SIGNIFIGANT WAVE HEIGHT 1.00 m
SPECTRUM TYPE IACS

***** DRIFT FORCE RESPONCE *****

NO-DIMENSION MEAN DRIFT FORCE FORCE($F/\rho_0 * g * L * H * H$) MOMENT ($M/\rho_0 * G * L * L * H * H$)

TZ (SEC.)	FX(DIF.)	FY(DIF)	FX(FREE)	FY(FREE)	MZ(DIF.)	MZ(FREE)
0.40000E+01	-0.20911E-01	-0.11600E-15	-0.23614E-01	-0.16089E-15	-0.42484E-07	-0.44082E-07
0.50000E+01	-0.19539E-01	-0.10310E-15	-0.35018E-01	-0.24036E-15	-0.35774E-07	-0.50094E-07
0.60000E+01	-0.14790E-01	-0.73557E-16	-0.38815E-01	-0.27033E-15	-0.23992E-07	-0.47174E-07
0.70000E+01	-0.10309E-01	-0.49550E-16	-0.31901E-01	-0.22343E-15	-0.14572E-07	-0.36315E-07
0.80000E+01	-0.74969E-02	-0.36136E-16	-0.23189E-01	-0.16280E-15	-0.43103E-08	-0.24769E-07

.
. .
.

LONG CRESTED IRREGULAR WAVE

B - Closing info of first loop

.

A - Second loop: Fixed IACS spectrum, fixed beta = 30, long crested, varying Tz

.

***** IRREGULAR WAVE RESPONSE SPECTRUM *****

DRIFT FORCE

SIGNIFICANT WAVE HEIGHT 1.0000 (m)
WAVE DIRECTION 30.0000 (deg.)
MOON POOL DAMPING epsi 0.0000

WAVE SPECTRUM IACS

No.	OMEGA(rad./sec.)	WAVE	FX(DIF.)	FY(DIF)	FX(FREE)	FY(FREE)	MZ(DIF.)	MZ(FREE)
WAVE DIRECTION	30.00000000000000			DEG.				
WAVE PERIOD TZ	4.00000000000000			SEC.				

1	0.10000	0.0000E+00	0.0000E+00	0.0000E+00	0.0000E+00	0.0000E+00	0.0000E+00	0.0000E+00
2	0.43000	0.7955E-23	-0.2268E-24	-0.1309E-24	-0.4504E-27	-0.5299E-27	0.3911E-24	0.8938E-23
3	0.76000	0.5735E-02	-0.5166E-03	-0.2982E-03	-0.3384E-02	-0.1932E-02	0.5369E-02	0.3335E-02
4	1.09000	0.7978E-01	-0.4028E-01	-0.2325E-01	-0.4495E-01	-0.2616E-01	0.1898E+00	0.1877E+00
5	1.42000	0.5210E-01	-0.2816E-01	-0.1623E-01	-0.2697E-01	-0.1556E-01	0.1036E+00	0.1035E+00
.								
.								
.								

B - Non-dimension mean drift force for each Tz=4:18 collected from previous list of results

LONG CRESTED IRREGULAR WAVE CONDITION

WAVE DIRECTION 30.00 DEG.
SIGNIFIGANT WAVE HEIGHT 1.00 m
SPECTRUM TYPE IACS

***** DRIFT FORCE RESPONCE *****

NO-DIMENSION MEAN DRIFT FORCE FORCE($F/\rho \cdot g \cdot L \cdot H \cdot H$) MOMENT ($M/\rho \cdot g \cdot L \cdot L \cdot H \cdot H$)

TZ (SEC.)	FX(DIF.)	FY(DIF)	FX(FREE)	FY(FREE)	MZ(DIF.)	MZ(FREE)
0.40000E+01	-0.18108E-01	-0.10448E-01	-0.20401E-01	-0.11838E-01	0.81507E-01	0.80135E-01
0.50000E+01	-0.16920E-01	-0.97647E-02	-0.30198E-01	-0.17407E-01	0.89379E-01	0.80254E-01
0.60000E+01	-0.12808E-01	-0.73922E-02	-0.33440E-01	-0.19198E-01	0.79204E-01	0.64798E-01

0.70000E+01	-0.89276E-02	-0.51530E-02	-0.27475E-01	-0.15751E-01	0.59577E-01	0.49444E-01
0.80000E+01	-0.64924E-02	-0.37475E-02	-0.19970E-01	-0.11442E-01	0.42481E-01	0.53731E-01

LONG CRESTED IRREGULAR WAVE

.
.
.

B - Closing info of first calculation

A - Repeats for the other beta values until 360 degrees

C - First loop: Fixed IACS spectrum, fixed beta = 0, short crested, varying Tz

SHORT CRESTED IRREGULAR WAVE CONDITION

WAVE DIRECTION	0.00	DEG.
SIGNIFIGANT WAVE HEIGHT	1.00	m
SPECTRUM TYPE	IACS	

***** DRIFT FORCE RESPONCE *****

NO-DIMENSION MEAN DRIFT FORCE FORCE($F/\rho \cdot g \cdot L \cdot H \cdot H$) MOMENT ($M/\rho \cdot g \cdot L \cdot L \cdot H \cdot H$)

TZ (SEC.)	FX(DIF.)	FY(DIF)	FX(FREE)	FY(FREE)	MZ(DIF.)	MZ(FREE)
-------------	----------	---------	----------	----------	----------	----------

0.40000E+01	-0.17653E-01	-0.75024E-02	-0.19901E-01	-0.84790E-02	0.58550E-01	0.57789E-01
0.50000E+01	-0.16495E-01	-0.70123E-02	-0.29471E-01	-0.12437E-01	0.64202E-01	0.59121E-01

0.60000E+01	-0.12486E-01	-0.53087E-02	-0.32644E-01	-0.13698E-01	0.56891E-01	0.48866E-01
0.70000E+01	-0.87031E-02	-0.37007E-02	-0.26823E-01	-0.11234E-01	0.42793E-01	0.37144E-01
0.80000E+01	-0.63291E-02	-0.26914E-02	-0.19497E-01	-0.81598E-02	0.30513E-01	0.36756E-01
0.90000E+01	-0.51841E-02	-0.22047E-02	-0.13684E-01	-0.57265E-02	0.22155E-01	0.45980E-01
0.10000E+02	-0.44827E-02	-0.19065E-02	-0.96078E-02	-0.40214E-02	0.16548E-01	0.52726E-01
0.11000E+02	-0.38354E-02	-0.16312E-02	-0.68389E-02	-0.28633E-02	0.12565E-01	0.52727E-01
0.12000E+02	-0.31997E-02	-0.13609E-02	-0.49574E-02	-0.20761E-02	0.96257E-02	0.48008E-01
0.13000E+02	-0.26188E-02	-0.11138E-02	-0.36622E-02	-0.15341E-02	0.74276E-02	0.41385E-01
0.14000E+02	-0.21215E-02	-0.90234E-03	-0.27551E-02	-0.11544E-02	0.57764E-02	0.34638E-01
0.15000E+02	-0.17129E-02	-0.72855E-03	-0.21081E-02	-0.88340E-03	0.45317E-02	0.28574E-01
0.16000E+02	-0.13846E-02	-0.58894E-03	-0.16382E-02	-0.68655E-03	0.35885E-02	0.23441E-01
0.17000E+02	-0.11237E-02	-0.47797E-03	-0.12910E-02	-0.54111E-03	0.28687E-02	0.19224E-01
0.18000E+02	-0.91706E-03	-0.39006E-03	-0.10305E-02	-0.43195E-03	0.23149E-02	0.15808E-01

C – Second loop: Fixed IACS spectrum, fixed beta = 30, short crested, varying Tz

SHORT CRESTED IRREGULAR WAVE CONDITION

WAVE DIRECTION 30.00 DEG.
SIGNIFIANT WAVE HEIGHT 1.00 m
SPECTRUM TYPE IACS

***** DRIFT FORCE RESPONCE *****

NO-DIMENSION MEAN DRIFT FORCE FORCE($F/\rho \cdot g \cdot L \cdot H \cdot H$) MOMENT ($M/\rho \cdot g \cdot L \cdot L \cdot H \cdot H$)

TZ (SEC.)	FX(DIF.)	FY(DIF)	FX(FREE)	FY(FREE)	MZ(DIF.)	MZ(FREE)
0.40000E+01	-0.15288E-01	-0.11140E-01	-0.17224E-01	-0.12587E-01	0.86937E-01	0.85947E-01
0.50000E+01	-0.14285E-01	-0.10412E-01	-0.25494E-01	-0.18458E-01	0.95330E-01	0.88730E-01
0.60000E+01	-0.10813E-01	-0.78824E-02	-0.28232E-01	-0.20327E-01	0.84475E-01	0.74052E-01
0.70000E+01	-0.75372E-02	-0.54947E-02	-0.23196E-01	-0.16670E-01	0.63541E-01	0.56206E-01
0.80000E+01	-0.54812E-02	-0.39961E-02	-0.16860E-01	-0.12108E-01	0.45307E-01	0.53425E-01
0.90000E+01	-0.44897E-02	-0.32735E-02	-0.11833E-01	-0.84972E-02	0.32897E-01	0.63864E-01
0.10000E+02	-0.38822E-02	-0.28308E-02	-0.83085E-02	-0.59671E-02	0.24571E-01	0.71591E-01
0.11000E+02	-0.33216E-02	-0.24221E-02	-0.59143E-02	-0.42487E-02	0.18657E-01	0.70854E-01
0.12000E+02	-0.27710E-02	-0.20207E-02	-0.42873E-02	-0.30807E-02	0.14293E-01	0.64176E-01
0.13000E+02	-0.22680E-02	-0.16539E-02	-0.31673E-02	-0.22764E-02	0.11029E-01	0.55161E-01
0.14000E+02	-0.18373E-02	-0.13398E-02	-0.23828E-02	-0.17130E-02	0.85772E-02	0.46086E-01
0.15000E+02	-0.14834E-02	-0.10818E-02	-0.18233E-02	-0.13109E-02	0.67290E-02	0.37976E-01
0.16000E+02	-0.11991E-02	-0.87447E-03	-0.14168E-02	-0.10188E-02	0.53284E-02	0.31130E-01
0.17000E+02	-0.97319E-03	-0.70969E-03	-0.11166E-02	-0.80297E-03	0.42596E-02	0.25515E-01
0.18000E+02	-0.79420E-03	-0.57917E-03	-0.89127E-03	-0.64098E-03	0.34374E-02	0.20973E-01
.						
.						
.						

C - Repeats for the other beta values until 360 degrees

.

REPEATS For JONSWAP spectrum

.

REPEATS For BRETSCHNEIDER spectrum

.

COMMENTS ON THE STRUCTURE OF THE OUTPUT FILE “CYLINDER -MOON-POOL-RAO.DAT”

Colors:

General information description of main objective

Information of local objective

Shape of data presentation

... Continues the same (can be in vertical position also)

General information and parameters of the simulated model

THREE-DIMENSIONAL PANEL METHOD

FOR RADIATION \& DIFFRACTION PROBLEMS

OF A FLOATING SHIP WITH ZERO SPEED

SHIP NAME : RING FLOATER MOONPOOL NO.1 30/3/2015

NUMBER OF HULL SURFACE ELEMENTS: NE = 704

NUMBER OF ADDED ELEMENTS : NADD = 9

NUMBER OF TOTAL ELEMENTS : NT = 713

LENGTH IN X-AXIS----- (LENGTH) ---= 41.000 m

LENGTH IN Y-AXIS----- (BREDTH) ---= 41.000 m

LENGTH IN Z-AXIS----- (DRAFT) ---= 7.000 m

BLOCK COEFFICIENT----- (CB) ---= 0.47860

WATER PLANE AREA COEFFICIENT---- (CW) ---= 0.47860

CENTER OF FLOATATION ----- 0.00000 m

IXX=VOL*(KXX**2);----- (KXX) ---= 23.45000 m

IYY=VOL*(KYY**2);----- (KYY) ---= 23.45000 m

IZZ=VOL*(KZZ**2);----- (KZZ) ---= 14.40000 m

POSITION OF GRAVITY FROM ORIGIN-- (OXG) ---= 0.00000 m

POSITION OF GRAVITY FROM ORIGIN-- (OYG) ---= 0.00000 m

POSITION OF GRAVITY FROM KEEL---- (KG) ---= 0.00000 m

METACENTRIC HEIGHT FOR PITCH ---- (GML) ---= 20.25000 m

METACENTRIC HEIGHT FOR ROLL ---- (GMB) ---= 20.25000 m

***** RESPONSE AMPLITUDE OPERATER *****

MP free surface elevation RAO for attack angle from 0 to 180 deg in several points: midship, foreship, aft, port and starboard

MOON POOL WATER SURFACE ELEVATION RAO

BETA = 0.00 DEG

RAMDA/L	OMEGA(RAD./SEC.)	T (SEC.)	MID	FORE	AFT.	PORT	STARBOARD
150.285	0.10000	62.83185	0.00018	0.00018	0.00025	0.00025	0.00025
8.128	0.43000	14.61206	0.07936	0.08335	0.23583	0.22808	0.22808
2.602	0.76000	8.26735	2.60476	2.69463	3.12687	3.09603	3.09603
1.265	1.09000	5.76439	1.36688	1.12359	0.75568	0.67591	0.67591
0.745	1.42000	4.42478	0.80427	1.11926	0.55943	0.47262	0.47262

MOON POOL WATER SURFACE ELEVATION RAO

BETA = 30.00 DEG

RAMDA/L	OMEGA(RAD./SEC.)	T (SEC.)	MID	FORE	AFT.	PORT	STARBOARD
150.285	0.10000	62.83185	0.00162	0.00483	0.01847	0.05447	0.05427
8.128	0.43000	14.61206	0.07907	0.08331	0.22587	0.25687	0.15405
2.602	0.76000	8.26735	2.60881	2.68283	2.99912	2.91880	3.09425
1.265	1.09000	5.76439	1.35733	1.16032	0.43159	0.33468	0.70798
0.745	1.42000	4.42478	0.82049	1.08423	0.34920	0.49944	0.50868

.
.
.

COMMENTS ON THE STRUCTURE OF THE OUTPUT FILE “COMMENTS ON CYLINDER -MOON-POOL-SPECTRUM.DAT”

Colors:

General information description of main objective

Information of local objective

Shape of data presentation

... Continues the same (can be in vertical position also)

Type of model simulated, main dimensions of the ship

THREE-DIMENSIONAL PANEL METHOD

FOR RADIATION \& DIFFRACTION PROBLEMS

OF A FLOATING SHIP WITH ZERO SPEED

SHIP NAME : RING FLOATER MOONPOOL NO.1 30/3/2015

NUMBER OF HULL SURFACE ELEMENTS: NE = 704

NUMBER OF ADDED ELEMENTS	: NADD =	9
NUMBER OF TOTAL ELEMENTS	: NT =	713
LENGTH IN X-AXIS-----	(LENGTH)---	41.000 m
LENGTH IN Y-AXIS-----	(BREDTH)---	41.000 m
LENGTH IN Z-AXIS-----	(DRAFT)---	7.000 m
BLOCK COEFFICIENT-----	(CB)---	0.47860
WATER PLANE AREA COEFFICIENT----	(CW)---	0.47860
CENTER OF FLOATATION -----		0.00000 m
IXX=VOL*(KXX**2);-----	(KXX)---	23.45000 m
IYY=VOL*(KYY**2);-----	(KYY)---	23.45000 m
IZZ=VOL*(KZZ**2);-----	(KZZ)---	14.40000 m
POSITION OF GRAVITY FROM ORIGIN--	(OXG)---	0.00000 m
POSITION OF GRAVITY FROM ORIGIN--	(OYG)---	0.00000 m
POSITION OF GRAVITY FROM KEEL----	(KG)---	0.00000 m
METACENTRIC HEIGHT FOR PITCH ----	(GML)---	20.25000 m
METACENTRIC HEIGHT FOR ROLL ----	(GMB)---	20.25000 m

Results of the Moon Pool's response in irregular waves: long crested and short crested for unit significant wave height, and standard deviation, for each wave spectrum – IACS, JONSWAP and Bretschneider. For each of the 5 values of frequency omega. Fixes wave spectrum, varies beta, Tz and omega:

```
For (wave spectrum = IACS, JONSWAP, Bretschneider){
  For (attack angle beta = 0:30:360){
```

```
For (period Tz = 4:18){
    For (omega = 1:5){
        Free surface height at mid
        Free surface height at fore
        Free surface height at aft
        Free surface height at port
        Free surface height at starboard
    }
}

Standard deviation of the response (sigma) for long crested condition
}

For (attack angle beta = 0:30:360){
    Standard deviation of the response (sigma) for short crested condition
}

}
```

LONG CRESTED IRREGULAR WAVE

***** IRREGULAR WAVE RESPONSE SPECTRUM *****

Water surface heights for fixed attack angle beta = 0

MOON POOL WAVER ELEVATIONS		
SIGNIFICANT WAVE HEIGHT	1.0000	(m)
WAVE DIRECTION	0.0000	(deg.)
MOON POOL DAMPING epsi	0.0000	

WAVE SPECTRUM IACS

No. OMEGA(rad./sec.) WAVE MIDD. FORE AFT. PROT STARBOARD

WAVE DIRECTION 0.000000000000000E+000 DEG.

WAVE PERIOD TZ 4.000000000000000 SEC.

ID omega(rad/s) wave Mid elevation Fore elev. Aft elev. Port elev. Starboard elev.

1	0.10000	0.0000E+00	0.0000E+00	0.0000E+00	0.0000E+00	0.0000E+00	0.0000E+00
2	0.43000	0.7955E-23	0.0000E+00	0.5010E-25	0.0000E+00	0.0000E+00	0.0000E+00
3	0.76000	0.5735E-02	0.0000E+00	0.3891E-01	0.0000E+00	0.0000E+00	0.0000E+00
4	1.09000	0.7978E-01	0.0000E+00	0.1491E+00	0.0000E+00	0.0000E+00	0.0000E+00
5	1.42000	0.5210E-01	0.0000E+00	0.3370E-01	0.0000E+00	0.0000E+00	0.0000E+00

WAVE DIRECTION 0.000000000000000E+000 DEG.

WAVE PERIOD TZ 5.000000000000000 SEC.

1	0.10000	0.0000E+00	0.0000E+00	0.0000E+00	0.0000E+00	0.0000E+00	0.0000E+00
2	0.43000	0.1114E-08	0.0000E+00	0.7019E-11	0.0000E+00	0.0000E+00	0.0000E+00
3	0.76000	0.7249E-01	0.0000E+00	0.4918E+00	0.0000E+00	0.0000E+00	0.0000E+00
4	1.09000	0.7350E-01	0.0000E+00	0.1373E+00	0.0000E+00	0.0000E+00	0.0000E+00
5	1.42000	0.2827E-01	0.0000E+00	0.1829E-01	0.0000E+00	0.0000E+00	0.0000E+00

.
.
.

Water surface heights for fixed attack angle beta=30 .

Standard deviation based on long crested condition for the previous TZ=4:18, IACS, beta=30 .

Standard deviation based on short crested condition for the previous TZ=4:18, IACS, beta=0

SHORT CRESTED IRREGULAR WAVE CONDITION

WAVE DIRECTION 0.00 DEG.
SIGNIFIGANT WAVE HEIGHT 1.00 m
SPECTRUM TYPE IACS

***** STANDARD DEVIATION OF RESPONCE *****

MOON POOL WAVER ELEVATIONS

TZ (SEC.)	MIDD. (m)	FORE (m)	AFT. (m)	PROT (m)	STARBOARD (m)
0.40000E+01	0.28747E+00	0.25849E+00	0.28488E+00	0.17342E+00	0.17342E+00
0.50000E+01	0.41138E+00	0.45888E+00	0.41194E+00	0.47575E+00	0.47575E+00
0.60000E+01	0.46283E+00	0.54766E+00	0.46507E+00	0.60235E+00	0.60235E+00
0.70000E+01	0.42848E+00	0.51504E+00	0.43099E+00	0.57450E+00	0.57450E+00
0.80000E+01	0.36921E+00	0.44557E+00	0.37154E+00	0.50019E+00	0.50019E+00

Standard deviation based on short crested condition for the previous TZ=4:18, IACS, beta=30

SHORT CRESTED IRREGULAR WAVE CONDITION

WAVE DIRECTION 30.00 DEG.
SIGNIFIGANT WAVE HEIGHT 1.00 m
SPECTRUM TYPE IACS

***** STANDARD DEVIATION OF RESPONCE *****

MOON POOL WAVER ELEVATIONS

TZ (SEC.)	MIDD. (m)	FORE (m)	AFT. (m)	PROT (m)	STARBOARD (m)
0.40000E+01	0.28147E+00	0.25780E+00	0.28615E+00	0.17836E+00	0.17836E+00
0.50000E+01	0.41285E+00	0.45888E+00	0.41326E+00	0.45972E+00	0.45972E+00
0.60000E+01	0.46827E+00	0.54805E+00	0.46641E+00	0.57899E+00	0.57899E+00
0.70000E+01	0.43449E+00	0.51551E+00	0.43215E+00	0.55160E+00	0.55160E+00
0.80000E+01	0.37450E+00	0.44600E+00	0.37220E+00	0.48025E+00	0.48025E+00

REPEATS For JONSWAP spectrum

.
.

REPEATS For BRETSCHNEIDER spectrum

.
.

COMMENTS ON THE STRUCTURE OF THE OUTPUT FILE “DRILL SHIP -MOTION-SPECTRUM.DAT”

Colors:

General information description of main objective

Information of local objective

Shape of data presentation

... Continues the same (can be in vertical position also)

General information and parameters of the simulated model

THREE-DIMENSIONAL PANEL METHOD

FOR RADIATION & DIFFRACTION PROBLEMS
OF A FLOATING SHIP WITH ZERO SPEED

SHIP NAME : DRILL SHIP MODEL 10/05/2016
NUMBER OF HULL SURFACE ELEMENTS: NE = 1162
NUMBER OF ADDED ELEMENTS : NADD = 40
NUMBER OF TOTAL ELEMENTS : NT = 1202

LENGTH IN X-AXIS----- (LENGTH)---= 203.363 m
LENGTH IN Y-AXIS----- (BREDTH)---= 29.027 m
LENGTH IN Z-AXIS----- (DRAFT)---= 11.613 m

BLOCK COEFFICIENT----- (CB)---= 0.76989
WATER PLANE AREA COEFFICIENT---- (CW)---= 0.18723
CENTER OF FLOATATION -----= 0.00000 m
IXX=VOL*(KXX**2);----- (KXX)---= 10.05000 m
IYY=VOL*(KYY**2);----- (KYY)---= 49.38000 m
IZZ=VOL*(KZZ**2);----- (KZZ)---= 49.38000 m
POSITION OF GRAVITY FROM ORIGIN-- (OXG)---= 0.00000 m
POSITION OF GRAVITY FROM ORIGIN-- (OYG)---= 0.00000 m
POSITION OF GRAVITY FROM ORIGIN-- (OZG)---= 1.00000 m
METACENTRIC HEIGHT FOR PITCH ---- (GML)---= 281.50000 m
METACENTRIC HEIGHT FOR ROLL ---- (GMB)---= 1.80000 m

MOON POOL WATER SURFACE DAMPING -----= 0.09000

LONG CRESTED IRREGULAR WAVE CONDITION

WAVE DIRECTION 0.00 DEG.
SIGNIFIGANT WAVE HEIGHT 1.00 m
SPECTRUM TYPE IACS

***** STANDARD DEVIATION OF RESPONCE *****

SHIP MOTIONS

TZ (SEC.)	SURGE (m)	SWAY (m)	HEAVE (m)	ROLL (deg.)	PITCH (deg.)	YAW (deg.)
0.40000E+01	0.46885E-03	0.00000E+00	0.68984E-03	0.00000E+00	0.18641E-01	0.00000E+00
0.50000E+01	0.86625E-03	0.00000E+00	0.18636E-02	0.00000E+00	0.45445E-01	0.00000E+00
0.60000E+01	0.13560E-02	0.00000E+00	0.24934E-02	0.00000E+00	0.68925E-01	0.00000E+00
0.70000E+01	0.21917E-02	0.00000E+00	0.25717E-02	0.00000E+00	0.99543E-01	0.00000E+00
0.80000E+01	0.31117E-02	0.00000E+00	0.25008E-02	0.00000E+00	0.12823E+00	0.00000E+00
0.90000E+01	0.38457E-02	0.00000E+00	0.24652E-02	0.00000E+00	0.14818E+00	0.00000E+00
0.10000E+02	0.43297E-02	0.00000E+00	0.24675E-02	0.00000E+00	0.15915E+00	0.00000E+00
0.11000E+02	0.45942E-02	0.00000E+00	0.24700E-02	0.00000E+00	0.16313E+00	0.00000E+00
0.12000E+02	0.46909E-02	0.00000E+00	0.24500E-02	0.00000E+00	0.16227E+00	0.00000E+00
0.13000E+02	0.46649E-02	0.00000E+00	0.24007E-02	0.00000E+00	0.15817E+00	0.00000E+00
0.14000E+02	0.45504E-02	0.00000E+00	0.23238E-02	0.00000E+00	0.15193E+00	0.00000E+00

0.15000E+02	0.43742E-02	0.00000E+00	0.22244E-02	0.00000E+00	0.14434E+00	0.00000E+00
0.16000E+02	0.41583E-02	0.00000E+00	0.21096E-02	0.00000E+00	0.13598E+00	0.00000E+00
0.17000E+02	0.39205E-02	0.00000E+00	0.19861E-02	0.00000E+00	0.12733E+00	0.00000E+00
0.18000E+02	0.36746E-02	0.00000E+00	0.18600E-02	0.00000E+00	0.11871E+00	0.00000E+00

Appendix F Output files pictures

EXAMPLE IMAGES OF AN OUTPUT FILE DRIFT RAO.DAT

```

1
2
3 *****
4   THREE-DIMENSIONAL PANEL METHOD
5   FOR RADIATION & DIFFRACTION PROBLEMS
6   OF A FLOATING SHIP WITH ZERO SPEED
7 *****
8
9   SHIP NAME      :      DRILL SHIP MODEL 10/05/2016
10  NUMBER OF HULL SURFACE ELEMENTS: NE   = 1162
11  NUMBER OF ADDED ELEMENTS      : NADD =   40
12  NUMBER OF TOTAL ELEMENTS      : NT   = 1202
13
14  LENGTH IN X-AXIS----- (LENGTH) ---      203.363 m
15  LENGTH IN Y-AXIS----- (BREDTH) ---      29.027 m
16  LENGTH IN Z-AXIS----- (DRAFT) ---      11.613 m
17
18  BLOCK COEFFICIENT----- ( CB ) ---      0.76989
19  WATER PLANE AREA COEFFICIENT---- ( CW ) ---      0.18723
20  CENTER OF FLOATATION -----      0.00000 m
21  IXX=VOL*(KXX**2);----- (KXX) ---      10.05000 m
22  IYY=VOL*(KYY**2);----- (KYY) ---      49.38000 m
23  IZZ=VOL*(KZZ**2);----- (KZZ) ---      49.38000 m
24  POSITION OF GRAVITY FROM ORIGIN-- (OXG) ---      0.00000 m
25  POSITION OF GRAVITY FROM ORIGIN-- (OYG) ---      0.00000 m
26  POSITION OF GRAVITY FROM ORIGIN-- (OZG) ---      1.00000 m
27  METACENTRIC HEIGHT FOR PITCH ---- (GML) ---      281.50000 m
28  METACENTRIC HEIGHT FOR ROLL ---- (GMB) ---      1.80000 m
29
30
31  MOON POOL WATER SURFACE DAMPING -----      0.09000
32
33
34
35
36
37 ***** RESPONSE AMPRITUDE OPERATER *****
38
39
40
41
42
43 BETA =      0.00 ( DEG )
44
45 ***** DRIFT FORCE BY FAR FIELD METHOD *****
46
47 DRIFTING FORCE  $\pm F/(D0*G**A) \pm M/(D0*G**A)$  WHERE A = WAVE AMPLITUDE  $\pm$ 

```

37

38

39

40

41

42

43

BETA = 0.00 (DEG)

44

45

***** DRIFT FORCE BY FAR FIELD METHOD *****

46

47

DRIFTING FORCE ++ F/(RO*G*A*A) M/(RO*G*A*A) WHERE A = WAVE AMPLITUDE ++

48

49

50

51

52

53

54

55

56

57

58

59

60

61

62

63

64

65

66

67

68

69

70

71

72

73

74

75

76

77

78

79

80

81

82

83

RAMDA/L	OMEGA (rad./sec.)	T (sec.)	DIFRCT(X)	DIFRCT(Y)	FREE (X)	FREE (Y)	MZ (FIX)	MZ (FREE)
4.852	0.25000	25.13274	-0.79565	-0.00000	-0.00006	0.00000	-0.00000	0.00000
3.868	0.28000	22.43995	-1.22916	0.00000	-0.00021	-0.00000	-0.00000	-0.00000
3.155	0.31000	20.26834	-1.66741	0.00000	-0.00067	-0.00000	-0.00000	0.00000
2.623	0.34000	18.47996	-2.00466	-0.00000	-0.00173	-0.00000	-0.00000	0.00000
2.215	0.37000	16.98158	-2.17428	0.00000	-0.00308	0.00000	-0.00000	-0.00000
1.895	0.40000	15.70796	-2.21649	-0.00000	-0.00309	0.00000	-0.00000	-0.00000
1.640	0.43000	14.61206	-2.28447	0.00000	-0.00215	0.00000	-0.00000	-0.00000
1.433	0.46000	13.65910	-2.54121	0.00000	-0.02086	-0.00000	-0.00000	-0.00000
1.263	0.49000	12.82283	-2.99327	-0.00000	-0.13468	-0.00000	-0.00000	0.00000
1.121	0.52000	12.08305	-3.42924	-0.00000	-0.48293	-0.00000	0.00000	0.00000
1.002	0.55000	11.42397	-3.60413	-0.00000	-1.17580	-0.00000	0.00000	0.00000
0.901	0.58000	10.83308	-3.52032	0.00000	-2.11655	0.00000	-0.00000	-0.00000
0.815	0.61000	10.30030	-3.43245	0.00000	-2.95649	0.00000	0.00000	-0.00000
0.740	0.64000	9.81748	-3.49827	0.00000	-3.36892	0.00000	-0.00000	-0.00000
0.676	0.67000	9.37789	-3.56663	-0.00000	-3.40381	-0.00000	0.00000	-0.00000
0.619	0.70000	8.97598	-3.49616	0.00000	-3.41871	0.00000	0.00000	-0.00000
0.569	0.73000	8.60710	-3.46424	0.00000	-3.77266	-0.00000	0.00000	-0.00000
0.525	0.76000	8.26735	-3.60422	0.00000	-4.92467	0.00000	0.00000	0.00000
0.486	0.79000	7.95340	-3.63889	-0.00000	-6.55793	-0.00000	0.00000	-0.00000
0.451	0.82000	7.66242	-3.43103	0.00000	-7.01464	-0.00000	0.00000	0.00000
0.420	0.85000	7.39198	-3.16486	0.00000	-5.77060	-0.00000	0.00000	0.00000
0.392	0.88000	7.13998	-2.93277	0.00000	-4.12251	-0.00000	0.00000	0.00000
0.366	0.91000	6.90460	-2.85303	0.00000	-3.29809	0.00000	0.00000	0.00000
0.343	0.94000	6.68424	-2.90553	0.00000	-3.22367	0.00000	0.00000	0.00000
0.322	0.97000	6.47751	-2.85312	-0.00000	-3.17318	-0.00000	0.00000	0.00000
0.303	1.00000	6.28319	-2.71531	-0.00000	-2.90973	-0.00000	0.00000	0.00000
0.286	1.03000	6.10018	-2.56653	-0.00000	-2.60266	-0.00000	0.00000	0.00000
0.270	1.06000	5.92753	-2.50115	-0.00000	-2.48113	0.00000	0.00000	0.00000
0.255	1.09000	5.76439	-2.50691	0.00000	-2.50669	0.00000	0.00000	0.00000
0.242	1.12000	5.60999	-2.42060	-0.00000	-2.44038	-0.00000	0.00000	0.00000
0.229	1.15000	5.46364	-2.27154	0.00000	-2.28681	0.00000	0.00000	0.00000
0.218	1.18000	5.32473	-2.14950	0.00000	-2.15169	0.00000	0.00000	0.00000
0.207	1.21000	5.18272	-2.04217	0.00000	-2.04102	0.00000	0.00000	0.00000

```

100      0.102      1.72000      3.65301      -1.31278      -0.00000      -1.30899      -0.00000      0.00000      0.00000
101      0.099      1.75000      3.59039      -1.11285      -0.00000      -1.11013      -0.00000      0.00000      0.00000
102
103
104
105 BETA =          30.00 ( DEG )
106
107 ***** DRIFT FORCE BY FAR FIELD METHOD *****
108
109 DRIFTING FORCE ++ F/(RO*G*A*A) M/(RO*G*A*A) WHERE A = WAVE AMPLITUDE ++
110
111 RAMDA/L  OMEGA (rad./sec.) T ( sec. ) DIFRCT(X) DIFRCT(Y) FREE(X) FREE(Y) MZ(FIX) MZ(FREE)
112
113      4.852      0.25000      25.13274      -0.71209      -0.50138      -0.00004      -0.00002      -185.57586      -3.60817
114      3.868      0.28000      22.43995      -1.12228      -0.87373      -0.00014      -0.00005      -256.74236      -6.38287
115      3.155      0.31000      20.26834      -1.56494      -1.39797      -0.00046      -0.00014      -338.29976      -10.17284
116      2.623      0.34000      18.47996      -1.94814      -2.08462      -0.00125      -0.00033      -425.17539      -14.80206
117      2.215      0.37000      16.98158      -2.19319      -2.93409      -0.00265      -0.00054      -509.69491      -18.39799
118      1.895      0.40000      15.70796      -2.29309      -3.94119      -0.00437      -0.00195      -582.00296      0.26292
119      1.640      0.43000      14.61206      -2.34410      -5.10070      -0.00445      -0.00357      -631.29803      4.29780
120      1.433      0.46000      13.65910      -2.50645      -6.41139      -0.01115      -0.01402      -648.29725      -0.05115
121      1.263      0.49000      12.82283      -2.88735      -7.87385      -0.06693      -0.07498      -628.75358      5.08836
122      1.121      0.52000      12.08305      -3.42135      -9.47584      -0.27302      -0.28944      -576.20825      13.14845
123      1.002      0.55000      11.42397      -3.88438      -11.16853      -0.77046      -0.85554      -501.13665      19.56700
124      0.901      0.58000      10.83308      -4.08953      -12.86364      -1.63420      -2.06043      -416.11284      19.13487
125      0.815      0.61000      10.30030      -4.09583      -14.48152      -2.73639      -4.19375      -331.28948      7.07943
126      0.740      0.64000      9.81748      -4.16032      -15.99768      -3.73152      -7.35188      -254.51951      -16.77498
127      0.676      0.67000      9.37789      -4.40241      -17.38475      -4.26964      -11.19518      -193.34725      -43.64881
128      0.619      0.70000      8.97598      -4.61918      -18.52550      -4.33013      -14.85486      -152.13670      -57.91962
129      0.569      0.73000      8.60710      -4.64064      -19.35787      -4.35894      -17.28067      -127.15665      -46.04762
130      0.525      0.76000      8.26735      -4.71275      -20.23501      -5.11903      -18.36057      -112.09217      0.50180
131      0.486      0.79000      7.95340      -5.01816      -21.55823      -6.62830      -19.25807      -108.21215      68.19250
132      0.451      0.82000      7.66242      -5.22493      -23.04968      -7.80067      -20.46562      -118.25609      119.12310
133      0.420      0.85000      7.39198      -5.16965      -24.39221      -8.31659      -21.60373      -138.29104      121.99983
134      0.392      0.88000      7.13998      -5.05996      -25.52880      -8.03293      -22.76107      -161.49817      52.89480
135      0.366      0.91000      6.90460      -4.98605      -26.52984      -6.98748      -24.27834      -192.61414      -59.42702
136      0.343      0.94000      6.68424      -4.98853      -27.44828      -5.88081      -26.03864      -230.79988      -151.60375
137      0.322      0.97000      6.47751      -5.15943      -28.30671      -5.28572      -27.54092      -266.67735      -198.16957
138      0.303      1.00000      6.28319      -5.31831      -29.09377      -5.11221      -28.51854      -307.80318      -232.97900
139      0.286      1.03000      6.10018      -5.28426      -29.73322      -5.04847      -29.07489      -350.69058      -285.59454
140      0.270      1.06000      5.92753      -5.19228      -30.30049      -4.99839      -29.58622      -391.24027      -355.12189
141      0.255      1.09000      5.76439      -5.14472      -30.74091      -4.95681      -30.21817      -433.18463      -422.20283
142      0.242      1.12000      5.60999      -5.16978      -31.01808      -4.96049      -30.76055      -467.93893      -461.15309
143      0.229      1.15000      5.46364      -5.14790      -31.07920      -4.90989      -30.92467      -502.62007      -487.64550
144      0.218      1.18000      5.32473      -4.84504      -30.78912      -4.62527      -30.60928      -536.48116      -521.47125
145      0.207      1.21000      5.19272      -4.49925      -30.37029      -4.34257      -30.16415      -571.01327      -565.23934
146      0.197      1.24000      5.06708      -4.20085      -29.05000      -4.21105      -29.80625      -591.56682      -591.22612

```


411	0.099	1.75000	3.59039	4.46150	-20.08074	4.46326	-20.14785	117.03084	116.97277
412									
413									
414									
415	BETA	=	180.00	(DEG)					
416									
417	***** DRIFT FORCE BY FAR FIELD METHOD *****								
418									
419	DRIFTING FORCE ++ F/(RO*G*A*A) M/(RO*G*A*A) WHERE A = WAVE AMPLITUDE ++								
420									
421	RAMDA/L	OMEGA (rad./sec.)	T (sec.)	DIFRCT(X)	DIFRCT(Y)	FREE(X)	FREE(Y)	MZ (FIX)	MZ (FREE)
422									
423	4.852	0.25000	25.13274	0.79435	-0.00000	0.00006	0.00000	0.00000	-0.00000
424	3.868	0.28000	22.43995	1.22634	-0.00000	0.00021	0.00000	0.00000	-0.00000
425	3.155	0.31000	20.26834	1.66283	-0.00000	0.00068	-0.00000	0.00000	-0.00000
426	2.623	0.34000	18.47996	2.00000	-0.00000	0.00173	-0.00000	0.00000	0.00000
427	2.215	0.37000	16.98158	2.17520	-0.00000	0.00308	-0.00000	0.00000	0.00000
428	1.895	0.40000	15.70796	2.23364	-0.00000	0.00311	0.00000	0.00000	0.00000
429	1.640	0.43000	14.61206	2.33139	-0.00000	0.00218	-0.00000	0.00000	0.00000
430	1.433	0.46000	13.65910	2.62940	-0.00000	0.02075	-0.00000	0.00000	-0.00000
431	1.263	0.49000	12.82283	3.12984	-0.00000	0.13337	-0.00000	0.00000	0.00000
432	1.121	0.52000	12.08305	3.62466	-0.00000	0.47727	-0.00000	0.00000	0.00000
433	1.002	0.55000	11.42397	3.88443	-0.00000	1.16119	-0.00000	0.00000	0.00000
434	0.901	0.58000	10.83308	3.91976	-0.00000	2.09553	-0.00000	0.00000	0.00000
435	0.815	0.61000	10.30030	3.95890	-0.00000	2.96203	-0.00000	0.00000	0.00000
436	0.740	0.64000	9.81748	4.12823	-0.00000	3.50860	-0.00000	0.00000	0.00000
437	0.676	0.67000	9.37789	4.34323	-0.00000	3.93495	-0.00000	0.00000	0.00000
438	0.619	0.70000	8.97598	4.66828	-0.00000	4.81457	-0.00000	0.00000	0.00000
439	0.569	0.73000	8.60710	5.35178	-0.00000	6.38907	-0.00000	0.00000	0.00000
440	0.525	0.76000	8.26735	5.93627	-0.00000	7.92643	-0.00000	0.00000	0.00000
441	0.486	0.79000	7.95340	5.81608	-0.00000	8.84862	-0.00000	0.00000	0.00000
442	0.451	0.82000	7.66242	5.86677	-0.00000	9.85165	-0.00000	0.00000	0.00000
443	0.420	0.85000	7.39198	6.70075	-0.00000	10.37201	-0.00000	0.00000	0.00000
444	0.392	0.88000	7.13998	7.76078	-0.00000	10.33638	-0.00000	0.00000	0.00000
445	0.366	0.91000	6.90460	8.43370	-0.00000	10.37037	-0.00000	0.00000	0.00000
446	0.343	0.94000	6.68424	8.58324	-0.00000	10.39626	-0.00000	0.00000	0.00000
447	0.322	0.97000	6.47751	8.70209	-0.00000	10.38383	-0.00000	0.00000	0.00000
448	0.303	1.00000	6.28319	9.57077	-0.00000	10.87043	-0.00000	0.00000	0.00000
449	0.286	1.03000	6.10018	10.99858	-0.00000	11.88604	-0.00000	0.00000	0.00000
450	0.270	1.06000	5.92753	12.01224	-0.00000	12.72365	-0.00000	0.00000	0.00000
451	0.255	1.09000	5.76439	11.88140	-0.00000	12.66627	-0.00000	0.00000	0.00000
452	0.242	1.12000	5.60999	11.43890	-0.00000	12.33249	-0.00000	0.00000	0.00000
453	0.229	1.15000	5.46364	12.62895	-0.00000	13.38043	-0.00000	0.00000	0.00000
454	0.218	1.18000	5.32473	14.22025	-0.00000	14.55601	-0.00000	0.00000	0.00000
455	0.207	1.21000	5.19272	13.09058	-0.00000	12.96245	-0.00000	0.00000	0.00000
456	0.197	1.24000	5.06708	12.43670	-0.00000	12.14346	-0.00000	-0.00000	-0.00000
457	0.188	1.27000	4.94730	11.76637	-0.00000	11.30134	-0.00000	0.00000	0.00000

440	0.525	0.76000	8.26735	5.93627	-0.00000	7.92643	-0.00000	0.00000	0.00000
441	0.486	0.79000	7.95340	5.81608	-0.00000	8.84862	-0.00000	0.00000	0.00000
442	0.451	0.82000	7.66242	5.86677	-0.00000	9.85165	-0.00000	0.00000	0.00000
443	0.420	0.85000	7.39198	6.70075	-0.00000	10.37201	-0.00000	0.00000	0.00000
444	0.392	0.88000	7.13998	7.76078	-0.00000	10.33638	-0.00000	0.00000	0.00000
445	0.366	0.91000	6.90460	8.43370	-0.00000	10.37037	-0.00000	0.00000	0.00000
446	0.343	0.94000	6.68424	8.58324	-0.00000	10.39626	-0.00000	0.00000	0.00000
447	0.322	0.97000	6.47751	8.70209	-0.00000	10.38383	-0.00000	0.00000	0.00000
448	0.303	1.00000	6.28319	9.57077	-0.00000	10.87043	-0.00000	0.00000	0.00000
449	0.286	1.03000	6.10018	10.99858	-0.00000	11.88604	-0.00000	0.00000	0.00000
450	0.270	1.06000	5.92753	12.01224	-0.00000	12.72365	-0.00000	0.00000	0.00000
451	0.255	1.09000	5.76439	11.88140	-0.00000	12.66627	-0.00000	0.00000	0.00000
452	0.242	1.12000	5.60999	11.43890	-0.00000	12.33249	-0.00000	0.00000	0.00000
453	0.229	1.15000	5.46364	12.62895	-0.00000	13.38043	-0.00000	0.00000	0.00000
454	0.218	1.18000	5.32473	14.22025	-0.00000	14.55601	-0.00000	0.00000	0.00000
455	0.207	1.21000	5.19272	13.09058	-0.00000	12.96245	-0.00000	0.00000	0.00000
456	0.197	1.24000	5.06708	12.43670	-0.00000	12.14346	-0.00000	-0.00000	-0.00000
457	0.188	1.27000	4.94739	14.17637	-0.00000	14.30134	-0.00000	-0.00000	-0.00000
458	0.179	1.30000	4.83322	13.62919	-0.00000	14.16133	-0.00000	-0.00000	-0.00000
459	0.171	1.33000	4.72420	12.31441	-0.00000	12.81503	-0.00000	0.00000	0.00000
460	0.164	1.36000	4.61999	13.76068	-0.00000	13.99233	-0.00000	0.00000	0.00000
461	0.157	1.39000	4.52028	13.81881	-0.00000	13.75159	-0.00000	0.00000	0.00000
462	0.150	1.42000	4.42478	11.60163	-0.00000	11.40946	-0.00000	-0.00000	-0.00000
463	0.144	1.45000	4.33323	12.76343	-0.00000	12.72905	-0.00000	-0.00000	-0.00000
464	0.138	1.48000	4.24540	14.43917	-0.00000	14.58750	-0.00000	-0.00000	-0.00000
465	0.133	1.51000	4.16105	11.51503	-0.00000	11.71863	-0.00000	0.00000	0.00000
466	0.128	1.54000	4.07999	11.82930	-0.00000	12.00921	-0.00000	0.00000	0.00000
467	0.123	1.57000	4.00203	14.86383	-0.00000	14.86808	-0.00000	-0.00000	-0.00000
468	0.118	1.60000	3.92699	11.13944	-0.00000	11.00971	-0.00000	0.00000	0.00000
469	0.114	1.63000	3.85471	12.01771	-0.00000	11.99652	-0.00000	0.00000	0.00000
470	0.110	1.66000	3.78505	15.60810	-0.00000	15.63287	-0.00000	0.00000	0.00000
471	0.106	1.69000	3.71786	10.60580	-0.00000	10.67008	-0.00000	0.00000	0.00000
472	0.102	1.72000	3.65301	15.14844	-0.00000	15.23267	-0.00000	0.00000	0.00000
473	0.099	1.75000	3.59039	12.93221	-0.00000	12.87911	-0.00000	0.00000	0.00000
474									

EXAMPLE IMAGES OF AN OUTPUT FILE MOON POOL RAO.DAT

```

1
2
3 *****
4 THREE-DIMENSIONAL PANEL METHOD
5 FOR RADIATION & DIFFRACTION PROBLEMS
6 OF A FLOATING SHIP WITH ZERO SPEED
7 *****
8
9 SHIP NAME : DRILL SHIP MODEL 10/05/2016
10 NUMBER OF HULL SURFACE ELEMENTS: NE = 1162
11 NUMBER OF ADDED ELEMENTS : NADD = 40
12 NUMBER OF TOTAL ELEMENTS : NT = 1202
13
14 LENGTH IN X-AXIS----- (LENGTH) --- 203.363 m
15 LENGTH IN Y-AXIS----- (BREDTH) --- 29.027 m
16 LENGTH IN Z-AXIS----- (DRAFT) --- 11.613 m
17
18 BLOCK COEFFICIENT----- ( CB ) --- 0.76989
19 WATER PLANE AREA COEFFICIENT---- ( CW ) --- 0.18723
20 CENTER OF FLOATATION ----- 0.00000 m
21 IXX=VOL*(KXX**2);----- (KXX) --- 10.05000 m
22 IYY=VOL*(KYY**2);----- (KYY) --- 49.38000 m
23 IZZ=VOL*(KZZ**2);----- (KZZ) --- 49.38000 m
24 POSITION OF GRAVITY FROM ORIGIN-- (OXG) --- 0.00000 m
25 POSITION OF GRAVITY FROM ORIGIN-- (OYG) --- 0.00000 m
26 POSITION OF GRAVITY FROM ORIGIN-- (OZG) --- 1.00000 m
27 METACENTRIC HEIGHT FOR PITCH ---- (GML) --- 281.50000 m
28 METACENTRIC HEIGHT FOR ROLL ---- (GMB) --- 1.80000 m
29
30
31 MOON POOL WATER SURFACE DAMPING ----- 0.09000
32
33
34
35
36
37 ***** RESPONSE AMPLITUDE OPERATOR *****
38
39
40
41 MOON POOL WATER SURFACE ELEVATION RAO
42
43 BETA = 0.00 DEG
44
45 RAMDA/L OMEGA (RAD./SEC.) T (SEC.) MID FORE AFT. PORT STARBOARD
46 4.852 0.25000 25.13274 0.06817 0.07030 0.06371 0.06122 0.06122
47 2.969 0.28000 22.42895 0.10211 0.10564 0.09844 0.09625 0.09625

```


40								
41	MOON POOL WATER SURFACE ELEVATION RAO							
42								
43	BETA =	0.00	DEG					
44								
45	RAMDA/L	OMEGA (RAD./SEC.)	T (SEC.)	MID	FORE	AFT.	PORT	STARBOARD
46	4.852	0.25000	25.13274	0.06817	0.07030	0.06371	0.06122	0.06122
47	3.868	0.28000	22.43995	0.10311	0.10564	0.09844	0.09625	0.09625
48	3.155	0.31000	20.26834	0.14842	0.15151	0.14345	0.14169	0.14169
49	2.623	0.34000	18.47996	0.20405	0.20790	0.19865	0.19758	0.19758
50	2.215	0.37000	16.98158	0.26856	0.27344	0.26269	0.26274	0.26274
51	1.895	0.40000	15.70796	0.33916	0.34532	0.33306	0.33514	0.33514
52	1.640	0.43000	14.61206	0.41283	0.42031	0.40763	0.41356	0.41356
53	1.433	0.46000	13.65910	0.48900	0.49717	0.48789	0.50111	0.50111
54	1.263	0.49000	12.82283	0.57338	0.58022	0.58298	0.60901	0.60901
55	1.121	0.52000	12.08305	0.67955	0.68120	0.71009	0.75564	0.75564
56	1.002	0.55000	11.42397	0.82513	0.81666	0.88781	0.95861	0.95861
57	0.901	0.58000	10.83308	1.02551	1.00268	1.12840	1.22734	1.22734
58	0.815	0.61000	10.30030	1.29292	1.25380	1.43814	1.56448	1.56448
59	0.740	0.64000	9.81748	1.63987	1.58581	1.82176	1.97060	1.97060
60	0.676	0.67000	9.37789	2.07240	2.00948	2.27507	2.43623	2.43623
61	0.619	0.70000	8.97598	2.55160	2.49299	2.74526	2.90137	2.90137
62	0.569	0.73000	8.60710	2.93561	2.90174	3.07662	3.20298	3.20298
63	0.525	0.76000	8.26735	3.03750	3.04740	3.08118	3.15155	3.15155
64	0.486	0.79000	7.95340	2.78750	2.84653	2.70670	2.70169	2.70169
65	0.451	0.82000	7.66242	2.27978	2.37470	2.08053	1.99702	1.99702
66	0.420	0.85000	7.39198	1.76300	1.87073	1.47606	1.32429	1.32429
67	0.392	0.88000	7.13998	1.41017	1.51139	1.06093	0.84688	0.84688
68	0.366	0.91000	6.90460	1.23771	1.32107	0.83618	0.55893	0.55893
69	0.343	0.94000	6.68424	1.19626	1.25766	0.73910	0.39983	0.39983
70	0.322	0.97000	6.47751	1.22763	1.26712	0.70538	0.31386	0.31386
71	0.303	1.00000	6.28319	1.28276	1.30029	0.69164	0.27581	0.27581
72	0.286	1.03000	6.10018	1.32543	1.31795	0.67715	0.29384	0.29384
73	0.270	1.06000	5.92753	1.33501	1.29557	0.66014	0.37449	0.37449
74	0.255	1.09000	5.76439	1.30681	1.22482	0.65164	0.50303	0.50303
75	0.242	1.12000	5.60999	1.24361	1.10540	0.66796	0.66987	0.66987
76	0.229	1.15000	5.46364	1.14311	0.93491	0.72792	0.87943	0.87943
77	0.218	1.18000	5.32473	0.99181	0.71433	0.84332	1.12322	1.12322
78	0.207	1.21000	5.19272	0.78175	0.49505	0.98787	1.34492	1.34492
79	0.197	1.24000	5.06708	0.53974	0.42016	1.10348	1.46946	1.46946
80	0.188	1.27000	4.94739	0.31172	0.51022	1.15727	1.47464	1.47464
81	0.179	1.30000	4.83322	0.12564	0.62348	1.15746	1.39319	1.39319
82	0.171	1.33000	4.72420	0.04355	0.70893	1.12811	1.27063	1.27063
83	0.164	1.36000	4.61999	0.13609	0.77026	1.09076	1.14236	1.14236
84	0.157	1.39000	4.52028	0.20836	0.82165	1.05667	1.03023	1.03023
85	0.150	1.42000	4.42478	0.25545	0.87633	1.02563	0.94752	0.94752
86	0.144	1.45000	4.32222	0.28261	0.91872	0.98722	0.88556	0.88556

376	0.118	1.60000	3.92699	1.14014	1.35930	0.20222	1.40926	0.67673
377	0.114	1.63000	3.85471	1.10753	1.36989	0.35752	1.37759	0.68220
378	0.110	1.66000	3.78505	1.07046	1.36626	0.54442	1.26529	0.72317
379	0.106	1.69000	3.71786	1.04876	1.40764	0.71514	1.06289	0.72593
380	0.102	1.72000	3.65301	1.00725	1.50284	0.85251	0.75059	0.53439
381	0.099	1.75000	3.59039	0.94015	1.61743	0.89622	0.62626	0.08141
382								
383	MOON POOL WATER SURFACE ELEVATION RAO							
384								
385	BETA =	180.00	DEG					
386								
387	RAMDA/L	OMEGA(RAD./SEC.)	T (SEC.)	MID	FORE	AFT.	PORT	STARBOARD
388	4.852	0.25000	25.13274	0.06834	0.07047	0.06381	0.06130	0.06130
389	3.868	0.28000	22.43995	0.10342	0.10596	0.09862	0.09637	0.09637
390	3.155	0.31000	20.26834	0.14902	0.15213	0.14377	0.14189	0.14189
391	2.623	0.34000	18.47996	0.20512	0.20902	0.19916	0.19783	0.19783
392	2.215	0.37000	16.98158	0.27020	0.27520	0.26316	0.26266	0.26266
393	1.895	0.40000	15.70796	0.34091	0.34748	0.33224	0.33296	0.33296
394	1.640	0.43000	14.61206	0.41252	0.42140	0.40117	0.40352	0.40352
395	1.433	0.46000	13.65910	0.48067	0.49309	0.46451	0.46851	0.46851
396	1.263	0.49000	12.82283	0.54492	0.56272	0.51954	0.52401	0.52401
397	1.121	0.52000	12.08305	0.61278	0.63836	0.57014	0.57140	0.57140
398	1.002	0.55000	11.42397	0.70172	0.73711	0.63035	0.62116	0.62116
399	0.901	0.58000	10.83308	0.83520	0.88054	0.72436	0.69552	0.69552
400	0.815	0.61000	10.30030	1.03280	1.08555	0.87893	0.82521	0.82521
401	0.740	0.64000	9.81748	1.30253	1.35815	1.11206	1.03800	1.03800
402	0.676	0.67000	9.37789	1.63658	1.68958	1.42573	1.34706	1.34706
403	0.619	0.70000	8.97598	1.99031	2.03493	1.78852	1.73253	1.73253
404	0.569	0.73000	8.60710	2.23647	2.26694	2.09314	2.09621	2.09621
405	0.525	0.76000	8.26735	2.18917	2.19875	2.16886	2.25753	2.25753
406	0.486	0.79000	7.95340	1.79965	1.77852	1.94658	2.10602	2.10602
407	0.451	0.82000	7.66242	1.32185	1.26017	1.62084	1.80414	1.80414
408	0.420	0.85000	7.39198	1.00797	0.90212	1.41939	1.60375	1.60375
409	0.392	0.88000	7.13998	0.84601	0.69937	1.35345	1.54719	1.54719
410	0.366	0.91000	6.90460	0.74626	0.56540	1.35100	1.56772	1.56772
411	0.343	0.94000	6.68424	0.65840	0.45087	1.35966	1.60490	1.60490
412	0.322	0.97000	6.47751	0.56932	0.34377	1.35295	1.62070	1.62070
413	0.303	1.00000	6.28319	0.48584	0.25348	1.31971	1.59099	1.59099
414	0.286	1.03000	6.10018	0.42267	0.20160	1.25860	1.50087	1.50087
415	0.270	1.06000	5.92753	0.39252	0.21828	1.17638	1.34611	1.34611
416	0.255	1.09000	5.76439	0.41195	0.33937	1.08776	1.14239	1.14239
417	0.242	1.12000	5.60999	0.51633	0.58183	1.01261	0.94707	0.94707
418	0.229	1.15000	5.46364	0.72109	0.92093	0.96177	0.86119	0.86119
419	0.218	1.18000	5.32473	0.97046	1.27109	0.91393	0.89453	0.89453
420	0.207	1.21000	5.19272	1.15184	1.49335	0.82293	0.87944	0.87944
421	0.197	1.24000	5.06708	1.18154	1.49454	0.67502	0.69879	0.69879
422	0.188	1.27000	4.94728	1.09447	1.32877	0.51572	0.45541	0.45541

414	0.286	1.03000	6.10018	0.42267	0.20160	1.25860	1.50087	1.50087
415	0.270	1.06000	5.92753	0.39252	0.21828	1.17638	1.34611	1.34611
416	0.255	1.09000	5.76439	0.41195	0.33937	1.08776	1.14239	1.14239
417	0.242	1.12000	5.60999	0.51633	0.58183	1.01261	0.94707	0.94707
418	0.229	1.15000	5.46364	0.72109	0.92093	0.96177	0.86119	0.86119
419	0.218	1.18000	5.32473	0.97046	1.27109	0.91393	0.89453	0.89453
420	0.207	1.21000	5.19272	1.15184	1.49335	0.82293	0.87944	0.87944
421	0.197	1.24000	5.06708	1.18154	1.49454	0.67502	0.69879	0.69879
422	0.188	1.27000	4.94739	1.09447	1.32977	0.51572	0.45541	0.45541
423	0.179	1.30000	4.83322	1.00863	1.15075	0.39883	0.47004	0.47004
424	0.171	1.33000	4.72420	1.00592	1.07300	0.33298	0.71858	0.71858
425	0.164	1.36000	4.61999	1.06253	1.08896	0.28915	0.94706	0.94706
426	0.157	1.39000	4.52028	1.10398	1.11297	0.24140	1.07929	1.07929
427	0.150	1.42000	4.42478	1.08100	1.07742	0.19434	1.10841	1.10841
428	0.144	1.45000	4.33323	1.00217	0.97329	0.17647	1.08207	1.08207
429	0.138	1.48000	4.24540	0.92623	0.84504	0.16949	1.06597	1.06597
430	0.133	1.51000	4.16105	0.91636	0.74964	0.14924	1.09066	1.09066
431	0.128	1.54000	4.07999	0.98074	0.72293	0.11542	1.15365	1.15365
432	0.123	1.57000	4.00203	1.05655	0.74759	0.12155	1.20515	1.20515
433	0.118	1.60000	3.92699	1.07997	0.77704	0.26135	1.16745	1.16745
434	0.114	1.63000	3.85471	1.06193	0.77337	0.44944	1.02029	1.02029
435	0.110	1.66000	3.78505	1.06734	0.74227	0.58189	0.85940	0.85940
436	0.106	1.69000	3.71786	1.10649	0.74376	0.70954	0.66357	0.66357
437	0.102	1.72000	3.65301	1.14792	0.78273	0.80178	0.45396	0.45396
438	0.099	1.75000	3.59039	1.17150	0.82202	0.81497	0.23309	0.23309
439								

PICTURES ON THE STRUCTURE OF THE OUTPUT FILE MOON POOL SPECTRUM.DAT

```

1
2
3 *****
4   THREE-DIMENSIONAL PANEL METHOD
5   FOR RADIATION & DIFFRACTION PROBLEMS
6   OF A FLOATING SHIP WITH ZERO SPEED
7 *****
8
9   SHIP NAME      :    DRILL SHIP MODEL 10/05/2016
10  NUMBER OF HULL SURFACE ELEMENTS: NE   = 1162
11  NUMBER OF ADDED ELEMENTS      : NADD =   40
12  NUMBER OF TOTAL ELEMENTS      : NT   = 1202
13
14  LENGTH IN X-AXIS----- (LENGTH)---      203.363 m
15  LENGTH IN Y-AXIS----- (BREDTH)---      29.027 m
16  LENGTH IN Z-AXIS----- (DRAFT)---       11.613 m
17
18  BLOCK COEFFICIENT----- ( CB )---         0.76989
19  WATER PLANE AREA COEFFICIENT---- ( CW )---         0.18723
20  CENTER OF FLOATATION -----          0.00000 m
21  IXX=VOL*(KXX**2);----- (KXX)---        10.05000 m
22  IYY=VOL*(KYY**2);----- (KYY)---        49.38000 m
23  IZZ=VOL*(KZZ**2);----- (KZZ)---        49.38000 m
24  POSITION OF GRAVITY FROM ORIGIN-- (OXG)---         0.00000 m
25  POSITION OF GRAVITY FROM ORIGIN-- (OYG)---         0.00000 m
26  POSITION OF GRAVITY FROM ORIGIN-- (OZG)---         1.00000 m
27  METACENTRIC HEIGHT FOR PITCH ---- (GML)---        281.50000 m
28  METACENTRIC HEIGHT FOR ROLL  ---- (GMB)---         1.80000 m
29
30
31  MOON POOL WATER SURFACE DAMPING -----          0.09000
32
33
34
35
36  LONG CRESTED IRREGULAR WAVE CONDITION
37
38  WAVE DIRECTION          0.00  DEG.
39  SIGNIFIGANT WAVE HEIGHT  1.00  m
40  SPECTRUM TYPE          IACS
41
42
43  ***** STANDARD DEVIATION OF RESPONCE *****
44
45  MOON POOL WAVER ELEVATIONS
46
47  TS ( SEC )      MIDR (m)      FORE (m)      AFT (m)      DECK (m)      SPAREBOARD (m)

```



```

40 SPECTRUM TYPE IACS
41
42
43 ***** STANDARD DEVIATION OF RESPONSE *****
44
45 MOON POOL WAVER ELEVATIONS
46
47 TZ ( SEC. ) MIDD. (m) FORE (m) AFT. (m) PROT (m) STARBOARD (m)
48 0.40000E+01 0.22049E+00 0.23896E+00 0.22264E+00 0.22804E+00 0.22804E+00
49 0.50000E+01 0.37134E+00 0.38070E+00 0.35056E+00 0.35067E+00 0.35067E+00
50 0.60000E+01 0.44904E+00 0.45323E+00 0.44175E+00 0.44995E+00 0.44995E+00
51 0.70000E+01 0.44389E+00 0.44493E+00 0.44675E+00 0.46014E+00 0.46014E+00
52 0.80000E+01 0.40241E+00 0.40204E+00 0.40967E+00 0.42449E+00 0.42449E+00
53 0.90000E+01 0.35280E+00 0.35198E+00 0.36122E+00 0.37546E+00 0.37546E+00
54 0.10000E+02 0.30607E+00 0.30519E+00 0.31422E+00 0.32710E+00 0.32710E+00
55 0.11000E+02 0.26534E+00 0.26457E+00 0.27272E+00 0.28407E+00 0.28407E+00
56 0.12000E+02 0.23084E+00 0.23021E+00 0.23734E+00 0.24725E+00 0.24725E+00
57 0.13000E+02 0.20188E+00 0.20137E+00 0.20754E+00 0.21618E+00 0.21618E+00
58 0.14000E+02 0.17757E+00 0.17717E+00 0.18250E+00 0.19004E+00 0.19004E+00
59 0.15000E+02 0.15709E+00 0.15677E+00 0.16139E+00 0.16801E+00 0.16801E+00
60 0.16000E+02 0.13974E+00 0.13949E+00 0.14351E+00 0.14935E+00 0.14935E+00
61 0.17000E+02 0.12497E+00 0.12477E+00 0.12829E+00 0.13348E+00 0.13348E+00
62 0.18000E+02 0.11231E+00 0.11215E+00 0.11526E+00 0.11989E+00 0.11989E+00
63
64
65 LONG CRESTED IRREGULAR WAVE CONDITION
66
67 WAVE DIRECTION 30.00 DEG.
68 SIGNIFIGANT WAVE HEIGHT 1.00 m
69 SPECTRUM TYPE IACS
70
71
72 ***** STANDARD DEVIATION OF RESPONSE *****
73
74 MOON POOL WAVER ELEVATIONS
75
76 TZ ( SEC. ) MIDD. (m) FORE (m) AFT. (m) PROT (m) STARBOARD (m)
77 0.40000E+01 0.25340E+00 0.27533E+00 0.26281E+00 0.31042E+00 0.23843E+00
78 0.50000E+01 0.46026E+00 0.47403E+00 0.44231E+00 0.45469E+00 0.42485E+00
79 0.60000E+01 0.54876E+00 0.55798E+00 0.53735E+00 0.54406E+00 0.53443E+00
80 0.70000E+01 0.53003E+00 0.53599E+00 0.52557E+00 0.53223E+00 0.53105E+00
81 0.80000E+01 0.47146E+00 0.47563E+00 0.47068E+00 0.47746E+00 0.47925E+00
82 0.90000E+01 0.40720E+00 0.41041E+00 0.40803E+00 0.41452E+00 0.41728E+00
83 0.10000E+02 0.34897E+00 0.35154E+00 0.35041E+00 0.35630E+00 0.35962E+00
84 0.11000E+02 0.29945E+00 0.30153E+00 0.30108E+00 0.30623E+00 0.31002E+00
85 0.12000E+02 0.25828E+00 0.25995E+00 0.25991E+00 0.26432E+00 0.26846E+00
86 0.13000E+02 0.22425E+00 0.22560E+00 0.22570E+00 0.22854E+00 0.23286E+00

```



```

382
383
384 LONG CRESTED IRREGULAR WAVE CONDITION
385
386 WAVE DIRECTION          360.00  DEG.
387 SIGNIFIGANT WAVE HEIGHT      1.00  m
388 SPECTRUM TYPE              IACS
389
390
391 ***** STANDARD DEVIATION OF RESPONCE *****
392
393 MOON POOL WAVER ELEVATIONS
394
395 TZ ( SEC. )      MIDD. (m)      FORE (m)      AFT. (m)      PROT (m)      STARBOARD (m)
396 0.40000E+01      0.22049E+00      0.23896E+00      0.22264E+00      0.22804E+00      0.22804E+00
397 0.50000E+01      0.37134E+00      0.38070E+00      0.35056E+00      0.35067E+00      0.35067E+00
398 0.60000E+01      0.44904E+00      0.45323E+00      0.44175E+00      0.44995E+00      0.44995E+00
399 0.70000E+01      0.44389E+00      0.44493E+00      0.44675E+00      0.46014E+00      0.46014E+00
400 0.80000E+01      0.40241E+00      0.40204E+00      0.40967E+00      0.42449E+00      0.42449E+00
401 0.90000E+01      0.35280E+00      0.35198E+00      0.36122E+00      0.37546E+00      0.37546E+00
402 0.10000E+02      0.30607E+00      0.30519E+00      0.31422E+00      0.32710E+00      0.32710E+00
403 0.11000E+02      0.26534E+00      0.26457E+00      0.27272E+00      0.28407E+00      0.28407E+00
404 0.12000E+02      0.23084E+00      0.23021E+00      0.23734E+00      0.24725E+00      0.24725E+00
405 0.13000E+02      0.20188E+00      0.20137E+00      0.20754E+00      0.21618E+00      0.21618E+00
406 0.14000E+02      0.17757E+00      0.17717E+00      0.18250E+00      0.19004E+00      0.19004E+00
407 0.15000E+02      0.15709E+00      0.15677E+00      0.16139E+00      0.16801E+00      0.16801E+00
408 0.16000E+02      0.13974E+00      0.13949E+00      0.14351E+00      0.14935E+00      0.14935E+00
409 0.17000E+02      0.12497E+00      0.12477E+00      0.12829E+00      0.13348E+00      0.13348E+00
410 0.18000E+02      0.11231E+00      0.11215E+00      0.11526E+00      0.11989E+00      0.11989E+00
411
412
413 SHORT CRESTED IRREGULAR WAVE CONDITION
414
415 WAVE DIRECTION          0.00  DEG.
416 SIGNIFIGANT WAVE HEIGHT      1.00  m
417 SPECTRUM TYPE              IACS
418
419
420 ***** STANDARD DEVIATION OF RESPONCE *****
421
422 MOON POOL WAVER ELEVATIONS
423
424 TZ ( SEC. )      MIDD. (m)      FORE (m)      AFT. (m)      PROT (m)      STARBOARD (m)
425 0.40000E+01      0.24588E+00      0.25957E+00      0.24759E+00      0.26388E+00      0.26388E+00
426 0.50000E+01      0.41966E+00      0.42705E+00      0.39807E+00      0.39696E+00      0.39696E+00
427 0.60000E+01      0.49452E+00      0.49800E+00      0.48160E+00      0.48339E+00      0.48339E+00
428 0.70000E+01      0.47867E+00      0.47882E+00      0.47880E+00      0.47826E+00      0.47826E+00

```

```

761 SHORT CRESTED IRREGULAR WAVE CONDITION
762
763 WAVE DIRECTION          360.00 DEG.
764 SIGNIFIGANT WAVE HEIGHT    1.00 m
765 SPECTRUM TYPE            IACS
766
767
768 ***** STANDARD DEVIATION OF RESPONSE *****
769
770 MOON POOL WAVER ELEVATIONS
771
772 TZ ( SEC. )      MIDD. (m)      FORE (m)      AFT. (m)      PROT (m)      STARBOARD (m)
773 0.40000E+01      0.24588E+00      0.25957E+00      0.24759E+00      0.26388E+00      0.26388E+00
774 0.50000E+01      0.41966E+00      0.42705E+00      0.39807E+00      0.39696E+00      0.39696E+00
775 0.60000E+01      0.49452E+00      0.49800E+00      0.48160E+00      0.48339E+00      0.48339E+00
776 0.70000E+01      0.47867E+00      0.47982E+00      0.47380E+00      0.47936E+00      0.47936E+00
777 0.80000E+01      0.42759E+00      0.42776E+00      0.42694E+00      0.43416E+00      0.43416E+00
778 0.90000E+01      0.37087E+00      0.37087E+00      0.37203E+00      0.37955E+00      0.37955E+00
779 0.10000E+02      0.31913E+00      0.31929E+00      0.32088E+00      0.32809E+00      0.32809E+00
780 0.11000E+02      0.27490E+00      0.27530E+00      0.27672E+00      0.28338E+00      0.28338E+00
781 0.12000E+02      0.23793E+00      0.23853E+00      0.23962E+00      0.24565E+00      0.24565E+00
782 0.13000E+02      0.20721E+00      0.20794E+00      0.20870E+00      0.21412E+00      0.21412E+00
783 0.14000E+02      0.18164E+00      0.18243E+00      0.18293E+00      0.18777E+00      0.18777E+00
784 0.15000E+02      0.16024E+00      0.16106E+00      0.16135E+00      0.16568E+00      0.16568E+00
785 0.16000E+02      0.14222E+00      0.14303E+00      0.14319E+00      0.14706E+00      0.14706E+00
786 0.17000E+02      0.12695E+00      0.12774E+00      0.12779E+00      0.13126E+00      0.13126E+00
787 0.18000E+02      0.11392E+00      0.11467E+00      0.11466E+00      0.11778E+00      0.11778E+00
788
789
790 *****
791
792
793 LONG CRESTED IRREGULAR WAVE CONDITION
794
795 WAVE DIRECTION          0.00 DEG.
796 SIGNIFIGANT WAVE HEIGHT    1.00 m
797 SPECTRUM TYPE            JONSWAP
798
799
800 ***** STANDARD DEVIATION OF RESPONSE *****
801
802 MOON POOL WAVER ELEVATIONS
803
804 TZ ( SEC. )      MIDD. (m)      FORE (m)      AFT. (m)      PROT (m)      STARBOARD (m)
805 0.40000E+01      0.21060E+00      0.21448E+00      0.21657E+00      0.24145E+00      0.24145E+00
806 0.50000E+01      0.33728E+00      0.34873E+00      0.28832E+00      0.27317E+00      0.27317E+00
807 0.60000E+01      0.51802E+00      0.52510E+00      0.50715E+00      0.51235E+00      0.51235E+00

```

```

1140
1141 LONG CRESTED IRREGULAR WAVE CONDITION
1142
1143 WAVE DIRECTION          360.00 DEG.
1144 SIGNIFIGANT WAVE HEIGHT    1.00 m
1145 SPECTRUM TYPE            JONSWAP
1146
1147
1148 ***** STANDARD DEVIATION OF RESPONCE *****
1149
1150 MOON POOL WAVER ELEVATIONS
1151
1152 TZ ( SEC. )      MIDD. (m)      FORE (m)      AFT. (m)      PROT (m)      STARBOARD (m)
1153 0.40000E+01      0.21060E+00      0.21448E+00      0.21657E+00      0.24145E+00      0.24145E+00
1154 0.50000E+01      0.33728E+00      0.34873E+00      0.28832E+00      0.27317E+00      0.27317E+00
1155 0.60000E+01      0.51802E+00      0.52510E+00      0.50716E+00      0.51235E+00      0.51235E+00
1156 0.70000E+01      0.49263E+00      0.48940E+00      0.50898E+00      0.53019E+00      0.53019E+00
1157 0.80000E+01      0.38688E+00      0.38458E+00      0.40037E+00      0.41901E+00      0.41901E+00
1158 0.90000E+01      0.32272E+00      0.32188E+00      0.33161E+00      0.34584E+00      0.34584E+00
1159 0.10000E+02      0.27700E+00      0.27656E+00      0.28395E+00      0.29552E+00      0.29552E+00
1160 0.11000E+02      0.23945E+00      0.23907E+00      0.24547E+00      0.25532E+00      0.25532E+00
1161 0.12000E+02      0.20795E+00      0.20760E+00      0.21327E+00      0.22182E+00      0.22182E+00
1162 0.13000E+02      0.18149E+00      0.18118E+00      0.18620E+00      0.19366E+00      0.19366E+00
1163 0.14000E+02      0.15933E+00      0.15907E+00      0.16348E+00      0.17002E+00      0.17002E+00
1164 0.15000E+02      0.14075E+00      0.14053E+00      0.14439E+00      0.15016E+00      0.15016E+00
1165 0.16000E+02      0.12506E+00      0.12489E+00      0.12828E+00      0.13338E+00      0.13338E+00
1166 0.17000E+02      0.11168E+00      0.11153E+00      0.11454E+00      0.11908E+00      0.11908E+00
1167 0.18000E+02      0.10019E+00      0.10007E+00      0.10275E+00      0.10683E+00      0.10683E+00
1168
1169
1170 SHORT CRESTED IRREGULAR WAVE CONDITION
1171
1172 WAVE DIRECTION          0.00 DEG.
1173 SIGNIFIGANT WAVE HEIGHT    1.00 m
1174 SPECTRUM TYPE            JONSWAP
1175
1176
1177 ***** STANDARD DEVIATION OF RESPONCE *****
1178
1179 MOON POOL WAVER ELEVATIONS
1180
1181 TZ ( SEC. )      MIDD. (m)      FORE (m)      AFT. (m)      PROT (m)      STARBOARD (m)
1182 0.40000E+01      0.22383E+00      0.22618E+00      0.23306E+00      0.26547E+00      0.26547E+00
1183 0.50000E+01      0.38932E+00      0.39950E+00      0.34521E+00      0.33101E+00      0.33101E+00
1184 0.60000E+01      0.58361E+00      0.58842E+00      0.56743E+00      0.56523E+00      0.56523E+00
1185 0.70000E+01      0.51750E+00      0.51527E+00      0.52368E+00      0.53580E+00      0.53580E+00
1186 0.80000E+01      0.40248E+00      0.40127E+00      0.40681E+00      0.41724E+00      0.41724E+00

```

```

1517
1518 SHORT CRESTED IRREGULAR WAVE CONDITION
1519
1520 WAVE DIRECTION          360.00 DEG.
1521 SIGNIFIGANT WAVE HEIGHT    1.00 m
1522 SPECTRUM TYPE            JONSWAP
1523
1524
1525 ***** STANDARD DEVIATION OF RESPONCE *****
1526
1527 MOON POOL WAVER ELEVATIONS
1528
1529 TZ ( SEC. )      MIDD. (m)      FORE (m)      AFT. (m)      PROT (m)      STARBOARD (m)
1530 0.40000E+01      0.22383E+00      0.22618E+00      0.23306E+00      0.26547E+00      0.26547E+00
1531 0.50000E+01      0.38932E+00      0.39950E+00      0.34521E+00      0.33101E+00      0.33101E+00
1532 0.60000E+01      0.58361E+00      0.58842E+00      0.56743E+00      0.56523E+00      0.56523E+00
1533 0.70000E+01      0.51750E+00      0.51527E+00      0.52368E+00      0.53580E+00      0.53580E+00
1534 0.80000E+01      0.40248E+00      0.40137E+00      0.40681E+00      0.41724E+00      0.41724E+00
1535 0.90000E+01      0.33552E+00      0.33549E+00      0.33747E+00      0.34526E+00      0.34526E+00
1536 0.10000E+02      0.28663E+00      0.28715E+00      0.28798E+00      0.29460E+00      0.29460E+00
1537 0.11000E+02      0.24662E+00      0.24772E+00      0.24781E+00      0.25397E+00      0.25397E+00
1538 0.12000E+02      0.21335E+00      0.21475E+00      0.21444E+00      0.22014E+00      0.22014E+00
1539 0.13000E+02      0.18556E+00      0.18673E+00      0.18661E+00      0.19158E+00      0.19158E+00
1540 0.14000E+02      0.16244E+00      0.16336E+00      0.16342E+00      0.16772E+00      0.16772E+00
1541 0.15000E+02      0.14318E+00      0.14398E+00      0.14406E+00      0.14784E+00      0.14784E+00
1542 0.16000E+02      0.12700E+00      0.12775E+00      0.12777E+00      0.13115E+00      0.13115E+00
1543 0.17000E+02      0.11327E+00      0.11398E+00      0.11395E+00      0.11698E+00      0.11698E+00
1544 0.18000E+02      0.10154E+00      0.10221E+00      0.10215E+00      0.10489E+00      0.10489E+00
1545
1546 *****
1547
1548
1549
1550 LONG CRESTED IRREGULAR WAVE CONDITION
1551
1552 WAVE DIRECTION          0.00 DEG.
1553 SIGNIFIGANT WAVE HEIGHT    1.00 m
1554 SPECTRUM TYPE            Bretchneider
1555
1556
1557 ***** STANDARD DEVIATION OF RESPONCE *****
1558
1559 MOON POOL WAVER ELEVATIONS
1560
1561 TZ ( SEC. )      MIDD. (m)      FORE (m)      AFT. (m)      PROT (m)      STARBOARD (m)
1562 0.40000E+01      0.21991E+00      0.23834E+00      0.22209E+00      0.22749E+00      0.22749E+00
1563 0.50000E+01      0.37041E+00      0.37875E+00      0.34867E+00      0.34878E+00      0.34878E+00

```


2260	0.60000E+01	0.51008E+00	0.50478E+00	0.50249E+00	0.49892E+00	0.49892E+00
2261	0.70000E+01	0.49579E+00	0.48996E+00	0.49407E+00	0.49580E+00	0.49580E+00
2262	0.80000E+01	0.44268E+00	0.43749E+00	0.44378E+00	0.44803E+00	0.44803E+00
2263	0.90000E+01	0.38334E+00	0.37932E+00	0.38541E+00	0.39066E+00	0.39066E+00
2264	0.10000E+02	0.32931E+00	0.32660E+00	0.33147E+00	0.33704E+00	0.33704E+00
2265	0.11000E+02	0.28327E+00	0.28170E+00	0.28519E+00	0.29075E+00	0.29075E+00
2266	0.12000E+02	0.24490E+00	0.24420E+00	0.24648E+00	0.25185E+00	0.25185E+00
2267	0.13000E+02	0.21307E+00	0.21299E+00	0.21435E+00	0.21941E+00	0.21941E+00
2268	0.14000E+02	0.18662E+00	0.18693E+00	0.18764E+00	0.19234E+00	0.19234E+00
2269	0.15000E+02	0.16452E+00	0.16507E+00	0.16534E+00	0.16966E+00	0.16966E+00
2270	0.16000E+02	0.14593E+00	0.14663E+00	0.14659E+00	0.15055E+00	0.15055E+00
2271	0.17000E+02	0.13020E+00	0.13096E+00	0.13074E+00	0.13435E+00	0.13435E+00
2272	0.18000E+02	0.11679E+00	0.11758E+00	0.11724E+00	0.12054E+00	0.12054E+00
2273						
2274						
2275	SHORT CRESTED IRREGULAR WAVE CONDITION					
2276						
2277	WAVE DIRECTION	360.00	DEG.			
2278	SIGNIFIGANT WAVE HEIGHT	1.00	m			
2279	SPECTRUM TYPE	Bretchneider				
2280						
2281						
2282	***** STANDARD DEVIATION OF RESPONCE *****					
2283						
2284	MOON POOL WAVER ELEVATIONS					
2285						
2286	TZ (SEC.)	MIDD. (m)	FORE (m)	AFT. (m)	PROT (m)	STARBOARD (m)
2287	0.40000E+01	0.24522E+00	0.25889E+00	0.24697E+00	0.26323E+00	0.26323E+00
2288	0.50000E+01	0.41860E+00	0.42598E+00	0.39707E+00	0.39596E+00	0.39596E+00
2289	0.60000E+01	0.49336E+00	0.49683E+00	0.48046E+00	0.48224E+00	0.48224E+00
2290	0.70000E+01	0.47760E+00	0.47874E+00	0.47273E+00	0.47827E+00	0.47827E+00
2291	0.80000E+01	0.42665E+00	0.42682E+00	0.42600E+00	0.43320E+00	0.43320E+00
2292	0.90000E+01	0.37007E+00	0.37007E+00	0.37122E+00	0.37873E+00	0.37873E+00
2293	0.10000E+02	0.31844E+00	0.31861E+00	0.32019E+00	0.32739E+00	0.32739E+00
2294	0.11000E+02	0.27431E+00	0.27471E+00	0.27613E+00	0.28277E+00	0.28277E+00
2295	0.12000E+02	0.23743E+00	0.23803E+00	0.23911E+00	0.24513E+00	0.24513E+00
2296	0.13000E+02	0.20677E+00	0.20750E+00	0.20826E+00	0.21366E+00	0.21366E+00
2297	0.14000E+02	0.18125E+00	0.18205E+00	0.18254E+00	0.18737E+00	0.18737E+00
2298	0.15000E+02	0.15990E+00	0.16072E+00	0.16101E+00	0.16533E+00	0.16533E+00
2299	0.16000E+02	0.14192E+00	0.14273E+00	0.14289E+00	0.14675E+00	0.14675E+00
2300	0.17000E+02	0.12668E+00	0.12747E+00	0.12752E+00	0.13099E+00	0.13099E+00
2301	0.18000E+02	0.11369E+00	0.11443E+00	0.11442E+00	0.11754E+00	0.11754E+00
2302						
2303						
2304	*****					
2305						

EXAMPLE IMAGES OF AN OUTPUT FILE MOTION SPECTRUM.DAT

```

1
2
3 *****
4   THREE-DIMENSIONAL PANEL METHOD
5   FOR RADIATION & DIFFRACTION PROBLEMS
6   OF A FLOATING SHIP WITH ZERO SPEED
7 *****
8
9   SHIP NAME      :      DRILL SHIP MODEL 10/05/2016
10  NUMBER OF HULL SURFACE ELEMENTS: NE   = 1162
11  NUMBER OF ADDED ELEMENTS      : NADD =   40
12  NUMBER OF TOTAL ELEMENTS      : NT   = 1202
13
14  LENGTH IN X-AXIS----- (LENGTH) --=      203.363 m
15  LENGTH IN Y-AXIS----- (BREDTH) --=      29.027 m
16  LENGTH IN Z-AXIS----- (DRAFT)  --=      11.613 m
17
18  BLOCK COEFFICIENT----- ( CB ) --=      0.76989
19  WATER PLANE AREA COEFFICIENT---- ( CW ) --=      0.18723
20  CENTER OF FLOATATION -----=      0.00000 m
21  IXX=VOL*(KXX**2);----- (KXX) --=     10.05000 m
22  IYY=VOL*(KYY**2);----- (KYY) --=     49.38000 m
23  IZZ=VOL*(KZZ**2);----- (KZZ) --=     49.38000 m
24  POSITION OF GRAVITY FROM ORIGIN-- (OXG) --=      0.00000 m
25  POSITION OF GRAVITY FROM ORIGIN-- (OYG) --=      0.00000 m
26  POSITION OF GRAVITY FROM ORIGIN-- (OZG) --=      1.00000 m
27  METACENTRIC HEIGHT FOR PITCH ---- (GML) --=     281.50000 m
28  METACENTRIC HEIGHT FOR ROLL ---- (GMB) --=      1.80000 m
29
30
31  MOON POOL WATER SURFACE DAMPING -----=      0.09000
32
33
34
35
36  LONG CRESTED IRREGULAR WAVE CONDITION
37
38  WAVE DIRECTION      0.00  DEG.
39  SIGNIFIGANT WAVE HEIGHT  1.00  m
40  SPECTRUM TYPE      IACS
41
42
43  ***** STANDARD DEVIATION OF RESPONCE *****
44
45  SHIP MOTIONS
46
47  PG. ( SEC )      SURGE (m)      SWAY (m)      HEAVE (m)      ROLL (deg.)

```

WAVE DIRECTION 0.00 DEG.
SIGNIFIGANT WAVE HEIGHT 1.00 m
SPECTRUM TYPE IACS

***** STANDARD DEVIATION OF RESPONCE *****

SHIP MOTIONS

TZ (SEC.)	SURGE (m)	SWAY (m)	HEAVE (m)	ROLL (deg.)	PITCH (deg.)	YAW (deg.)
0.40000E+01	0.46885E-03	0.00000E+00	0.68984E-03	0.00000E+00	0.18641E-01	0.00000E+00
0.50000E+01	0.86625E-03	0.00000E+00	0.18636E-02	0.00000E+00	0.45445E-01	0.00000E+00
0.60000E+01	0.13560E-02	0.00000E+00	0.24934E-02	0.00000E+00	0.68925E-01	0.00000E+00
0.70000E+01	0.21917E-02	0.00000E+00	0.25717E-02	0.00000E+00	0.99543E-01	0.00000E+00
0.80000E+01	0.31117E-02	0.00000E+00	0.25008E-02	0.00000E+00	0.12823E+00	0.00000E+00
0.90000E+01	0.38457E-02	0.00000E+00	0.24652E-02	0.00000E+00	0.14818E+00	0.00000E+00
0.10000E+02	0.43297E-02	0.00000E+00	0.24675E-02	0.00000E+00	0.15915E+00	0.00000E+00
0.11000E+02	0.45942E-02	0.00000E+00	0.24700E-02	0.00000E+00	0.16313E+00	0.00000E+00
0.12000E+02	0.46909E-02	0.00000E+00	0.24500E-02	0.00000E+00	0.16227E+00	0.00000E+00
0.13000E+02	0.46649E-02	0.00000E+00	0.24007E-02	0.00000E+00	0.15817E+00	0.00000E+00
0.14000E+02	0.45504E-02	0.00000E+00	0.23238E-02	0.00000E+00	0.15193E+00	0.00000E+00
0.15000E+02	0.43742E-02	0.00000E+00	0.22244E-02	0.00000E+00	0.14434E+00	0.00000E+00
0.16000E+02	0.41583E-02	0.00000E+00	0.21096E-02	0.00000E+00	0.13598E+00	0.00000E+00
0.17000E+02	0.39205E-02	0.00000E+00	0.19861E-02	0.00000E+00	0.12733E+00	0.00000E+00
0.18000E+02	0.36746E-02	0.00000E+00	0.18600E-02	0.00000E+00	0.11871E+00	0.00000E+00

LONG CRESTED IRREGULAR WAVE CONDITION

WAVE DIRECTION 30.00 DEG.
SIGNIFIGANT WAVE HEIGHT 1.00 m
SPECTRUM TYPE IACS

***** STANDARD DEVIATION OF RESPONCE *****

SHIP MOTIONS

TZ (SEC.)	SURGE (m)	SWAY (m)	HEAVE (m)	ROLL (deg.)	PITCH (deg.)	YAW (deg.)
0.40000E+01	0.55295E-03	0.40729E-03	0.10365E-02	0.15482E-01	0.22975E-01	0.74302E-02
0.50000E+01	0.90562E-03	0.79080E-03	0.24672E-02	0.43200E-01	0.48293E-01	0.14671E-01
0.60000E+01	0.16306E-02	0.11376E-02	0.29930E-02	0.62524E-01	0.81776E-01	0.28703E-01
0.70000E+01	0.26624E-02	0.14333E-02	0.29931E-02	0.81280E-01	0.11749E+00	0.45137E-01
0.80000E+01	0.35608E-02	0.21606E-02	0.29380E-02	0.13432E+00	0.14368E+00	0.58402E-01
0.90000E+01	0.41728E-02	0.32830E-02	0.29287E-02	0.20543E+00	0.15847E+00	0.67451E-01
0.10000E+02	0.45154E-02	0.42525E-02	0.28270E-02	0.26040E+00	0.16423E+00	0.72688E-01


```

409 0.17000E+02 0.39205E-02 0.00000E+00 0.19861E-02 0.00000E+00 0.12733E+00 0.00000E+00
410 0.18000E+02 0.36746E-02 0.00000E+00 0.18600E-02 0.00000E+00 0.11871E+00 0.00000E+00
411
412
413 SHORT CRESTED IRREGULAR WAVE CONDITION
414
415 WAVE DIRECTION 0.00 DEG.
416 SIGNIFIGANT WAVE HEIGHT 1.00 m
417 SPECTRUM TYPE IACS
418
419
420 ***** STANDARD DEVIATION OF RESPONCE *****
421
422 SHIP MOTIONS
423
424 TZ ( SEC. ) SURGE (m) SWAY (m) HEAVE (m) ROLL (deg.) PITCH (deg.) YAW (deg.)
425 0.40000E+01 0.64710E-03 0.60324E-03 0.10308E-02 0.16875E-01 0.29189E-01 0.11294E-01
426 0.50000E+01 0.14145E-02 0.85472E-03 0.22718E-02 0.32144E-01 0.71832E-01 0.25332E-01
427 0.60000E+01 0.22052E-02 0.11362E-02 0.31002E-02 0.47084E-01 0.10468E+00 0.40946E-01
428 0.70000E+01 0.29870E-02 0.14091E-02 0.34232E-02 0.75504E-01 0.13024E+00 0.52970E-01
429 0.80000E+01 0.36694E-02 0.20634E-02 0.34984E-02 0.13377E+00 0.14857E+00 0.60626E-01
430 0.90000E+01 0.41562E-02 0.30934E-02 0.34736E-02 0.20095E+00 0.15899E+00 0.64815E-01
431 0.10000E+02 0.44372E-02 0.40126E-02 0.33982E-02 0.25135E+00 0.16267E+00 0.66413E-01
432 0.11000E+02 0.45495E-02 0.45930E-02 0.32891E-02 0.27795E+00 0.16148E+00 0.66077E-01
433 0.12000E+02 0.45379E-02 0.48464E-02 0.31556E-02 0.28502E+00 0.15710E+00 0.64387E-01
434 0.13000E+02 0.44389E-02 0.48613E-02 0.30047E-02 0.27927E+00 0.15072E+00 0.61812E-01
435 0.14000E+02 0.42788E-02 0.47243E-02 0.28416E-02 0.26623E+00 0.14311E+00 0.58692E-01
436 0.15000E+02 0.40776E-02 0.45004E-02 0.26710E-02 0.24964E+00 0.13480E+00 0.55266E-01
437 0.16000E+02 0.38516E-02 0.42330E-02 0.24978E-02 0.23182E+00 0.12619E+00 0.51712E-01
438 0.17000E+02 0.36141E-02 0.39499E-02 0.23265E-02 0.21408E+00 0.11760E+00 0.48167E-01
439 0.18000E+02 0.33754E-02 0.36683E-02 0.21609E-02 0.19716E+00 0.10925E+00 0.44727E-01
440
441
442 SHORT CRESTED IRREGULAR WAVE CONDITION
443
444 WAVE DIRECTION 30.00 DEG.
445 SIGNIFIGANT WAVE HEIGHT 1.00 m
446 SPECTRUM TYPE IACS
447
448
449 ***** STANDARD DEVIATION OF RESPONCE *****
450
451 SHIP MOTIONS
452
453 TZ ( SEC. ) SURGE (m) SWAY (m) HEAVE (m) ROLL (deg.) PITCH (deg.) YAW (deg.)
454 0.40000E+01 0.65101E-03 0.21837E-02 0.19543E-02 0.17797E-01 0.28875E-01 0.11829E-01
455 0.50000E+01 0.12222E-02 0.25260E-03 0.40410E-02 0.28210E-01 0.67242E-01 0.24002E-01

```

```

786 0.17000E+02 0.36141E-02 0.39499E-02 0.23265E-02 0.21408E+00 0.11760E+00 0.48167E-01
787 0.18000E+02 0.33754E-02 0.36683E-02 0.21609E-02 0.19716E+00 0.10925E+00 0.44727E-01
788
789
790 *****
791
792
793 LONG CRESTED IRREGULAR WAVE CONDITION
794
795 WAVE DIRECTION 0.00 DEG.
796 SIGNIFIGANT WAVE HEIGHT 1.00 m
797 SPECTRUM TYPE JONSWAP
798
799
800 ***** STANDARD DEVIATION OF RESPONCE *****
801
802 SHIP MOTIONS
803
804 TZ ( SEC. ) SURGE (m) SWAY (m) HEAVE (m) ROLL (deg.) PITCH (deg.) YAW (deg.)
805 0.40000E+01 0.47106E-03 0.00000E+00 0.42464E-03 0.00000E+00 0.11181E-01 0.00000E+00
806 0.50000E+01 0.70772E-03 0.00000E+00 0.14861E-02 0.00000E+00 0.37192E-01 0.00000E+00
807 0.60000E+01 0.13715E-02 0.00000E+00 0.29339E-02 0.00000E+00 0.73250E-01 0.00000E+00
808 0.70000E+01 0.17221E-02 0.00000E+00 0.29381E-02 0.00000E+00 0.83079E-01 0.00000E+00
809 0.80000E+01 0.27822E-02 0.00000E+00 0.22665E-02 0.00000E+00 0.12590E+00 0.00000E+00
810 0.90000E+01 0.39661E-02 0.00000E+00 0.22199E-02 0.00000E+00 0.15858E+00 0.00000E+00
811 0.10000E+02 0.46862E-02 0.00000E+00 0.24218E-02 0.00000E+00 0.17267E+00 0.00000E+00
812 0.11000E+02 0.49572E-02 0.00000E+00 0.25362E-02 0.00000E+00 0.17377E+00 0.00000E+00
813 0.12000E+02 0.49873E-02 0.00000E+00 0.25484E-02 0.00000E+00 0.16929E+00 0.00000E+00
814 0.13000E+02 0.48757E-02 0.00000E+00 0.24884E-02 0.00000E+00 0.16194E+00 0.00000E+00
815 0.14000E+02 0.46894E-02 0.00000E+00 0.23893E-02 0.00000E+00 0.15336E+00 0.00000E+00
816 0.15000E+02 0.44720E-02 0.00000E+00 0.22748E-02 0.00000E+00 0.14453E+00 0.00000E+00
817 0.16000E+02 0.42302E-02 0.00000E+00 0.21487E-02 0.00000E+00 0.13551E+00 0.00000E+00
818 0.17000E+02 0.39172E-02 0.00000E+00 0.19874E-02 0.00000E+00 0.12492E+00 0.00000E+00
819 0.18000E+02 0.35754E-02 0.00000E+00 0.18121E-02 0.00000E+00 0.11382E+00 0.00000E+00
820
821
822 LONG CRESTED IRREGULAR WAVE CONDITION
823
824 WAVE DIRECTION 30.00 DEG.
825 SIGNIFIGANT WAVE HEIGHT 1.00 m
826 SPECTRUM TYPE JONSWAP
827
828
829 ***** STANDARD DEVIATION OF RESPONCE *****
830
831 SHIP MOTIONS
832

```

1140	
1141	LONG CRESTED IRREGULAR WAVE CONDITION
1142	
1143	WAVE DIRECTION 360.00 DEG.
1144	SIGNIFIGANT WAVE HEIGHT 1.00 m
1145	SPECTRUM TYPE JONSWAP
1146	
1147	
1148	***** STANDARD DEVIATION OF RESPONCE *****
1149	
1150	SHIP MOTIONS
1151	
1152	TZ (SEC.) SURGE (m) SWAY (m) HEAVE (m) ROLL (deg.) PITCH (deg.) YAW (deg.)
1153	0.40000E+01 0.47106E-03 0.00000E+00 0.42464E-03 0.00000E+00 0.11181E-01 0.00000E+00
1154	0.50000E+01 0.70772E-03 0.00000E+00 0.14861E-02 0.00000E+00 0.37192E-01 0.00000E+00
1155	0.60000E+01 0.13715E-02 0.00000E+00 0.29339E-02 0.00000E+00 0.73250E-01 0.00000E+00
1156	0.70000E+01 0.17221E-02 0.00000E+00 0.29381E-02 0.00000E+00 0.83079E-01 0.00000E+00
1157	0.80000E+01 0.27822E-02 0.00000E+00 0.22665E-02 0.00000E+00 0.12590E+00 0.00000E+00
1158	0.90000E+01 0.39661E-02 0.00000E+00 0.22199E-02 0.00000E+00 0.15858E+00 0.00000E+00
1159	0.10000E+02 0.46862E-02 0.00000E+00 0.24218E-02 0.00000E+00 0.17267E+00 0.00000E+00
1160	0.11000E+02 0.49572E-02 0.00000E+00 0.25362E-02 0.00000E+00 0.17377E+00 0.00000E+00
1161	0.12000E+02 0.49873E-02 0.00000E+00 0.25484E-02 0.00000E+00 0.16929E+00 0.00000E+00
1162	0.13000E+02 0.48757E-02 0.00000E+00 0.24884E-02 0.00000E+00 0.16194E+00 0.00000E+00
1163	0.14000E+02 0.46894E-02 0.00000E+00 0.23893E-02 0.00000E+00 0.15336E+00 0.00000E+00
1164	0.15000E+02 0.44720E-02 0.00000E+00 0.22748E-02 0.00000E+00 0.14453E+00 0.00000E+00
1165	0.16000E+02 0.42302E-02 0.00000E+00 0.21487E-02 0.00000E+00 0.13551E+00 0.00000E+00
1166	0.17000E+02 0.39172E-02 0.00000E+00 0.19874E-02 0.00000E+00 0.12492E+00 0.00000E+00
1167	0.18000E+02 0.35754E-02 0.00000E+00 0.18121E-02 0.00000E+00 0.11382E+00 0.00000E+00
1168	
1169	
1170	SHORT CRESTED IRREGULAR WAVE CONDITION
1171	
1172	WAVE DIRECTION 0.00 DEG.
1173	SIGNIFIGANT WAVE HEIGHT 1.00 m
1174	SPECTRUM TYPE JONSWAP
1175	
1176	
1177	***** STANDARD DEVIATION OF RESPONCE *****
1178	
1179	SHIP MOTIONS
1180	
1181	TZ (SEC.) SURGE (m) SWAY (m) HEAVE (m) ROLL (deg.) PITCH (deg.) YAW (deg.)
1182	0.40000E+01 0.53584E-03 0.58731E-03 0.74495E-03 0.13746E-01 0.18401E-01 0.10389E-01
1183	0.50000E+01 0.11717E-02 0.83673E-03 0.19607E-02 0.29352E-01 0.60018E-01 0.19857E-01
1184	0.60000E+01 0.21930E-02 0.10855E-02 0.34067E-02 0.46696E-01 0.11098E+00 0.39196E-01
1185	0.70000E+01 0.28640E-02 0.14521E-02 0.37617E-02 0.63053E-01 0.12923E+00 0.54904E-01
1186	0.80000E+01 0.36374E-02 0.17156E-02 0.35351E-02 0.88785E-01 0.15222E+00 0.62825E-01


```

1518 SHORT CRESTED IRREGULAR WAVE CONDITION
1519
1520 WAVE DIRECTION          360.00 DEG.
1521 SIGNIFIGANT WAVE HEIGHT    1.00 m
1522 SPECTRUM TYPE            JONSWAP
1523
1524
1525 ***** STANDARD DEVIATION OF RESPONCE *****
1526
1527 SHIP MOTIONS
1528
1529 TZ ( SEC. )      SURGE (m)      SWAY (m)      HEAVE (m)      ROLL (deg.)      PITCH (deg.)      YAW (deg.)
1530 0.40000E+01      0.53584E-03      0.58731E-03      0.74495E-03      0.13746E-01      0.18401E-01      0.10389E-01
1531 0.50000E+01      0.11717E-02      0.83673E-03      0.19607E-02      0.29352E-01      0.60018E-01      0.19857E-01
1532 0.60000E+01      0.21930E-02      0.10855E-02      0.34067E-02      0.46696E-01      0.11098E+00      0.39196E-01
1533 0.70000E+01      0.28640E-02      0.14521E-02      0.37617E-02      0.63053E-01      0.12923E+00      0.54904E-01
1534 0.80000E+01      0.36374E-02      0.17156E-02      0.35251E-02      0.98785E-01      0.15232E+00      0.63935E-01
1535 0.90000E+01      0.43489E-02      0.23400E-02      0.34482E-02      0.16074E+00      0.16787E+00      0.67939E-01
1536 0.10000E+02      0.47375E-02      0.34522E-02      0.34193E-02      0.23930E+00      0.17200E+00      0.68861E-01
1537 0.11000E+02      0.48144E-02      0.49738E-02      0.33224E-02      0.32139E+00      0.16783E+00      0.68296E-01
1538 0.12000E+02      0.47330E-02      0.59205E-02      0.31789E-02      0.35108E+00      0.16046E+00      0.66674E-01
1539 0.13000E+02      0.45599E-02      0.56680E-02      0.30058E-02      0.31413E+00      0.15159E+00      0.62825E-01
1540 0.14000E+02      0.43421E-02      0.49914E-02      0.28224E-02      0.26711E+00      0.14228E+00      0.58438E-01
1541 0.15000E+02      0.41105E-02      0.44437E-02      0.26426E-02      0.23448E+00      0.13318E+00      0.54442E-01
1542 0.16000E+02      0.38672E-02      0.40437E-02      0.24654E-02      0.21190E+00      0.12422E+00      0.50698E-01
1543 0.17000E+02      0.35713E-02      0.36924E-02      0.22661E-02      0.19314E+00      0.11420E+00      0.46600E-01
1544 0.18000E+02      0.32562E-02      0.33672E-02      0.20616E-02      0.17633E+00      0.10394E+00      0.42432E-01
1545
1546
1547 *****
1548
1549
1550 LONG CRESTED IRREGULAR WAVE CONDITION
1551
1552 WAVE DIRECTION          0.00 DEG.
1553 SIGNIFIGANT WAVE HEIGHT    1.00 m
1554 SPECTRUM TYPE            Bretchnneider
1555
1556
1557 ***** STANDARD DEVIATION OF RESPONCE *****
1558
1559 SHIP MOTIONS
1560
1561 TZ ( SEC. )      SURGE (m)      SWAY (m)      HEAVE (m)      ROLL (deg.)      PITCH (deg.)      YAW (deg.)
1562 0.40000E+01      0.46763E-03      0.00000E+00      0.68775E-03      0.00000E+00      0.18585E-01      0.00000E+00
1563 0.50000E+01      0.86401E-03      0.00000E+00      0.18587E-02      0.00000E+00      0.45326E-01      0.00000E+00
1564 0.60000E+01      0.12524E-02      0.00000E+00      0.24875E-02      0.00000E+00      0.68746E-01      0.00000E+00

```

2260	0.60000E+01	0.20660E-02	0.25645E-02	0.52058E-02	0.60981E-01	0.98928E-01	0.39066E-01
2261	0.70000E+01	0.28511E-02	0.25277E-02	0.54536E-02	0.96848E-01	0.12460E+00	0.52288E-01
2262	0.80000E+01	0.35186E-02	0.29688E-02	0.52727E-02	0.16690E+00	0.14232E+00	0.61636E-01
2263	0.90000E+01	0.39741E-02	0.40313E-02	0.49541E-02	0.24777E+00	0.15175E+00	0.67363E-01
2264	0.10000E+02	0.42226E-02	0.50787E-02	0.46105E-02	0.30858E+00	0.15452E+00	0.70129E-01
2265	0.11000E+02	0.43087E-02	0.57547E-02	0.42779E-02	0.34064E+00	0.15270E+00	0.70581E-01
2266	0.12000E+02	0.42798E-02	0.60450E-02	0.39656E-02	0.34903E+00	0.14798E+00	0.69362E-01
2267	0.13000E+02	0.41719E-02	0.60489E-02	0.36741E-02	0.34186E+00	0.14151E+00	0.67016E-01
2268	0.14000E+02	0.40102E-02	0.58698E-02	0.34009E-02	0.32584E+00	0.13401E+00	0.63942E-01
2269	0.15000E+02	0.38133E-02	0.55860E-02	0.31442E-02	0.30551E+00	0.12597E+00	0.60433E-01
2270	0.16000E+02	0.35958E-02	0.52504E-02	0.29030E-02	0.28369E+00	0.11773E+00	0.56708E-01
2271	0.17000E+02	0.33696E-02	0.48969E-02	0.26775E-02	0.26198E+00	0.10957E+00	0.52935E-01
2272	0.18000E+02	0.31439E-02	0.45460E-02	0.24681E-02	0.24127E+00	0.10169E+00	0.49236E-01
2273							
2274							
2275	SHORT CRESTED IRREGULAR WAVE CONDITION						
2276							
2277	WAVE DIRECTION	360.00	DEG.				
2278	SIGNIFIGANT WAVE HEIGHT	1.00	m				
2279	SPECTRUM TYPE	Bretchnneider					
2280							
2281							
2282	***** STANDARD DEVIATION OF RESPONCE *****						
2283							
2284	SHIP MOTIONS						
2285							
2286	TZ (SEC.)	SURGE (m)	SWAY (m)	HEAVE (m)	ROLL (deg.)	PITCH (deg.)	YAW (deg.)
2287	0.40000E+01	0.64531E-03	0.60173E-03	0.10278E-02	0.16829E-01	0.29102E-01	0.11263E-01
2288	0.50000E+01	0.14108E-02	0.85257E-03	0.22659E-02	0.32061E-01	0.71643E-01	0.25264E-01
2289	0.60000E+01	0.21995E-02	0.11334E-02	0.30927E-02	0.46963E-01	0.10442E+00	0.40841E-01
2290	0.70000E+01	0.29795E-02	0.14055E-02	0.34151E-02	0.75294E-01	0.12992E+00	0.52840E-01
2291	0.80000E+01	0.36603E-02	0.20577E-02	0.34903E-02	0.13340E+00	0.14821E+00	0.60480E-01
2292	0.90000E+01	0.41462E-02	0.30852E-02	0.34656E-02	0.20042E+00	0.15861E+00	0.64662E-01
2293	0.10000E+02	0.44267E-02	0.40024E-02	0.33905E-02	0.25072E+00	0.16229E+00	0.66259E-01
2294	0.11000E+02	0.45389E-02	0.45819E-02	0.32816E-02	0.27729E+00	0.16111E+00	0.65925E-01
2295	0.12000E+02	0.45275E-02	0.48351E-02	0.31485E-02	0.28436E+00	0.15675E+00	0.64241E-01
2296	0.13000E+02	0.44288E-02	0.48501E-02	0.29980E-02	0.27864E+00	0.15038E+00	0.61673E-01
2297	0.14000E+02	0.42691E-02	0.47137E-02	0.28353E-02	0.26564E+00	0.14279E+00	0.58561E-01
2298	0.15000E+02	0.40685E-02	0.44904E-02	0.26651E-02	0.24909E+00	0.13450E+00	0.55144E-01
2299	0.16000E+02	0.38431E-02	0.42237E-02	0.24924E-02	0.23131E+00	0.12592E+00	0.51599E-01
2300	0.17000E+02	0.36062E-02	0.39413E-02	0.23215E-02	0.21362E+00	0.11734E+00	0.48062E-01
2301	0.18000E+02	0.33681E-02	0.36604E-02	0.21562E-02	0.19674E+00	0.10901E+00	0.44630E-01
2302							
2303							
2304	*****						
2305							

Appendix G Code

1. Avaliacao.m

```
function [ q ] = Avaliacao( F, q, t )
%Function which evaluate if it is the moment to stop looping,
%changing 'q' from 1 to 0.

a1 = F(t)-F(t-1) ; % Compare the current value of 'F' with the last one.

a2 = F(t-1)-F(t-2); % Compare the last value of 'F' with
%the value before it.

if (a1<0.1)&&(a2<0.1)
    q = 0; % If in the tree last loops, 'F' did not increase so much,
           %it is better to stop.
end
end
```

2. Build_Moonpools.m

```
function [ notas, GR ] = Build_Moonpools( I, LS, folder_str )
% Organize the groups of individuals to build and evaluate each one

disp('enter buildmoonpools');

% Read data from files to build the moon pools -----%

% Input parameters
fileID = fopen('Optimization_Parameters.dat','r') ;
line_data = textscan(fileID, '%*[^']' %f',1,'HeaderLines',8);

% Typical distance between nodes.
divs(1) = line_data{1} ;

fclose(fileID) ;

% Ship hull without opening
% v is the list of coordinates of the grid
% e is the variable that receives the elements data from the file
[ v, e ] = Pre_Leitor;
```

```

s          = v(:,4)          ; % 'z' values.
H          = max(s)          ; % ship height

divs(2)    = H                ; % H is the MP height. It is not a division,
                                % but was added for convenience to divs.

% Create for each individual in I (columns) a folder ----- %
% the values of mi should better be multiples of dx and dy respectively
for i=1:size(I,2),
    shape = I(:,i);
    folder_name = [folder_str,num2str(i)];

    folder_name

    mkdir(folder_name);
    % Copy files to each folder the kits for generation and
    %hydrodynamic calculation
    copyfile('input_hull.txt',folder_name)          ; %
    copyfile('d_Geom_Pontos.m',folder_name)          ; % mesh
                                                % generation
                                                % kit

    copyfile('d_Elim_Linhas_Pontos.m',folder_name)    ; %
    copyfile('centroide.m',folder_name)              ; %
    copyfile('d_Pre_Escrevedor.m',folder_name)       ; %
    copyfile('Principal.drillship.MoonPool.dat',folder_name); %
    copyfile('WAVE.CONDITION.RAO-IRREGULAR.DAT',folder_name); % hydrody-
                                                % namic simu-
                                                % lation kit

    copyfile('Hydrodynamic.exe',folder_name)         ; % (module)
    copyfile('d_Runcommand.m',folder_name)           ; % function
                                                % that uses
                                                % both kits

    % Enter in the folder and run the mesh generation and hydrodynamic
    % module inside there
    command      = 'cd'          ; % system command line: "inform
                                % present path"
    [status,cmdout] = system(command); % send command, receive answer
                                % in cmdout
    cd (folder_name)            % enter in the folder of the
                                % individual

    % Run the function Runcommand inside there. Inside the function, it

```

```

% has a command to return to the path in cmdout
[eval] = d_Runcommand(cmdout, v, e, LS, shape, divs);

% Came back from the individual's folder, then continue
if eval == 1
    % Calculate the Operability of the ship-moonpool -----%
    disp('calling evaldata')          ;
    [ nota, P ] = Eval_Data(folder_name);
    disp('eval done')                  ;
    % If the file was mistaken as good but inside data was bad
    if isnan(nota(1,1)) == 1 || isnan(nota(2,1)) == 1 || ...
        isnan(nota(3,1)) == 1
        nota = zeros(3,1);
        P     = zeros(7,4);
    end
else
    % if the files in that folder were not eligible for evaluation
    nota = zeros(3,1);
    P     = zeros(7,4); % 7 axis of the radar chart (incidence angles
                        % beta), 4 criteria
end

% Keep the grades in 'notas' and data for radar chart in 'GR' -----%
notas(:,i) = nota;
GR{i,1}    = P    ; % GR is a cell array
end
disp('exit buildmoonpools');
GR
end

```

4. Crossover.m

```

function [ I ] = Crossover( I4, I, ni )
% Function to generate new individuals as sons of two input individuals.
% The 'father' is the first column of 'I4' and the 'mother' is the second.

for i=1:ni
    for j      = 1:size(I4,1),
        a      = randi(2,1,1); % If 'a'=1, the new individual receives
                                % information from its 'father'.

        I(j,i) = I4(j,a);      % If 'a'=2, the new individual receives
                                % information from its 'mother'.
    end
end
end

```

end

5.D_Elim_Linhas_Pontos.m

```
function [v, e] = d_Elim_Linhas_Pontos( v, e, contour, H )
% Function to eliminate the elements located inside the moon pool

contour      = [[contour(1,1) -1] ; contour ; ...
               [contour(size(contour,1),1) -1]]      ;
closedpol    = [contour ; contour(1,:)]              ;

% Identification of elements inside the opening ----- %
tot = size(e,1);
for i = 1:tot
    clear DT K IDgrids
    clear DT1 K1 quad1 DT2 K2 quad2 DT3 K3 quad3 quad
    clear quad22 DT22 K22 x1 y1 x2 y2 x3 y3

    % find the intersection between border(:,2:3) and each of the elements
    % of listIn and store them. Then make the appropriate treatment using
    % those calculated intersection points
    a      = [e(i,2) e(i,3) e(i,5) e(i,4)]      ;
    nodesClosed = v(a,2:3)                      ; % coordinates of all
    nodesClosed = [nodesClosed ; nodesClosed(1,:)]; % grids of the current
                                                    % element sorted in

    [xi, yi] = polyxpoly(contour(:,1),contour(:,2), nodesClosed(:,1),...
                        nodesClosed(:,2));

    % Identifies the elements with at least 1 grid inside the opening,
    % lists them with their respective grid ID for inside MP(listIN) and on
    % border (listOn).
    % *****Obs: on is also considered in***** %

    [in, on] = inpolygon(v(a,2),v(a,3),closedpol(:,1),closedpol(:,2));

    % find ids of the grids in each condition: inside, out of and on border
    idsin = in.*v(a,1)                      ;
    idsin(~any(idsin,2)) = []                ;
    if ~isempty(idsin)
        isinCoord = v(idsin,:) ; %IDs of grids inside and on border
    else
        isinCoord = []                    ;
    end
end
```

```

idsout = ~in.*v(a,1)                ;
idsout(~any(idsout,2))=[]           ;
if ~isempty(idsout)
    isoutCoord = v(idsout,:)         ; %coordinates of grids out of border
else
    isoutCoord = []                 ;
end

idson = on.*v(a,1)                  ;
idson(~any(idson,2)) = []           ;
if ~isempty(idson)
    isonCoord = v(idson,:)          ; % coordinates of grids on border
else
    isonCoord = []                 ;
end

if size(isinCoord,1) == 4
    e(i,1) = 0                      ; % zeroes IDs of elements that are
                                   % totally inside MP from e
else
    if ~isempty(xi) % Adjust the elements intercepted by border or
                    % inside MP
        intercepted = size(xi,1);
        % search for ID of already existent intersection point or add
        % a new to v
        addpoint = [];
        for j = 1: size(xi,1)
            isThereInv = ismember(v(:,2:3),[xi(j) yi(j)]) ; % check if
            % there is already such coordinates in v
            idIntersec = find(sum(isThereInv')' == 2)      ; % take the
            % existent grid's ID
            if isempty(idIntersec)
                addpoint(j,:) = [size(v,1)+1 xi(j) yi(j) H]; % there
                % isn't grid with those coordinates: create
                v = [v ; addpoint(j,:)] ;
            else
                if v(idIntersec,4) == H
                    addpoint(j,:) = v(idIntersec,:) ;
                    % take the already-existent ID to use
                else
                    addpoint(j,:) = [size(v,1)+1 xi(j) yi(j) H] ;
                    % there isn't grid with those coordinates: create
                    v = [v ; addpoint(j,:)] ;
                end
            end
        end
    end
end

```

```

end

grids_on_border = size(isonCoord,1);
grids_inside    = size(isinCoord,1);
% Start adjusting by cases
switch grids_on_border
    case 0 % no grids on border
        switch grids_inside
            case 3
                % if there are 3 inside
                % the MP, find the one in
                % hull to adjust and
                % create a triangle
                e(i,2:5) = [isoutCoord(1,1) addpoint(2,1) ...
                    addpoint(1,1) addpoint(1,1)]; % triangle
            case 2
                % if there are 2 inside the
                % MP, find the intersection
                % and create the new quadrangle
                if intercepted <= 2
                    % define if the border cuts the element on
                    % vertical or horizontal
                    deltaout = isoutCoord(1,:)-isoutCoord(2,:);
                    % create quadrangle element
                    if abs(deltaout(1,2)) > abs(deltaout(1,3))
                        addpoint = sortrows(addpoint,2) ;
                        isoutCoord = sortrows(isoutCoord,2);
                        e(i,2:5) = [addpoint(1,1) ...
                            addpoint(2,1) isoutCoord(1,1) ...
                            isoutCoord(2,1)];
                    else
                        addpoint = sortrows(addpoint,3) ;
                        isoutCoord = sortrows(isoutCoord,3);
                        if v(e(i,2:5),2) > 0
                            e(i,2:5) = [addpoint(1,1) ...
                                isoutCoord(1,1) addpoint(2,1) ...
                                isoutCoord(2,1)];
                        else
                            e(i,2:5) = [addpoint(1,1) ...
                                addpoint(2,1) isoutCoord(1,1) ...
                                isoutCoord(2,1)];
                        end
                    end
                end
            case 1
                % if there are 2 grids
                % inside MP and more
                % than 2 intersections
                quad22 = [isoutCoord;addpoint] ;
                DT22 = delaunayTriangulation(quad22...
                    (:,2),quad22(:,3));
        end
    end
end

```

```

        K22      = convexHull(DT22)                ;
        quad22   = quad22(K22(1:size(K22,1)), :)   ;
        IDgrids  = quad22(K22(1:size(K22,1)-1), 1)';
        e(i,2:5) = [IDgrids(1:2) IDgrids(4:-1:3)] ;

    end
case 1                                     % if there is 1 grid inside
                                     % create the triangle with
                                     % the existent points and a
                                     % quadrangle

    DT      = delaunayTriangulation(isoutCoord...
        (:,2), isoutCoord(:,3));
    K        = convexHull(DT)                ;
    tr1l     = isoutCoord(K(1:size(K,1)), :)   ;
    IDgrids   = tr1l(K(1:size(K,1)-1), 1) '    ;
    e(i,2:5)  = [IDgrids IDgrids(3)]          ;
    outpoints = [isoutCoord ; isoutCoord(1,:)] ;
    for k = 1:3
        closedtri = [isinCoord(1,2)...
            isinCoord(1,3); outpoints(k,2)...
            outpoints(k,3); outpoints(k+1,2)...
            outpoints(k+1,3); isinCoord(1,2)...
            isinCoord(1,3)];
        [xx, yy] = polyxpoly(contour(:,1),...
            contour(:,2), closedtri(:,1),...
            closedtri(:,2));
        compare  = [xx yy];
        intersec = [xi yi];
        found    = 0 ;
        for count = 1:size(compare,1) % compares
            % in all the possible orders if there
            % is coincidence or not
            b = intersec ...
                - ones(2,1)*compare(count,:);
            b(abs(b) < 0.0001) = 0

            if sum(any(b,2)) == 1
                found = found + 1
            end
        end
    end
    if found == 2
        % define the order should be in
        % vertical or horizontal direction
        deltaint = [xi(1) yi(1)]...
            - [xi(2) yi(2)] ;
        % create quadrangle element
    end
end
;
;

```

```

        if abs(deltaint(1,1)) ...
            > abs(deltaint(1,2))
            addpoint = sortrows(addpoint,2);
            toelement = sortrows(outpoints...
                (k:k+1,:),2);
            newElement = [size(e,1)+1 ...
                addpoint(1,1) addpoint(2,1) ...
                toelement(1,1) toelement(2,1)];
            % create the quadrangle
            e = [e ; newElement] ;
        else
            addpoint = sortrows(addpoint,3) ;
            toelement = ...
                sortrows(outpoints(k:k+1,:),3);
            if v(e(i,2:5),2) < 0
                addpoint = flipud(addpoint) ;
                toelement = flipud(toelement) ;
            end
            newElement = [size(e,1)+1 ...
                addpoint(1,1) toelement(1,1) ...
                addpoint(2,1) toelement(2,1)];
            % create the quadrangle
            e = [e ; newElement] ;
        end
    end
end
otherwise % grids_inside == 0 (rhombus)
    switch intercepted
        case 4 % grids_inside == 0,
            % onborder == 0
            pair = [] ;
            isoutCoord = v(e(i,2:5),:);
            for k = 1: size(addpoint,1)
                position = dsearchn(isoutCoord(:,...
                    2:3),addpoint(k,2:3));
                pair(k,1)= isoutCoord(position,1) ;
            end
            quad1 = [addpoint(1,:); ...
                v(pair(1,:),:); addpoint(2,:); ...
                v(pair(2,:),:)];
            quad2 = [addpoint(1,:); ...
                v(pair(1,:),:); addpoint(3,:); ...
                v(pair(3,:),:)];
            quad3 = [addpoint(1,:); ...
                v(pair(1,:),:); addpoint(4,:); ...
                v(pair(4,:),:)];

```

```

DT1      = ...
    delaunayTriangulation(quad1(:,1),...
    quad1(:,2));
K1        = convexHull(DT1)          ;
quad1     = quad1(K1(1:size(K1,1)), :) ;
DT2      = ...
    delaunayTriangulation(quad2(:,1),...
    quad2(:,2));
K2        = convexHull(DT2)          ;
quad2     = quad2(K2(1:size(K2,1)), :) ;
DT3      = ...
    delaunayTriangulation(quad3(:,1),...
    quad3(:,2));
K3        = convexHull(DT3)          ;
quad3     = quad3(K3(1:size(K3,1)), :) ;

quad = {[quad1] ; [quad2] ; [quad3]};

% find number of intersections between the previously created triangle and
% decide which has less intersection. This set of grids + the intersection
% point that makes the pair with the current point in use will be one of
% the quadrangles. The other quadrangle is made with what remained.

[x1, y1] = polyxpoly(closedpol(:,1),...
    closedpol(:,2), quad1(:,2),...
    quad1(:,3));
[x2, y2] = polyxpoly(closedpol(:,1),...
    closedpol(:,2), quad2(:,2),...
    quad2(:,3));
[x3, y3] = polyxpoly(closedpol(:,1),...
    closedpol(:,2), quad3(:,2),...
    quad3(:,3));
y1 = [x1, y1]          ;
y2 = [x2, y2]          ;
y3 = [x3, y3]          ;
x1 = size(unique(y1, 'rows'),1);
x2 = size(unique(y2, 'rows'),1);
x3 = size(unique(y3, 'rows'),1);

[val,I] = min([x1, x2, x3])      ;
IDgrids = quad{I}(:,1:4)        ;
e(i,2:5) = [IDgrids(1:2) ...
    IDgrids(4:-1:3)];

others    = ...
    addpoint(~ismember(addpoint(:,1),...
    IDgrids),:);

```

```

        otherpair = ...
            pair(~ismember(addpoint(:,1),...
                IDgrids),:);

        quad22 = [others;v(otherpair,:)] ;
        DT22 = ...
            delaunayTriangulation(quad22(:,2),...
                quad22(:,3));
        K22 = convexHull(DT22) ;
        quad22 = ...
            quad22(K22(1:size(K22,1)),:);
        IDgrids = ...
            quad22(K22(1:size(K22,1)-1),1)';
        e = ...
            [e ; size(e,1)+1 IDgrids(1:2) ...
                IDgrids(4:-1:3)] ;

    case 3
        % find peak of the triangle that
        % determines the opening of MP
        [test, I] = max(addpoint(:,2:3)) ;
        others = addpoint(addpoint(:,...
            3)~=addpoint(I(2),3),:);
        others = sortrows(others,2) ;
        if (others(1,2) < addpoint(I(2),2)) ...
            && (others(2,2) ...
                > addpoint(I(2),2))
            peak = addpoint(I(2),:) ;
        else
            others = addpoint(addpoint(:,3) ...
                ~=addpoint(I(1),3),:);
            others = sortrows(others,3) ;
            if (others(1,3) ...
                < addpoint(I(1),3)) ...
                && (others(2,3) ...
                    > addpoint(I(1),3))
                peak = addpoint(I(1),:) ;
            end
        end
        % find the grids of the element that
        % make pairs with the intersection
        % points.
        pair = [] ;
        isoutCoord = v(e(i,2:5),:);
        options = isoutCoord ;
        for k = 1: size(others,1)
            position = ...

```

```

                                dsearchn(isoutCoord(:,2:3),...
                                others(k,2:3));
                                options(position,:) = 0
;

                                pair(k,1) = ...
                                isoutCoord(position,1) ;
end
options(~any(options,2),:) = [] ;
tri1 = [peak(2:3); others(1,2:3) ; ...
        others(2,2:3) ; peak(2:3)];
quad1 = [peak; options(1,:); ...
        v(pair(1,:),:); others(1,:)] ;
quad2 = [peak; options(2,:); ...
        v(pair(1,:),:); others(1,:)] ;
DT1 = ...
    delaunayTriangulation(quad1(:,1),...
    quad1(:,2)) ;
K1 = convexHull(DT1) ;
quad1 = quad1(K1(1:size(K1,1)),:);
DT2 = ...
    delaunayTriangulation(quad2(:,1),...
    quad2(:,2)) ;
K2 = convexHull(DT2) ;
quad2 = quad2(K2(1:size(K2,1)),:);

% find number of intersections between the previously created triangle and
% decide which has less intersection. This set of grids + the intersection
% point that makes the pair with the current point in use will be one of
% the quadrangles. The other quadrangle is made with what remained.

[x1, y1] = polyxpoly(tri1(:,1), ...
    tri1(:,2), quad1(:,1),quad1(:,2));
[x2, y2] = polyxpoly(tri1(:,1), ...
    tri1(:,2), quad2(:,1),quad2(:,2));
y1 = [x1, y1] ;
y2 = [x2, y2] ;
x1 = size(unique(y1, 'rows'),1);
x2 = size(unique(y2, 'rows'),1);

if x1 < x2
    IDgrids = ...
        quad1(K1(1:size(K1,1)-1),1)' ;
    e(i,2:5)= ...
        [IDgrids(1:2) IDgrids(4:-1:3)];
    quad2 = ...
        [peak; options(2,:); ...
        v(pair(2,:),:); others(2,:)] ;

```



```

DT2      = ...
          delaunayTriangulation(quad2...
                                (:,1),quad2(:,2));
K2       = convexHull(DT2)      ;
quad2    = ...
          quad2(K2(1:size(K2,1)),:);
IDgrids  = ...
          quad2(K2(1:size(K2,1)-1),1)';
e        = [e ; size(e,1)+1 ...
            IDgrids(1:2) IDgrids(4:-1:3)] ;
else
    IDgrids = ...
          quad2(K2(1:size(K2,1)-1),1)';
e(i,2:5) = ...
          [IDgrids(1:2) IDgrids(4:-1:3)];
quad1    = ...
          [peak; options(1,:); ...
           v(pair(2,:),:); others(2,:)] ;
DT1      = ...
          delaunayTriangulation(quad1...
                                (:,1),quad1(:,2))      ;
K1       = convexHull(DT1)      ;
quad1    = ...
          quad1(K1(1:size(K1,1)),:);
IDgrids  = ...
          quad1(K1(1:size(K1,1)-1),1)';
e        = ...
          [e ; size(e,1)+1 ...
            IDgrids(1:2) IDgrids(4:-1:3)] ;
end
case 2
% otherwise % if intercepted > 1
% find how many grids of MP are
% inside the element
[in, on] = inpolygon(closedpol(:,1),...
                    closedpol(:,2),nodesClosed(:,1),...
                    nodesClosed(:,2));
% find ids of the grids in each
% condition: inside, out of and on
% border
coordsin = closedpol(in,:);
% if there is any point from border
% also inside the element, but is not
% the peak
if size(coordsin,1) > 1
    % find peak of the triangle that
    % determines the opening of MP

```

```

[ test, I ] = max(coordsin(:,1:2))
;

posContour = find(sum(ismember...
    (contour,coordsin(I(2),:))' )'...
    )== 2);
if (contour(posContour,1) ...
    <= contour(posContour-1,1)) ...
    && contour(posContour,1) ...
    >= contour(posContour+1,1)
    peak = contour(posContour,:);
else
    posContour = ...
        find(sum(ismember...
            (contour,coordsin(I(1),...
                :))' )' )== 2)
    if(contour(posContour,2) ...
        <= contour(posContour-1,...
            2)) && contour(posContour,...
            2) >= contour(posContour+1,2)
        peak = ...
            contour(posContour,:) ;
    end
end
else
    peak = coordsin;
end
for j = 1: size(peak,1)
    isThereInv = ...
        ismember(v(:,2:3),peak) ;
    % check if there is already such
    % coordinates in v
    idIntersec = find(sum...
        (isThereInv')' == 2);
    % take the existent grid's ID

    if isempty(idIntersec)
        intruder = [size(v,1)+1 peak H];
        % there isn't grid with those
        % coordinates: create
        v = [v ; intruder(j,:)] ;
    else
        if v(idIntersec,4) == H
            intruder = v(idIntersec,:);
            % take the already-existent
            % ID to use
        else
            intruder = [size(v,1)+1 ...

```

```

                                peak H]                                ;
                                % there isn't grid with those
                                % coordinates: create
                                v      = [v ; ...
                                intruder(j,:)]                        ;

                                end
                                end
                                end

% create triangle opposite to the line with intersection tries the
% combinations of triangles formed by pairs of grid + intruder point,
% first west/east, then north/south. The triangle containing the two
% intersections will indicate the pair of grid NOT to be used in the
% wanted triangle

ord      = ...
          sortrows(isoutCoord(),2);
% sort to try west/east
tril      = [intruder(1,2:3); ...
          ord(1,2:3) ; ord(2,2:3) ; ...
          intruder(1,2:3)];
[alfa, beta] = ...
  inpolygon(addpoint(:,2),...
  addpoint(:,3),tril(:,1),...
  tril(:,2));
if sum(beta) == 2
  if v(e(i,2:5),2) > 0
    e(i,:) = [i intruder(1,1) ...
      ord(3,1) ord(4,1) ...
      ord(4,1)]; % triangle
  else
    e(i,:) = [i intruder(1,1) ...
      ord(4,1) ord(3,1) ...
      ord(3,1)]; % triangle
  end
else
  tril      = [intruder(1,2:3); ...
    ord(3,2:3) ; ord(4,2:3) ;...
    intruder(1,2:3)];
  [alfa, beta] = ...
    inpolygon(addpoint(:,2),...
    addpoint(:,3),tril(:,1),...
    tril(:,2));
  if sum(beta) == 2
    if v(e(i,2:5),2) > 0
      e(i,:) = [i ...
        intruder(1,1) ...

```

```

ord(1,1) ord(2,1) ...
ord(2,1)]; % triangle
else
    e(i,:) = [i ...
        intruder(1,1) ...
        ord(2,1) ord(1,1) ...
        ord(1,1)]; % triangle
end
else % sort to try north/south
    ord = ...
    sortrows(isoutCoord,3)

;

    tril = ...
    [intruder(1,2:3); ...
    ord(1,2:3); ord(2,2:3); ...
    intruder(1,2:3)];
    [alfa, beta] = ...
    inpolygon(addpoint(:,2),...
    addpoint(:,3),tril(:,1),...
    tril(:,2)) ;
    if sum(beta) == 2
        if v(e(i,2:5),2) > 0
            e(i,:) = [i ...
                intruder(1,1) ...
                ord(3,1) ord(4,1) ...
                ord(4,1)]; % triangle
        else
            e(i,:) = [i ...
                intruder(1,1) ...
                ord(4,1) ord(3,1) ...
                ord(3,1)]; % triangle
        end
    else
        tril = ...
        [intruder(1,2:3); ...
        ord(3,2:3); ...
        ord(4,2:3); ...
        intruder(1,2:3)];
        [alfa, beta] = ...
        inpolygon(addpoint(:,...
        2),addpoint(:,3),...
        tril(:,1),tril(:,2));
        if sum(beta) == 2
            if v(e(i,2:5),2) > 0
                e(i,:) = [i ...
                    intruder(1,1) ...
                    ord(1,1) ...

```

```

ord(2,1) ...
ord(2,1)]; % triangle
else
    e(i,:) = [i ...
intruder(1,1) ...
ord(2,1) ...
ord(1,1) ...
ord(1,1)]; % triangle
end
else
    i % unpredicted
      % situation
end
end
end
end

% Make the quadrangles
% first find the grids of the element
% that make pairs with the
% intersection points.
pair = [];
options = isoutCoord;
for k = 1: size(addpoint,1)
    position = ...
        dsearchn(isoutCoord(:,2:3), ...
        addpoint(k,2:3));
    options(position,:) = 0
;

    pair(k,1) = ...
        isoutCoord(position,1) ;
end
options(~any(options,2),:) = []
;

% make trial triangles with the
% intruder, one of the grids of the
% pair and the two options of grids
% that don't make pairs with the
% intersections. (pairs = closest)
firsttri = [e(i,2) e(i,3) e(i,4) ...
e(i,2)];
firsttri = v(firsttri,2:3) ;
secondtri = [intruder(1,2:3); ...
addpoint(1,2:3); addpoint(2,2:3); ...
intruder(1,2:3)];
quad1 = [intruder(1,2:3); ...

```

```

        addpoint(1,2:3); ...
        v(pair(1,:),2:3); options(1,2:3)] ;
quad2      = [intruder(1,2:3); ...
        addpoint(1,2:3); ...
        v(pair(1,:),2:3); options(2,2:3)] ;
DT          = ...
        delaunayTriangulation(quad1(:,1),...
        quad1(:,2));
K           = convexHull(DT)                ;
quad1       = quad1(K(1:size(K,1)),:);      ;
DT          = ...
        delaunayTriangulation(quad2(:,1),...
        quad2(:,2));
K           = convexHull(DT)                ;
quad2       = quad2(K(1:size(K,1)),:);      ;

% find number of intersections between
% the previously created triangle of
% the beginning and decide which has
% less intersection. This set of grids
% + the intersection point that makes
% the pair with the current point in
% use will be one of the quadrangles.
% The other quadrangle is made with
% what remained.

[x1, y1] = polyxpoly(firsttri(:,1), ...
        firsttri(:,2), quad1(:,1),...
        quad1(:,2));
[x2, y2] = polyxpoly(firsttri(:,1), ...
        firsttri(:,2), quad2(:,1),...
        quad2(:,2));
y1        = [x1, y1]                        ;
y2        = [x2, y2]                        ;
x1        = size(unique(y1, 'rows'),1) ;
x2        = size(unique(y2, 'rows'),1) ;
if x1 == x2
    [x1, y1] = ...
        polyxpoly(secondtri(:,1), ...
        secondtri(:,2), quad1(:,1),...
        quad1(:,2));
    [x2, y2] = ...
        polyxpoly(secondtri(:,1), ...
        secondtri(:,2), quad2(:,1),...
        quad2(:,2));
y1        = [x1, y1]                        ;
y2        = [x2, y2]                        ;

```

```

        x1      = size(unique(y1, ...
            'rows'),1);
        x2      = size(unique(y2, ...
            'rows'),1);
    end
    if x1 < x2
        listofpoints1 = [intruder; ...
            v(pair(1,:), options(1,:); ...
            addpoint(1,:)] ;
        listofpoints2 = [intruder; ...
            v(pair(2,:), options(2,:); ...
            addpoint(2,:)] ;
    else
        listofpoints1 = [intruder; ...
            v(pair(2,:), options(2,:); ...
            addpoint(1,:)] ;
        listofpoints2 = [intruder; ...
            v(pair(1,:), options(1,:); ...
            addpoint(2,:)] ;
    end

    % element of listofpoints1
    DT      = ...
        delaunayTriangulation(...
        listofpoints1(:,2),...
        listofpoints1(:,3));
    K      = convexHull(DT)          ;
    IDgrids = ...
        listofpoints1(K(1:size(K,1)-1),1)';
    e      = [e ; size(e,1)+1 ...
        IDgrids(1:2) IDgrids(4:-1:3)]    ;

    % element of listofpoints2
    DT      = ...
        delaunayTriangulation(...
        listofpoints2(:,2),...
        listofpoints2(:,3));
    K      = convexHull(DT)          ;
    IDgrids = listofpoints2(K(1:size...
        (K,1)-1),1)'                ;
    e      = [e ; size(e,1)+1 ...
        IDgrids(1:2) IDgrids(4:-1:3)]    ;
case 1
    % do nothing
end
end
case 1

```

```

        if grids_inside == 3 % if there are
            % 3 inside the MP, and 1 on border create the
            % triangle
            e(i,2:5) = [isoutCoord(1,1) addpoint(1,1) ...
                isonCoord(1,1) isonCoord(1,1)]; % triangle
        elseif grids_inside == 2 % if there are
            % 2 inside the MP, find the intersection and create
            % a quadrangle
            deltaout = isoutCoord(1,:) - isoutCoord(2,:);
            if abs(deltaout(1,2)) > abs(deltaout(1,3))
                addpoint = sortrows([isonCoord ; addpoint],2);
                isoutCoord = sortrows(isoutCoord,2) ;
            else
                addpoint = sortrows([isonCoord ; addpoint],3);
                isoutCoord = sortrows(isoutCoord,3) ;
            end
            % create quadrangle elements
            e(i,2:5) = [isoutCoord(1,1) isoutCoord(2,1) ...
                addpoint(2,1) addpoint(1,1)];
        else % if grids inside is 1
            % stay as it is, since on border is considered
            % inside also, this is the one on border
        end
    case 2 % grids_inside cannot be == 1 because the 2 on
        % border are also considered inside
        if grids_inside == 3 % if there are 3 inside the MP,
            % and 2 on border
            e(i,2:5) = [isoutCoord(1,1) isonCoord(1,1) ...
                isonCoord(2,1) isonCoord(2,1)]; % triangle
        else % grids_inside == 2 % if there are 2
            % inside the MP, both on
            % border
            % stay as it is, since on border is considered
            % inside also
        end
    otherwise
        grids_on_border
        grids_inside
        % if grids_inside == 3, the element cannot be inside the moon
        % pool. Also, grids_inside cannot be less than 3, since the
        % ones on border are also considered inside
    end
end
end
end
stay = find(e(:,1)) ;
e = [[1:size(stay,1)]' e(stay,2:5)];

```



```
disp('fim')
end
```

6. D_Geom_Pontos.m

```
function [realpar] = d_Geom_Pontos( v, e, LS, shape, divs)
% Function that makes the moonpool points data matrix.

l1 = LS(1); %
l2 = LS(2); %
l3 = LS(3); %
m1 = shape(1); %
m2 = shape(2); %
m3 = shape(3); % ASSIGN PARAMETERS.
m4 = shape(4); %
nf = shape(5); %
nt = shape(6); %
div = divs(1); %
H = divs(2); %

% Rounding m-parameter values to avoid tiny elements on SF—————%
% deciding if ellipses should exist or not, in mkEllipse
% deciding if middle rectangle should exist or not, in mkMidRec
% deciding if ext rectangles should exist or not, in mkExRec

mkEllipsef = 1;
mkExRecf = 1;
mkEllipsea = 1;
mkExReca = 1;
mkMidRec = 1;

% fore ellipse and external rectangle
if m1 >= 0.98*l2
    m1 = 12;
    m2 = 11;
    mkEllipsef = 0 ;
elseif m1 < 0.1*div
    m1 = 0 ;
    mkExRecf = 0 ;
end
if m2 >= 0.98*l1
    m2 = 11;
    m1 = 12;
    mkEllipsef = 0 ;
    mkExRecf = 0 ;
```

```

end

% aft ellipse and external rectangle
if m4 >= 0.98*l2
    m4          = 12;
    m3          = 13;
    mkEllipsea  = 0 ;
elseif m4 < 0.1*div
    m4          = 0 ;
    mkExReca   = 0 ;
end

if m3 >= 0.98*l3
    m3          = 13;
    m4          = 12;
    mkEllipsea  = 0 ;
    mkExReca   = 0 ;
end

% mid rectangle
if m2+m3 < 0.1*div
    m2          = 0 ;
    m3          = 0 ;
    mkMidRec    = 0 ;
end

% Prepare division values to space grids -----%
numdivz      = max(1, floor(H/div))      ;
dz           = H/numdivz                 ;
numDivRecExtxf = max(1, floor((l1-m2)/div)); % number of x divisions in
                                           % the external rectangles fore
numDivRecExtyf = max(1, floor(m1/div))    ; % number of y divisions in the
                                           % external rectangles fore
numDivRecExtxa = max(1, floor((l3-m3)/div)); % number of x divisions in the
                                           % external rectangles aft
numDivRecExtya = max(1, floor(m4/div))    ; % number of y divisions in the
                                           % external rectangles aft
ndxMd        = max(1, floor((m2+m3)/div)); % number of x divisions in the
                                           % mid rectangle
numdivyMd    = max(1, floor(l2/div))      ;
dxmf         = (l1-m2)/numDivRecExtxf    ; % dx of the external rectangle
                                           % fore
dxa          = (l3-m3)/numDivRecExtxa    ; % dx of the external rectangle
                                           % aft
dxMd         = (m2+m3)/ndxMd             ; % dx of the mid rectangle
dyf          = m1/numDivRecExtyf         ; % dy of the external rectangle
                                           % fore

```

```
dya          = m4/numDivRecExtYa      ; % dy of the external rectangle  
                                         % aft  
dyMd         = l2/numdivyMd           ; % dy of the mid rectangle  
numdivForeEllipsey = floor((l2-m1)/div) ; % number of vertical divisions  
                                         % of the fore ellipse fore  
numdivAftEllipseY   = floor((l2-m4)/div) ; % number of vertical divisions  
                                         % of the fore ellipse aft  
  
% % % % % % % % % % % % % % % % % % % the two following parameters should  
% disappear but they are used as input for FORTRAN! Make adaptations in  
% Fortran to be independent of them  
numdivx       = numDivRecExtxf + ndxMd + numDivRecExtxa;  
numdivy       = numdivyMd           ;  
% % % % % % % % % % % % % % % % % % % % % % % % % % % % % % % % % % % % % %  
  
% Generate the coordinates for the fore elliptical corner -----  
if mkEllipsef == 1  
    a = l1-m2      ; % First radius of the fore quarter of ellipse.  
    b = l2-m1      ; % Second radius of the fore quarter of ellipse.  
    % number of offsets of the fore quarter of ellipse: bigger subdivision  
    % due to exaggerated areas in polar elements  
    nda = floor((1.5*numDivRecExtxf+1.5*numdivForeEllipsey)/2);  
    da = a/max(nda,1); % dx of the horizontal radius of fore quarter of  
                        % ellipse  
    db = b/max(nda,1); % dy of the vertical radius of fore quarter of  
                        % ellipse  
  
    dthetaf = pi/2/nf; % Determ. 'dtheta' angular interval of fore quarter  
                        % of ellipse.  
    x1 = l1          ; % initiate x1 with the first position at theta = 0  
    y1 = m1          ; % idem for y1  
  
    nfreal = 1;  
    thetarealf = 0;  
    for theta = dthetaf:dthetaf:pi/2  
        xi = m2 + a*cos(theta);  
        yi = m1 + b*sin(theta);  
        if sqrt((xi - x1(size(x1,1),1))^2+ ...  
            (yi - y1(size(y1,1),1))^2) >= div/4  
            x1 = [x1 ; xi];  
            y1 = [y1 ; yi];
```

```

        nfrealf = nfrealf + 1;
        thetarealf = [thetarealf theta];
    end
end

nfrealf = nfrealf - 1;    % When increasing inside if, it counts
                        % the points. Converting to number of segments
if sqrt((xi - x1(size(x1,1),1))^2 + (yi - y1(size(y1,1),1))^2) <= div/4
    x1 = x1(1:size(x1,1)-1,1);
    y1 = y1(1:size(y1,1)-1,1);
    thetarealf(size(thetarealf,2)) = pi/2;
end

x1 = [x1 ; xi];
y1 = [y1 ; yi];
end

% Generate the coordinates for the aft elliptical corner -----%
if mkEllipsea == 1
    c = l3-m3          ; % First radius of the aft quarter of ellipse.
    d = l2-m4          ; % Second radius of the aft quarter of ellipse.
    % number of offsets of the fore quarter of ellipse: bigger subdivision
    % due to exaggerated areas in polar elements
    ndc = floor((1.5*numDivRecExtxa+1.5*numdivAftEllipsey)/2);
    dc = c/max(ndc,1); % dx of the horizontal radius of aft
                    % quarter of ellipse
    dd = d/max(ndc,1); % dy of the vertical radius of aft
                    % quarter of ellipse

    dthetat = pi/2/nt; % Determine the 'dtheta' angular interval of
                    % the aft quarter of ellipse.
    x2 = -m3          ; % initiate x2 with the first position at theta = 0
    y2 = l2            ;

    ntreal = 1;
    thetareala = pi/2;
    for theta = pi/2 + dthetat:dthetat:pi
        xi = -m3 + c*cos(theta);
        yi = m4 + d*sin(theta);
        if sqrt((xi - x2(size(x2,1),1))^2 + ...
            (yi - y2(size(y2,1),1))^2) >= div/4
            x2 = [x2 ; xi];
            y2 = [y2 ; yi];
            ntreal = ntreal + 1;
            thetareala = [thetareala theta];
        end
    end
end

```

```

    ntreal = ntreal - 1;    % When increasing inside if, it counts
                           % the points. Converting to number of segments
    if sqrt((xi - x2(size(x2,1),1))^2+(yi - y2(size(y2,1),1))^2) <= div/4
        x2 = x2(1:size(x2,1)-1,1);
        y2 = y2(1:size(y2,1)-1,1);
        thetareala(size(thetareala,2)) = pi;
    end
    x2 = [x2 ; xi];
    y2 = [y2 ; yi];
end

% Generate the sequence of points of straight line and curves -----%
sequence = [l1 0];
% Fore vertical line
if m1 ~= 0
    yvalsf = 0                ; % y values of external
                               % fore rectangle to offset later

    for i = 1:numDivRecExtyf
        yvalsf = [yvalsf ; i*dyf] ;
    end
    offsetyef = ones(size(yvalsf)) ; % offset vertical lines vector for
                                       % external rectangle fore
    sequence = [sequence ; [l1*offsetyef yvalsf]];
end

% Fore ellipse
if mkEllipsef == 1
    sequence = [sequence ; [x1 y1]];
end

% Mid horizontal straight line
if m2+m3 == 0
    sequence = [sequence ; [0 l2]];
else
    xvalsmid = m2;            % x values of mid rectangle to offset later
    for i = 1:ndxMd
        xvalsmid = [xvalsmid ; m2-i*dxMd];
    end
    offsetxmd = ones(size(xvalsmid)); % offset horizontal
                                       %lines vector for mid rectangle
    sequence = [sequence ; [xvalsmid l2*offsetxmd]];
end

% aft ellipse
if mkEllipsea == 1
    sequence = [sequence ; [x2 y2]];
end

```

```

end
% Aft vertical line
if m4 ~= 0
    yvalsa = m4;
    for i = 1:numDivRecExtya
        yvalsa = [yvalsa ; m4-i*dya];
    end
    offsetyea = ones(size(yvalsa)); % offset vertical lines vector
                                     % for external rectangle aft
    sequence = [sequence ; [-l3*offsetyea yvalsa]];
end

% Clean repeated points -----
for i = 1: size(sequence, 1)          % truncating values to be able
                                     % to find repeated
    for j = 1: size (sequence, 2)
        sequence(i,j) = round(sequence(i,j)/0.001)*0.001;
    end
end

contour = sequence(1,:);

for i = 2: size (sequence,1)          % copy sequence, skipping repeated grid
    deltax = sequence(i,1) - sequence(i-1,1); % if there is a big
                                               % distance, discretizes
    deltay = sequence(i,2) - sequence(i-1,2);
    if deltax ~= 0 || deltay ~= 0
        dist = sqrt(deltax^2+deltay^2);
        if dist > div
            kdiv = floor(dist/div); % number of possible divisions
            if (kdiv == 1) && (dist/div >= 1.5*div)
                contour = [contour ; [sequence(i-1,1)+deltax/2 ...
                    sequence(i-1,2)+deltay/2]];
            else
                dxplusdiv = deltax/kdiv;
                dyplusdiv = deltay/kdiv;
                for j = 1: kdiv - 1
                    contour = [contour ; [sequence(i-1,1)+j*dxplusdiv ...
                        sequence(i-1,2)+j*dyplusdiv]];
                end
            end
        end
        contour = [contour ; sequence(i,:)];
    end
end

% Adjust grid border ID to be a sequence of v later -----

```

```

startMP = size(v,1) + 1 ;

[ v, e ] = d_Elim_Linhas_Pontos( v, e, contour, H );

idv = size(v,1);      % last grid ID
ide = size(e,1);      % last element ID

% Rewrite the input elements in format and order of indices for gmsh -----%
countq = 1 ;
countt = 1 ;

for i = 1: size(e,1)
    if e(i,2) == e(i,3)
        e(i,:) = [e(i,1) e(i,2) e(i,4) e(i,5) e(i,5)] ;
    elseif e(i,2) == e(i,4)
        e(i,:) = [e(i,1) e(i,2) e(i,3) e(i,5) e(i,5)] ;
    elseif e(i,2) == e(i,5)
        e(i,:) = [e(i,1) e(i,2) e(i,3) e(i,4) e(i,4)] ;
    elseif e(i,3) == e(i,4)
        e(i,:) = [e(i,1) e(i,2) e(i,3) e(i,5) e(i,5)] ;
    elseif e(i,3) == e(i,5)
        e(i,:) = [e(i,1) e(i,2) e(i,3) e(i,4) e(i,4)] ;
    end
end

% Write vertical coordinates for each water plane offset of contour -----%
% 0 is the top of moon pool and H is the base.
sizecontour = size(contour,1) ;
zc = [] ;
for i=1:(numdivz+1) % each column is one ordinate defined by dz
    zc(:,i) = dz*(numdivz+1-i)*ones(sizecontour,1);
end

% Build the moonpool points data matrix -----%
points = [contour zc(:,1)]; % offset the contour for each height
for i=2:numdivz+1 % the number of levels is divz+1
    points = [points ; [contour zc(:,i)]];
end
MPpoints = [];
for i = 1:size(points,1) % assign ID to the MP
    MPpoints(i,:) = [idv+i points(i,:)] ;
end

% Elements of MP wall -----%
MPparam = idv + 1 ; % parameter to compose the element
o = size(contour,1); % size of 1 loop of grids
MPmesh = [] ;

```

```

counter      = 1                      ;
for i = 1:(o-1)*numdivz
    MPmesh(i,:)      = [ide+i MPparam MPparam+1 MPparam+o MPparam+1+o];
    MPparam          = MPparam + 1;
    if counter == o-1          % skips 1 number in counter when
                                % the element column ends
        MPparam = MPparam + 1;
        counter = 1          ;
    else
        counter = counter + 1;
    end
end

idv      = idv + size(MPpoints,1)  ;
ide      = ide + size(MPmesh,1)    ;
startSFv = idv + 1                 ;
startSFe = ide + 1                 ;

totgrid  = [v ; MPpoints]          ;
totelem  = [e ; MPmesh ]           ;

% Create the free surface grid -----%
% Can only be done in this stage because the repeated points were
% eliminated at the creation of matrix contour. Decision upon making or
% not each piece are made here with mkEllipse, mkExRec etc.

% vectors of radii a and b to generate the free surface mesh grid of fore
% ellipse

% Generate grid and elements of fore ellipse -----%
if mkEllipsef == 1
    % vector of the points that divide the horiz radius of fore ellipse
    vecta = 11;
    if nda > 0
        for i = 1:nda
            vecta = [vecta ; (11-i*da)]; % subtracts da, creating from
                                           % outside in
        end
    end
    % vector of the points that divide the vert radius of fore ellipse
    vectb = 12;
    if nda > 0
        for i = 1:nda
            vectb = [vectb ; (12-i*db)];
        end
    end
end

```



```

gx1 = x1; % initializing the grids with the
gy1 = y1; % already calculated part in contour
% fore ellipse grid
oa = size(vecta,1); % size of 1 loop of grids fore ellipse
if oa > 1 % if there is more than the external arch
    for i = 2:oa-1 % starts from 2 because the first value
        % was already used
        a = vecta(i) - m2; % First radius of the fore quarter
        % of ellipse.
        b = vectb(i) - m1; % Second radius of the fore quarter
        % of ellipse.
        for j = 1:size(thetarealf,2)
            gx1 = [gx1 ; m2 + a*cos(thetarealf(j))];
            gy1 = [gy1 ; m1 + b*sin(thetarealf(j))];
        end
    end
end
gx1 = [gx1 ; m2];
gy1 = [gy1 ; m1];

elgridf = [(idv+1):(idv+size(gx1,1))] ' gx1 gy1 zeros(size(gy1));

% fore ellipse elements
param = idv + 1; % parameter to compose the element
counter = 1 ;

ellf = []; % creates ellf
for i = 1:(nfreal)*(oa-2) % elements of fore ellipse
    ellf(i,:) = [ide+i param param+1 param+nfreal+1 ...
        param+nfreal+2];
    param = param + 1;
    if counter == nfreal % skips 1 number in counter
        % when the element column ends
        param = param + 1;
        counter = 1 ;
    else
        counter = counter + 1;
    end
end

if isempty(i); i = 0; end
idv = idv + size(elgridf,1);
ide = ide + i ;

nn = size(elgridf,1) ; % triangle elements of fore corner.

for i = 1:nfreal

```

```

        ellf = [ellf ; [ide+i elgridf(nn,1) elgridf(nn-nfreal-2+i,1) ...
        elgridf(nn-nfreal-1+i,1) elgridf(nn-nfreal-1+i,1)]];
    end

    ide      = ide + i      ;
    totgrid = [totgrid ; elgridf];
    totelem = [totelem ; ellf  ];
end

% Generate grid and elements of aft ellipse ----- %
if mkEllipsea == 1
    % vector of the points that divide the horiz radius of aft ellipse
    vectc = -l3;
    if ndc > 0
        for i = 1:ndc
            vectc = [-(l3-i*dc) ; vectc];
        end
    end

    % vector of the points that divide the vert radius of aft ellipse
    vectd = l2;
    if ndc > 0
        for i = 1:ndc
            vectd = [ l2-i*dd ; vectd];
        end
    end

    % Generate grid of the elliptical corners ----- %
    gx2 = x2; % initializing the grids with the
    gy2 = y2; % already calculated part in contour

    % aft ellipse grid
    vectc = flipud(vectc);
    vectd = flipud(vectd);
    oc = size(vectc,1) ; % size of 1 loop of grids aft ellipse
    if oc > 1
        for i = 2:oc-1 % starts from 2 because the first
            % value was already used
            c = vectc(i) + m3; % First radius of the aft quarter
            % of ellipse.
            d = vectd(i) - m4; % Second radius of the aft quarter
            % of ellipse.
            for j = 1:size(thetareala,2)
                gx2 = [gx2 ; -(m3 + c*cos(thetareala(j)))];
                gy2 = [gy2 ; m4 + d*sin(thetareala(j)) ];
            end
        end
    end

    gx2 = [gx2 ; -m3];

```

```

gy2 = [gy2 ; m4];

elgrida = [(idv+1):(idv+size(gx2,1))] ' gx2 gy2 zeros(size(gy2));

% aft ellipse elements
param = idv + 1; % parameter to compose the element
counter = 1 ;

ell = []; % creates ell
for i = 1:(ntreal)*(oc-2) % elements of aft ellipse
    ell = [ell ; [ide+i param param+1 param+ntreal+1 ...
        param+ntreal+2]];
    param = param + 1;
    if counter == ntreal % skips 1 number in counter when
        % the element column ends
        param = param + 1;
        counter = 1 ;
    else
        counter = counter + 1;
    end
end

if isempty(i); i = 0; end
idv = idv + size(elgrida,1);
ide = ide + i ;

% triangle elements of aft corner
nn = size(elgrida,1);
for i = 1:ntreal
    ell = [ell ; [ide+i elgrida(nn,1) elgrida(nn-ntreal-2+i,1) ...
        elgrida(nn-ntreal-1+i,1) elgrida(nn-ntreal-1+i,1)]];
end

ide = ide + i ;
totgrid = [totgrid ; elgrida] ;
totelem = [totelem ; ell ] ;
end

% Generate grid and elements of external fore rectangle -----%
if mkExRecf == 1
    gridexrecf = [l1*offsetyef yvalsf]; % grid external rectangle fore
    for i = 1: numDivRecExtxf
        gridexrecf = [gridexrecf ; ((l1-i*dxf)*offsetyef yvalsf)];
    end
    gridexrecf = [v(1:size(gridexrecf,1),1)+idv gridexrecf ...
        zeros(size(gridexrecf,1),1)];

```

```

% elements
param = idv+1          ;
o      = size(offsetyef,1);          % number of grid in one
                                       %single loop fore ext rectangle
for i = 1:numDivRecExtxf*numDivRecExtyf
    elexrecf(i,:) = [ide+i param param+1 param+o param+o+1];
    param          = param + 1          ;
    if counter == o-1          % skips 1 number in counter
                                % when the element column ends
        param      = param + 1;
        counter    = 1          ;
    else
        counter = counter + 1;
    end

end

idv      = idv + size(gridexrecf,1);
ide      = ide + i          ;
totgrid = [totgrid ; gridexrecf] ;
totelem = [totelem ; elexrecf  ] ;
end

% Generate grid and elements of external aft rectangle -----%
if mkExReca == 1
    yvalsa      = flipud(yvalsa);          % flip upside down because of
                                           % the order it is used in contour
    gridexreca   = [-l3*offsetyea yvalsa]; % grid external rectangle aft
    for i = 1: numDivRecExtxa
        gridexreca = [[-(l3-i*dxa)*offsetyea yvalsa] ; gridexreca];
    end
    gridexreca = [v(1:size(gridexreca,1),1)+idv gridexreca ...
        zeros(size(gridexreca,1),1)];

    % elements
    param = idv+1          ;
    o      = size(offsetyea,1);          % number of grid in one single
                                           % loop aft ext rectangle
    for i = 1:numDivRecExtxa*numDivRecExtya
        elexreca(i,:) = [ide+i param param+1 param+o param+o+1];
        param          = param + 1          ;
        if counter == o-1          % skips 1 number in counter when
                                    % the element column ends
            param      = param + 1 ;
            counter    = 1          ;
        else
            counter = counter + 1;
        end
    end
end

```

```

        end
    end
    idv      = idv + size(gridexreca,1);
    ide      = ide + size(elexreca,1) ;
    totgrid = [totgrid ; gridexreca] ;
    totelem = [totelem ; elexreca  ] ;
end
% Generate grid of the mid rectangle -----%
if mkMidRec == 1
    valsynd = 0;                % values in y column of the mid rectangle
                                % to offset
    for i = 1: numdivyMd
        valsynd = [valsynd ; i*dyMd] ;
    end
    gridRecMd = [m2*ones(size(valsynd)) valsynd];
    for i = 1:ndxMd
        gridRecMd = [gridRecMd ; [(m2-i*dxMd)*ones(size(valsynd)) valsynd]];
    end
    gridRecMd = [v(1:size(gridRecMd,1),1)+idv gridRecMd ...
        zeros(size(gridRecMd,1),1)];

    % elements
    param = idv+1 ;
    o      = size(valsynd,1);    % number of grid in one single loop mid
                                % rectangle
    for i = 1:ndxMd*numdivyMd
        elmd(i,:) = [ide+i param param+1 param+o param+o+1];
        param     = param + 1;
        if counter == o-1    % skips 1 number in counter when the
                            % element column ends
            param = param + 1 ;
            counter = 1 ;
        else
            counter = counter + 1;
        end
    end
    ide      = ide + i ;
    idv      = idv + size(gridRecMd,1);
    totgrid = [totgrid ; gridRecMd ] ;
    totelem = [totelem ; elmd      ] ;
end

% Collection of grids and elements -----%
n_grid_SF = size(totgrid,1)-startSFv+1;
n_elem_SF = size(totelem,1)-startSFe+1;

```

```
d_Pre_Escritor(totgrid, totelem, l1, l2, l3, H, numdivx, ...
    numdivy, numdivz, n_grid_SF, n_elem_SF, startMP);

if mkEllipsef == 0
    nfreal = 999;
end
if mkEllipsea == 0
    ntreal = 999;
end

realpar = [m1; m2; m3; m4; nfreal; ntreal];

disp('fim')
end
```

7. D_Pre_Escrevedor.m

```
function d_Pre_Escrevedor(totgrid, totelem, l1, l2, l3, H, divx, divy,...  
    divz, startSFv, startSFe,startMp)  
% Writes three files: one .msh file for Gmsh visualization, one .dat input  
% for the .exe module and a .vtk file for ParaView visualization.  
  
% % % % % .dat file % % % % % % % % % % % % % % % % % % % % % % % % % % % % % %  
mpdamping = textread('input_hull.txt','%.2f', 1,'headerlines',2);  
  
% Create file for the hydrodynamic response module _____%  
fidl = fopen('PANEL.drill-ship.dat','wt');  
% fidl = fopen(fullfile(folder_name,'\PANEL.drill-ship.dat'),'wt');  
  
fprintf(fidl, '''Panel data ''\n') ;  
fprintf(fidl, '''Opening front x coordinate (m) '' %.2f\n',l1) ;  
fprintf(fidl, '''Opening aft. x coordinate (m) '' %.2f\n',-l3);  
fprintf(fidl, '''Width (half) (m) '' %.3f\n',l2) ;  
fprintf(fidl, '''Height (m) '' %.3f\n',H) ;  
  
fprintf(fidl, '''Total Grid '' %u %u %u \n',...  
    size(totgrid,l),startSFv,startMp);% actually startSFv is dummy  
fprintf(fidl, '''Total Panel & Free surface panel '' %u %u\n',...  
    size(totelem,l),startSFe);  
  
fprintf(fidl, '''Moon pool data''\n') ;  
fprintf(fidl, '''Fore Division '' %u\n',divy) ;  
fprintf(fidl, '''Side Division '' %u\n',divx) ;  
fprintf(fidl, '''Height Division '' %u\n',divz) ;  
fprintf(fidl, '''Rayleigh Damping '' %.2f\n',mpdamping);  
fprintf(fidl, '''Grid coordinate No. x y z (m)''\n') ;
```

```
% Print the grid -----%
fprintf(fid1,sprintf('%u %0.9f %0.9f %0.9f\n',totgrid.'));

% Print the mesh -----%

fprintf(fid1,sprintf('%u %u %u %u %u\n',totelem.'));

fclose(fid1);


%% .msh file %%%%%%%%%%%%%%
fid2 = fopen('PANEL.drill-ship.msh','wt');      % creates file gmsh file

fprintf(fid2,'$MeshFormat\n');                  % headings begin
fprintf(fid2,'2.2 0 8\n');
fprintf(fid2,'$EndMeshFormat\n');
fprintf(fid2,'$Nodes\n');                      % headings end
fprintf(fid2,'%u\n', size(totgrid,1));          % number of grid

% Print the grid -----%

fprintf(fid2,sprintf('%u %0.9f %0.9f %0.9f\n',totgrid.'));

% Headings elements -----%

fprintf(fid2,'$Elements\n');                   % headings end
fprintf(fid2,'%u\n', size(totelem,1));         % number of elements

% Print the mesh -----%

for i=1:size(totelem,1),
    if totelem(i,4) ~= totelem(i,5)
        fprintf(fid2,'%u %u %u %u %u %u %u %u\n', totelem(i,1), 3, 2,...
            0, 6, totelem(i,2), totelem(i,3), totelem(i,5), totelem(i,4).');
    else
        fprintf(fid2,'%u %u %u %u %u %u %u %u\n', totelem(i,1), 2, 2, 0,...
            6, totelem(i,2), totelem(i,3), totelem(i,4).');
    end
end

% Finish and close file -----%

fprintf(fid2,'$EndElements\n');                % end of file
fclose(fid2);
```



```

disp('enter runcommand');

status      = 1000                                ; % initializing with
% an improbable value from system output
[realpar] = d_Geom_Pontos( v, e, LS, shape, divs); % generate
% individual's mesh
eval        = 0                                    ; % initializing
% information of eligibility of output files with 'no'

% Write the log in the file 'log.txt' -----%
fid = fopen('logs.txt','wt')                        ;
fprintf(fid,'Criteria for evaluation and deletion used for this ...
folder\n')      ;
fprintf(fid,['initiated eval (0): ',num2str(eval),'\n'])      ;
fprintf(fid,'L1, L2, L3:\n')                                  ;
fprintf(fid,sprintf('%0.9f\n %0.9f\n %0.9f\n',LS.'))          ;
fprintf(fid,'m1, m2, m3, m4, nf, nt:\n')                    ;
fprintf(fid,sprintf('%0.9f\n %0.9f\n %0.9f\n %0.9f\n %0.9f\n %0.9f\n',...
    shape.')) ;
fprintf(fid,'div, H:\n')                                      ;
fprintf(fid,sprintf('%0.9f\n %0.9f\n',divs.'))                ;
fprintf(fid,'real parameters after mesh generation')         ;
fprintf(fid,sprintf('%0.9f\n %0.9f\n %0.9f\n %0.9f\n %0.9f\n %0.9f\n',...
    realpar.'));

% Run analysis until the system informs its end -----%
while status == 1000
    % execute the hydrodynamic calculation module
    command = 'Hydrodynamic.exe'                        ;
    status = system(command)                             ;
    fprintf(fid,['status after running fortran (0): ',num2str(status),...
        '\n']);
end
disp('finished hydrodynamic module');

% Check if the files of interest are ok and register log -----%
dirStruct1 = dir('DRILL SHIP -MOTION-SPECTRUM.DAT')      ;
dirStruct2 = dir('DRILL SHIP -MOON-POOL-SPECTRUM.DAT')    ;
dirStruct3 = dir('DRILL SHIP -DRIFT-FORCE-SPECTRUM.DAT');

if ~isempty(dirStruct1) && ~isempty(dirStruct2) && ~isempty(dirStruct3)
    fileSize1 = dirStruct1.bytes; % return the file size
    fileSize2 = dirStruct2.bytes; % return the file size
    fileSize3 = dirStruct3.bytes; % return the file size
    fprintf(fid,['MOTION-SPECTRUM(154Kb): ',num2str(fileSize1),'\n']) ;
    fprintf(fid,['MOON-POOL-SPECTRUM(137Kb): ',num2str(fileSize2),...
        '\n']) ;

```

```

fprintf(fid, ['DRIFT-FORCE-SPECTRUM(158Kb): ', num2str(fileSize3), ...
    '\n']);
if fileSize1 >= 153000 % no problem file has 154Kb
    fprintf(fid, 'fileSize1 (MOTION-SPECTRUM) approved\n');
    if fileSize2 >= 136000 % no problem file has 137Kb
        fprintf(fid, 'fileSize2 (MOON-POOL-SPECTRUM) approved\n');
        if fileSize3 >= 157000 % no problem file has 158Kb
            fprintf(fid, ...
                'fileSize3 (DRIFT-FORCE-SPECTRUM) approved\n');
            eval = 1; % if all the files are OK,
                    % eligibility becomes 'yes'
            disp ('simulation ok');
        end
    end
end
end
end
% Delete copied files to save space. Has to be done here because the
% folder will not be accessed by Eval_data, since eval = 0
delete('d_*.*)' ;
delete('input_hull.txt') ;
delete('WAVE.CONDITION*.*)' ;
delete('Principal.DrillShip*.*)' ;
delete('*.exe') ;

fprintf(fid, ['eval after deletion: ', num2str(eval), '\n']);
if eval ~= 1 && eval ~= 0
    fprintf(fid, 'eval neither defined as 1 nor 0\n') ;
end
centroide ;
cd ../../../../ % return to folder of origin where Gamma
                % file is placed

fclose(fid);
disp('exit runcommand');
end

```

9. Eval_Data.m

```

function [ nota, P ] = Eval_Data(folder_name)
% A: radar chart area ; D1, D2: tiebreak grades; GR: resultant
% polygon points

disp('enter eval_data');

% Read input parameters.-----%
fileID = fopen('Optimization_Parameters.dat', 'r') ;

```

```

% Sea states to perform analysis
line_data = textscan(fileID, '%*[^']' %d', 6, 'HeaderLines', 18);
sea_opt    = line_data{1}                                ;

% Choose significant wave periods to perform analysis
line_data = textscan(fileID, '%f', 'HeaderLines', 2)      ;
T_opt      = transpose(line_data{1})                      ;
fclose(fileID)                                           ;

sea_states = {'IACS LONG CRESTED'; 'IACS SHORT CRESTED';
              'JONSWAP LONG CRESTED'; 'JONSWAP SHORT CRESTED';
              'Bretschneider LONG CRESTED'; 'Bretschneider SHORT CRESTED'};

% Find location of the data of interest -----%
C = textread(fullfile(folder_name, 'DRILL SHIP -MOTION-SPECTRUM.DAT'), ...
              '%s', 'delimiter', '\n') ;
line_mark1 = [];
for i = 1:size(C,1);
    if strcmp(C{i}, '***** STANDARD DEVIATION OF RESPONSE *****')
        line_mark1{end+1} = i;
    end
end

D = textread(fullfile(folder_name, ...
                      'DRILL SHIP -MOON-POOL-SPECTRUM.DAT'), '%s', 'delimiter', '\n');
line_mark2 = [];
for i = 1:size(D,1);
    if strcmp(D{i}, '***** STANDARD DEVIATION OF RESPONSE *****')
        line_mark2{end+1} = i;
    end
end

E = textread(fullfile(folder_name, ...
                      'DRILL SHIP -DRIFT-FORCE-SPECTRUM.DAT'), '%s', 'delimiter', '\n');
line_mark3 = [];
for i = 1:size(E,1);
    if strcmp(E{i}, '***** DRIFT FORCE RESPONSE *****')
        line_mark3{end+1} = i;
    end
end

F = textread(fullfile(folder_name, ...
                      'DRILL SHIP -VERTICAL-BENDING-MOMENT-SPECTRUM.DAT'), ...
              '%s', 'delimiter', '\n');
line_mark4 = [];
for i = 1:size(F,1);
    if strcmp(F{i}, '***** STANDARD DEVIATION OF RESPONSE *****')

```

```

        line_mark4{end+1} = i;
    end
end

% Search and pick data starting from line_marks -----%
exec_id = 0; % Counter of pick loops execution
for i=1:size(sea_opt,1) % for each position of matrix sea_opt
    if sea_opt(i) % if value is 1, i.e., if this one is required
        j = 1+13*(i-1); % position of the matrix line_mark where the first
            % occurrence of the spectrum's output data starts
            % Since the blocks of standard dev. for each beta
            % go from 0:30:360deg, there are 13 blocks until
            % the next spectrum (e.g. IACS long ends IACS short
            % starts)
        for m=1:size(T_opt,2) % for each significant wave period
            exec_id = exec_id+1;
            T         = T_opt(m) ;

            % allocate treshhold matrices to save computing time.
            H_str = zeros(1,7); %
            H_mpw = zeros(1,7); % 7 is the number of divisions of the incid.
            H_ben = zeros(1,7); % angles (0:30:180 deg). radar chart is
            H_dri = zeros(1,7); % symmetric, so pick 1 hemisphere only
            H_opt = zeros(1,7); %

            for k = 0:6 % k is attack angle counter.
                str_motion = C{line_mark1{j+k}+T+1}; %
                str_moon   = D{line_mark2{j+k}+T+1}; % placing the marker
                str_drift   = E{line_mark3{j+k}+T+1}; % at the data line
                str_mment   = F{line_mark4{j+k}+T+1}; %
                % concluded finding data of interest location.

                % acquiring values from marked lines.
                resp_moon   = textscan(str_moon , '%f');
                resp_motion = textscan(str_motion, '%f');
                resp_mment   = textscan(str_mment , '%f');
                resp_drift   = textscan(str_drift , '%f');

                % Overflow in the middle of the moon-pool criterion
                H_mpw(:,k+1) = Tres_Height(1, resp_moon{1}(2), T,...
                    folder_name) ;

                % Heave compensator criterion (stroke)
                H_str(:,k+1) = Tres_Height(2, resp_motion{1}(4), T,...
                    folder_name);

                % Vertical bending moment at midship criterion

```

```

        H_ben(:,k+1) = Tres_Height(3, resp_mment{1}(2), T,...
            folder_name) ;

        % Drift force criterion
        % water specific weight value took from fortran code
        resultant = (resp_drift{1}(4)^2 +...
            resp_drift{1}(5)^2)^0.5 ;
        H_dri(:,k+1) = Tres_Height(4,resultant, T, folder_name) ;
    end

    % Radar chart area: makes matrix of points (P), calls function
    % to calculate the area (SA) only, without plotting (0)
    P = [H_str' H_mpw' H_ben' H_dri'];
    [SA] = Radar_area_calc (P, 0) ;

    %-----%
    % Verify if the criteria for this combination of sea state
    % and significant wave period is critical and store it if
    % it is.-----%
    A = Inf;

    if SA<A
        A = SA ; % grade
        crit_sea_state = sea_states(i);
        T_crit = T ;
        H_str_min = H_str ;
        H_mpw_min = H_mpw ;
        H_ben_min = H_ben ;
        H_dri_min = H_dri ;
    end
end
end
end

% Tie break parameters -----%
% Find the minimum value in each incidence angle (radar chart axis)
for l = 1:size(H_opt,2)
    H_opt(:,l) = min([H_str(:,l),H_mpw(:,l),H_ben(:,l), H_dri(:,l)]);
end
D1 = H_opt(1,4) ; % tiebreak 1
D2 = H_opt(1,7) ; % tiebreak 2

nota = [A ; D1 ; D2] ;
P = [H_str_min' H_mpw_min' H_ben_min' H_dri_min'];

% Write in 'radar.txt' file the set of points of each criterion's radar

```

```
% chart values-----%
fid = fopen(fullfile(folder_name, '\radar.txt'), 'wt') ;
fprintf(fid, 'Critical sea state: %s\n', crit_sea_state{1});
fprintf(fid, 'Critical significant period: %d\n', T_crit) ;
fprintf(fid, ['overfl', ' ', num2str(H_str_min), '\n']) ;
fprintf(fid, ['str ', ' ', num2str(H_mpw_min), '\n']) ;
fprintf(fid, ['mom ', ' ', num2str(H_ben_min), '\n']) ;
fprintf(fid, ['drift ', ' ', num2str(H_dri_min), '\n']) ;
fprintf(fid, ['op_score ', ' ', num2str(A), '\n']) ;
fclose(fid) ;

fclose all;

disp('exit evaldata');
end
```

10. GAMMA.m

```
delete(gcp)
clear all
close all
clc

tic % start counting elapsed time
rng('shuffle'); % generate random numbers that are different

% Read main input parameters -----%
fileID = fopen('Optimization_Parameters.dat', 'r');

line_data = textscan(fileID, '%*[^']' %d', 1) ;
ni = line_data{1} ; % Total number of
% individuals to each evaluation.

line_data = textscan(fileID, '%f', 'HeaderLines', 2);
L1 = transpose(line_data{1}); % Based on the typical moonpool lenght and
% width, set values for L1.

line_data = textscan(fileID, '%f', 'HeaderLines', 1);
L2 = transpose(line_data{1}); % Based on the typical moonpool lenght and
% width, set values for L2.

line_data = textscan(fileID, '%f', 'HeaderLines', 1);
L3 = transpose(line_data{1}); % Based on the typical moonpool lenght and
% width, set values for L3.
```

```

line_data = textscan(fileID, '%*[^']' %f', 1) ;
p_no = line_data{1} ; % Percentage of the individuals to
                        % be selected as the best.
fclose(fileID) ;

% Finish reading main input parameters -----%

% Create main folder -----%
mkdir('Files');

% Parallel computing -----%
% parpool('local',2) % notebooks in general % creating pool of workers
parpool('local',4) % desktops in general % to call parfor

% Start silly search -----%
L = {L1; L2; L3} ; % compress data in 1 variable to pass
                        % to next function no. of columns of
colsK = size(L2,2)*size(L3,2); % Kn, KR, KI in the output of
grades = [] ; % Otherloops pre-allocating first
individuals = [] ; % position to use parfor without
radars = {} ; % index manipulation.

parfor w1 = 1:size(L1,2) % loop in L1
    [ Kn, KR, KI ] = Otherloops( w1, ni, p_no, L );
    for i = 1: colsK % store results from
        grades = [grades Kn(:,i)] ;
        individuals = [individuals KI(:,i)];
        radars = [radars KR(:,i)] ;
    end
end

% % % %- Select the best of the bests -----%
n = 1 ; % number of individuals
                        % to select as best

radars = (radars)';
[ I10, nota10, GR10 ] = Selecao( grades, individuals, n, radars );

% Search for and store its important parameters -----%
for i = 1:size(grades,2) % find index of the champion
    if nota10 == grades(:,i)
        indexIndiv = i;
    end
end

BestOfAll = individuals(:,indexIndiv); % recover the parameters of the

```

```

                                % individual
% Recover the data to generate the mesh again ----- %

fileID    = fopen('Optimization_Parameters.dat','r')           ;
line_data = textscan(fileID, '%*[^']' %f', 1, 'HeaderLines', 8);
divs(1)    = line_data{1}                                     ;
fclose(fileID)                                              ;

% divs are the number of divisions of the prismatic moon pool part (x,y,z)
% acquire the closed hull data to generate the ship again with the MP
[ v, e ] = Pre_Leitor      ;
LS        = BestOfAll(1:3,1);
shape     = BestOfAll(4:9,1);

s         = v(:,4)          ; % 'z' values.
H         = max(s)          ; % ship height

divs(2)   = H               ; % H is the MP height. It is not a division,
                                % but was added for convenience to divs.

% Generate and plots the mesh and radar chart ----- %
[realpar] = d_Geom_Pontos( v, e, LS, shape, divs)    % generate the mesh
fid = fopen('champion.txt','wt')                    ;
fprintf(fid, 'L1, L2, L3:\n')                       ;
fprintf(fid, sprintf('%0.9f\n %0.9f\n %0.9f\n', LS.)) ;
fprintf(fid, 'm1, m2, m3, m4, nf, nt:\n')           ;
fprintf(fid, sprintf('%0.9f\n %0.9f\n %0.9f\n %0.9f\n %0.9f\n %0.9f\n', ...
    shape.)) ;
fprintf(fid, 'div, H:\n')                           ;
fprintf(fid, sprintf('%0.9f\n %0.9f\n', divs.))      ;
fprintf(fid, 'real parameters after mesh generation') ;
fprintf(fid, sprintf('%0.9f\n %0.9f\n %0.9f\n %0.9f\n %0.9f\n %0.9f\n', ...
    realpar.));
fprintf(fid, '\n grade:\n')                          ;
fprintf(fid, sprintf('%0.9f\n', notal0'))            ;
fclose(fid);

winopen('PANEL.drill-ship.msh')                      ;    % open mesh visualization
Radar_area_calc (radars{indexIndiv}, 1);
disp('last radar chart data');
radars{indexIndiv}
save results.mat

Best_result ={'l1' BestOfAll(1); 'l2' BestOfAll(2); 'l3' BestOfAll(3); ...
'm1' BestOfAll(4); 'm2' BestOfAll(5); 'm3' BestOfAll(6); ...
'm4' BestOfAll(7); 'nf' BestOfAll(8); 'nt' BestOfAll(9)}
disp(sprintf ( '\n\t\t\t\t\t **** Finished optimization ****\n\n' ) )

```



```

toc                % stop counting and display elapsed time
%%%%%%%%%%%%%%%%%%%% parallel computing
delete(gcf)        % terminate existing parallel session
%-----%
```

11. Geracao_De_Individuos.m

```

function [ I ] = Geracao_de_Individuos( p, n )
% Random generation of individuals just for the first loop.

for i=1:n                % for each individual
    for j=1:6            % There are 6 parameters in m's and n's.
        % rng('shuffle')
        e = randi(size(p,1),1,1); % Choose a random position in 'p'.
        I(j,i) = p(e,j)      ; % Assign that position value in 'I'.
    end
end
end
end
```

12. Geracao_De_Parametros.m

```

function [ p ] = Geracao_de_Parametros (l1, l2, l3)
% Function to fix the available values for each parameter.]

dy = 12/9; % This way, we can have ten possible values for m1 and m4
dx1 = 11/9; % This way, we can have ten possible values for m2 and m3.
dx3 = 13/9; % This way, we can have ten possible values for m2 and m3.

t = 1;
for i = 0:dy:l2
    m1(t) = i; % Construction of m1.
    m4(t) = i; % Construction of m4
    t = t+1 ;
end
m1(t-1) = 12 - 0.01;
m4(t-1) = 12 - 0.01;

t = 1;
for i = 0:dx1:l1
    m2(t) = i; % Construction of m2.
```

```

        t = t+1 ;
end
m2(t-1) = l1 - 0.01;

t = 1;
for i = 0:dx3:13
    m3(t) = i; % Construction of m3.
    t = t+1 ;
end
m3(t-1) = l3 - 0.01;

% % % % THE NUMBER OF ELEMENTS IN m'S AND n'S HAVE TO BE THE SAME DUE TO p

nf = [1:10]; % number of sides of the quarter of polygon
           % which will represent the first rounding
           % corner. A 'Ten sides' is enough refined.

nt = [1:10]; % number of sides of the quarter of polygon
           % which will represent the second rounding
           % corner. A 'Ten sides' is enough refined.

p = [m1' m2' m3' m4' nf' nt'];
end

```

13. Mutacao.m

```

function [ I2 ] = Mutacao( I1, p )
% Creates a mutant from each individual
disp('enter mutacao');

I2 = I1 ; % matrix with the
           % originals modify

for i = 1:size(I1,2)
    e1 = randi(size(I1,1),1,3) ;
    [ G ] = Geracao_de_Individuos(p, size(I1,2)) ; % Generate random
                                                    % individuals in 'H'

    I2(e1(1),i) = G(e1(1),i) ; % Modify the individuals
                                % from 'I2' with parts
                                % of the 'H' ones.

    I2(e1(2),i) = G(e1(2),i) ; % Same as above.
    I2(e1(3),i) = G(e1(3),i) ; % Same as above.

```

```

end
disp('exit mutacao');
end

```

14. Otherloops.m

```

function [ Kn, KR, KI ] = Otherloops( w1, ni, p_no, L )

% Rest of the silly search loops with the genetic algorithm inside
disp('enter otherloops');

L1 = L{1}; %
L2 = L{2}; % separate the vectors again
L3 = L{3}; %
Kn = [] ;
KR = {} ;
KI = [] ;
for w2=1:size(L2,2)           % loop in L2
    for w3=1:size(L3,2)       % loop in L3
        l1 = L1(w1);          % Varying l1;
        l2 = L2(w2);          % Varying l2;
        l3 = L3(w3);          % Varying l3;

% Create main folder for a given L1 x L2 x L3 combination -----%
        folder_name_par = ['Files\','Parameter combination ',...
            num2str(l1), ' x ', num2str(l2), ' x ', num2str(l3)];
        mkdir(folder_name_par);

% Parameter generation according the chosen l1, l2 and l3 -----%
        [ p ] = Geracao_de_Parametros (l1, l2, l3);
% p are the parameters to combine and create individual meshes%

        t = 1; % Counter to know if it is in the first loop.
        q = 1; % Breaking variable.

        while q == 1           % while genetic algorithm doesn't converge
            clear GR ;
            clear GR1;
            clear GR2;
            clear GR3;
            clear GR4;

% Create folder to store all individuals created in the current iteration -%
            folder_name = [folder_name_par, '\Iteration ', num2str(t)];
            mkdir(folder_name);

```

```

        if t==1
            [ I ] = Geracao_de_Individuos( p, ni );% Initial
                                                    % generation
                                                    % just for the
                                                    % first loop.
        else
            [ I ] = Crossover( I4, I, ni )           ;% New
                                                    % generation
                                                    % for all the
                                                    % other loops.
        end

        % Create string with partial name of the original
        % individual, to be completed when the individual is
        % finally created.
        folder_str = [folder_name, '\I0-'];

% Build and evaluate moonpools in 'I' _____%
        disp('Silly search combination in execution:');
        LS = [11, 12, 13]

        % Get grade and tiebreaks, radar chart data for this group
        [ nota , GR ] = Build_Moonpools( I, LS, folder_str );

        % Percentage of the individuals to be selected as the best
        no = round(p_no*ni) ;
        while sum(nota(1,:)) == 0 % checks if there is at least one
                                    % individual with non-zero grade.
                                    % If all are zeroes, record the
                                    % parameters and generate 1
                                    % nonzero-graded individual.

            % Write the log in the file 'allzeros.txt'
            fid1 = fopen(folder_name, 'allzeros.txt', 'a') ;
            fprintf(fid1,...
                'All the generation resulted in zero grades.\n') ;
            fprintf(fid1,...
                ' A new unique individual will be generated.\n') ;
            fprintf(fid1,...
                sprintf('%0.9f %0.9f %0.9f %0.9f %0.9f\n %0.9f'...
                    ' %0.9f %0.9f %0.9f %0.9f\n %0.9f %0.9f %0.9f %0.9f'...
                    ' %0.9f\n %0.9f %0.9f %0.9f %0.9f %0.9f\n %0.9f %0.9f'...
                    ' %0.9f %0.9f %0.9f\n %0.9f %0.9f %0.9f %0.9f %0.9f'...
                    '\n,I.')) ;
            fclose(fid1) ;
            [ I ] = Geracao_de_Individuos( p, 1 ) ;
            [ nota , GR ] = Build_Moonpools( I, LS,...

```



```

% it is the moment to
% break.

end

t=t+1 ; % Increase 't'.

if t > 50
    disp('number of loops '...
        ' in while exceeded 50. Breaking here');
    q = 0;
    continue
end

end

Kn(:,size(Kn,2)+1) = nota4(:,1) ; % collection of grades
% and tiebreaks in columns
KR(:,size(KR,2)+1) = GR4(1,1) ; % collection of radar
% chart points in lines
KI(:,size(KI,2)+1) = [LS' ; I4(:,1)] ; % collection of
%parameters of individuals in columns:
% [l1; l2; l3; m1; m2; m3; m4; nf; nt]

% register successful exit from the folder
fid1 = fopen(fullfile(folder_name_par,...
    '\parameter_successful_exit.txt'),'wt');
fprintf(fid1,sprintf('Kn: \n')) ;
fprintf(fid1,sprintf('%u %u %u\n',Kn(:,size(Kn,2)).')) ;
fprintf(fid1,sprintf('\n KI: \n')) ;

for i=1:size(KI,1)
    fprintf(fid1,sprintf('%f \n ' ,KI(i,size(KI,2)))) ;
end
fprintf(fid1,sprintf('\n KR = %u \n',size(KR,2))) ;
for j=1:size(KR{size(KR,1)},1)
    for k=1:size(KR{size(KR,1)},2)
        fprintf(fid1,sprintf('%u \t' ,KR{1,size(KR,2)}(j,k))) ;
    end
    fprintf(fid1,sprintf('\n')) ;
end
fclose(fid1) ;

Kn
KR
KI

end
end

```

```
disp('exit otherloops');
end
```

15. Pre_Leitor.m

```
function [ v, e ] = Pre_Leitor
% Function which reads the data from the ship geometry file and make data
% matrices.

% Catch the amount of points and elements -----%
num_vertices = textread('input_hull.txt','%u', 1);
num_elem = textread('input_hull.txt','%u', 1,'headerlines',1);

% Catch the points coordinates from the ship geometry file -----%
v=zeros(num_vertices,4); % memory allocation for vertices coordinates

for i=1:num_vertices,
    [a b c d]=textread('input_hull.txt','%f %f %f %f',1,...
        'headerlines',i+2);
    v(i,1)=a;
    v(i,2)=b;
    v(i,3)=c;
    v(i,4)=d;
end

% Catch the elements from the ship geometry file -----%
for i=1:num_elem,
    [e(i,1) e(i,2) e(i,3) e(i,4) e(i,5)]=textread('input_hull.txt',...
        '%u %u %u %u %u',1,'headerlines',i+num_vertices+2);
end
end
```

16. Radar_Area_Calc.m

```
function [Area] = Radar_area_calc (P, plotyn)

% function [Area] = Radar_area_calc (P, plotyn)
% This program will calculate the minimum area between radar plot graphs.
% It will be done by the calculation of smaller polygons, inside the
% main area.
% P is the matrix of points. Lines are for each radial axis, columns for
% each criterion
```

```

% plot indicates 1 for yes, plot the last chart, and 0 for no, do not plot

nPoints      = size(P,2); %number of criteria
nDimensions = size(P,1); %number of data of each criteria

%this program works for 4 criteria, 8 data numbers for each criteria. For
%more criteria and more data numbers, it needs to be adapted.

% create data base for each sector (pair of axes) -----%
for i = 1:nDimensions
    % Transform the minimum of each axis from polar to cartesian
    a = min(P(i,:)) ;
    [mPx(i) mPy(i)] = pol2cart((i-1)*pi/(nDimensions-1),a);
    % list the criteria located at minimum in the axis
    sectordata{i} = find(P(i,:) == min(P(i,:))) ;
end

% analyze if there will be intersection or not, obtain the intercection
% point and calculate area for each sector
% Calc. area of intersection polygons for each pair of axis -----%
% Identify which case of intersection area is between pairs of axis
% Area is calculated for one hemisphere only, due to symmetry
Area = 0 ;
RP = [mPx(1) mPy(1)];
for i = 1:nDimensions-1
    a = intersect(sectordata{i},sectordata{i+1});
    if size(a,2) == 0
        % disp('different colors: there is intersection')
        % the intersection point needs to be calculated, and the area will
        % be a four side polygon.
        % take in the opposite axis the min. val. or radius corresponding
        % to the set of colors that belong to the point under analysis,
        % convert to cartesian
        b = min(P(i+1,sectordata{i})) ;
        c = min(P(i,sectordata{i+1})) ;
        [xi2 yi2] = pol2cart(i*pi/(nDimensions-1),b) ;
        [xi1 yi1] = pol2cart((i-1)*pi/(nDimensions-1),c);

        % find intersection point
        q = calculopontos(mPx(i),mPy(i),xi2,yi2,mPx(i+1),...
            mPy(i+1),xi1,yi1) ;
        Area = Area + polyarea([0 mPx(i) q(1) mPx(i+1)],...
            [0 mPy(i) q(2) mPy(i+1)]);
        RP = [ RP ; q' ; [ mPx(i+1) mPy(i+1)]] ;
    else
        % disp('same colors: no intersection')
        % belong to the same criterion, there is no crossing between lines

```



```

        % and the area is the triangle between the two lowest values and
        % the origin.
        Area = Area + polyarea([0 mPx(i) mPx(i+1)], [0 mPy(i) mPy(i+1)]);
        RP    = [ RP ; [ mPx(i+1) mPy(i+1)]] ;
    end
end

Area = 2*Area;

% Prepare matrix for 0:360 deg (mirror P) and plot chart -----%
if plotyn == 1
    % mirror P and RP
    PP = [P ; flipud(P(2:nDimensions-1,:))] ;
    RPx = [RP(:,1) ; flipud(RP(2:size(RP,1)-1,1))] ; % for the patch usage
    RPy = [RP(:,2) ; -flipud(RP(2:size(RP,1)-1,2))] ; % for the patch usage

    [theta,rho] = cart2pol(RPx,RPy); % converting for plot
    % creating variable to send to plot
    dataplot = {PP, [theta,rho]};
    % aesthetic configuration of chart
    pointNames = arrayfun( @(i)sprintf('p_{{d}}', i), 1:nPoints,...
        'UniformOutput', false);
    close all;
    figure('Name','Safety limits of significant wave height',...
        'NumberTitle','off')
    Radar_final_plot(dataplot, '-', 'LineWidth', 1.5,...
        'MarkerFaceColor', [0,0,0] )
    ax = gca ;

    ax.Position = [0.095 0.02 0.7750 0.8150];
    legend('Stroke ', 'Overflow ', 'Moment ', 'DPS ',...
        'Location', 'northeastOutside', 'Orientation', 'Vertical');
    TitleH = title('Operable area') ;
    set(TitleH, 'Position', [5, 18], 'FontSize', 18,...
        'VerticalAlignment', 'top' )
end

```

18. Selecao.m

```

function [ K2, f2, radar2 ] = Selecao( f, K, a, GR )
% Function to select the individuals with best grades.

% f: list of grades and tiebreaks (3 x :)
% K: list of individuals (6 x :)

```

```

% a: number of best to pick          (1 x 1)
% GR: collection of radar chart data of each individual
% column cellarray { : , 1 }(7 x 4)
disp('enter selecao');

clear radar2;

% Create a matrix of the information used to sort the individuals -----%
tot          = size(f,2)              ; % Number of grades
ids          = (1:tot)                ; % vector from 1:1:tot to store the
                                     % original positions of the grades
                                     % and track later their other
                                     % properties in the other vectors
orderindiv   = [f' ids']              ; % creates a set of grade, tiebreaks
                                     % and individuals
classifiedind = sortrows(orderindiv) ; % classifies them in crescent order
                                     % (from worst to best)
lst          = flipud(classifiedind); % flips matrix to have descending
                                     % order (from best to worst)

% First individual of the champions -----%
IDbest       = lst(1,4)               ;
K2           = K(:,IDbest)            ;
f2           = f(:,IDbest)            ;
radar2(1,1) = GR(IDbest,1)            ;

% Pick the rest in descendent order -----%
for i = 2:size(K,2)-1
    ID = lst(i,4);
    if sum(K(:,ID) == K2(:,size(K2,2))) ~= size(K,1) % check if is
                                                    % neither repeated
                                                    % nor null
                                                    %
        if lst(i,1) ~= 0 && size(K2,2) < a
            K2 = [K2 K(:,ID)];
            f2 = [f2 f(:,ID)];
            radar2(size(K2,2),1) = GR(ID,1) ;
        end
    end
end

disp('exit selecao');

K2
f2
radar2

end

```

19. Tres_Height.m

```

function [H_tres] = Tres_Height(mode, variance, T, folder_name)

% Choose mode according to criterion:
% 1: wave overflow
% 2: stroke compensation
% 3: bending moment
% 4: drift force

if mode == 1 || mode == 2      % green water / stroke
    % Read input parameters.-----%
    fileID = fopen('Optimization_Parameters.dat','r') ;
    line_data = textscan(fileID, '%*[^']' %f', 2, 'HeaderLines', ...
        9 + 2*mode) ;
    xq = line_data{1}(1) ;
    Nn1 = line_data{1}(2) ;
    fclose(fileID) ;
elseif mode == 3 || mode == 4 % bending moment / drift
    % Read input parameters.-----%
    fileID = fopen('Optimization_Parameters.dat','r') ;
    line_data = textscan(fileID, '%*[^']' %f', 1, 'HeaderLines', ...
        12 + mode) ;
    param = line_data{1}(1) ;
    % dummy for bending moment (using iacs max and min)
    fclose(fileID) ;

    fileID = fopen(fullfile(folder_name, ...
        'DRILL SHIP -DRIFT-FORCE-SPECTRUM.DAT'));
    line_data = textscan(fileID, ...
        '%*[          LENGTH IN X-AXIS----- (LENGTH)---=' ...
        '] %f', 1, 'headerlines', 13);
    % ignores the text between brackets and takes the float that comes
    % after. Skips 17 lines until the desired one.
    lpp = line_data{1};
    line_data = textscan(fileID, '%*[          LENGTH IN' ...
        'Y-AXIS----- (BREDTH)---=          ] %f', 1, 'headerlines', 1);
    B = line_data{1};
    line_data = textscan(fileID, '%*[          BLOCK      COEFFICIENT' ...
        '----- ( CB )---=          ] %f', 1, 'headerlines', 3);
    Cb = line_data{1};
    fclose(fileID);
end

switch mode

```

```

case 1 % overflow
    Nn          = 3*3600/T/Nn1          ;
    H_tres       = xq/(variance*(2*log(Nn))^0.5);
case 2 % heave compensator
    Nn          = 3*3600/T/Nn1          ;
    H_tres       = xq/(variance*(2*log(Nn))^0.5);
case 3 % vertical bending moment at midship
    % conversion from long to short term: 10^8 is the criterion,
    % divided by 25 years*12months, all divided by log(10^8), for 1 month
    long2short   = log((10^8)/(25*12))/log(10^8)      ;
    nshort       = 10^(-8)*long2short                 ;
    timen        = (30*24*60*60/T)                   ; % 1 month
                                                    % exposure
    Nn           = timen/nshort                       ;
    if (Lpp >= 90) && (Lpp < 300)
        C        = 10.75 - ((300 - Lpp)/100)^1.5      ;
    elseif (Lpp >= 300) && (Lpp < 350)
        C        = 10.75                             ;
    elseif (Lpp >= 350) && (Lpp < 500)
        C        = 10.75 - ((Lpp - 350)/150)^1.5     ;
    end

    superioru    = 110*C*Lpp^2*B*(Cb+0.7)*long2short*0.001;
    inferioru    = 190*C*Lpp^2*B*Cb*long2short*0.001;
    xq           = min(superioru,inferioru)            ;

    % disp('bending moment')
    H_tres       = xq/(variance*(2*log(Nn))^0.5);
case 4 % drift
    % disp('drift')
    specWeight    = 1025                          ; % actually
    % should be multiplied
    Dy_dimsens    = variance*specWeight*Lpp        ; % by H, which
    % will be considered
    H_tres        = (param/(Dy_dimsens*(2*pi/T)))^(1/3) ; % in
    % Tres_Height calculation
end
end

```